



# Low Frequency Transmission

*Final Project Report*

**Power Systems Engineering Research Center**

*Empowering Minds to Engineer  
the Future Electric Energy System*



# **Low Frequency Transmission**

## **Final Project Report**

### **Project Team**

#### **Faculty:**

**Sakis A. P. Meliopoulos, Project Leader**  
**Georgia Institute of Technology**

**Dionysios Aliprantis, Iowa State University**

#### **Graduate Research Assistants:**

**Yongnam Cho, Dongbo Zhao, and Anupama Keeli**  
**Georgia Institute of Technology**

**Hao Chen**  
**Iowa State University**

**PSERC Publication 12-28**

**October 2012**

**For information about this project, contact:**

Sakis Meliopoulos  
Georgia Power Distinguished Professor  
School of Electrical and Computer Engineering  
Georgia Institute of Technology  
Atlanta, Georgia 30332-0250  
Phone: 404-894-2926  
E-mail: sakis.m@gatech.edu

**Power Systems Engineering Research Center**

This is a project report from the Power Systems Engineering Research Center (PSERC). PSERC is a multi-university Center conducting research on challenges facing a restructuring electric power industry and educating the next generation of power engineers. More information about PSERC can be found at the Center's website: <http://www.pserc.wisc.edu>.

**For additional information, contact:**

Power Systems Engineering Research Center  
Arizona State University  
527 Engineering Research Center  
Tempe, Arizona 85287-5706  
Phone: 480-965-1643  
Fax: 480-965-0745

**Notice Concerning Copyright Material**

PSERC members are given permission to copy without fee all or part of this publication for internal use if appropriate attribution is given to this document as the source material. This report is available for downloading from the PSERC website.

**© 2012 Georgia Institute of Technology and Iowa State University.  
All rights reserved.**

## Acknowledgements

This is the final report for the Power Systems Engineering Research Center (PSERC) research project S-42 titled “Low Frequency Transmission”. We express our appreciation for the support provided by PSERC’s industrial members and by the National Science Foundation’s Industry / University Cooperative Research Center program.

The authors wish to recognize their postdoctoral researchers and student graduate research assistants (GRA) who contributed to the research and creation of the report:

Georgia Institute of Technology:

- Yongnam Cho, GRA
- Dongbo Zhao, GRA
- Anupama Keeli, GRA

Iowa State University:

- Hao Chen, GRA

The authors thank the following individuals for their technical advice on the project, especially (the companies shown were as of time of this project work):

- Bob Pierce, Duke Energy
- Floyd Galvan and Shannon Watts, Entergy
- Bruce Fardanesh and George Stefopoulos, New York Power Authority
- Jianzhong Tong, PJM
- Olivier Despouys, Sebastien Henry and Patrick Panciatici, RTE
- Andrew Taylor, Southern Company Services Transmission Planning

## **Executive Summary**

The goal of this project is to evaluate alternative transmission systems from remote wind farms to the main grid using low-frequency AC technology. Low frequency means a frequency lower than nominal frequency (60/50Hz). To minimize costs, cyclo-converter technology is utilized resulting in systems of 20/16.66 Hz (for 60/50Hz systems respectively). The technical and economic performance of low-frequency AC transmission technology is compared to HVDC transmission and conventional AC transmission in different configurations. The issue is quite important since wind potential exists in remote and off-shore locations and the transmission system required to bring wind energy to the main power grid represents a substantial expenditure of the overall wind energy projects. The end result of this study is a comprehensive method for evaluating and selecting the design parameters for alternative configurations of wind projects and typical results of these evaluations for selected example systems.

In this project we have identified a number of possible configurations that are mainly based on the three main options: (a) interconnection of a wind farm to the main power grid via AC transmission, (b) interconnection of the wind farm to the main power grid via DC transmission, and (c) interconnection of the wind farm to the main power grid via low frequency AC transmission (LFAC). Using these three distinct transmission options, eight alternative configurations were developed that include the above three options. These alternative configurations were analyzed from several points of view. Specifically, the following evaluations were performed: (a) optimal kV levels for each specific alternative configuration, (b) reliability performance of each one of the alternative configurations, (c) transfer capability of each one of the configurations, and (d) transient stability analysis of each one of the configurations. For each one of these evaluations, a parametric study has been performed when warranted. A summary for the final report is provided below.

Chapter 1 provides an overview of the project and the reasons that the project was initiated.

Chapter 2 provides an overview of the overall approach to the stated objectives for the proposal. Specifically, the approach is based on developing comprehensive models for the proposed technologies and to use these models to evaluate their performance and compare them to competing technologies. The models developed are described in more detail in the Appendices B and C.

Chapter 3 provides a literature survey for alternate connection methods of wind farm to the main power grid using HVDC, conventional AC and LFAC technologies. Based on the survey, eight alternate wind farm configurations have been proposed in Chapter 4 of the report, including different combinations of in-farm technologies and out-farm transmission technologies (HVDC, conventional AC or LFAC).

Chapter 4 describes alternative topologies for low-frequency transmission. Chapter 5 provides a methodology for determining the optimal kV level selection and equipment rating. The selection methods are formulated based on the minimization of the total cost,

which contains the operational cost and the acquisition cost. Specific analysis of the selection of optimal kV level and equipment ratings based on the formulation of the total cost for each of the eight proposed configurations has been performed. Examples of these computations are provided in the section for each one of the eight alternative configurations. The example results are summarized at the end of the chapter and presented here. It should be emphasized that the values of the table below are valid only for the considered example systems.

Configuration	kV Level Selection	Minimum Annualized Total Cost (M\$/year)
1	12	0.48
2	10	0.50
3	8	0.52
4	2	1.05
5	18	1.20
6	4	0.82
7	7	0.75
8	2	1.25

In Chapter 6, the operational study presents the comparison of maximum power transfer capability between nominal-frequency systems and LFAC transmission systems. The maximum power transfer capability is computed by gradually increasing the power transfer until one of the operating constraints or static stability limits are violated. The operational constraints are voltage limits, loading limits and electric current limits. The stability constraints are the static stability limits. Example results are also presented for specific example systems. For convenience we present one example of transmission at 76 kV below. The much higher power transfer capability of the low frequency AC system is clearly apparent.

Maximum Transmission Capability at the Operation Voltage 76kV

	Capability of Power Transmission (MW)										
Distance (miles)	10	30	50	70	90	100	120	140	160	180	200
Transfer Capability (MW) at 60Hz	180.3	82.8	57.54	44.17	36.78	34.31	30.56	27.98	26.19	24.84	23.38
Transfer Capability (MW) at 20Hz	225.3	141.3	106.1	86.28	73.49	68.29	60.19	54.27	49.22	45.21	41.96

Chapter 7 describes the overall approach for performing transient analysis of wind farm systems and provides case studies for voltage stability.

Chapters 8 and 9 describe the requirements for transient stability studies to determine the suitability and operational robustness of these systems. These studies are important for better understanding the dynamic behavior of these systems that include complex power electronic systems. These studies also provide the generation of harmonics by these systems. They are critical for understanding the harmonic content generated by wind farms and LFAC transmission systems. The methods can be used to determine the need for harmonic filters and if filters are needed, the method can be also used for the design of these filters. Also, the power transient study allows the close observation of control performance of power transients. Chapter 8 presents the overall approach for transient analysis of the proposed low frequency AC transmission systems and presents the controls of the power electronic subsystems for this operation. Design details for these systems are also addressed, such as harmonic filter design, etc. Chapter 9 describes a numerical integration of the basic models using the advanced quadratic integration. Details of the simulation method are presented and results for specific systems are presented. The ability of the proposed systems to control the power transferred and to control the operation of these systems is demonstrated.

Chapter 10 provides an analysis of the eight alternative configurations from the reliability point of view. Reliability analysis methods have been proposed for the alternative wind farm configurations. Both the structural reliability model and the wind variability model are considered in the reliability study. Monte Carlo models of the components and probabilistic approaches of the topologies are utilized to formulate the reliability analysis and reliability indices calculation. Case studies for each of the eight configurations are provided and the reliability indices results are compared. Specifically, the reliability of the wind farms is assessed in terms of the following reliability indices: EGWE (Expected Generated Wind Energy) and CF (Capacity Factor). Results for example systems (one example per proposed alternative configurations) are provided. A summary of these results is given below for convenience.

Configuration	EGWE	IWP	CF
1	22.98	60	0.383
2	22.42	60	0.374
3	20.82	60	0.347
4	26.22	60	0.437
5	12.31	60	0.205
6	25.86	60	0.431
7	20.54	60	0.342
8	26.27	60	0.438

Conclusions and future work is discussed in Chapter 11. Since wind energy is the most rapidly developed generating systems from all renewable resources and the forecast is that they may be forming a large percentage of the generation system, their performance is of paramount importance to the reliability of the power system of the near and far future. The models developed in this research project can be utilized to study other very important operational characteristics and capabilities of these systems. One main concern is that as the percentage of wind generating systems become very large (even 100% in some systems) what will be the operational challenges of these new systems from the stability, control, operation and protection point of view. Suggestions are provided in Chapter 11.

A total of four students contributed to this project (three at Georgia Tech and one at Iowa State University). One Master's thesis was written on the subject and two PhD theses were written on the subject. In addition, nine publications were generated that describe the work of this project. These publications and the three Theses (Dissertations) compliment this main report.

### **Project Publications:**

1. Yongnam Cho, Georgy J. Cokkinides, and A. P. Meliopoulos, "Time Domain Simulation of a Three-Phase Cycloconverter for LFAC Transmission Systems," 2012 IEEE Power and Energy Society Transmission and Distribution Conference and Exhibition, Orlando, Florida, May 2012.
2. Yongnam Cho, George J. Cokkinides, A. P. Meliopoulos, "Transient Simulation Technique for HVDC Systems," in Proceedings of the International conference on Power Systems Transients, Delft, the Netherlands, June 2011.
3. Yongnam Cho, George J. Cokkinides, A. P. Meliopoulos, "LFAC-Transmission Systems for Remote Wind Farms Using a Three-phase, Six-pulse Cycloconverter," in Power Electronics and Machines in Wind Applications-PEMWA 2012, Denver, Co, July 2012.
4. Yongnam Cho, Georgy J. Cokkinides, and A. P. Meliopoulos, "Advanced Time Domain Method for Remote Wind Farms with LFAC Transmission Systems: Power Transfer and Harmonics," in North American Power Symposium, Urbana, Illinois, September 2012.
5. Dongbo Zhao, A. P. Meliopoulos, George J. Cokkinides, Ramazan Caglar, "Reliability Analysis of Alternate Wind Energy Farms and Interconnections," in Proceedings of 12th International Conf. on Probabilistic Methods Applied to Power Systems, Istanbul, Turkey, June 2012.
6. Dongbo Zhao, A. P. Meliopoulos, Rui Fan, Zhenyu Tan and Yongnam Cho, "Reliability Evaluation with Cost Analysis of Alternate Wind Energy Farms and Interconnections," in North American Power Symposium, Urbana, Illinois, September 2012.



7. H. Chen, N. David, and D. C. Aliprantis, "Analysis of permanent magnet synchronous generator with Vienna rectifier for wind energy conversion system," to appear in IEEE Trans. Sustainable Energy.
8. H. Chen and D. C. Aliprantis, "Analysis of squirrel-cage induction generator with Vienna rectifier for wind energy conversion system," IEEE Trans. Energy Conv., Vol. 26, No. 3, pp. 967-975, Sep. 2011.
9. H. Chen and D. C. Aliprantis, "Induction generator with Vienna rectifier: feasibility study for wind power generation," in Proc. IEEE Int. Conf. Electrical Machines, Rome, Italy, Sep. 2010.

**Student Theses and Dissertations:**

1. Anupama, K. "Low Frequency Transmission for Remote Power Generating Systems," Master's Thesis, Georgia Institute of Technology, 2011.
2. H. Chen, "Advances in Wind Power Generation, Transmission, and Simulation Technology," PhD dissertation, Iowa State University, Aug. 2012.
3. Yongnam Cho, "Transient Modeling of Converters for HVDC system and LFAC Systems," PhD dissertation, Georgia Institute of Technology, to be defended in Spring 2013.

## Table of Contents

Acknowledgements .....	i
Executive Summary .....	i
Table of Contents .....	vi
List of Figures .....	ix
List of Tables .....	xv
1        Project Description .....	1
2        Technical Approach .....	3
3        Literature Survey .....	7
4        Alternative Topologies for Low-Frequency Transmission .....	9
4.1    Wind System Configuration 1: AC Wind Farm, Nominal Frequency, Network Connection .....	9
4.2    Wind System Configuration 2: AC Wind Farm, AC/DC Transmission, Network Connection .....	11
4.3    Wind System Configuration 3: Series DC Wind Farm, Nominal Frequency, Network Connection .....	12
4.4    Wind System Configuration 4: Parallel Dc Wind Farm, Nominal Frequency, Network Connection .....	13
4.5    Wind System Configuration 5: Series DC Wind Farm, Low Frequency Radial AC Transmission .....	15
4.6    Wind System Configuration 6: Parallel DC Wind Farm, Low Frequency, Radial Transmission .....	16
4.7    Wind System Configuration 7: Series DC Wind Farm, Low Frequency AC Transmission Network .....	16
4.8    Wind System Configuration 8: Parallel DC Wind Farm, Low Frequency AC Transmission Network .....	18
5        Optimal kV Level, Equipment Ratings and Cost Analysis of Alternate Configurations .....	19
5.1    Approach Description .....	19
5.2    kV Levels, Equipment Ratings and Wind Farm Cost Analysis of Configuration 2 .....	32
5.3    kV Levels, Equipment Ratings and Wind Farm Cost Analysis of Configuration 3 .....	37
5.4    kV Levels, Equipment Ratings and Wind Farm Cost Analysis of Configuration 4 .....	41

## **Table of Contents (continued)**

5.5	kV Levels, Equipment Ratings and Wind Farm Cost Analysis of Configuration 5 .....	45
5.6	kV Levels, Equipment Ratings and Wind Farm Cost Analysis of Configuration 6 .....	48
5.7	kV Levels, Equipment Ratings and Wind Farm Cost Analysis of Configuration 7 .....	51
5.8	kV Levels, Equipment Ratings and Wind Farm Cost Analysis of Configuration 8 .....	55
5.9	Summary and Conclusions .....	58
6	Operational Studies – Power Transfer Capability .....	59
6.1	Technical Approach of Power Transfer Capability Study .....	59
6.2	Methodology for Simulation Models in Steady State .....	60
6.3	Case Studies of Power-Transfer Capability .....	69
7	Transient Stability Studies .....	73
7.1	Description and Technical Approach of Transient Stability Studies .....	73
7.2	Case Studies of Voltage-Stability Study .....	75
8	Time-Domain Studies-I.....	83
8.1	System Configuration and Control .....	83
8.2	Sending End Control.....	83
8.3	Receiving End Control.....	84
8.4	System Design .....	87
8.5	Case Study .....	92
8.6	Simulation Results .....	95
8.7	Conclusion .....	98
9	Time-Domain Studies-II .....	99
9.1	Technical Approach of Time-Domain Studies .....	99
9.2	Methodology for Simulation Models in Time-Domain .....	101
9.3	Power-Transient Studies of LFAC Transmission Systems .....	121
9.4	Harmonics Study of LFAC Transmission Systems .....	128
10	Reliability Analysis of Wind Farm Configurations .....	132
10.1	Approach Description .....	132
10.2	Reliability Analysis of Wind Farm Configuration 1 .....	135

## **Table of Contents (continued)**

10.3	Reliability Analysis of Wind Farm Configuration 2.....	146
10.4	Reliability Analysis of Wind Farm Configuration 3.....	150
10.5	Reliability Analysis of Wind Farm Configuration 4.....	154
10.6	Reliability Analysis of Wind Farm Configuration 5.....	159
10.7	Reliability Analysis of Wind Farm Configuration 6.....	162
10.8	Reliability Analysis of Wind Farm Configuration 7.....	165
10.9	Reliability Analysis of Wind Farm Configuration 8.....	170
10.10	Summary and Conclusions .....	174
11	Conclusions .....	175
Appendix A:	Nomenclature.....	181
Appendix B:	Example Wind Farm Model.....	183
Appendix C:	Advanced Time-Domain Method (Quadratic).....	186
Appendix D:	Reliability Model Parameters .....	191
Appendix E:	Cost Parameters .....	193

## List of Figures

Figure 2.1:	Typical Interconnection and Topology of Wind Farms and Collector Substations .....	4
Figure 4.1.1:	Wind System Configuration 1: AC Wind Farm, Nominal Frequency, Network Connection .....	10
Figure 4.2.1:	Wind System Configuration 2: AC Wind Farm, AC/DC Transmission, Network Connection .....	11
Figure 4.3.1:	Wind System Configuration 3: Series DC Wind Farm, Nominal Frequency, Network Connection .....	12
Figure 4.4.1:	Wind System Configuration 4: Parallel DC Wind Farm, Nominal Frequency, Network Connection .....	14
Figure 4.5.1:	Wind System Configuration 5: Series DC Wind Farm, Low Frequency Radial AC Transmission .....	15
Figure 4.6.1:	Wind System Configuration 6: Parallel DC Wind Farm, Low Frequency, Radial Transmission.....	16
Figure 4.7.1:	Wind System Configuration 7: Series DC Wind Farm, Low Frequency AC Transmission Network .....	17
Figure 4.8.1:	Wind System Configuration 8: Parallel DC Wind Farm, Low Frequency AC Transmission Network .....	18
Figure 5.1.1:	Alternative Configuration 1 - Example Configuration for Transmission Loss Analysis .....	20
Figure 5.1.2:	Acquisition Cost of Wind Turbine System vs. kV Level .....	27
Figure 5.1.3:	Operating Cost of Example Configuration .....	30
Figure 5.1.4:	Annualized Acquisition Cost of Example Configuration .....	31
Figure 5.1.5:	Annualized Total Cost of Example Configuration .....	32
Figure 5.2.1:	Alternative Wind Farm Configuration 2 .....	33
Figure 5.2.2:	Annualized Total Cost of Configuration 2.....	36
Figure 5.3.1:	Alternative Wind Farm Configuration 3.....	37
Figure 5.3.2:	Annualized Total Cost of Configuration 3.....	40
Figure 5.4.1:	Alternative Wind Farm Configuration 4.....	41
Figure 5.4.2:	Annualized Total Cost of Configuration 4.....	44
Figure 5.5.1:	Alternative Wind Farm Configuration 5.....	45
Figure 5.5.2:	Annualized Total Cost of Configuration 5.....	47

## List of Figures (continued)

Figure 5.6.1:	Alternative Wind Farm Configuration 6.....	48
Figure 5.6.2:	Annualized Total Cost of Configuration 6.....	50
Figure 5.7.1:	Alternative Wind Farm Configuration 7.....	51
Figure 5.7.2:	Annualized Total Cost of Configuration 7.....	54
Figure 5.8.1:	Alternative Wind Farm Configuration 8.....	55
Figure 5.8.2:	Annualized Total Cost of Configuration 8.....	57
Figure 6.1.1:	Two Types of Transmission Configurations for Case Studies .....	59
Figure 6.2.1:	Three-Phase Transformer.....	62
Figure 6.2.2:	Three-Phase Overhead Transmission Line .....	62
Figure 6.2.3:	The Equivalent Circuit of a Single-Phase Transformer.....	63
Figure 6.2.4:	The PI-Equivalent Circuit of a Single Phase Line .....	63
Figure 6.2.5:	115-kV Overhead Transmission Line: Left figure: equivalent circuit at 60 Hz. Right figure: equivalent circuit at 20 Hz. ....	65
Figure 6.2.6:	230-kV Overhead Transmission Line: Left figure: equivalent circuit at 60 Hz. Right figure: equivalent circuit at 20 Hz. ....	65
Figure 6.2.7:	345-kV Overhead Transmission Line: Left figure: equivalent circuit at 60 Hz. Right figure: equivalent circuit at 20 Hz. ....	66
Figure 6.2.8:	Power Electronic Systems (a) Three-Phase, Six-Pulse Converter, (b) Three-Phase, PWM Converter, and (c) Three-Phase, Six-Pulse Cycloconverter.....	67
Figure 6.3.1:	Power Transmission Capability of the Operation Voltage 38-kV .....	70
Figure 6.3.2:	Power Transmission Capability of the Operation Voltage 76-kV .....	71
Figure 6.3.3:	Power Transmission Capability of the Operation Voltage 115-kV .....	72
Figure 7.1.1:	NERC PRC-024-1 Voltage-Ride-Through Requirement Curve.....	74
Figure 7.2.1:	Single-Line Diagram of a LFAC Transmission System Connecting a Series LFAC Wind Farm to the Main Grid.....	75
Figure 7.2.2:	Configuration 1: Voltage Magnitude of Phase A at (A) Remote Grid and (B) Local Grid, and (C) Before the Cycloconverter during a Three-Phase Fault at Remote Grid .....	76
Figure 7.2.3:	Configuration 1: (A) Operating Frequency and (B) Real Power at Remote Grid during a Three-Phase Fault at Remote Grid.....	76

## List of Figures (continued)

Figure 7.2.4:	Configuration 1: Voltage Magnitude of Phase A at (A) Remote Grid, (B) Local Grid, and (C) Before the Cycloconverter during the Recloser Operation.....	77
Figure 7.2.5:	Configuration 1: (A) Operating Frequency and (B) Real Power at Remote Grid during the Recloser Operation.....	77
Figure 7.2.6:	Configuration 1: (A) Voltage Magnitude of Phase A and (B) Operating Frequency during the Three-Phase Fault at Local Grid.....	78
Figure 7.2.7:	Single-Line Diagram of LFAC Transmission Network Connecting a Series DC Wind Farm .....	79
Figure 7.2.8:	Configuration 2: Voltage Magnitude of Phase A (A) at Remote Grid, (B) at Local Grid 1, and (C) Before the Cycloconverter during a Three-Phase Fault at Remote Grid .....	80
Figure 7.2.9:	Configuration 2: (A) Operating Frequency and (B) Real Power at Remote Grid during a Three-Phase Fault at Remote Grid.....	80
Figure 7.2.10:	Configuration 2: Magnitude of Phase A Voltages at (A) Remote Grid and (B) Local Grid 1, and (C) Real Power and Operating Frequency at Remote Grid during a Three-Phase Fault at Local Grid 1 .....	81
Figure 7.2.11:	Configuration 2: Magnitude of Phase A voltages at (A) Remote Grid and (B) Local Grid 1 during Recloser Operation at RECLOSOR-LFAC2-TR.....	82
Figure 7.2.12:	Configuration 2: Magnitude of Phase A Voltages at (A) Remote Grid and (B) Local Grid 1 during Recloser Operation at RECLOSOR-LFAC1-TR.....	82
Figure 8.1.1:	Configuration of the Proposed LFAC Transmission System .....	83
Figure 8.2.1:	Sending End DC/AC Inverter Control.....	84
Figure 8.3.1:	Receiving End Cycloconverter Control.....	86
Figure 8.3.2:	Details of the Signal Conditioning Block .....	86
Figure 8.3.3:	Modulator for Phase A.....	87
Figure 8.4.1:	Equivalent Circuit of 20 Hz Transmission System.....	90
Figure 8.4.2:	Equivalent Circuit of 20 Hz Transmission System for Harmonic Analysis.....	90
Figure 8.4.3:	Harmonic Voltage Amplitudes Generated by the Cycloconverter at the 20 Hz Side .....	92
Figure 8.5.1:	Equivalent Circuit of 60 Hz Transmission System.....	93

## List of Figures (continued)

Figure 8.5.2:	Sending End Active Power vs. Max. Transmission Distance.....	94
Figure 8.5.3:	<i>LC</i> Filter Design.....	95
Figure 8.5.4:	Equivalent Impedance Magnitude Seen from the Receiving End .....	95
Figure 8.6.1:	Simulated Voltage and Current Waveforms .....	97
Figure 8.6.2:	Transient Waveforms.....	98
Figure 9.1.1:	Wind Farm Configuration: LFAC Wind Farm and LFAC Transmission .....	100
Figure 9.1.2:	Wind Farm Configuration: Series DC Wind Farm and LFAC Transmission .....	100
Figure 9.2.1:	(A) Three-Phase Y- $\Delta$ Isolation Transformer and (B) Single Phase Transformer.....	102
Figure 9.2.2:	Three-Phase, Six-Pulse Cycloconverter.....	106
Figure 9.2.3:	Electrical Valve.....	107
Figure 9.2.4:	Circulating Current Circuit Model.....	108
Figure 9.2.5:	Control Algorithm for the Cycloconverter .....	111
Figure 9.2.6:	Close Loop Control Algorithm for (a) Magnitude of Voltage and (b) Output Power.....	112
Figure 9.2.7:	Three-Phase PWM Converter .....	114
Figure 9.2.8:	Three-Phase PWM Converter .....	115
Figure 9.2.9:	Constant-Frequency Controller using Direct-Power Algorithm with Space-Vector Modulation .....	116
Figure 9.2.10:	Variable-Frequency Controller using Direct-Power Algorithm with Hysteresis Controllers.....	116
Figure 9.2.11:	Block Diagram of DPC Control Algorithm .....	118
Figure 9.2.12:	(A) SVM Diagram and (B) Mirror Image in SVM Diagram.....	120
Figure 9.3.1:	Wind Farm Configuration: LFAC Wind Farm and LFAC Transmission .....	122
Figure 9.3.2:	Three-Phase (a) Line-to-Line Voltages and (d) Currents at 60Hz AC Transmission Connected to the Cycloconverter; Three-Phase (c) Voltages and (b) Currents at LFAC Transmission Connected to the Cycloconverter; and (e) Real Power from Wind Farm and (f) RMS Voltage at the LFAC from 0.0 to 7.0 Seconds .....	123



## List of Figures (continued)

Figure 9.3.3:	Three-Phase (a) Line-to-Line Voltage and (d) Currents at 60Hz AC Transmission Connected to the Cycloconverter; Three-Phase (c) Voltages and (b) Currents at LFAC Transmission Connected to the Cycloconverter; and (e) Real Power from Wind Farm and (f) RMS Voltage at the LFAC from 2.8 to 3.4 Seconds.....	123
Figure 9.3.4:	Three-Phase (a) Line-to-Line Voltage and (d) Current at 60Hz AC Transmission Connected to the Cycloconverter; Three-Phase (c) Voltages and (b) Currents at LFAC Transmission Connected to the Cycloconverter; and (e) Real Power from Wind Farm and (f) RMS Voltage at the LFAC from 6.75 to 7.0 Seconds .....	124
Figure 9.3.5:	Single-Line Diagram of a Power Transient Test System.....	125
Figure 9.3.6:	(a) Three-Phase Line-to-Line Voltages and (b) Three-Phase Currents at 60Hz AC Transmission Connected to the Cycloconverter; Three-Phase (c) Voltages and (b) Currents at LFAC Transmission Connected to the Cycloconverter; and (e) Real Power from Wind Farm and (f) RMS Voltage at the LFAC from 0.0 to 8.0 Seconds.....	126
Figure 9.3.7:	(a) Three-Phase Line-to-Line Voltages and (b) Three-Phase Currents at 60Hz AC Transmission Connected to the Cycloconverter; and Three-Phase (c) Voltages and (b) Currents at LFAC Transmission Connected to the Cycloconverter during Steady State from 4.846 to 5.0 Seconds ..	126
Figure 9.3.8:	(a) Three-Phase Line-to-Line Voltages and (b) Three-Phase Currents at 60Hz AC Transmission Connected to the Cycloconverter; Three-Phase (c) Voltages and (b) Currents at LFAC Transmission Connected to the Cycloconverter during Steady State from 9.785 to 8.0 Seconds ..	127
Figure 9.3.9:	(a) Three-Phase Currents at 60Hz AC Transmission Connected to the Cycloconverter; and Three-Phase (b) Voltages and (c) Currents at LFAC Transmission Connected to the Cycloconverter during Steady State from 0.0 to 0.500 Seconds. ....	127
Figure 9.3.10:	(a) Three-Phase Currents at 60Hz AC Transmission Connected to the Cycloconverter; and Three-Phase (b) Voltages and (c) Currents at LFAC Transmission Connected to the Cycloconverter during Steady State from 4.867 to 5.423 Seconds .....	128
Figure 9.4.1:	(A) Line-to-Line Voltage between Phase A and Phase B; (B) Current at Phase A; (C) Phase Voltage and (D) Phase Current at Phase A .....	129
Figure 9.4.2:	Harmonic Spectrums: (A) Line-to-Line Voltage between Phase A and Phase B, (B) Current at Phase A, (C) Phase Voltage at Phase A, and (D) Phase Current at Phase A .....	129
Figure 9.4.3:	Harmonic Spectrums of the Phase Voltage at the LFAC Side .....	130

## **List of Figures (continued)**

Figure 9.4.4: Harmonic Spectrums of the Phase Voltage at the LFAC Side: (Blue) Full Circulating-Current Mode and (Red) 50% Circulating-Current Mode...	131
Figure 10.1.1: Wind Speed Probabilistic Distribution [27].....	134
Figure 10.1.2: A Typical Wind Turbine Output Considering Wind Speed Variation ...	134
Figure 10.2.1: Wind Farm Configuration 1 .....	136
Figure 10.2.2: A 30 WT Case Study Configuration for Configuration 1 .....	144
Figure 10.3.1: Wind Farm Configuration 2.....	147
Figure 10.4.1: Wind Farm Configuration 3.....	151
Figure 10.5.1: Wind Farm Configuration 4.....	155
Figure 10.6.1: Wind Farm Configuration 5.....	159
Figure 10.7.1: Wind Farm Configuration 6.....	162
Figure 10.8.1: Wind Farm Configuration 7 .....	166
Figure 10.9.1: Wind Farm Configuration 8.....	170

## List of Tables

Table 5.1.1:	Current Capability vs. Cable Size and Type .....	29
Table 5.9.1:	Summary of kV Level Selection Results of the 8 Configurations.....	58
Table 6.3.1:	Operating Voltages for Power Transfer Studies .....	69
Table 6.3.2:	Maximum Transmission Capability at the Operation Voltage 38kV .....	70
Table 6.3.3:	Maximum Transmission Capability at the Operation Voltage 76kV .....	71
Table 6.3.4:	Maximum Transmission Capability at the Operation Voltage 115kV .....	72
Table 7.1.1:	NERC PRC-024-1 Voltage-Ride-Through Requirement .....	73
Table 8.6.1:	LFAC System Simulation Parameters .....	96
Table 8.6.2:	Parameters of PI Controllers with Transfer Function $K(1 + 1\tau s)$ .....	97
Table 9.2.1:	Connectivity Pointer of Three Single-Phase Transformers .....	105
Table 9.4.1:	Numerical Values of Harmonic Contents of the Phase Voltage at LFAC .....	130
Table 9.4.2:	Numerical Values of Harmonic Contents of the Phase Voltage at LFAC Side in Both Full- and Fifty Percent-Circulating Current Modes.....	131
Table 10.2.1:	Components and their Quantities in Configuration 1 .....	137
Table 10.2.2:	States of the $i$ th Circuit and Power Transmitted in Configuration 1.....	138
Table 10.2.3:	States of the $m$ Parallel Circuits (Lines) .....	139
Table 10.2.4:	States of Entire Configuration and Probabilities .....	140
Table 10.2.5:	States and Corresponding Probabilities .....	141
Table 10.2.6:	Definition and Expression of Reliability indices .....	143
Table 10.2.7:	Case Study Output States and Probabilities.....	145
Table 10.2.8:	Summary of Reliability Indices for Alternate Configuration 1 .....	146
Table 10.3.1:	Summary of Reliability Indices for Alternate Configuration 2 .....	150
Table 10.4.1:	Summary of Reliability Indices for Alternate Configuration 3 .....	154
Table 10.5.1:	Summary of Reliability Indices for Alternate Configuration 4 .....	159
Table 10.6.1:	Summary of Reliability Indices for Alternate Configuration 5 .....	161
Table 10.7.1:	Summary of Reliability Indices for Alternate Configuration 6 .....	165
Table 10.8.1:	Summary of Reliability Indices for Alternate Configuration 7 .....	170
Table 10.9.1:	Summary of Reliability Indices for Alternate Configuration 8 .....	174
Table 10.10.1:	Summary of Reliability Indices for the 8 Alternate Configurations.....	174

# 1 Project Description

The project's goal is to evaluate alternative transmission systems from remote wind farms to the main grid using low-frequency AC technology. Low frequency means a frequency lower than nominal frequency (60/50Hz). To minimize costs cyclo-converter technology will be utilized resulting in systems of 20/16.66 Hz (for 60/50Hz systems respectively). The technical and economic performance of low-frequency AC transmission technology will be compared to HVDC transmission (including HVDC Light) and conventional AC transmission. Electric power generation from wind is increasing at a fast rate. Plans to install hundreds of GW of wind turbine generation in the next few years are in place in the US, Europe, and China. Typically, geographic sites that are suitable for wind farm development are in remote land locations or offshore locations, far from the main transmission grid and major load centers. For instance, this is the case in the US, with abundant wind potential in the scarcely populated Midwestern states, as well as for offshore sites that could be located tens of miles from the coast. In these cases, the transmission of wind power to the main grid is a major expenditure that adversely affects the economics of these systems. The most economical approach depends on distance and electric power (capacity) to be transmitted. Presently well-established technologies are AC transmission or HVDC transmission (including HVDC Light). HVDC technology is mature and offers significant advantages for long-distance point-to-point transmission, as generally required by wind farm applications. However, one main disadvantage attributed to HVDC is increased cost due to the complexity of the power electronics converters at the two ends of the lines. HVDC Light technology tries to limit the cost but it is still higher than AC technology. As a lower-cost alternative to HVDC or AC transmission, we propose transmission by a low-frequency AC system, using thyristor-based AC/DC and AC/AC converters. The proposed system is expected to have costs substantial lower than HVDC – the cost savings will come from the fact that we propose to use cyclo-converters which are much lower in cost than the typical six-pulse converters for HVDC. The disadvantage of using cyclo-converters is that the frequency reduction is fixed – the most practical system is 20 Hz. Other savings can come from optimizing the topology of the wind farms. Another advantage of the proposed topologies is that existing transformers designed for 60 Hz can be used for the proposed topologies (for example a 345kV/69 kV, 60Hz transformer can be used for a 115 kV/23kV, 20 Hz system). We propose to use alternative topologies that will provide additional cost savings (operational and investment cost) by minimizing the power electronic transformations. The proposed configurations might indeed provide similar advantages to HVDC at reduced cost and high reliability, therefore improving the financial viability of remote wind power plants. The goal of this project is to perform a comprehensive evaluation of the technical performance and economics of low-frequency AC transmission, in comparison to HVDC and power-frequency AC transmission. It is expected that a comprehensive evaluation may allow the industry to make better-informed decisions for the type of transmission for large wind farm projects in remote inland or offshore sites. It is also expected that the proposed topologies will enable a more comprehensive evaluation of storage at the wind

farm site, and will shape our thinking of the merits of storage in connection to wind energy.

The major potential benefit from this technology will be a significant cost reduction of the transmission system for remote or offshore wind farms (compared to the alternatives of HVDC transmission or power-frequency AC transmission). This could make the economics of wind energy more favorable, and aid our nation's goal of 20% wind penetration by 2030, by allowing utilities to tap into rich wind potential of remote onshore or offshore areas. The proposed topologies have numerous operational benefits as well, such as high reliability, capability of voltage and reactive power support, energy storage, and enhanced dispatchability of the wind resource. The expected outcomes of the project are: (a) a comprehensive methodology for determining the optimal topology, kV levels, etc. of a low-frequency AC transmission system for wind farms and a given distance of the wind farms from major power grid substations, (b) a monitoring and control system for the proposed technologies that will allow enhanced dispatchability of the wind resource and ability to provide ancillary services such as voltage and reactive power support, and (c) a comprehensive methodology to evaluate the reliability of the proposed topologies and the expected capacity credit of wind farms to the power grid.

This project will result in high-fidelity simulation models to analyze all different aspects of the proposed low-frequency AC transmission technology for wind power plants. PSERC industrial members could use these models to study the feasibility of such configurations in their systems.

## 2 Technical Approach

The desirability of providing at least part of the required electric power from renewable sources has made wind energy the leading renewable energy source because of the favorable economics as compared to other renewables. Still there are few problems that make wind energy economics higher than other forms of electric power generation. Two main issues are: (a) the cost for transmission of wind power from remote sites where large wind farms can be developed, and (b) the unpredictability of the wind that results in low capacity credits for the operation of the integrated power system. We propose to investigate alternative topologies and transmission systems operating at low frequency for the purpose of decreasing the cost of transmission and making the wind farm a more reliable power source so that the capacity credit can increase. The general approach for defining these topologies is illustrated in Figure 2.1 which illustrates one alternative configuration. Note that we envision that the configuration will include sections of DC transmission as well as AC transmission and LF AC transmission, within and outside the wind farm. This will enable to directly rectify the output of wind generators via a standard transformer to DC of appropriate kV level. The system can be optimized depending on the area covered by the wind farm. Storage can be provided at the DC bus. While the proposed use of storage is not unique to the proposed low frequency transmission, the proposed topology facilitates a more efficient and centralized utilization of storage. An inverter can transform DC to AC of low frequency, preferably of 1/3 of the normal power frequency. This low-frequency AC can be transformed to higher voltages for transmission at higher kV levels. Standard transformers can be used as long as the V/Hz operating value remains the same; for example, a 13.8kV/230kV 60 Hz transformer can be used for 4.6kV/76.6kV 20 Hz operation. The low-frequency AC network will be connected to the power grid at major substations via cyclo-converters that provide a low-cost interconnection and synchronization with the main grid. The cost reduction enabled with cyclo-converters is substantial as compared with HVDC options with the limitation that the frequency reduction is fixed at 20 Hz. Transmission line design procedures developed for 60 Hz systems can be equally applied to transmission lines operating at 20 Hz. Overall, 20 Hz transmission systems can be constructed with existing components and technology. The proposed topologies will enable (a) optimization of the overall transmission network for wind energy with substantial economic benefits, (b) a more reliable operation because the number of conversion will be smaller (only one conversion process per wind farm versus per wind turbine today), (c) a more dispatchable operation of the wind farms since all wind turbines deposit their output to one DC bus (the net output of many wind turbines is smoother than the output of a single wind turbine) plus the storage on the DC bus will enable the overall wind farm to better respond to dispatchers' controls, and (d) the presence of the inverter and cyclo-converter will allow the wind farm to provide ancillary services and in particular voltage and reactive power control. The above-described basic approach can produce a number of alternative topologies for specific geographical arrangements. In addition, it will allow the more economical development of other forms of storage systems, such as hydro or pumped hydro that may be located in remote areas.

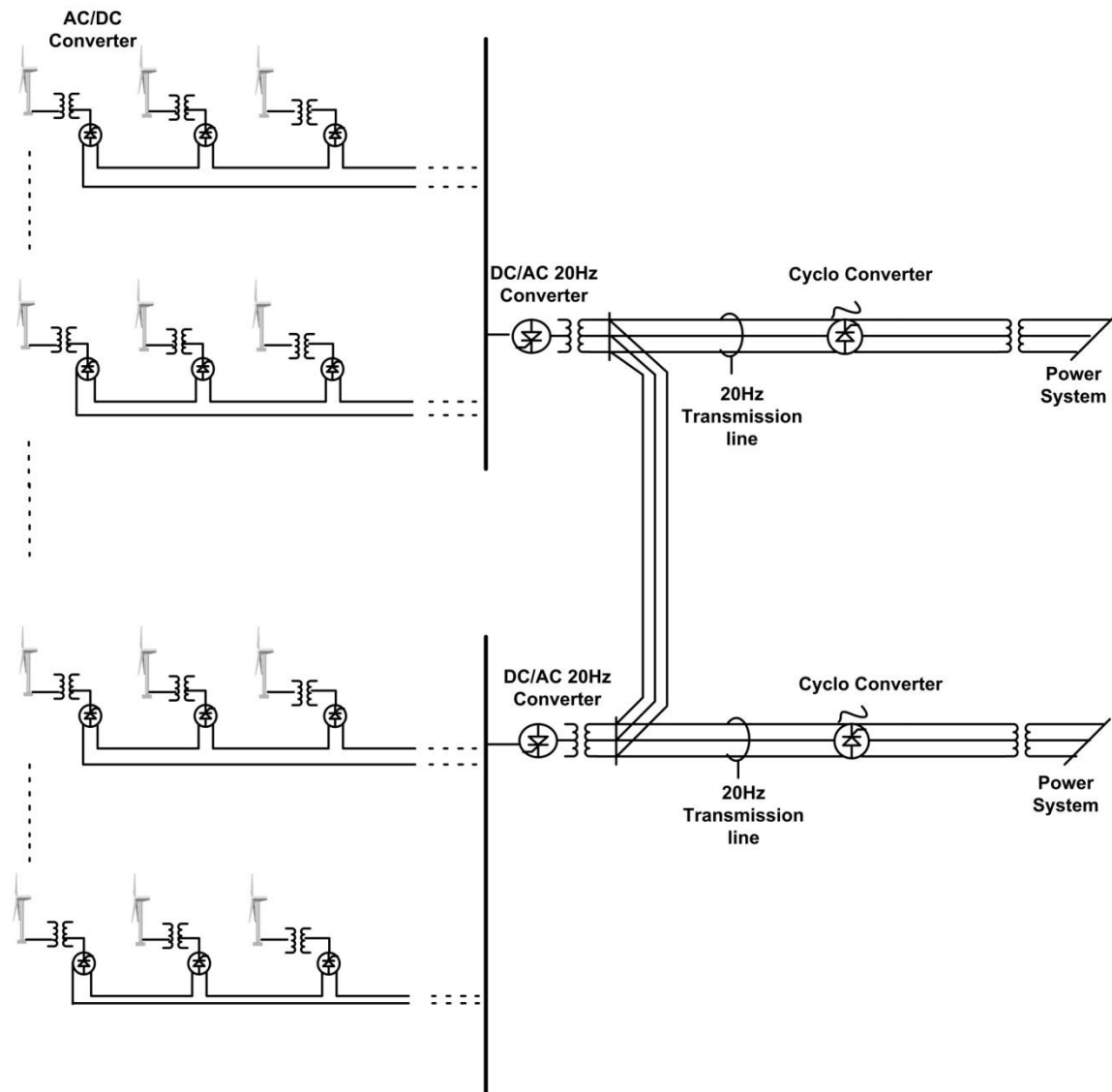


Figure 2.1: Typical Interconnection and Topology of Wind Farms and Collector Substations

Since there are competing technologies for transmission and storage, the proposed project will be focusing on a comprehensive comparative evaluation of three competing technologies: (a) AC transmission at power frequency (60 Hz or 50 Hz), (b) HVDC transmission, including HVDC Light, and (c) the proposed low-frequency (20 Hz) transmission topologies. The criteria for the comparative evaluation will be: (1) overall cost—investment and operational cost, (2) voltage regulation/ reactive power control, (3) fault currents, protection schemes and overall reliability, (4) dispatchability with and without storage, (5) stability and transfer capability, (6) ability to provide ancillary services to the main power grid, and (7) scalability. To minimize the system cost, commercial off-the-shelf transformers designed for 60 Hz operation can be used in the 20

Hz transmission system. Simply, in order to maintain rated magnetic flux in their iron cores, their nominal voltage ratings need to be scaled down by a factor of 3. For instance, a 60 Hz 13.8kV/230kV transformer is de-rated to operate at 4.6kV/76.6kV at 20 Hz. In addition, hysteresis and eddy current losses in the core are also significantly reduced, thus increasing transmission efficiency. In particular, the use of the medium-voltage (a few kVs) DC bus has the following advantages: (a) It allows for the easy interconnection of a large battery energy storage system (BESS), which could be used to enable a more predictable and dispatchable power output from the wind farm. The size of the BESS will be a function of the stochastic nature of wind at the wind farm site, and of the power system operators' requirements for the plant's maximum ramp down/up rates. The battery technology (*i.e.*, chemistry) also will have an impact on cost and efficiency.

(b) The AC/DC converters that connect each wind turbine to the DC bus represent some very interesting control possibilities. Essentially, they may be considered as power electronics drives, similar in principle to industrial motor drives, which decouple the turbines' terminal voltage magnitude and frequency from the nominal system values. This forces us to re-think the design of wind turbine control schemes (designed to allow variable-speed operation and maximum power point tracking). For all turbine generator types (*i.e.*, induction machines, wound-rotor and doubly-fed induction machines, or synchronous machines), these converters can be controlled in such a way as to provide maximum efficiency and energy capture from the wind. For instance, the converter's AC voltage and frequency could be varied (in some constant V/f fashion) to control the turbine's speed and/or minimize iron core losses in the transformer and generator, thereby potentially eliminating the need for more advanced and expensive power electronics that are found in DFIG and SG turbines (such as converters with AC-DC-AC topologies). (c) The overall topology can be optimized independently from any other systems, for example the DC-bus kV level can be optimally selected to minimize the losses within the area of the wind farm. The size, design and controls of the low-frequency inverter can be also optimized to enable efficient conversion, coordination with storage, and ancillary services.

The comprehensive evaluation was performed as follows. First, test systems and specific topologies were developed in collaboration with the industry advisors. The derived test systems are described in Section 4. A total of eight different alternative configurations were developed that include the alternative technologies, *i.e.* AC transmission, LFAC transmission, DC transmission, DC wind farm distribution, AC wind farm distribution, and series or parallel connection of wind turbine systems. For each one of the alternative configurations a number of scenarios was developed. These scenarios include (a) stochastic processes that define the time model of wind speeds at the various points of the wind turbine systems, (b) stochastic processes that define the time model of marginal power prices and demand for electric power at the interfacing substations to the main grid (these processes will represent the overall operation of the power grid). The time scale for simulation of these systems has been selected to be one year. For each one of the alternative configurations and the scenarios of wind speeds and operations of the main power grid, the following studies have been performed:



- A.** Operational analysis of the entire system on 15 minute intervals. The operational analysis has been characterized with the following metrics: (1) voltage profile index; (2) total transmission losses from wind turbines to the interconnecting substations to the main power grid; (3) dispatchability index in terms of how many MW can be dispatched if needed for the specific operating conditions and wind speeds; (4) transfer capability index in terms of MW that can be transferred over and above the operating conditions before violating constraints; (5) required BESS size and cost.
- B.** Transient stability analysis, using average-value models of the converters' operation. This analysis has been used: (1) to design the outer-loop high-level controls used to interface the wind farm(s) with the power system, with particular emphasis on the control infrastructure requirements, and the ability to provide inertial frequency control and other ancillary services; (2) to study the stability of the power system under contingencies; (3) to determine the transient discharge/charge rates of the storage scheme and optimize its operation, and (4) to study the ability of the system to provide voltage ancillary services to the power grid under various conditions including shortcoming of reactive power in the grid, delayed voltage recovery in the grid, and oscillatory voltage fluctuations.
- C.** Detailed EMTP-type simulation including switching events to analyze phenomena with shorter time constants. This type of analysis has been used: (1) to design the inner-loop controls at the power electronic converters; (2) to predict fault currents under symmetric and asymmetric faults at the AC side, as well as short-circuits at the DC bus (the most severe case); (3) to design the protective relaying system; (4) to study the impact of harmonics on the system performance and cost. The thyristor-based converters introduce low-frequency harmonics (compared to IGBT-based converters that switch at much higher frequencies), and thus can significantly degrade the system's power quality; (5) to evaluate the harmonic losses and power quality, and investigate the need for inclusion of harmonic filters; (6) to study in detail the effects of communication delays between the two ends of the transmission line (*i.e.*, how they impact the protection system).

### 3 Literature Survey

The possible solutions for wind farm transmission are HVAC, Line commutated HVDC and voltage source based HVDC (VSC-HVDC). The various wind farm designs have been studied in the past with these technologies. In this study the low frequency AC transmission technology is proposed for various designs of the wind farms.

The author in [1] presents an algorithm to derive a probabilistic wind turbine generator model to determine the annual energy output of a wind farm connected to the grid. The model focuses on generation and transmission system reliability and wind speed variation is only considered as an occurrence probability. Thus the wind speed variation effect is weakened in the evaluation. In the present study the total cost of the energy production including the infrastructure and maintenance cost is evaluated. It is expected that the cost of transmission and generation remains more or less the same compared to the previous methods of transmission.

In reference [2] Thomas et al., proposed that a series connection of the wind farm leads to the elimination of the offshore platform and the turbines output would be DC voltage. As a result the desired transmission voltage can be obtained directly without a large centralized DC/DC converter. Various wind farm designs with low frequency and nominal frequency transmission are proposed in the study.

S. Lundberg in reference [7] proposed a control strategy for the series connected wind turbines showing that the wind farm was able to operate successfully even though there were large variations in the individual turbine powers. A key result of the study is that a wind farm layout utilizing series connected wind turbines with a DC voltage output has a very promising energy production cost, if the transmission distance is above 20 km. The current study is concentrating on onshore as well as offshore power transmission involving variable distances.

Cost of energy production of a wind turbine is an important element in this study. There are many factors contributing to the cost and productivity of the wind farm. For low frequency transmission the transmission cable as well as the related expenditure would be same as for the nominal frequency transmission. In order for the wind farms to be economically reasonable it is important to keep the energy production cost down. This can be done by having a site with high average wind speed, a wind park layout that fits the site and to keep the number of operation hours high. The energy production of various wind parks is calculated in [17, 18, 19].

The estimated cost of the produced electric energy is presented in the references [20, 17, 21, 19, 23]. In [22], R. Barthelmie and S. Pryor presented the economics of some offshore wind farms that are built and are planned to be built. The investment and operational cost of the wind farm are investigated in this study. From this it can be said that the cost of the cable can be determined by the number of cables, the transmission voltage and the transmitted power by each cable.

In [24] the cost of cable per kilometer depending on the transmission voltage for the off-shore wind farms is given. In this evaluation for cases with more than one line needing to connect to onshore the author considered that all the submarine cables are installed together. Different studies about the cost of energy based on the investments made and the produced energy are carried out. These analyses are centered on the comparison between AC and DC transmission. Particularly the analysis in [26] is based on very high powers 400 – 100MW. As different transmission options are not considered in detail in these studies the present study tries to complete the analysis.

## **4 Alternative Topologies for Low-Frequency Transmission**

The literature survey indicates that many topologies and systems have been proposed for transmitting power from wind farms to the main power grid. We have also proposed variations of topologies that it is believed to have additional advantages. In this section we present a number of topologies and systems that are further evaluated of their advantages or shortcomings.

A wind farm is a group of a number of wind turbines located in the same geographical area and interconnected. Individual wind turbines are interconnected with a medium voltage power collection system. In order to connect the local wind turbine grid to the transmission system the voltage is increased. Wind farm has the following elements: wind turbines, local wind turbine grid, collecting point, transmission system, wind farm interface to the point of common connection (PCC). The power from the wind turbine units is collected at the collecting point where the voltage is increased to a level suitable for transmission. The power is then transmitted to the wind farm grid interface over the transmission system. The following are the different wind farm topologies.

### **4.1 Wind System Configuration 1: AC Wind Farm, Nominal Frequency, Network Connection**

Wind farms that have been built today have an AC electrical system from the wind turbines to the PCC. Two different types of AC wind farms referred in the study are radial and network connections. The idea with the radial wind farm is that it should be suitable for small wind farms with a short transmission distance. In the small AC wind farm, the local wind farm grid is used both for connecting all wind turbines in a radial fashion together and to transmit the generated power to the wind farm grid interface. The other type of wind farm is the network connection. Large AC wind farms generally have network connection of wind farms. In this type of configuration the local wind farm grid has a lower voltage level than the transmission system. This system requires an offshore platform for the transformer and switch gear. Horns Rev Wind Farm is built according to this principle.

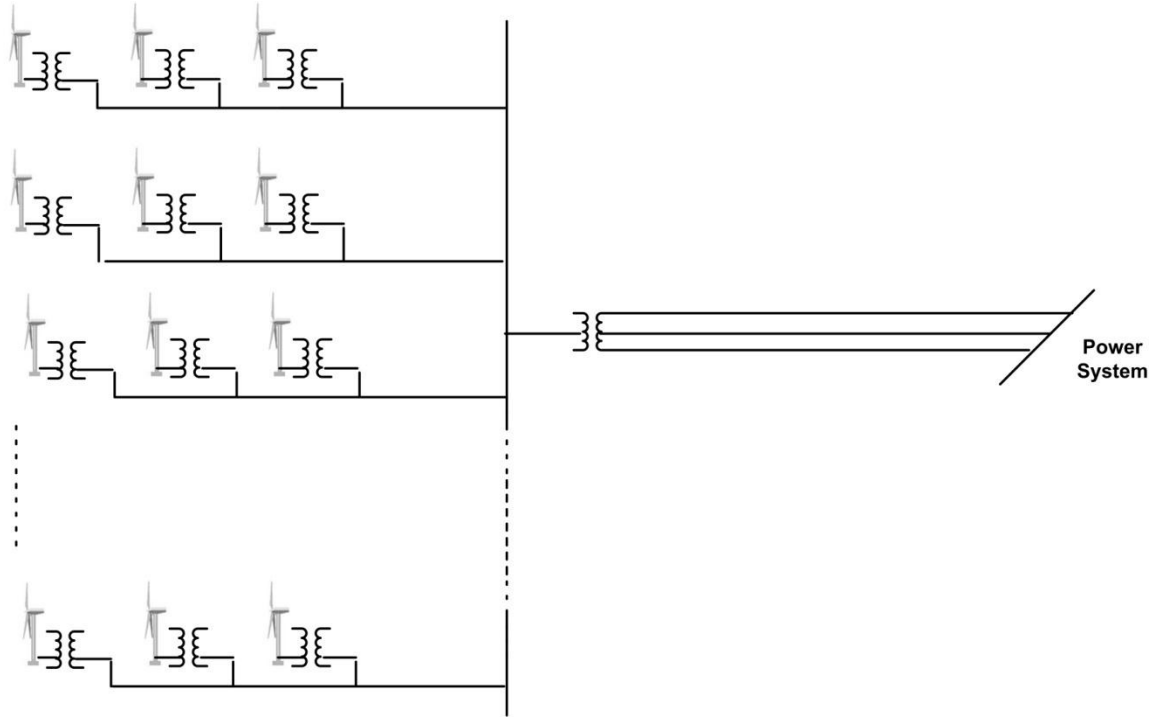


Figure 4.1.1: Wind System Configuration 1: AC Wind Farm, Nominal Frequency, Network Connection

The wind system configuration shown in Figure 4.1.1 has an AC wind farm. The wind turbines are connected in network fashion and nominal frequency transmission is adopted. For the purpose of the study a network of 10 radial feeders is considered with 5 wind turbines in each feeder. Selection of the optimal voltage levels is described in Section 5.

This configuration is described with the following parameters:

- N: Number of radial feeders
- $N_i$ : Number of wind turbines in feeder  $i$
- $d$ : Spacing between the wind turbines
- $P_t$ : Rating of the wind turbine
- $R$ : Resistance of the cable
- kVdc: DC voltage level

In this configuration the wind turbines are interconnected with medium voltage.  $N$ , the number of radial feeders and  $N_i$ , the number of wind turbines in the feeder  $i$  are decided based on the total electrical output required from the wind farm. Wind turbines with rating ( $P_t$ ) 1MW, 1.75MW, 2.25MW or 3.6MW are considered in the study. Spacing between the turbines  $d$ , is fixed based on the size of the wind turbine. As per requirements the cable is chosen based on its resistance.

## 4.2 Wind System Configuration 2: AC Wind Farm, AC/DC Transmission, Network Connection

In this system, the AC transmission is replaced with a DC transmission. This wind farm will be referred to as the AC/DC wind farm. This type of system does not exist today, but is frequently proposed when the distance to the PCC is long or if the AC grid that the wind farm is connected to is weak. The system is shown in Figure 4.2.1. In this system we have an independent local AC system in which both the voltage and the frequency are fully controllable with the offshore converter station. This can be utilized for a collective variable speed system of all wind turbines in the farm. The benefits with this are that the aerodynamic and electrical efficiency can be increased.

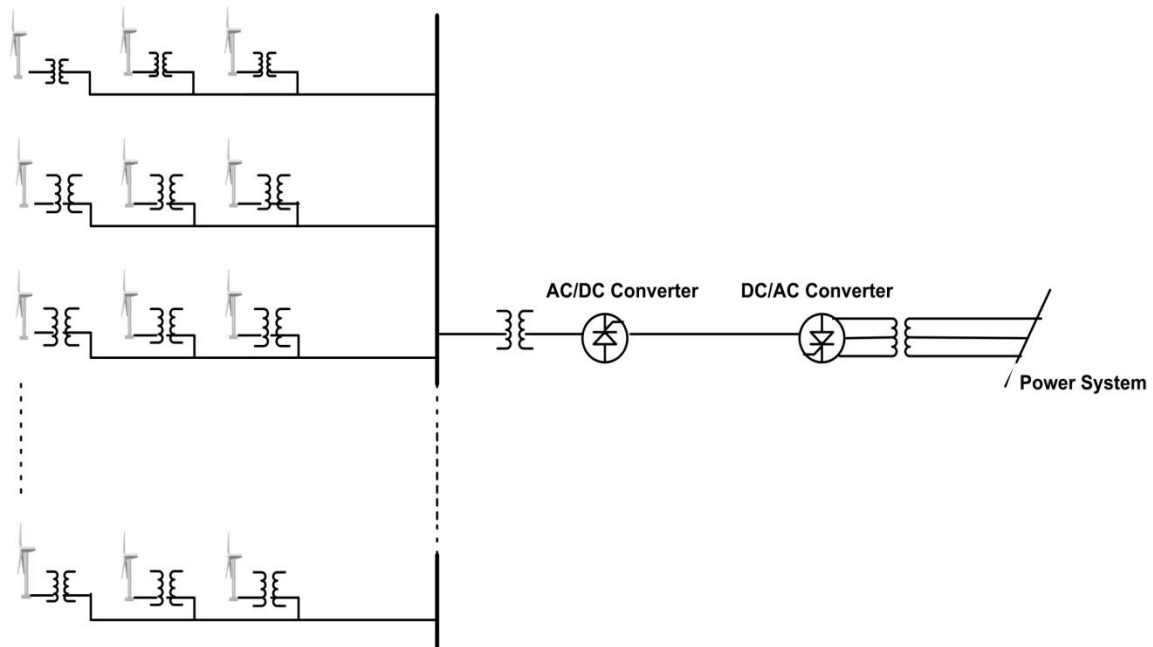


Figure 4.2.1: Wind System Configuration 2: AC Wind Farm, AC/DC Transmission, Network Connection

The wind system configuration shown in figure has a AC wind farm. The wind turbines in the farm are connected in network fashion and DC transmission is adopted. Selection of optimal voltage levels is described in Section 5.

This configuration is described with the following parameters:

- N: Number of radial feeders
- $N_i$ : Number of wind turbines in feeder  $i$
- $d$ : Spacing between the wind turbines
- $P_t$ : Rating of the wind turbine

R: Resistance of the cable

kVdc: DC voltage level.

The AC wind farm configuration is similar to the wind system configuration 1 except for the transmission part. The AC transmission is replaced by the DC transmission here.

#### 4.3 Wind System Configuration 3: Series DC Wind Farm, Nominal Frequency, Network Connection

The layout of the DC wind farm somewhat differs from the AC wind farm. The difference is in the number transformation steps it requires to increase the DC voltage at the local wind turbine grid to the level suitable for transmission. The number of transformations depends on the DC voltage level in the local wind turbine grid. If the voltage level is high *i.e.* 20-40kV DC then only one transformation step is required. But if the output voltage of the wind turbine is lower *i.e.* 5kV, two steps are required. All wind turbines within one cluster are connected one by one to the first transformation step. If only one step is used, the wind turbines are connected in radials directly to the second DC transformer step, similarly as for the AC wind farm.

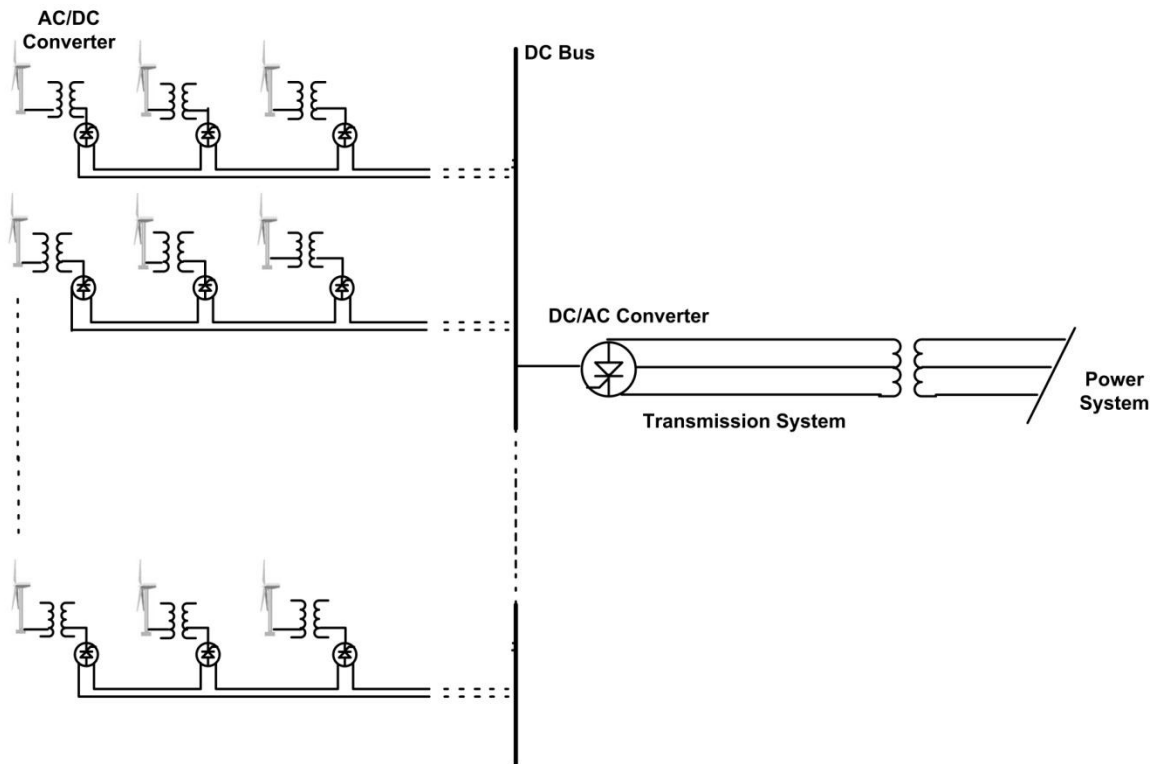


Figure 4.3.1: Wind System Configuration 3: Series DC Wind Farm, Nominal Frequency, Network Connection

The wind system configuration shown in figure has a DC wind farm. The wind turbines are connected in network fashion and nominal frequency transmission is adopted. Selection of the optimal voltage levels is described in Section 5.

This configuration is described with the following parameters:

- N: Number of radial feeders
- N<sub>i</sub>: Number of wind turbines in feeder i
- d: Spacing between the wind turbines
- P<sub>t</sub>: Rating of the wind turbine
- R: Resistance of the cable
- kV<sub>dc</sub>: DC voltage level

The local wind farm is a DC wind farm and the wind turbines are connected in series. N, the number of radial feeders and N<sub>i</sub>, the number of wind turbines in the feeder i is decided based on the total electrical output required from the wind farm. Wind turbines with rating (P<sub>t</sub>) 1MW, 1.75MW, 2.25MW or 3.6MW are considered in the study. Spacing between the turbines d, is fixed based on the size of the wind turbine. As per requirements the cable is chosen based on its resistance.

#### **4.4 Wind System Configuration 4: Parallel Dc Wind Farm, Nominal Frequency, Network Connection**

The configuration differs from the wind system configuration 4 only in the local wind farm. Here the wind turbines are connected in parallel. The wind system configuration shown in figure 4.4.1 has a DC wind farm. The wind turbines are connected in network fashion and nominal frequency transmission is adopted. Selection of the optimal voltage levels is described in Section 5.



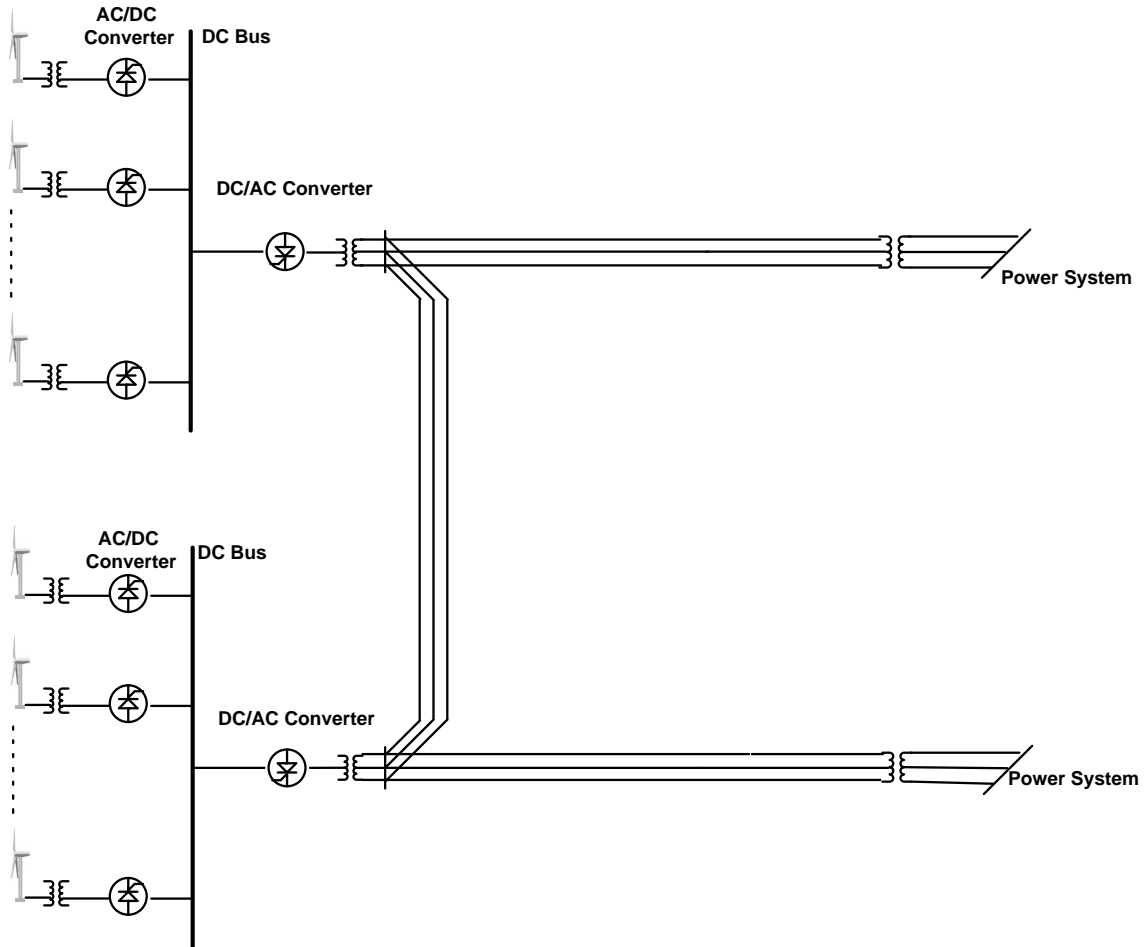


Figure 4.4.1: Wind System Configuration 4: Parallel DC Wind Farm, Nominal Frequency, Network Connection

This configuration is described with the following parameters:

- N: Number of radial feeders
- $N_i$ : Number of wind turbines in feeder  $i$
- $d$ : Spacing between the wind turbines
- $P_t$ : Rating of the wind turbine
- $R$ : Resistance of the cable
- $kV_{dc}$ : DC voltage level

The local wind farm is a DC wind farm and the wind turbines are connected in parallel.  $N$ , the number of radial feeders and  $N_i$ , the number of wind turbines in the feeder  $i$  is decided based on the total electrical output required from the wind farm. Wind turbines with rating ( $P_t$ ) 1MW, 1.75MW, 2.25MW or 3.6MW are considered in the study. Spacing

between the turbines  $d$ , is fixed based on the size of the wind turbine. As per requirements the cable is chosen based on its resistance.

#### 4.5 Wind System Configuration 5: Series DC Wind Farm, Low Frequency Radial AC Transmission

The proposed Low frequency AC transmission configuration would significantly reduce the transmission system loss for remote or offshore wind farms. This makes the economics of wind energy more favorable and increase the wind resources penetration easy. Existing transmission line design, breakers and protection can be used and cycloconverters offer an inexpensive conversion technology for conversion of frequency from 60/50 Hz to 20/16.67Hz.

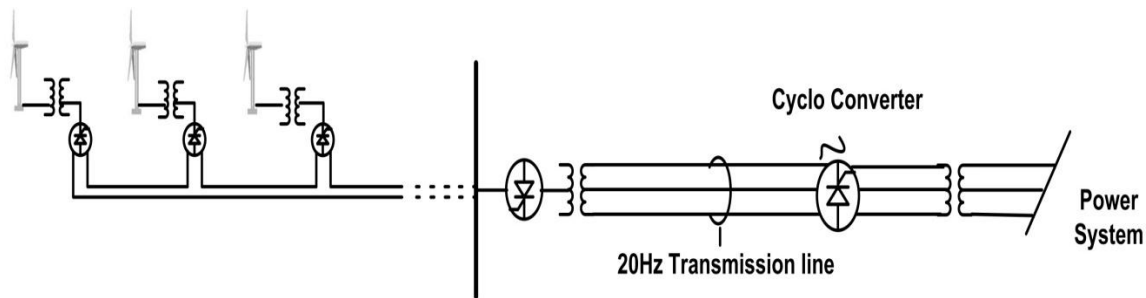


Figure 4.5.1: Wind System Configuration 5: Series DC Wind Farm, Low Frequency Radial AC Transmission

Wind system configuration shown in the figure has a DC wind farm. The wind turbines are connected in series, radial fashion and low frequency transmission is adopted. Selection of the optimal voltage levels is described in Section 5.

This configuration is described with the following parameters:

- N: Number of radial feeders
- $N_i$ : Number of wind turbines in feeder  $i$
- $d$ : Spacing between the wind turbines
- $P_t$ : Rating of the wind turbine
- R: Resistance of the cable
- kVdc: DC voltage level

The wind turbines in the local wind farm are connected in series. It has low frequency transmission (20Hz/16.66Hz). The number of radial feeders is one. The total number of wind turbines in the wind farm is decided depending upon the requirements of the electrical output. The losses of the system are also to be taken into consideration while designing the system.

#### 4.6 Wind System Configuration 6: Parallel DC Wind Farm, Low Frequency, Radial Transmission

The proposed system adopts low frequency of 20/16.67Hz. The wind system configuration shown in figure has a DC wind farm. The wind turbines are connected in parallel, radial fashion and low frequency transmission is adopted. Selection of the optimal voltage levels is described in Section 5.

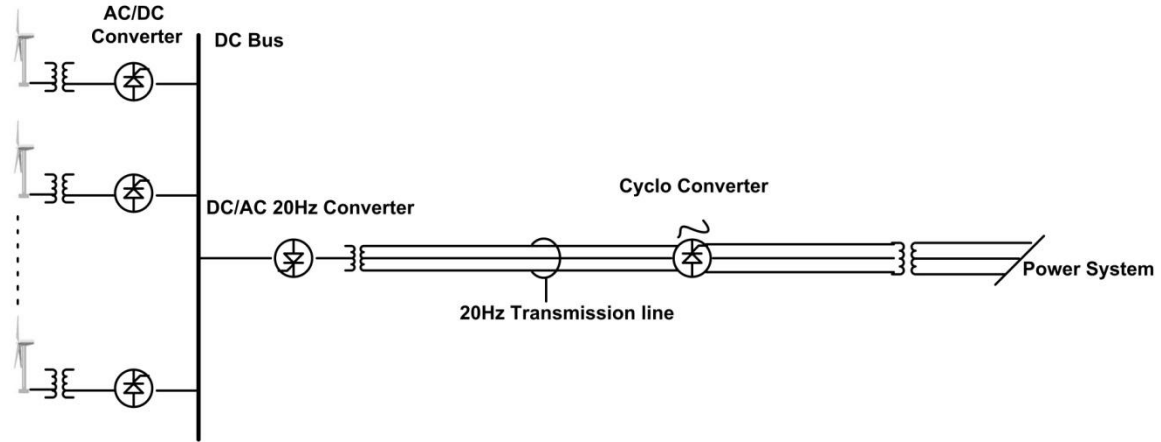


Figure 4.6.1: Wind System Configuration 6: Parallel DC Wind Farm, Low Frequency, Radial Transmission

This configuration is described with the following parameters:

- N: Number of radial feeders
- $N_i$ : Number of wind turbines in feeder  $i$
- $d$ : Spacing between the wind turbines
- $P_t$ : Rating of the wind turbine
- $R$ : Resistance of the cable
- $kV_{dc}$ : DC voltage level

#### 4.7 Wind System Configuration 7: Series DC Wind Farm, Low Frequency AC Transmission Network

The wind system configuration shown in figure has a DC wind farm. The wind turbines are connected in series, network fashion and low frequency transmission is adopted. Selection of the optimal voltage levels is described in Section 5.

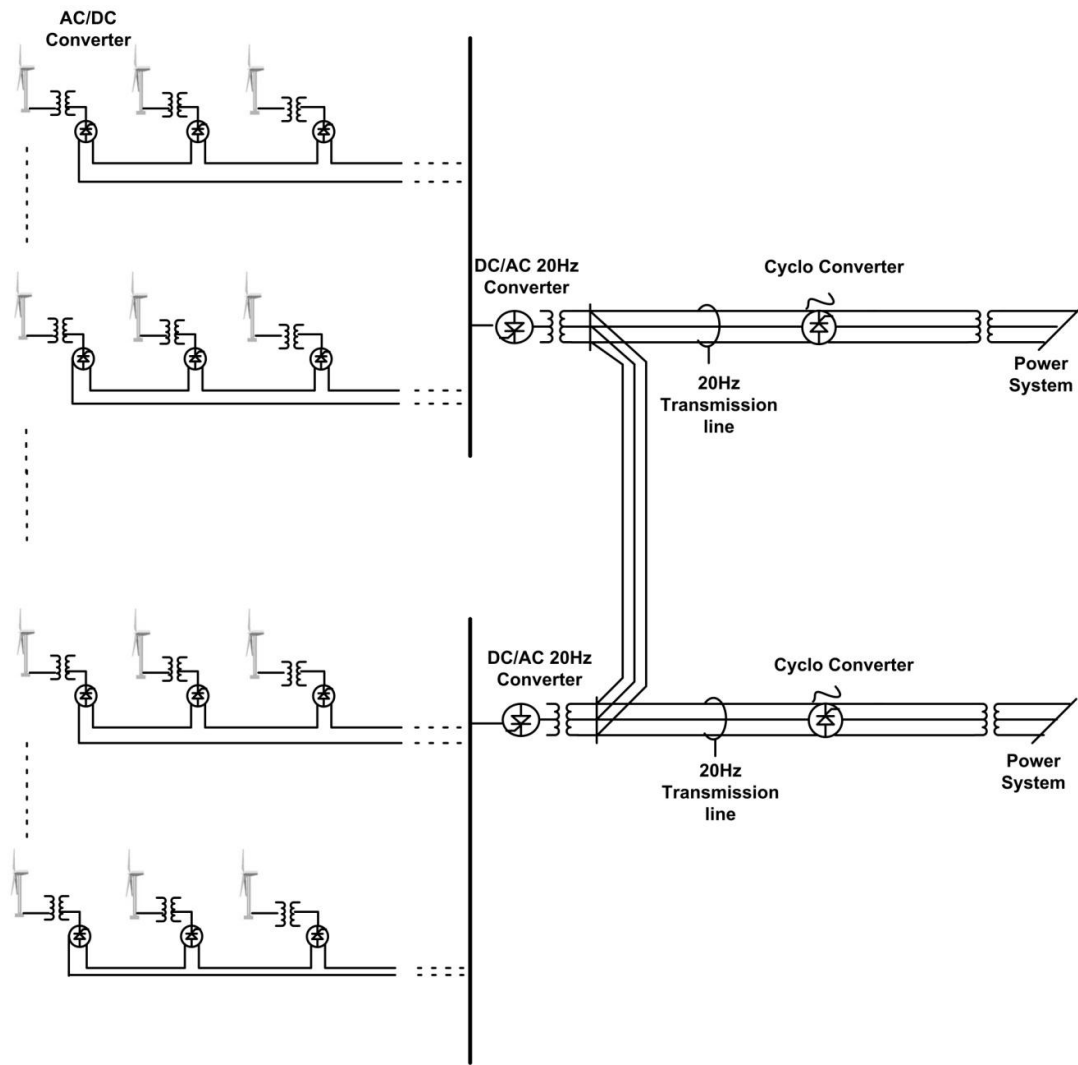


Figure 4.7.1: Wind System Configuration 7: Series DC Wind Farm, Low Frequency AC Transmission Network

This configuration is described with the following parameters:

- N: Number of radial feeders
- $N_i$ : Number of wind turbines in feeder  $i$
- $d$ : Spacing between the wind turbines
- $P_t$ : Rating of the wind turbine
- $R$ : Resistance of the cable
- $kV_{dc}$ : DC voltage level

#### 4.8 Wind System Configuration 8: Parallel DC Wind Farm, Low Frequency AC Transmission Network

The wind system configuration shown in figure has a DC wind farm. The wind turbines are connected in parallel, network fashion and low frequency transmission is adopted. Selection of the optimal voltage levels is described in Section 5.

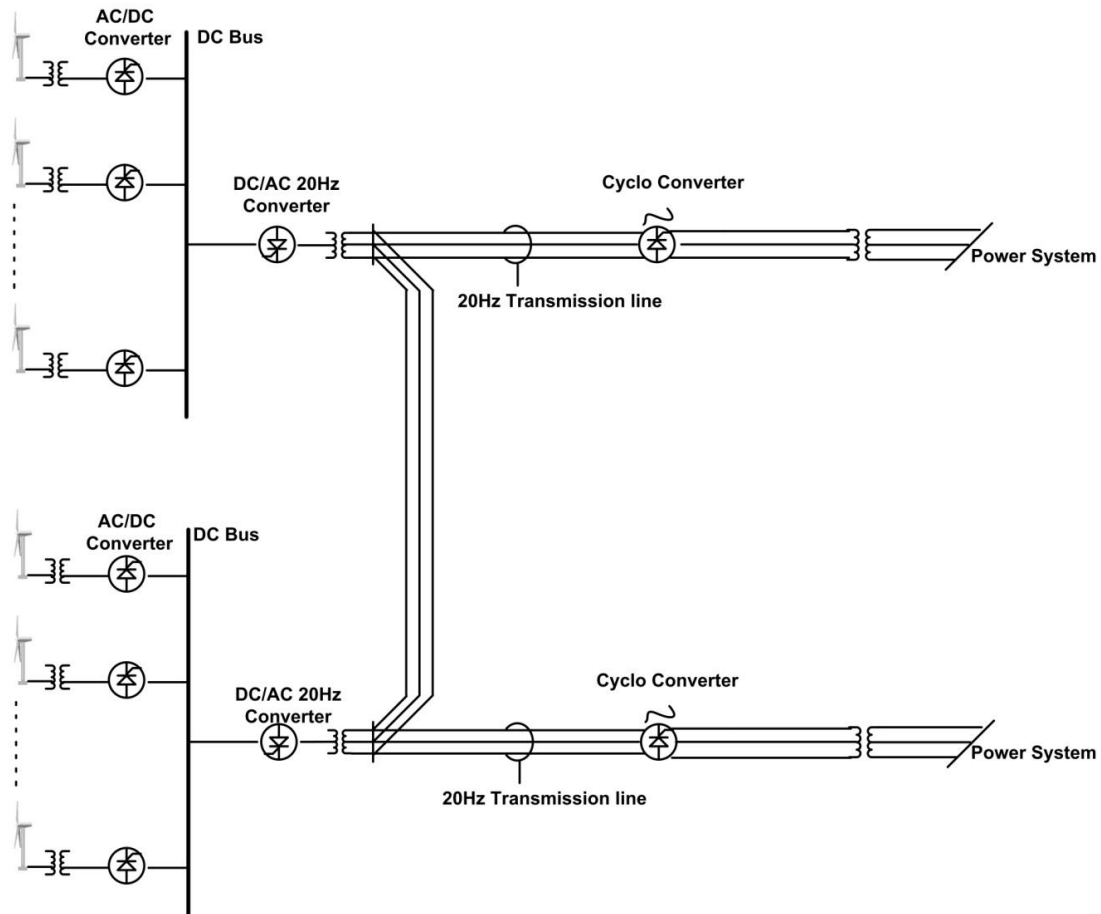


Figure 4.8.1: Wind System Configuration 8: Parallel DC Wind Farm, Low Frequency AC Transmission Network

This configuration is described with the following parameters:

- N: Number of radial feeders
- $N_i$ : Number of wind turbines in feeder  $i$
- $d$ : Spacing between the wind turbines
- $P_t$ : Rating of the wind turbine
- $R$ : Resistance of the cable
- $kV_{dc}$ : DC voltage level

## **5 Optimal kV Level, Equipment Ratings and Cost Analysis of Alternate Configurations**

In this section, the optimal kV level and the equipment ratings for each alternate configuration listed in Section 4 are discussed and analyzed. The optimal kV level for transmission is selected on the basis of the minimum total cost consisting of operating costs, maintenance costs and acquisition costs. In the analysis presented in this section we consider mainly the transmission power loss cost and the acquisition cost. Maintenance costs can be added but in general their influence in determining optimal kV levels is small. Since the selection of optimal kV levels is dependent on total cost, this section presents formulae for cost accounting for each wind farm configuration. Subsection 5.1 provides the general formulation of the methods used in the optimal kV level and equipment ratings selection analysis, and cost analysis methods, using Configuration 1 as the example. Subsequent subsections provide optimal kV level analysis, equipment ratings, operational cost and acquisition cost analysis for each configurations listed in Section 4. A 30 wind turbine case study is made for each configuration, and the results of optimal kV level and minimum total cost are compared.

### **5.1 Approach Description**

The determination of the optimal kV level is based on minimizing the total cost of the wind farm. The total cost consists of mainly three components: (a) operating costs - mainly losses, (b) maintenance cost, and (c) acquisition costs. The basic approach in determining the optimal kV levels for a wind farm is to develop expressions for the total cost of wind farms and then find the value of kV level that will minimize the total cost. This process can be applied to any wind farm configuration. In general distances between wind turbine systems will vary, cable sizes will vary, etc., in which case the analysis for specific wind farms must be done numerically by necessity. Since this report is not focused on any specific site, some simplifying assumptions will be imposed, such as distance between any two wind turbine systems will be fixed, cable size will be determined by the rating of the wind turbine systems, etc. These assumptions enable the development of simplified models for the cost and provide a compact determination of optimal kV levels. It should be understood that the methodology presented here can be directly applied to specific sites with specific configuration and equipment rating selections.

In subsequent paragraphs expressions for the total costs are developed. In this subsection we present the basic approach for developing these expressions using Configuration 1 as an example. In subsequent subsections, the approach is applied to each of the other alternate configurations of the wind farms defined in section 4.

### 5.1.1 Formulation of Operating Cost

Configuration 1 in Section 4 is used as an example to explain the derivation of formulas for the operating cost, mainly transmission loss in the wind farm. Configuration 1 is shown in Figure 5.1.1. Variables related to the analysis of transmission loss are marked in the figure.

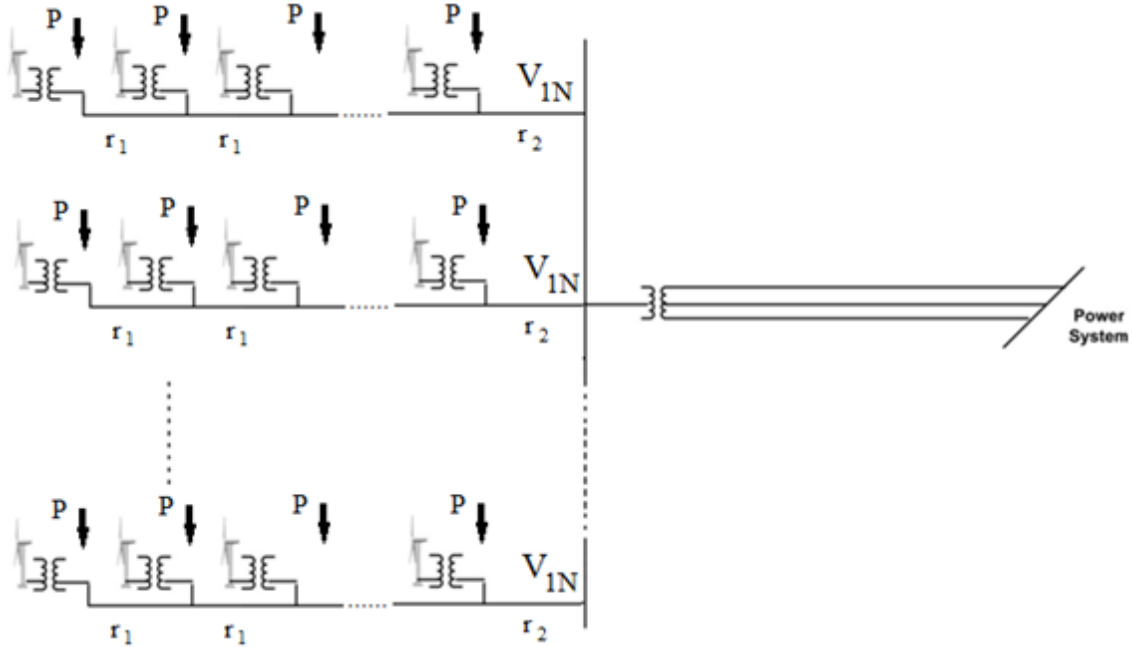


Figure 5.1.1: Alternative Configuration 1 - Example Configuration for Transmission Loss Analysis

This configuration consists of an AC wind farm and AC transmission, with a radial connection within the farm. Assume that there are identical numbers of turbines in each radial feeder, and all turbines are identical in generation capacity. Some of the parameters in this configuration are listed as:

- $m$ :** Number of radial feeders (circuits in parallel)
- $n$ :** Number of turbines in each feeder
- $P$ :** Generation capacity of each wind turbine
- $r_1$ :** Resistance of the transmission line between two wind turbines on a single feeder
- $r_2$ :** Resistance of the transmission line between the last wind turbine and the AC bus on a single feeder
- $V_{1N}$ :** The kV level of every feeder

Note that there is interdependency between the kV level, the wind turbine power, number of wind turbines in a string and the resistance of the circuits in the wind farm. In general the rating of the cable (power circuit in the wind farm) is selected from discrete size cable. As an example, for a ten unit string of 2.2 MVA wind turbine systems and operating kV level of 25 kV, then the cable size “350kcm, copper” will be selected (specifically, the current at the last power circuit section will be  $\frac{2.2MVA}{\sqrt{3} \cdot 25kV} = 0.5kA$ . The current carrying capability of a 350 kcm copper cable is approximately 550 A). Once this selection is made, the values for the resistances will be obtained from the characteristics of the cables.

In this section, only the in-farm transmission loss is considered. This loss refers to the loss in the transmission lines connecting turbine-turbine, or turbines-AC bus. Therefore, the total loss is in the form below.

$$\text{Total Loss} = m \cdot [\text{Loss between Turbines in Single Line} + \text{Loss from Turbines to Bus in Single Line}] \quad (5.1.1)$$

The two elements in the bracket is defined as below.

**Power Loss between Turbines in a Single Feeder:** Summing up the loss between the turbines in a single feeder, the formulation is as below.

$$\text{Loss between Turbines in Single Line} = r_1 \cdot \left(\frac{P}{V_{1N}}\right)^2 + r_1 \cdot \left(\frac{2P}{V_{1N}}\right)^2 + r_1 \cdot \left(\frac{3P}{V_{1N}}\right)^2 + \dots + r_1 \cdot \left(\frac{(n-1)P}{V_{1N}}\right)^2$$

**Power Loss on the Line Connecting the Turbines and the AC Bus:** The loss on the line connecting the bunch of turbines with the bus in a single feeder is listed as below.

$$\text{Loss from Turbines to Bus in Single Line} = r_2 \cdot \left(\frac{nP}{V_{1N}}\right)^2$$

Therefore, from (5.1.1), the total loss is defined as below.

**Total Power Loss:** The total power loss is the sum of the losses listed above. Before the deduction of the total loss, a mathematical lemma that is to be used in the simplification of the formula is provided.

$$\text{Lemma: } 1^2 + 2^2 + 3^2 + \dots + k^2 = \frac{k(k+1)(2k+1)}{6} \quad \text{for } k=1,2,3$$

**Proof:** Using mathematical induction,

$$\text{For } k=1, 1^2 = \frac{1(1+1)(2 \cdot 1 + 1)}{6}, \text{ the statement is true;}$$

If for  $k=j-1$  case the statement is true, which is:

$$1^2 + 2^2 + 3^2 + \dots + (j-1)^2 = \frac{(j-1)j(2j-1)}{6}$$



Then for  $k=j$  case, the left side of the statement is:

$$1^2 + 2^2 + \dots + (j-1)^2 + j^2 = \frac{(j-1)(j)(2j-1)}{6} + j^2 = \frac{(j-1)(j)(2j-1) + 6 \cdot j^2}{6} = \frac{j \cdot [(j-1)(2j-1) + 6 \cdot j]}{6} = \frac{j(j+1)(2j+1)}{6}$$

which is the form of the right side of the statement.

Based on these cases, the lemma is proved for all  $k, k=1,2,3,\dots$

### End of Proof.

Taking the two deducted types of loss above into (5.1.1), the total loss is provided as below.

$$\text{Total Loss} = m \cdot [\text{Loss between Turbines in Single Line} + \text{Loss from Turbines to Bus in Single Line}]$$

$$\begin{aligned} &= m \cdot \left[ r_1 \cdot \left( \frac{P}{V_{1N}} \right)^2 + r_1 \cdot \left( \frac{2P}{V_{1N}} \right)^2 + r_1 \cdot \left( \frac{3P}{V_{1N}} \right)^2 + \dots + r_1 \cdot \left( \frac{(n-1)P}{V_{1N}} \right)^2 + r_2 \cdot \left( \frac{nP}{V_{1N}} \right)^2 \right] \\ &= P^2 \cdot m \cdot \left[ r_1 \cdot \left( \frac{1}{V_{1N}} \right)^2 + r_1 \cdot \left( \frac{2}{V_{1N}} \right)^2 + r_1 \cdot \left( \frac{3}{V_{1N}} \right)^2 + \dots + r_1 \cdot \left( \frac{(n-1)}{V_{1N}} \right)^2 + r_2 \cdot \left( \frac{n}{V_{1N}} \right)^2 \right] \\ &= P^2 \cdot m \cdot \left( \frac{r_1}{V_{1N}^2} \right) \cdot [1^2 + 2^2 + 3^2 + \dots + (n-1)^2] + P^2 \cdot m \cdot n^2 \cdot \left( \frac{r_2}{V_{1N}^2} \right) \\ &\quad \text{(using the lemma)} \\ &= P^2 \cdot m \cdot \left( \frac{r_1}{V_{1N}^2} \right) \cdot \frac{(n-1)n(2n-1)}{6} + P^2 \cdot m \cdot n^2 \cdot \left( \frac{r_2}{V_{1N}^2} \right) \end{aligned}$$

Hence the formulation of the total loss for this configuration is:

$$\text{Total Loss} = P^2 \cdot \left[ m \cdot \left( \frac{r_1}{V_{1N}^2} \right) \cdot \frac{(n-1)n(2n-1)}{6} + m \cdot n^2 \cdot \left( \frac{r_2}{V_{1N}^2} \right) \right] \quad (5.1.2)$$

Note that the total loss in (5.1.2) is in terms of power. It can be discovered that the wind turbine capacity  $P$  is denoted as constant in here. However, the generating capacity  $P$  is variable during a year, especially with the influence of the varying wind speed. Therefore, the constant  $P$  in the above formulae is to be substituted by the transient power  $P$  at time  $t$ , which is  $P(t)$ , and the total energy loss in a year is the integral of the product of the power above and the time, which will be provided in the subsection of formulating the expression of operating cost below.

**Comments on Sensitivity of Loss:** From the formulation of the total power loss, it can be found that the total loss is proportional to the second order of the turbine capacity  $P$ , i.e., proportional to  $P^2$ . The loss is inversely proportional to the second order of the kV level in farm, i.e., inversely proportional to  $V_{1N}^2$ . In addition, the increase of line

resistance  $r_1$  and  $r_2$  will cause the increase of the total loss linearly. The increase of the structure parameters,  $m$  and  $n$ , can also cause the increase of the total loss.

The percentage of the total loss in the total generation capacity is:

$$\begin{aligned} \text{Percentage of Total Loss} &= \frac{\text{Total Loss}}{\text{Total Generation}} = \frac{\text{Total Loss}}{m \cdot n \cdot P} \\ &= \frac{P^2 \cdot m \cdot \left(\frac{r_1}{V_{1N}^2}\right) \cdot \frac{(n-1)n(2n-1)}{6} + P^2 \cdot m \cdot n^2 \cdot \left(\frac{r_2}{V_{1N}^2}\right)}{m \cdot n \cdot P} \\ &= P \cdot \left[ \left(\frac{r_1}{V_{1N}^2}\right) \cdot \frac{(n-1)(2n-1)}{6} + n \cdot \left(\frac{r_2}{V_{1N}^2}\right) \right] \end{aligned}$$

While  $(1 - \text{Percentage of Total Loss})$  is the transmission efficiency.

**Annual Operating Cost:** The annual operating cost, which is mainly the cost of loss, is proportional to the transmission power loss, which is analyzed using example configuration in the subsections above. The transmission loss is in terms of power, and the cost of it is an accumulative cost in terms of \$/year or Million \$/year. Note here the aging of the components is not considered in both the transmission loss and the cost analysis. Therefore, the formulation of the cost of loss in a year is like below.

$$\text{Operating Cost} = \text{Cost of loss} = \int_0^{365 \cdot 24} [k(t) \cdot \text{Total Power Loss}(t)] dt \quad (5.1.3)$$

where  $k(t)$  is determined by primarily the electricity price at time  $t$ .  $t$  is in “hour” basis. For example, if the total loss is 200kW at time  $t$ , then the total energy loss at time  $t$  is 200kW·dt, and the cost of loss at time  $t$  is  $k(t) \cdot 200\text{kW} \cdot dt$ , where  $k(t)$  is the electricity price at time  $t$ . Substituting the total power loss part in (5.1.3) by the total power loss formula (5.1.2), the expression (5.1.3) becomes as below,

$$\begin{aligned} \text{Operating Cost} &= \int_0^{365 \cdot 24} [k(t) \cdot \text{Total Power Loss}(t)] dt = \int_0^{365 \cdot 24} \left[ k(t) \cdot P^2(t) \cdot \right. \\ &\quad \left. \left[ m \cdot \left(\frac{r_1}{V_{1N}^2}\right) \cdot \frac{(n-1)n(2n-1)}{6} + m \cdot n^2 \cdot \left(\frac{r_2}{V_{1N}^2}\right) \right] \right] dt = \left[ m \cdot \left(\frac{r_1}{V_{1N}^2}\right) \cdot \frac{(n-1)n(2n-1)}{6} + m \cdot n^2 \cdot \right. \\ &\quad \left. \left(\frac{r_2}{V_{1N}^2}\right) \right] \cdot \int_0^{365 \cdot 24} [k(t) \cdot P^2(t)] dt \quad (5.1.4) \end{aligned}$$

where  $P(t)$  is the output power of the wind turbine at time  $t$ . This value can be found in the output distribution of the wind turbine in a year;  $k(t)$  is the electricity price at time  $t$ .  $t$  is in “hour” basis.

### 5.1.2 Formulation of Acquisition Cost

The total cost of an alternate wind farm configuration consists of both the acquisition cost and the operation cost. In this subsection, the acquisition cost related to the configurations listed in Section 4 is analyzed.

The acquisition cost, known also as the capital cost and the installation cost, is the one-time cost used for installing the apparatus, constructing the wind farm, and building the interconnections and is amortized over the economic life of the project. This process provides the annualized acquisition cost. The annual acquisition cost is in “dollars per year” basis. When the component in the wind farm is within its life time, the total capital cost remains unchanged. However, when a component reaches its maximum life time, the replacement cost becomes an essential part of the acquisition cost. Here the presented calculation is a demonstration of the method of cost analysis.

The formulation of the annualized acquisition cost (AAC), in “dollars per year” basis, is shown as:

First the total acquisition cost is considered for each component of the wind farm as well as the expected economic life of the component. The main components of the wind farm are:

1. Wind turbine and generator: cost  $C_1$ , expected economic life  $N_1$
2. Power Electronics: cost  $C_2$ , expected economic life  $N_2$
3. Power Circuits: cost  $C_3$ , expected economic life  $N_3$
4. Switchgear at the point of common coupling: cost  $C_4$ , expected economic life  $N_4$

The annualized acquisition cost is computed on the basis of equal present worth value of the annual cost to the total acquisition cost at a reference time, for example at start of project.

Using the above principle the AAC is for a specific wind farm with  $n_1$  wind turbine/generators,  $n_2$  power electronics,  $n_3$  power circuits, and  $n_4$  switchgear at the point of common coupling. In this subsection, the components are listed in these 4 categories above for a demonstration of the method.

The derivation of the annual acquisition cost follows the principle of present worth value (equal Net Present Value, NPV), *i.e.*, the sum of the net present value of the equivalent annual acquisition cost is the initial total acquisition cost. With the equivalence of NPV for a component, the capital cost paid at the beginning (year 0) equals to the summation of the individual equivalent annual acquisition cost, formulated as:

$$\text{Total AC} = \text{NPV} = \sum_{t=1}^{N_i} \frac{R_t}{(1+r)^t} \quad (5.1.5)$$

where:

$R_t$ : is the net cash flow at time t. Counting in years in this case,  $R_t$  is the equivalent annual acquisition cost at year t;

$r$ : is the interest rate;

$N_i$ : is the life time of the component.

Based on the assumption of equal yearly acquisition rate,  $R_t$  stays unchanged with years. Representing  $R_t$  by  $R$ , it is derived from (5.1.5),  $R = \frac{\text{Total AC}}{\sum_{t=1}^{N_i} \frac{1}{(1+r)^t}}$ . From math deduction, the denominator

$$\sum_{t=1}^{N_i} \frac{1}{(1+r)^t} = \frac{1 - \frac{1}{(1+r)^{N_i}}}{r} = \frac{1 - \frac{1}{(1+r)^{N_i}}}{r} = \frac{(1+r)^{N_i} - 1}{r \cdot (1+r)^{N_i}},$$

Therefore,

$$R = \frac{\text{Total AC}}{\sum_{t=1}^{N_i} \frac{1}{(1+r)^t}} = \frac{\text{Total AC}}{\frac{(1+r)^{N_i} - 1}{r \cdot (1+r)^{N_i}}} = \frac{\text{Total AC} \cdot r \cdot (1+r)^{N_i}}{(1+r)^{N_i} - 1} = \frac{r \cdot (1+r)^{N_i}}{(1+r)^{N_i} - 1} \cdot \text{Total AC} \quad (5.1.6)$$

For component  $i$ , the annualized acquisition cost (AAC) is therefore:

$$\text{AAC}_i = \frac{C_i}{\sum_{t=1}^{N_i} \frac{1}{(1+r)^t}} = \frac{C_i}{\frac{(1+r)^{N_i} - 1}{r \cdot (1+r)^{N_i}}} = \frac{C_i \cdot r \cdot (1+r)^{N_i}}{(1+r)^{N_i} - 1} = \frac{r \cdot (1+r)^{N_i}}{(1+r)^{N_i} - 1} \cdot C_i \quad (5.1.7)$$

$i=1,2,3,4$ .

The annualized acquisition cost of the entire configuration is the sum of the AAC of the components:

$$\text{AAC} = \sum_{i=1}^4 [n_i \cdot \text{AAC}_i] = \sum_{i=1}^4 [n_i \cdot \frac{r \cdot (1+r)^{N_i}}{(1+r)^{N_i} - 1} \cdot C_i] \quad (5.1.8)$$

### 5.1.3 Formulation of Maintenance Cost

In this subsection, the maintenance cost is defined. This cost is in “dollars per year” basis. The maintenance cost, MC, is normally considered as a fixed cost.

The maintenance cost is formulated as the sum of the maintenance cost of each component. The main components of the wind farm are:

1. Wind turbine and generator: maintenance cost  $MC_1$
2. Power Electronics: cost  $MC_2$
3. Power Circuits: cost  $MC_3$
4. Switchgear at the point of common coupling: cost  $MC_4$

Using the above principle the MC is for a specific wind farm with  $n_1$  wind turbine/generators,  $n_2$  power electronics,  $n_3$  power circuits, and  $n_4$  switchgear at the point of common coupling.

$$MC = \sum_{i=1}^4 [n_i \cdot MC_i] \quad (5.1.9)$$

As discussed above, the maintenance cost has little impact on the selection of kV level and equipment ratings.

#### 5.1.4 Formulation of Total Cost as a Function of kV Level

Summing all the costs (operational, acquisition, maintenance) and expressing these as functions of the kV level, the following is obtained.

The annualized total cost is:

Annual Total Cost = Operational Cost + Annual Acquisition Cost + Maintenance Cost.

Abbreviating the terms into ATC, OC, AAC, and MC, the above formula of calculating the total cost is shown below:

$$ATC = OC + AAC + MC = \int_0^{365 \cdot 24} [k(t) \cdot \text{Total Power Loss}(t)] dt + \sum_{i=1}^4 [n_i \cdot AAC_i] + \sum_{i=1}^4 [n_i \cdot MC_i] = \int_0^{365 \cdot 24} [k(t) \cdot \text{Total Power Loss}(t)] dt + \sum_{i=1}^4 [n_i \cdot \frac{r \cdot (1+r)^{N_i}}{(1+r)^{N_i} - 1} \cdot C_i] + \sum_{i=1}^4 [n_i \cdot MC_i] \quad (5.1.10)$$

In this expression (5.1.10), the total power loss is a function of the kV level, such as the one shown above in (5.1.4). The acquisition costs of the components,  $C_i$ , are also functions of the kV level, since the acquisition cost of the devices at different kV level differs greatly. For example, the acquisition cost of wind turbines vs kV level is shown in Figure 5.1.2.

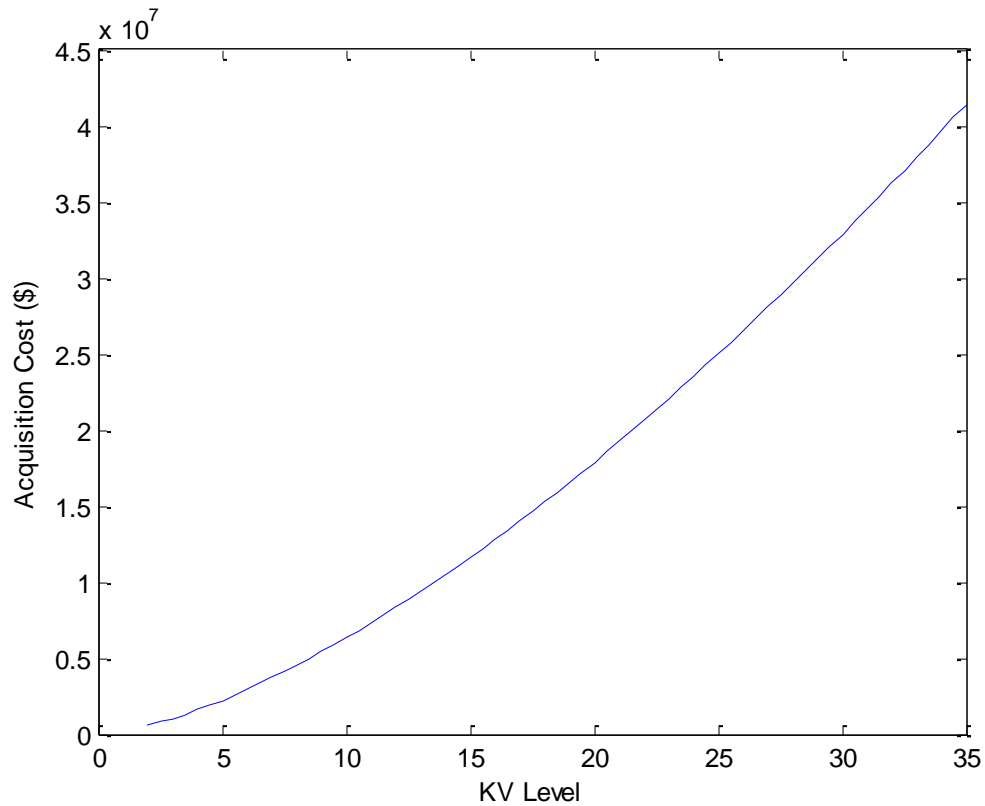


Figure 5.1.2: Acquisition Cost of Wind Turbine System vs. kV Level

Similarly, the maintenance costs of the components are functions of the kV level. But since the maintenance costs are limited as compared with the annualized acquisition cost, the impact of the maintenance costs on the selection of kV level is very small. In the following analysis, the process of selecting the kV level does not take into account the maintenance costs.

From the analysis above, the annualized total cost, ATC, is the sum of functions of kV level, which is therefore also a function of kV level.

### 5.1.5 Optimal kV Level Computation

The optimal kV level is obtained by finding the kV level that will yield the minimum annualized total cost of a wind farm (ATC). The approach is illustrated in a graphical manner, by simply graphing the total cost versus kV level. An example for configuration 1 is provided below with a detailed process of the kV level computation. As discussed above, the maintenance costs, which have little impact on the selection of kV level, are not considered in the graphs.

The process of deriving the optimal kV level is provided:

**Step 1:** Calculate the current range of the cable;

**Step 2:** Select the cable size and get the resistance value;

**Step 3:** Based on the distribution of wind turbine output  $P(t)$ , calculate the total power loss; Based on the price difference  $k(t)$ , derive the operating cost expression and plot it as a curve variable to the kV level;

**Step 4:** Based on the acquisition cost characteristics of the components variable to the kV level, derive the expression of the annualized acquisition cost and plot it as a curve variable to the kV level;

**Step 5:** Add the curves of operating cost and annualized acquisition cost to form the curve of the annualized total cost;

**Step 6:** Find the minimum point of the annualized total cost curve, and obtain the corresponding kV level.

#### 5.1.6 Example Case of Finding the Optimal kV Level – Configuration 1

Configuration 1 is used as an example to show the process of finding the kV level.

The assumed parameters of Configuration 1 are:

- a) Number of parallel lines:  $m = 3$ ;
- b) Number of wind turbines in each line:  $n = 10$ ;
- c) Rating of wind turbines: 2.2MVA at 25kV;
- d) The distance between the wind turbines is 200ft; the distance from the last turbine in the feeder to the bus is 500 ft;
- e) The interest rate is 5%, which means,  $r = 0.05$ ;
- f)  $k(t)$  is assumed to be a stable factor,  $k(t) = \$0.1/\text{kwh}$ ;
- g) Based on assumption f),

$$\int_0^{365 \cdot 24} [k(t) \cdot P^2(t)] dt = \int_0^{365 \cdot 24} [0.1 \cdot P^2(t)] dt = 0.1 \cdot \int_0^{365 \cdot 24} [P^2(t)] dt$$

It is in further assumed that  $\int_0^{365 \cdot 24} [P^2(t)] dt = 2 \cdot 10^{10} (\text{kw})^2 \cdot h$ , which is based on the typical distribution of  $P$  over a year. Therefore,

$$\int_0^{365 \cdot 24} [k(t) \cdot P^2(t)] dt = \frac{\$0.1}{\text{kwh}} \cdot 2 \cdot 10^{10} (\text{kw})^2 \cdot h = 2 \cdot 10^9 \text{kw}$$

- h) The life time of the components in years:

Wind turbine and generator:  $N_1=30$

Power Electronics:  $N_2=20$

Power Circuits:  $N_3=40$

Switchgear at the point of common coupling:  $N_4=20$

The above process in Subsection 5.1.5 is provided as below.

**Step 1:** Calculate the current range of the cable:  $\frac{10 \cdot 2.2 MVA}{\sqrt{3} \cdot 25 kV} = 0.5 kA$

**Step 2:** Select the cable size and get the resistance value: 350 kcm copper cable is selected since the current capability of a 350 kcm copper cable is around 550A. A list of current capability vs cable size is provided in Table 5.1.1.

Table 5.1.1: Current Capability vs. Cable Size and Type

Current (A)	50-250	250-300	300-350	350-500	500-550	550-600	600-1000	1000-2000
Cable Size (kcm)	105.5	133.1	211.6	500	350	750	1093	2250
Type	Aluminum	Copper	Aluminum	Aluminum	Copper	Copper	Copper	Copper

The resistance value of a 350 kcm copper cable is obtained: 0.03 ohm/1000ft. Therefore,

$$r_1 = \frac{0.03 ohm}{1000 ft} \cdot 200 ft = 0.006 ohm; r_2 = \frac{0.03 ohm}{1000 ft} \cdot 500 ft = 0.015 ohm$$

**Step 3:** Calculate the total power loss from (5.1.2),

$$\begin{aligned} Total Power Loss &= P^2(t) \cdot \left[ m \cdot \left( \frac{r_1}{V_{1N}^2} \right) \cdot \frac{(n-1)n(2n-1)}{6} + m \cdot n^2 \cdot \left( \frac{r_2}{V_{1N}^2} \right) \right] \\ &= P^2(t) \cdot \left[ 3 \cdot \left( \frac{0.006}{V_{1N}^2} \right) \cdot \frac{(10-1)10(20-1)}{6} + 3 \cdot 10^2 \cdot \left( \frac{0.015}{V_{1N}^2} \right) \right] = P^2(t) \cdot \frac{9.63}{V_{1N}^2} \end{aligned}$$

Based on the price  $k(t) = \$0.1/kwh = \$10^{-4}/w \cdot h$  assumption and the assumption of  $P(t)$ , derive the operating cost expression from (5.1.4),

$$Operating cost = 10^{-4} \cdot 2 \cdot 10^{10} \cdot \frac{9.63}{V_{1N}^2} = 19260000 \cdot \frac{1}{V_{1N}^2}$$

where  $V_{1N}$  is in kV and is in the range of 2kV - 35kV.

The plot is shown in Figure 5.1.3.



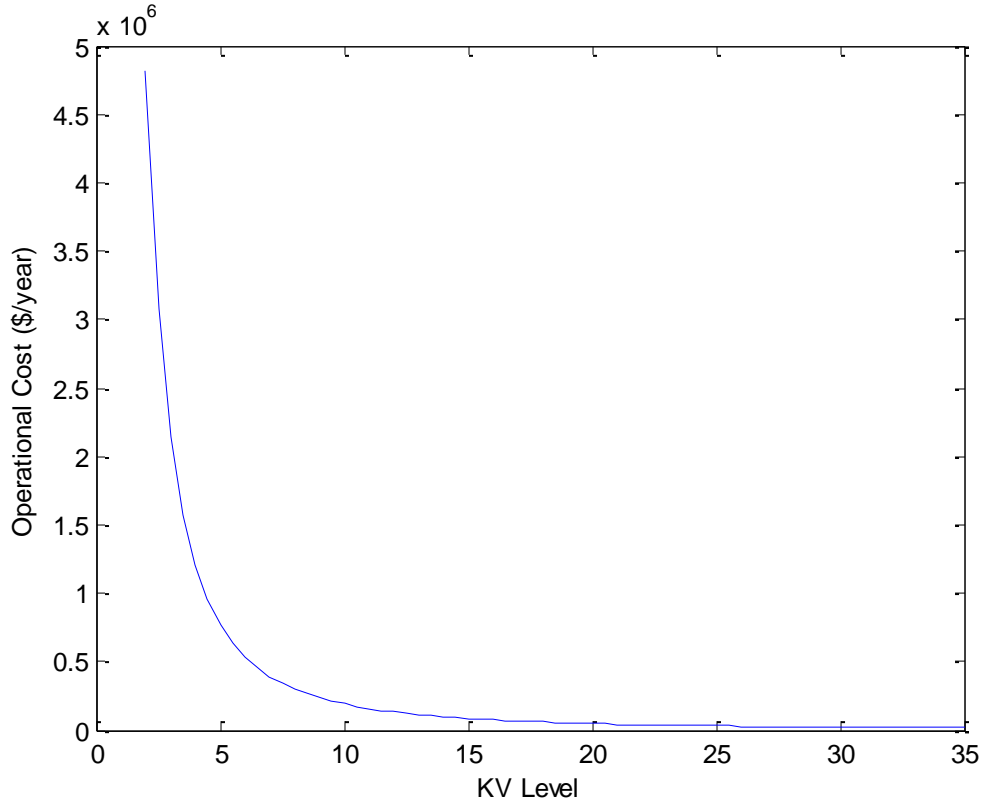


Figure 5.1.3: Operating Cost of Example Configuration

**Step 4:** Based on the acquisition cost characteristics of the components variable to the kV level, derive the expression of the annualized acquisition cost:

$$\text{From (5.1.8), } AAC = \sum_{i=1}^4 [n_i \cdot AAC_i] = \sum_{i=1}^4 \left[ n_i \cdot \frac{r \cdot (1+r)^{N_i}}{(1+r)^{N_i-1}} \cdot C_i \right]$$

The curve of the annual acquisition cost vs kV level is provided in Figure 5.1.4.

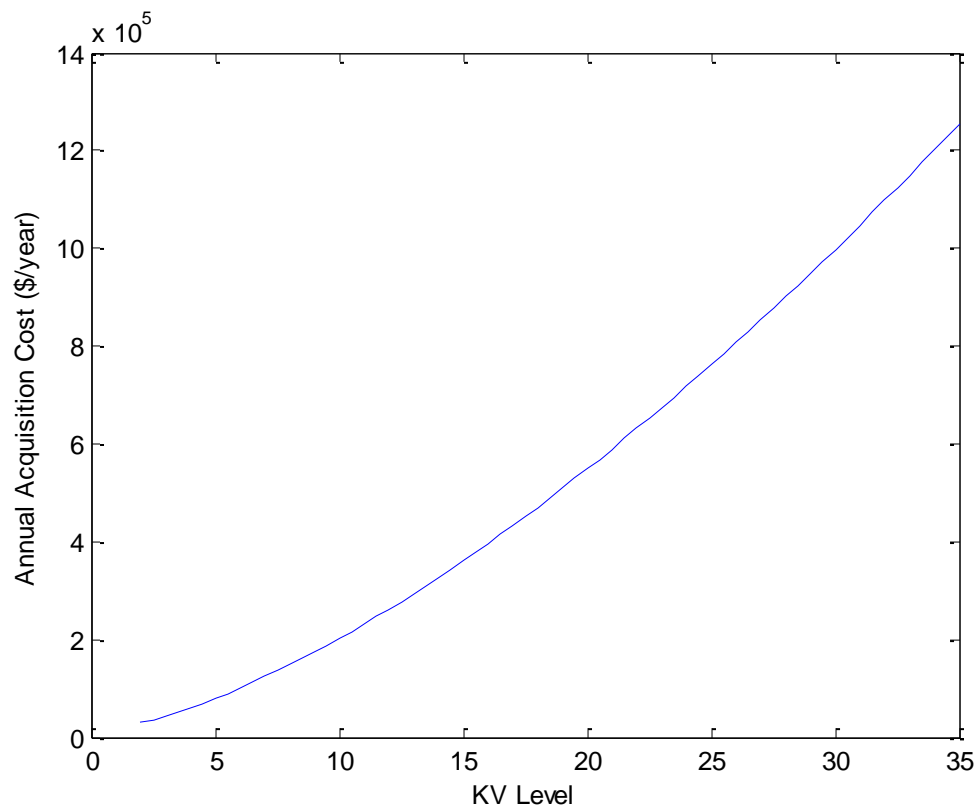


Figure 5.1.4: Annualized Acquisition Cost of Example Configuration

**Step 5:** Add the curves of operating cost and annualized acquisition cost to form the curve of the annualized total cost:

From (5.1.10), the curve is plotted as shown in Figure 5.1.5.

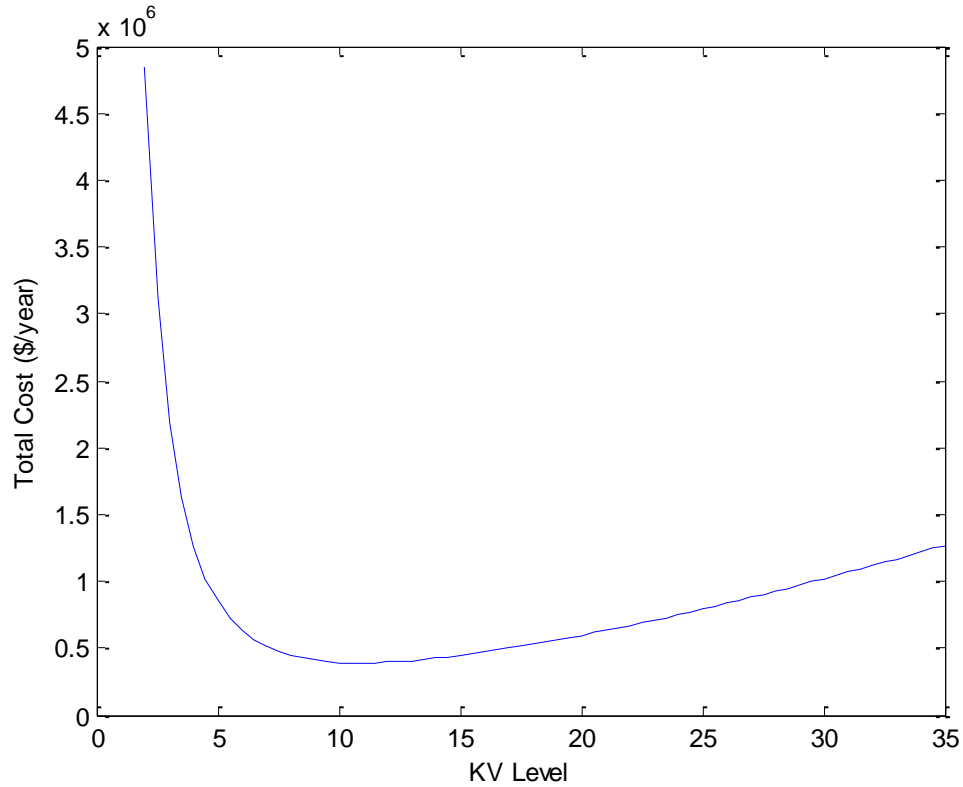


Figure 5.1.5: Annualized Total Cost of Example Configuration

**Step 6:** Find the minimum point of the annualized total cost curve, and obtain the corresponding kV level.

From Figure 5.1.5, it can be found that the minimum point of the annualized total cost is at kV level = 12kV, when the annualized total cost = 0.48 million \$/year.

This provides the optimal kV level  $V_{1N}=12$  kV.

For configuration 1, this subsection has provided the complete analysis for kV level and cost formulation. In the subsections below from Subsection 5.2 to 5.8, similar analysis will be provided for all the other 7 configurations, followed by a 30 wind turbine case study for each configuration.

## 5.2 kV Levels, Equipment Ratings and Wind Farm Cost Analysis of Configuration 2

In this subsection, Configuration 2 is analyzed for the kV levels, equipment ratings, and cost. The configuration is shown in Figure 5.2.1.

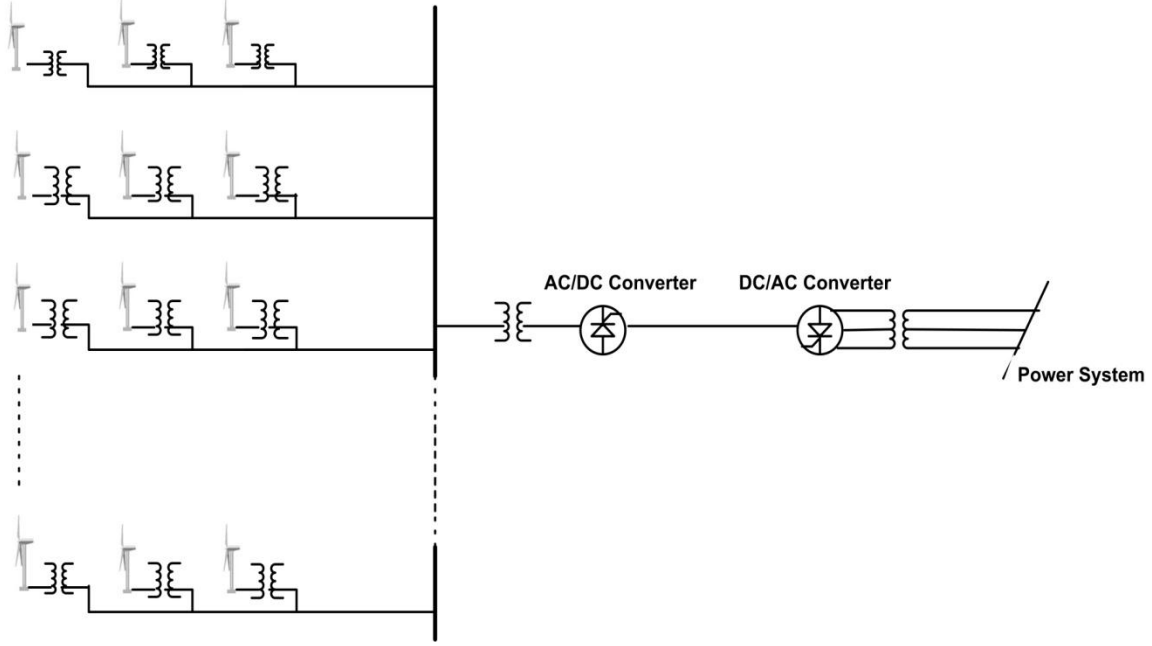


Figure 5.2.1: Alternative Wind Farm Configuration 2

### 5.2.1 Formulation of Operating Cost

Since the in-farm transmission is identical to Configuration 1, the formulation of operational cost is exactly the same as shown in Configuration 1.

$$\begin{aligned} \text{Operating Cost} &= \int_0^{365 \cdot 24} [k(t) \cdot \text{Total Power Loss}(t)] dt = \int_0^{365 \cdot 24} \left[ k(t) \cdot P^2(t) \cdot \left[ m \cdot \left( \frac{r_1}{V_{1N}^2} \right) \cdot \right. \right. \\ &\quad \left. \left. \frac{(n-1)n(2n-1)}{6} + m \cdot n^2 \cdot \left( \frac{r_2}{V_{1N}^2} \right) \right] \right] dt = \left[ m \cdot \left( \frac{r_1}{V_{1N}^2} \right) \cdot \frac{(n-1)n(2n-1)}{6} + m \cdot n^2 \cdot \left( \frac{r_2}{V_{1N}^2} \right) \right] \cdot \int_0^{365 \cdot 24} [k(t) \cdot P^2(t)] dt \end{aligned} \quad (5.2.1)$$

### 5.2.2 Formulation of Acquisition Cost

The main components of the wind farm are:

1. Wind turbine and generator: cost  $C_1$ , expected economic life  $N_1$
2. Power Electronics: cost  $C_2$ , expected economic life  $N_2$
3. Power Circuits: cost  $C_3$ , expected economic life  $N_3$
4. Switchgear at the point of common coupling: cost  $C_4$ , expected economic life  $N_4$

For this specific wind farm with  $n_1$  wind turbine/generators,  $n_2$  power electronics,  $n_3$  power circuits, and  $n_4$  switchgear at the point of common coupling, the annualized acquisition cost, AAC, is:

$$AAC = \sum_{i=1}^4 [n_i \cdot AAC_i] = \sum_{i=1}^4 [n_i \cdot \frac{r \cdot (1+r)^{N_i}}{(1+r)^{N_i-1}} \cdot C_i] \quad (5.2.2)$$

### 5.2.3 Formulation of Total Cost as a Function of kV Level

Similar as (5.1.10), the annualized total cost, ATC, is formulated by summing (5.2.1) and (5.2.2). As discussed in the subsections above, the maintenance cost is not to be considered.

$$ATC = \left[ m \cdot \left( \frac{r_1}{V_{1N}^2} \right) \cdot \frac{(n-1)n(2n-1)}{6} + m \cdot n^2 \cdot \left( \frac{r_2}{V_{1N}^2} \right) \right] \cdot \int_0^{365 \cdot 24} [k(t) \cdot P^2(t)] dt + \sum_{i=1}^4 [n_i \cdot AAC_i] =$$

$$\left[ m \cdot \left( \frac{r_1}{V_{1N}^2} \right) \cdot \frac{(n-1)n(2n-1)}{6} + m \cdot n^2 \cdot \left( \frac{r_2}{V_{1N}^2} \right) \right] \cdot \int_0^{365 \cdot 24} [k(t) \cdot P^2(t)] dt + \sum_{i=1}^4 [n_i \cdot \frac{r \cdot (1+r)^{N_i}}{(1+r)^{N_i-1}} \cdot C_i] \quad (5.2.3)$$

### 5.2.4 Example Case of Finding the Optimal kV Level – Configuration 2

In this subsection, a 30 wind turbine example is provided to show the process of finding the optimal kV level of Configuration 2.

The assumed parameters of Configuration 2 are:

- a) Number of parallel lines:  $m = 3$ ;
- b) Number of wind turbines in each line:  $n = 10$ ;
- c) Rating of wind turbines: 2.2MVA at 25kV;
- d) The distance between the wind turbines is 200ft; the distance from the last turbine in the feeder to the bus is 500 ft;
- e) The interest rate is 5%, which means,  $r = 0.05$ ;
- f)  $k(t)$  is assumed to be a stable factor,  $k(t) = \$0.1/\text{kwh}$ ;
- g) Based on assumption f),

$$\int_0^{365 \cdot 24} [k(t) \cdot P^2(t)] dt = \int_0^{365 \cdot 24} [0.1 \cdot P^2(t)] dt = 0.1 \cdot \int_0^{365 \cdot 24} [P^2(t)] dt$$

It is in further assumed that  $\int_0^{365 \cdot 24} [P^2(t)] dt = 2 \cdot 10^{10} (\text{kw})^2 \cdot h$ , which is based on the typical distribution of  $P$  over a year. Therefore,

$$\int_0^{365 \cdot 24} [k(t) \cdot P^2(t)] dt = \frac{\$0.1}{\text{kwh}} \cdot 2 \cdot 10^{10} (\text{kw})^2 \cdot h = 2 \cdot 10^9 \text{kw}$$

- h) The life time of the components in years:

Wind turbine and generator:  $N_1=30$

Power Electronics:  $N_2=20$

Power Circuits:  $N_3=40$

Switchgear at the point of common coupling:  $N_4=20$

The analysis process is provided as below.

**Step 1:** Calculate the current range of the cable:  $\frac{10 \cdot 2.2 MVA}{\sqrt{3} \cdot 25 kV} = 0.5 kA$

**Step 2:** Select the cable size and get the resistance value: 350 kcm copper cable is selected since the current capability of a 350 kcm copper cable is around 550A. The resistance value of a 350 kcm copper cable is obtained: 0.03 ohm/1000ft. Therefore,

$$r_1 = \frac{0.03 ohm}{1000 ft} \cdot 200 ft = 0.006 ohm; r_2 = \frac{0.03 ohm}{1000 ft} \cdot 500 ft = 0.015 ohm$$

**Step 3:** Based on the distribution of wind turbine output  $P(t)$ , calculate the total power loss:

$$\begin{aligned} Total Power Loss &= P^2(t) \cdot \left[ m \cdot \left( \frac{r_1}{V_{1N}^2} \right) \cdot \frac{(n-1)n(2n-1)}{6} + m \cdot n^2 \cdot \left( \frac{r_2}{V_{1N}^2} \right) \right] \\ &= P^2(t) \cdot \left[ 3 \cdot \left( \frac{0.006}{V_{1N}^2} \right) \cdot \frac{(10-1)10(20-1)}{6} + 3 \cdot 10^2 \cdot \left( \frac{0.015}{V_{1N}^2} \right) \right] \\ &= P^2(t) \cdot \frac{9.63}{V_{1N}^2} \end{aligned}$$

From (5.2.1),

$$Operating\ cost = 10^{-4} \cdot 2 \cdot 10^{10} \cdot \frac{9.63}{V_{1N}^2} = 19260000 \cdot \frac{1}{V_{1N}^2}$$

where  $V_{1N}$  is in kV and is in the range of 2 kV - 35kV.

**Step 4:** Based on the acquisition cost characteristics of the components variable to the kV level, derive the expression of the annualized acquisition cost as in (5.2.2).

**Step 5:** Add the operating cost and annualized acquisition cost to form the annualized total cost: from (5.2.3), the curve is plotted as shown in Figure 5.2.2.

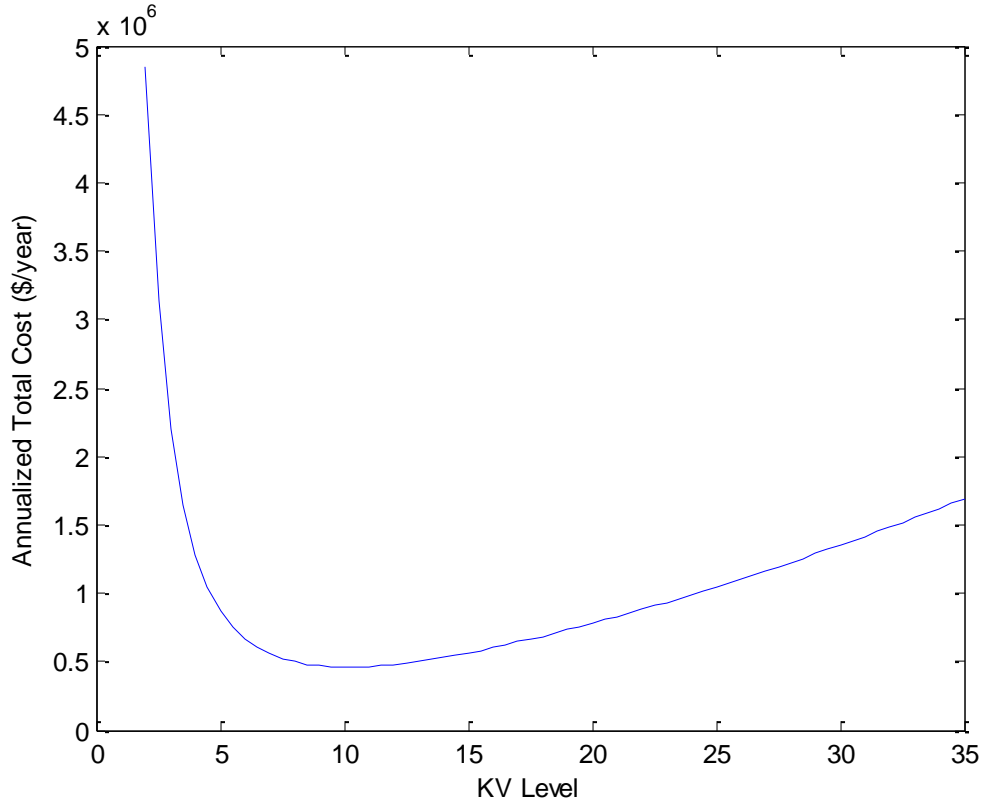


Figure 5.2.2: Annualized Total Cost of Configuration 2

**Step 6:** Find the minimum point of the annualized total cost curve, and obtain the corresponding kV level. From Figure 5.2.2, it can be found that the minimum point of the annualized total cost is at kV level = 10kV, when the annualized total cost = 0.50 million \$/year.

This provides the optimal kV level  $V_{1N}=10$  kV. The reason that the optimal kV level is smaller than that of Configuration 1 is that the acquisition cost of this configuration is larger than Configuration 1, since more electronic devices are added to achieve the DC transmission.

In the subsections below for Configuration 3 to 8, the result of the annualized total cost will be provided right after Step 2, without detailed results from Step 3 and Step 4.

### 5.3 kV Levels, Equipment Ratings and Wind Farm Cost Analysis of Configuration 3

In this subsection, Configuration 3 is analyzed for the kV levels, equipment ratings, and cost. The configuration is shown in Figure 5.3.1.

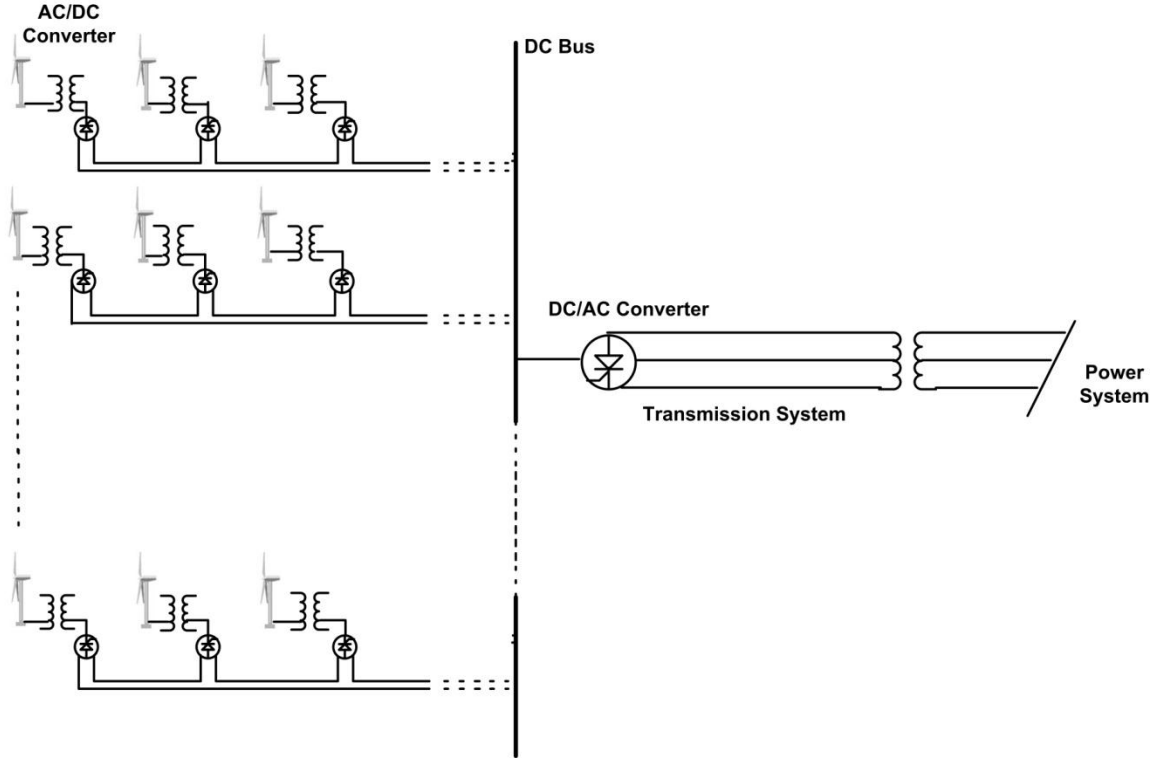


Figure 5.3.1: Alternative Wind Farm Configuration 3

#### 5.3.1 Formulation of Operating Cost

Similar as Configuration 1,

$$\begin{aligned} \text{Operating Cost} &= \int_0^{365 \cdot 24} [k(t) \cdot \text{Total Power Loss}(t)] dt = \int_0^{365 \cdot 24} \left[ k(t) \cdot P^2(t) \cdot \left[ m \cdot \left( \frac{r_1}{V_{1N}^2} \right) \cdot \right. \right. \\ &\quad \left. \left. \frac{(n-1)n(2n-1)}{6} + m \cdot n^2 \cdot \left( \frac{r_2}{V_{1N}^2} \right) \right] \right] dt = \left[ m \cdot \left( \frac{r_1}{V_{1N}^2} \right) \cdot \frac{(n-1)n(2n-1)}{6} + m \cdot n^2 \cdot \left( \frac{r_2}{V_{1N}^2} \right) \right] \cdot \int_0^{365 \cdot 24} [k(t) \cdot \\ &\quad P^2(t)] dt \end{aligned} \quad (5.3.1)$$

#### 5.3.2 Formulation of Acquisition Cost

The main components of the wind farm are:

1. Wind turbine and generator: cost  $C_1$ , expected economic life  $N_1$



2. Power Electronics: cost  $C_2$ , expected economic life  $N_2$
3. Power Circuits: cost  $C_3$ , expected economic life  $N_3$
4. Switchgear at the point of common coupling: cost  $C_4$ , expected economic life  $N_4$

For this specific wind farm with  $n_1$  wind turbine/generators,  $n_2$  power electronics,  $n_3$  power circuits, and  $n_4$  switchgear at the point of common coupling, the annualized acquisition cost, AAC, is:

$$AAC = \sum_{i=1}^4 [n_i \cdot AAC_i] = \sum_{i=1}^4 [n_i \cdot \frac{r \cdot (1+r)^{N_i}}{(1+r)^{N_i}-1} \cdot C_i] \quad (5.3.2)$$

### 5.3.3 Formulation of Total Cost as a Function of kV Level

Similar as (5.1.10), the annualized total cost, ATC, is formulated by summing (5.3.1) and (5.3.2). As discussed in the subsections above, the maintenance cost is not to be considered.

$$\begin{aligned} ATC = & \left[ m \cdot \left( \frac{r_1}{V_{1N}^2} \right) \cdot \frac{(n-1)n(2n-1)}{6} + m \cdot n^2 \cdot \left( \frac{r_2}{V_{1N}^2} \right) \right] \cdot \int_0^{365 \cdot 24} [k(t) \cdot P^2(t)] dt + \sum_{i=1}^4 [n_i \cdot \\ & AAC_i] = \left[ m \cdot \left( \frac{r_1}{V_{1N}^2} \right) \cdot \frac{(n-1)n(2n-1)}{6} + m \cdot n^2 \cdot \left( \frac{r_2}{V_{1N}^2} \right) \right] \cdot \int_0^{365 \cdot 24} [k(t) \cdot P^2(t)] dt + \\ & \sum_{i=1}^4 [n_i \cdot \frac{r \cdot (1+r)^{N_i}}{(1+r)^{N_i}-1} \cdot C_i] \end{aligned} \quad (5.3.3)$$

### 5.3.4 Example Case of Finding the Optimal kV Level – Configuration 3

In this subsection, a 30 wind turbine example is provided to show the process of finding the optimal kV level of Configuration 3.

The assumed parameters of Configuration 3 are:

- a) Number of parallel lines:  $m = 3$ ;
- b) Number of wind turbines in each line:  $n = 10$ ;
- c) Rating of wind turbines: 2.2MVA at 25kV;
- d) The distance between the wind turbines is 200ft; the distance from the last turbine in the feeder to the bus is 500 ft;
- e) The interest rate is 5%, which means,  $r = 0.05$ ;
- f)  $k(t)$  is assumed to be a stable factor,  $k(t) = \$0.1/\text{kwh}$ ;
- g) Based on assumption f),

$$\int_0^{365 \cdot 24} [k(t) \cdot P^2(t)] dt = \int_0^{365 \cdot 24} [0.1 \cdot P^2(t)] dt = 0.1 \cdot \int_0^{365 \cdot 24} [P^2(t)] dt$$

It is further assumed that  $\int_0^{365 \cdot 24} [P^2(t)] dt = 2 \cdot 10^{10} (\text{kw})^2 \cdot h$ , which is based on the typical distribution of  $P$  over a year. Therefore,

$$\int_0^{365 \cdot 24} [k(t) \cdot P^2(t)] dt = \frac{\$0.1}{\text{kwh}} \cdot 2 \cdot 10^{10} (\text{kw})^2 \cdot h = 2 \cdot 10^9 \text{kw}$$

**h)** The life time of the components in years:

Wind turbine and generator:  $N_1=30$

Power Electronics:  $N_2=20$

Power Circuits:  $N_3=40$

Switchgear at the point of common coupling:  $N_4=20$

The analysis process is provided as below.

**Step 1:** Calculate the current range of the cable:  $\frac{10 \cdot 2.2 \text{MVA}}{\sqrt{3} \cdot 25 \text{kV}} = 0.5 \text{kA}$

**Step 2:** Select the cable size and get the resistance value: 350 kcm copper cable is selected since the current capability of a 350 kcm copper cable is around 550A. The resistance value of a 350 kcm copper cable is obtained: 0.03 ohm/1000ft. Therefore,

$$r_1 = \frac{0.03 \text{ohm}}{1000 \text{ft}} \cdot 200 \text{ft} = 0.006 \text{ohm}; r_2 = \frac{0.03 \text{ohm}}{1000 \text{ft}} \cdot 500 \text{ft} = 0.015 \text{ohm}$$

**Step 3:** Add the operating cost and annualized acquisition cost to form the annualized total cost: from (5.3.3), the curve is plotted as shown in Figure 5.3.2.

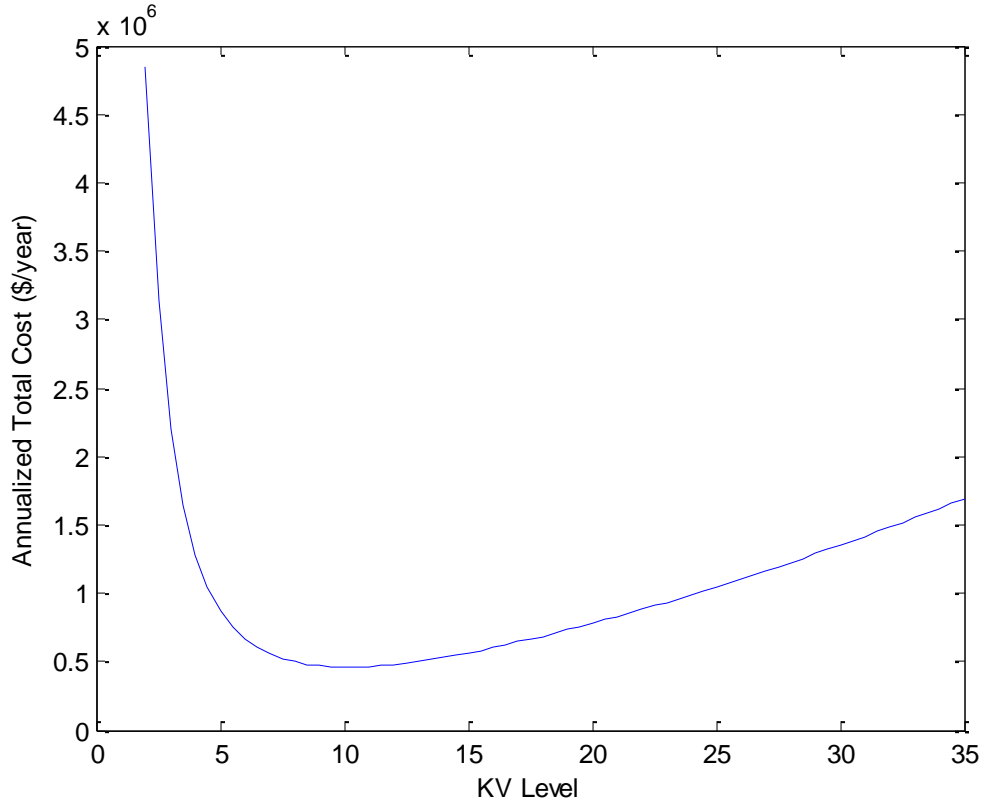


Figure 5.3.2: Annualized Total Cost of Configuration 3

**Step 4:** From Figure 5.3.2, it can be found that the minimum point of the annualized total cost is at kV level = 8kV, when the annualized total cost = 0.52 million \$/year.

This provides the optimal kV level  $V_{1N}=8$  kV. The reason that the optimal kV level is smaller than that of Configuration 1 and 2 is that the acquisition cost of this configuration is larger than Configuration 1 and 2, since more electronic devices are added to achieve the in-farm DC transmission.

## 5.4 kV Levels, Equipment Ratings and Wind Farm Cost Analysis of Configuration 4

In this subsection, Configuration 4 is analyzed for the kV levels, equipment ratings, and cost. The configuration is shown in Figure 5.4.1.

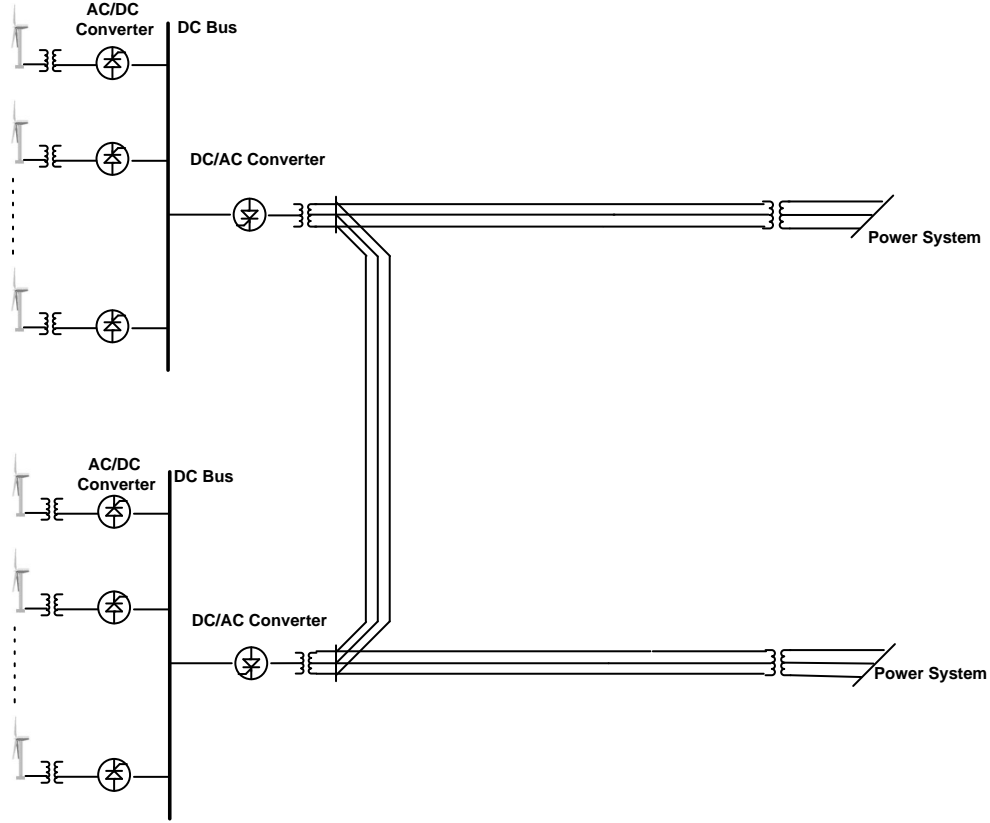


Figure 5.4.1: Alternative Wind Farm Configuration 4

### 5.4.1 Formulation of Operating Cost

The operating cost is formulated for Configuration 4 as below.

$$\text{Operating Cost} = \int_0^{365 \cdot 24} [k(t) \cdot \text{Total Power Loss}(t)] dt = \int_0^{365 \cdot 24} \left[ k(t) \cdot P^2(t) \cdot \left[ m \cdot n \cdot \left( \frac{r_2}{V_{1N}^2} \right) \right] \right] dt = \left[ m \cdot n \cdot \left( \frac{r_2}{V_{1N}^2} \right) \right] \cdot \int_0^{365 \cdot 24} [k(t) \cdot P^2(t)] dt \quad (5.4.1)$$

### 5.4.2 Formulation of Acquisition Cost

The main components of the wind farm are:

1. Wind turbine and generator: cost  $C_1$ , expected economic life  $N_1$
2. Power Electronics: cost  $C_2$ , expected economic life  $N_2$
3. Power Circuits: cost  $C_3$ , expected economic life  $N_3$
4. Switchgear at the point of common coupling: cost  $C_4$ , expected economic life  $N_4$

For this specific wind farm with  $n_1$  wind turbine/generators,  $n_2$  power electronics,  $n_3$  power circuits, and  $n_4$  switchgear at the point of common coupling, the annualized acquisition cost, AAC, is:

$$AAC = \sum_{i=1}^4 [n_i \cdot AAC_i] = \sum_{i=1}^4 [n_i \cdot \frac{r \cdot (1+r)^{N_i}}{(1+r)^{N_i-1}} \cdot C_i] \quad (5.4.2)$$

### 5.4.3 Formulation of Total Cost as a Function of kV Level

Similar as (5.1.10), the annualized total cost, ATC, is formulated by summing (5.4.1) and (5.4.2). As discussed in the subsections above, the maintenance cost is not to be considered.

$$ATC = \left[ m \cdot n \cdot \left( \frac{r_2}{V_{1N}^2} \right) \right] \cdot \int_0^{365 \cdot 24} [k(t) \cdot P^2(t)] dt + \sum_{i=1}^4 [n_i \cdot \frac{r \cdot (1+r)^{N_i}}{(1+r)^{N_i-1}} \cdot C_i] \quad (5.4.3)$$

### 5.4.4 Example Case of Finding the Optimal kV Level – Configuration 4

In this subsection, a 30 wind turbine example is provided to show the process of finding the optimal kV level of Configuration 4.

The assumed parameters of Configuration 4 are:

- a) Number of buses:  $m = 3$ ;
- b) Number of wind turbines connecting to each bus:  $n = 10$ ;
- c) Rating of wind turbines: 2.2MVA at 25kV;
- d) The distance from the turbine to the bus is 500 ft ;
- e) The interest rate is 5%, which means,  $r = 0.05$ ;
- f)  $k(t)$  is assumed to be a stable factor,  $k(t) = \$0.1/\text{kwh}$ ;
- g) Based on assumption f),

$$\int_0^{365 \cdot 24} [k(t) \cdot P^2(t)] dt = \int_0^{365 \cdot 24} [0.1 \cdot P^2(t)] dt = 0.1 \cdot \int_0^{365 \cdot 24} [P^2(t)] dt$$

It is further assumed that  $\int_0^{365 \cdot 24} [P^2(t)] dt = 2 \cdot 10^{10} (\text{kw})^2 \cdot h$ , which is based on the typical distribution of  $P$  over a year. Therefore,

$$\int_0^{365 \cdot 24} [k(t) \cdot P^2(t)] dt = \frac{\$0.1}{\text{kwh}} \cdot 2 \cdot 10^{10} (\text{kw})^2 \cdot h = 2 \cdot 10^9 \text{kw}$$

**h)** The life time of the components in years:

Wind turbine and generator:  $N_1=30$

Power Electronics:  $N_2=20$

Power Circuits:  $N_3=40$

Switchgear at the point of common coupling:  $N_4=20$

The analysis process is provided as below.

**Step 1:** Calculate the current range of the cable:  $\frac{2.2 \text{MVA}}{\sqrt{3} \cdot 25 \text{kV}} = 51 \text{A}$

**Step 2:** Select the cable size and get the resistance value: 105.5 kcm aluminum cable is selected. The resistance value of a 105.5 kcm aluminum cable is obtained: 0.07 ohm/1000ft. Therefore,

$$r_2 = \frac{0.07 \text{ohm}}{1000 \text{ft}} \cdot 500 \text{ft} = 0.035 \text{ ohm}$$

**Step 3:** Add the operating cost and annualized acquisition cost to form the annualized total cost: from (5.4.3), the curve is plotted as shown in Figure 5.4.2.

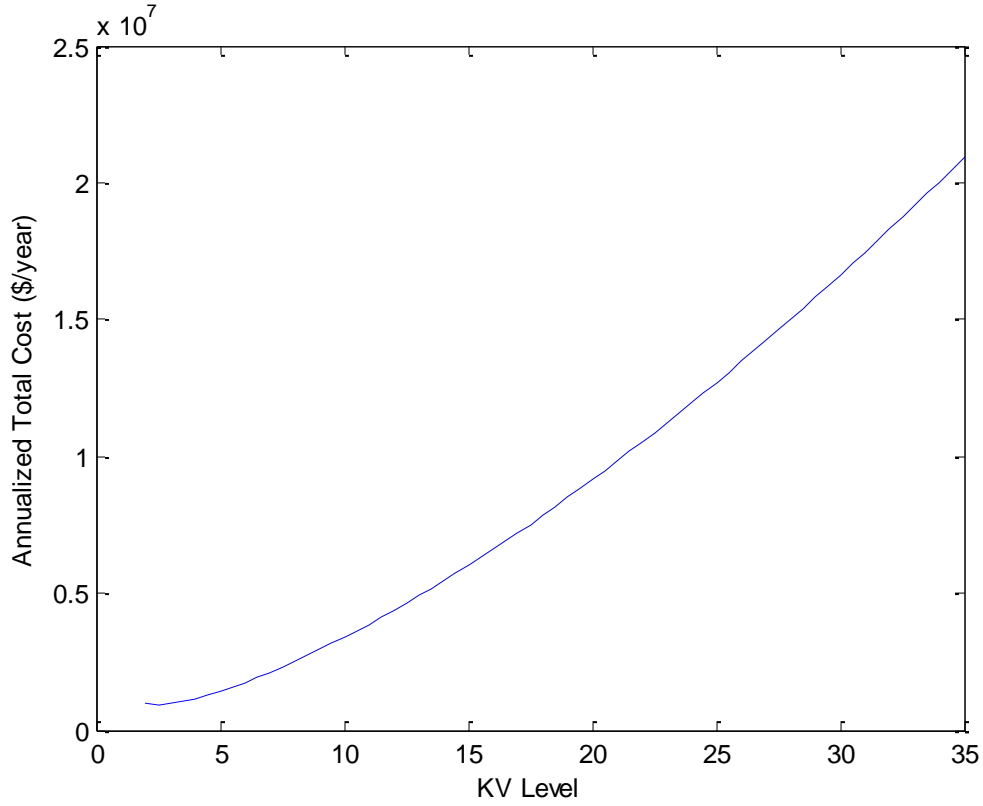


Figure 5.4.2: Annualized Total Cost of Configuration 4

**Step 4:** From Figure 5.4.2, it can be found that the minimum point of the annualized total cost is hard to be determined based on the minimum of the total cost. The kV level is selected to be the lowest value in the accepted range, *i.e.*, 2kV in this case. The annualized total cost is approximately 1.05 million \$/year.

This provides the optimal kV level  $V_{1N}=2$  kV. The reason that the optimal kV level is much smaller than that of most of the other configurations is that the acquisition cost of this configuration is much larger, while the operating cost is much lower.

## 5.5 kV Levels, Equipment Ratings and Wind Farm Cost Analysis of Configuration 5

In this subsection, Configuration 5 is analyzed for the kV levels, equipment ratings, and cost. The configuration is shown in Figure 5.5.1.

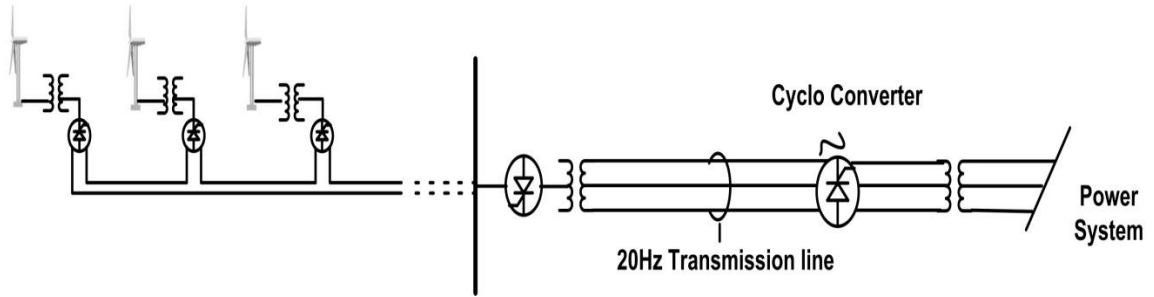


Figure 5.5.1: Alternative Wind Farm Configuration 5

### 5.5.1 Formulation of Operating Cost

The operating cost is formulated for Configuration 5 as below.

$$\text{Operating Cost} = \int_0^{365 \cdot 24} [k(t) \cdot \text{Total Power Loss}(t)] dt = \int_0^{365 \cdot 24} \left[ k(t) \cdot P^2(t) \cdot \left[ m \cdot \left( \frac{r_1}{V_1 N^2} \right) \cdot \frac{(n-1)n(2n-1)}{6} + m \cdot n^2 \cdot \left( \frac{r_2}{V_1 N^2} \right) \right] \right] dt = \left[ m \cdot \left( \frac{r_1}{V_1 N^2} \right) \cdot \frac{(n-1)n(2n-1)}{6} + m \cdot n^2 \cdot \left( \frac{r_2}{V_1 N^2} \right) \right] \cdot \int_0^{365 \cdot 24} [k(t) \cdot P^2(t)] dt \quad (5.5.1)$$

### 5.5.2 Formulation of Acquisition Cost

The main components of the wind farm are:

1. Wind turbine and generator: cost  $C_1$ , expected economic life  $N_1$
2. Power Electronics: cost  $C_2$ , expected economic life  $N_2$
3. Power Circuits: cost  $C_3$ , expected economic life  $N_3$
4. Switchgear at the point of common coupling: cost  $C_4$ , expected economic life  $N_4$

For this specific wind farm with  $n_1$  wind turbine/generators,  $n_2$  power electronics,  $n_3$  power circuits, and  $n_4$  switchgear at the point of common coupling, the annualized acquisition cost, AAC, is:

$$\text{AAC} = \sum_{i=1}^4 [n_i \cdot \text{AAC}_i] = \sum_{i=1}^4 \left[ n_i \cdot \frac{r \cdot (1+r)^{N_i}}{(1+r)^{N_i} - 1} \cdot C_i \right] \quad (5.5.2)$$



### 5.5.3 Formulation of Total Cost as a Function of kV Level

Similar as (5.1.10), the annualized total cost, ATC, is formulated by summing (5.5.1) and (5.5.2). As discussed in the subsections above, the maintenance cost is not to be considered.

$$ATC = \left[ m \cdot \left( \frac{r_1}{V_{1N}^2} \right) \cdot \frac{(n-1)n(2n-1)}{6} + m \cdot n^2 \cdot \left( \frac{r_2}{V_{1N}^2} \right) \right] \cdot \int_0^{365 \cdot 24} [k(t) \cdot P^2(t)] dt + \sum_{i=1}^4 \left[ n_i \cdot \frac{r \cdot (1+r)^{N_i}}{(1+r)^{N_i} - 1} \cdot C_i \right] \quad (5.5.3)$$

### 5.5.4 Example Case of Finding the Optimal kV Level – Configuration 5

In this subsection, a 30 wind turbine example is provided to show the process of finding the optimal kV level of Configuration 5.

The assumed parameters of Configuration 5 are:

- a) Number of parallel lines:  $m = 1$ ;
- b) Number of wind turbines in each Line:  $n = 30$
- c) Rating of wind turbines: 2.2MVA at 25kV;
- d) The distance between the wind turbines is 200ft; the distance from the last turbine to the bus is 500 ft;
- e) The interest rate is 5%, which means,  $r = 0.05$ ;
- f)  $k(t)$  is assumed to be a stable factor,  $k(t) = \$0.1/\text{kwh}$ ;
- g) Based on assumption f),

$$\int_0^{365 \cdot 24} [k(t) \cdot P^2(t)] dt = \int_0^{365 \cdot 24} [0.1 \cdot P^2(t)] dt = 0.1 \cdot \int_0^{365 \cdot 24} [P^2(t)] dt$$

It is in further assumed that  $\int_0^{365 \cdot 24} [P^2(t)] dt = 2 \cdot 10^{10} (\text{kw})^2 \cdot h$ , which is based on the typical distribution of  $P$  over a year. Therefore,

$$\int_0^{365 \cdot 24} [k(t) \cdot P^2(t)] dt = \frac{\$0.1}{\text{kwh}} \cdot 2 \cdot 10^{10} (\text{kw})^2 \cdot h = 2 \cdot 10^9 \text{kw}$$

- h) The life time of the components in years:

Wind turbine and generator:  $N_1=30$

Power Electronics:  $N_2=20$

Power Circuits:  $N_3=40$

Switchgear at the point of common coupling:  $N_4=20$

The analysis process is provided as below.

**Step 1:** Calculate the current range of the cable:  $\frac{30 \cdot 2.2 MVA}{\sqrt{3} \cdot 25 kV} = 1.5 kA$

**Step 2:** Select the cable size and get the resistance value: 2250 kcm copper cable is selected since the current capability of a 2250 kcm copper cable is around 2kA. The resistance value of a 2250 kcm copper cable is obtained: 0.01 ohm/1000ft. Therefore,

$$r_1 = \frac{0.01 ohm}{1000 ft} \cdot 200 ft = 0.002 ohm; r_2 = \frac{0.01 ohm}{1000 ft} \cdot 500 ft = 0.005 ohm$$

**Step 3:** Add the operating cost and annualized acquisition cost to form the annualized total cost: from (5.5.3), the curve is plotted as shown in Figure 5.5.2.

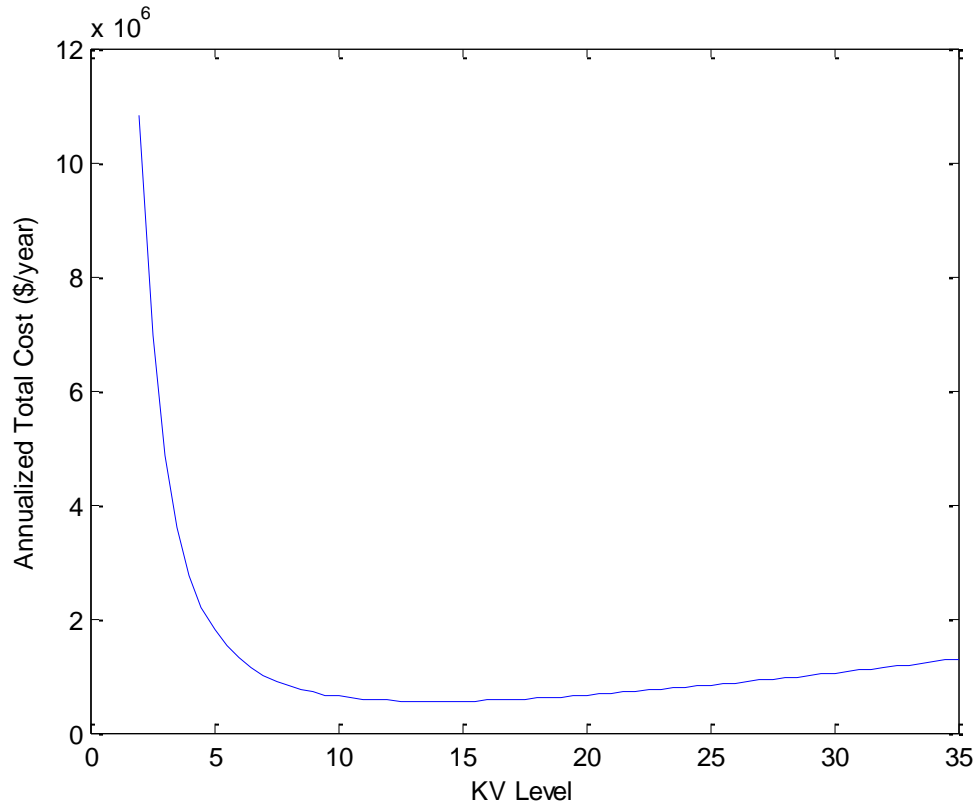


Figure 5.5.2: Annualized Total Cost of Configuration 5

**Step 4:** From Figure 5.5.2, it can be found that the minimum point of the annualized total cost is at at kV level = 18kV, when the annualized total cost = 1.20 million \$/year.

This provides the optimal kV level  $V_{1N}=18$  kV. The reason that the optimal kV level is larger than some of the other configurations is that the operational cost of this configuration is larger.

## 5.6 kV Levels, Equipment Ratings and Wind Farm Cost Analysis of Configuration 6

In this subsection, Configuration 6 is analyzed for the kV levels, equipment ratings, and cost. The configuration is shown in Figure 5.6.1.

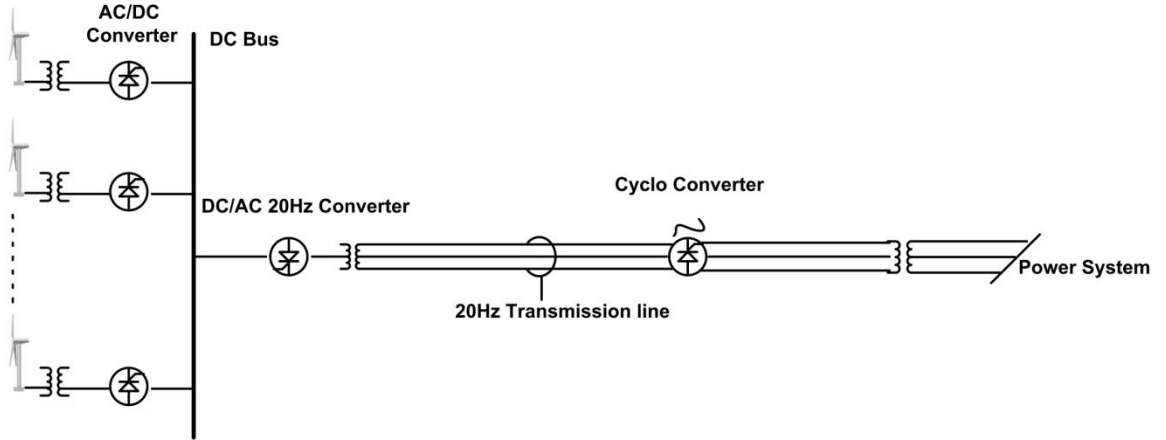


Figure 5.6.1: Alternative Wind Farm Configuration 6

### 5.6.1 Formulation of Operating Cost

The operating cost is formulated for Configuration 5 as below.

$$\text{Operating Cost} = \int_0^{365 \cdot 24} [k(t) \cdot \text{Total Power Loss}(t)] dt = \int_0^{365 \cdot 24} \left[ k(t) \cdot P^2(t) \cdot \left[ m \cdot n \cdot \left( \frac{r_2}{V_{1N}^2} \right) \right] \right] dt = \left[ m \cdot n \cdot \left( \frac{r_2}{V_{1N}^2} \right) \right] \cdot \int_0^{365 \cdot 24} [k(t) \cdot P^2(t)] dt \quad (5.6.1)$$

### 5.6.2 Formulation of Acquisition Cost

The main components of the wind farm are:

1. Wind turbine and generator: cost  $C_1$ , expected economic life  $N_1$
2. Power Electronics: cost  $C_2$ , expected economic life  $N_2$
3. Power Circuits: cost  $C_3$ , expected economic life  $N_3$
4. Switchgear at the point of common coupling: cost  $C_4$ , expected economic life  $N_4$

For this specific wind farm with  $n_1$  wind turbine/generators,  $n_2$  power electronics,  $n_3$  power circuits, and  $n_4$  switchgear at the point of common coupling, the annualized acquisition cost, AAC, is:

$$AAC = \sum_{i=1}^4 [n_i \cdot AAC_i] = \sum_{i=1}^4 [n_i \cdot \frac{r \cdot (1+r)^{N_i}}{(1+r)^{N_i-1}} \cdot C_i] \quad (5.6.2)$$

### 5.6.3 Formulation of Total Cost as a Function of kV Level

Similar as (5.1.10), the annualized total cost, ATC, is formulated by summing (5.6.1) and (5.6.2). As discussed in the subsections above, the maintenance cost is not to be considered.

$$ATC = \left[ m \cdot n \cdot \left( \frac{r_2}{V_1 N^2} \right) \right] \cdot \int_0^{365 \cdot 24} [k(t) \cdot P^2(t)] dt + \sum_{i=1}^4 [n_i \cdot \frac{r \cdot (1+r)^{N_i}}{(1+r)^{N_i-1}} \cdot C_i] \quad (5.6.3)$$

### 5.6.4 Example Case of Finding the Optimal kV Level – Configuration 6

In this subsection, a 30 wind turbine example is provided to show the process of finding the optimal kV level of Configuration 6.

The assumed parameters of Configuration 6 are:

- a) Number of feeders  $m = 30$ ;
- b) Number of wind turbines on each feeder:  $n = 1$
- c) Rating of wind turbines: 2.2MVA at 25kV;
- d) The distance from the turbine to the bus is 500 ft;
- e) The interest rate is 5%, which means,  $r = 0.05$ ;
- f)  $k(t)$  is assumed to be a stable factor,  $k(t) = \$0.1/\text{kwh}$ ;
- g) Based on assumption f),

$$\int_0^{365 \cdot 24} [k(t) \cdot P^2(t)] dt = \int_0^{365 \cdot 24} [0.1 \cdot P^2(t)] dt = 0.1 \cdot \int_0^{365 \cdot 24} [P^2(t)] dt$$

It is in further assumed that  $\int_0^{365 \cdot 24} [P^2(t)] dt = 2 \cdot 10^{10} (\text{kw})^2 \cdot h$ , which is based on the typical distribution of  $P$  over a year. Therefore,

$$\int_0^{365 \cdot 24} [k(t) \cdot P^2(t)] dt = \frac{\$0.1}{\text{kwh}} \cdot 2 \cdot 10^{10} (\text{kw})^2 \cdot h = 2 \cdot 10^9 \text{kw}$$

- h) The life time of the components in years:

Wind turbine and generator:  $N_1=30$

Power Electronics:  $N_2=20$

Power Circuits:  $N_3=40$

Switchgear at the point of common coupling:  $N_4=20$

The analysis process is provided as below.

**Step 1:** Calculate the current range of the cable:  $\frac{2.2MVA}{\sqrt{3} \cdot 25kV} = 51A$

**Step 2:** Select the cable size and get the resistance value: 105.5 kcm aluminum cable is selected. The resistance value of a 105.5 kcm aluminum cable is obtained: 0.07 ohm/1000ft. Therefore,

$$r_2 = \frac{0.07 \text{ ohm}}{1000 \text{ ft}} \cdot 500 \text{ ft} = 0.035 \text{ ohm}$$

**Step 3:** Add the operating cost and annualized acquisition cost to form the annualized total cost: from (5.6.3), the curve is plotted as shown in Figure 5.6.2.

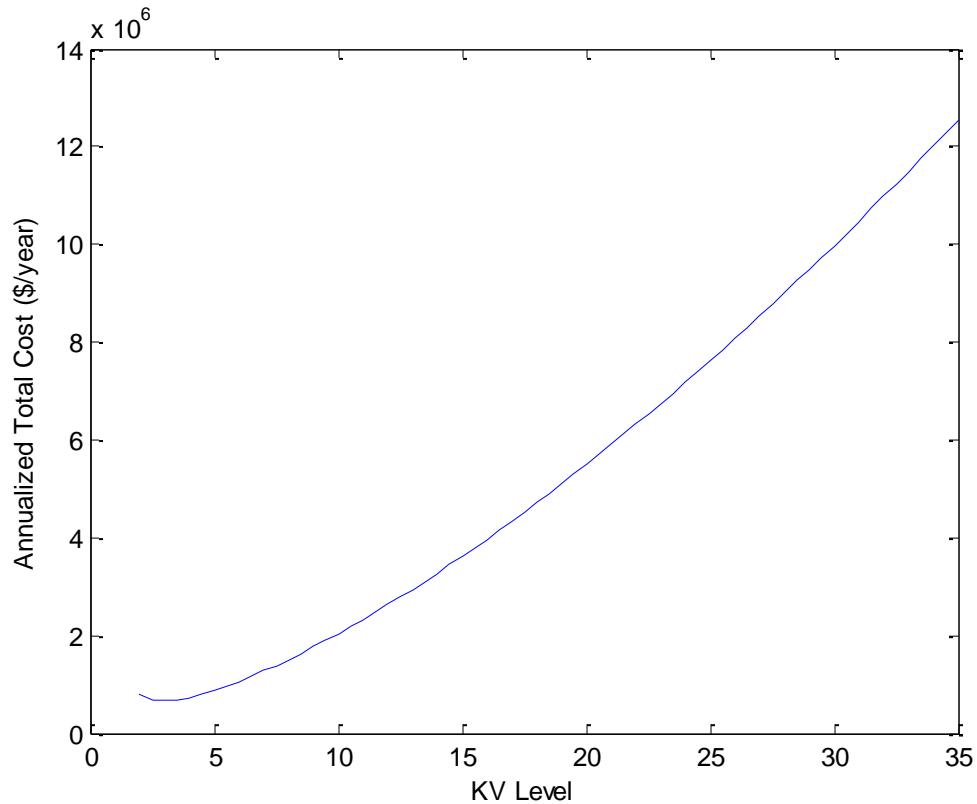


Figure 5.6.2: Annualized Total Cost of Configuration 6

**Step 4:** From Figure 5.6.2, it can be found that the minimum point of the annualized total cost is at kV level = 4kV in this case. The annualized total cost is approximately 0.82 million \$/year.

This provides the optimal kV level  $V_{1N}=4$  kV. The reason that the optimal kV level is much smaller than that of most of the other configurations is that the acquisition cost of this configuration is much larger, while the operating cost is much lower.

## 5.7 kV Levels, Equipment Ratings and Wind Farm Cost Analysis of Configuration 7

In this subsection, Configuration 7 is analyzed for the kV levels, equipment ratings, and cost. The configuration is shown in Figure 5.7.1.

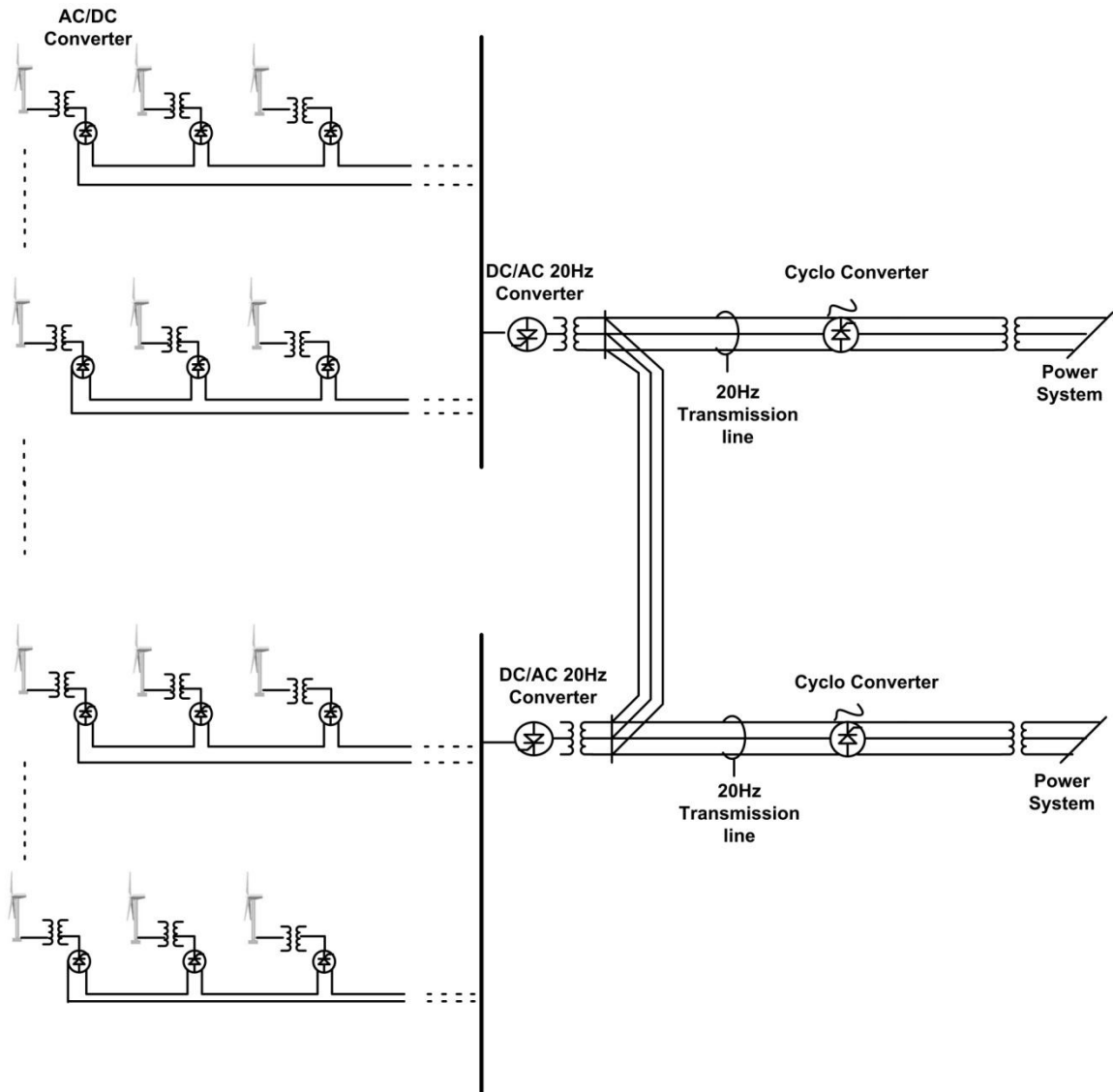


Figure 5.7.1: Alternative Wind Farm Configuration 7

### 5.7.1 Formulation of Operating Cost

The operating cost is formulated for Configuration 7 as below.

$$\text{Operating Cost} = \int_0^{365 \cdot 24} [k(t) \cdot \text{Total Power Loss}(t)] dt = \int_0^{365 \cdot 24} \left[ k(t) \cdot P^2(t) \cdot \left[ m \cdot \left( \frac{r_1}{V_{1N}^2} \right) \cdot \frac{(n-1)n(2n-1)}{6} + m \cdot n^2 \cdot \left( \frac{r_2}{V_{1N}^2} \right) \right] \right] dt = \left[ m \cdot \left( \frac{r_1}{V_{1N}^2} \right) \cdot \frac{(n-1)n(2n-1)}{6} + m \cdot n^2 \cdot \left( \frac{r_2}{V_{1N}^2} \right) \right] \cdot \int_0^{365 \cdot 24} [k(t) \cdot P^2(t)] dt \quad (5.7.1)$$

### 5.7.2 Formulation of Acquisition Cost

The main components of the wind farm are:

1. Wind turbine and generator: cost  $C_1$ , expected economic life  $N_1$
2. Power Electronics: cost  $C_2$ , expected economic life  $N_2$
3. Power Circuits: cost  $C_3$ , expected economic life  $N_3$
4. Switchgear at the point of common coupling: cost  $C_4$ , expected economic life  $N_4$

For this specific wind farm with  $n_1$  wind turbine/generators,  $n_2$  power electronics,  $n_3$  power circuits, and  $n_4$  switchgear at the point of common coupling, the annualized acquisition cost, AAC, is:

$$\text{AAC} = \sum_{i=1}^4 [n_i \cdot \text{AAC}_i] = \sum_{i=1}^4 \left[ n_i \cdot \frac{r \cdot (1+r)^{N_i}}{(1+r)^{N_i-1}} \cdot C_i \right] \quad (5.7.2)$$

### 5.7.3 Formulation of Total Cost as a Function of kV Level

Similar as (5.1.10), the annualized total cost, ATC, is formulated by summing (5.7.1) and (5.7.2). As discussed in the subsections above, the maintenance cost is not to be considered.

$$\text{ATC} = \left[ m \cdot \left( \frac{r_1}{V_{1N}^2} \right) \cdot \frac{(n-1)n(2n-1)}{6} + m \cdot n^2 \cdot \left( \frac{r_2}{V_{1N}^2} \right) \right] \cdot \int_0^{365 \cdot 24} [k(t) \cdot P^2(t)] dt + \sum_{i=1}^4 \left[ n_i \cdot \frac{r \cdot (1+r)^{N_i}}{(1+r)^{N_i-1}} \cdot C_i \right] \quad (5.7.3)$$

### 5.7.4 Example Case of Finding the Optimal kV Level – Configuration 7

In this subsection, a 30 wind turbine example is provided to show the process of finding the optimal kV level of Configuration 7.

The assumed parameters of Configuration 7 are:

- a) Number of Buses: 1; Number of parallel lines connected to a bus:  $m = 3$ ;
- b) Number of wind turbines in each Line:  $n = 10$

- c) Rating of wind turbines: 2.2MVA at 25kV;
- d) The distance between the wind turbines is 200ft; The distance from the last turbine to the bus is 500 ft;
- e) The interest rate is 5%, which means,  $r = 0.05$ ;
- f)  $k(t)$  is assumed to be a stable factor,  $k(t) = \$0.1/\text{kwh}$ ;
- g) Based on assumption f),

$$\int_0^{365 \cdot 24} [k(t) \cdot P^2(t)] dt = \int_0^{365 \cdot 24} [0.1 \cdot P^2(t)] dt = 0.1 \cdot \int_0^{365 \cdot 24} [P^2(t)] dt$$

It is in further assumed that  $\int_0^{365 \cdot 24} [P^2(t)] dt = 2 \cdot 10^{10} (\text{kw})^2 \cdot h$ , which is based on the typical distribution of  $P$  over a year. Therefore,

$$\int_0^{365 \cdot 24} [k(t) \cdot P^2(t)] dt = \frac{\$0.1}{\text{kwh}} \cdot 2 \cdot 10^{10} (\text{kw})^2 \cdot h = 2 \cdot 10^9 \text{kw}$$

- h) The life time of the components in years:

Wind turbine and generator:  $N_1=30$

Power Electronics:  $N_2=20$

Power Circuits:  $N_3=40$

Switchgear at the point of common coupling:  $N_4=20$

The analysis process is provided as below.

**Step 1:** Calculate the current range of the cable:  $\frac{10 \cdot 2.2 \text{MVA}}{\sqrt{3} \cdot 25 \text{kV}} = 0.5 \text{kA}$

**Step 2:** Select the cable size and get the resistance value: 350 kcm copper cable is selected since the current capability of a 350 kcm copper cable is around 550A. The resistance value of a 350 kcm copper cable is obtained: 0.03 ohm/1000ft. Therefore,

$$r_1 = \frac{0.03 \text{ohm}}{1000 \text{ft}} \cdot 200 \text{ft} = 0.006 \text{ohm}; r_2 = \frac{0.03 \text{ohm}}{1000 \text{ft}} \cdot 500 \text{ft} = 0.015 \text{ohm}$$

**Step 3:** Add the operating cost and annualized acquisition cost to form the annualized total cost: from (5.7.3), the curve is plotted as shown in Figure 5.7.2.



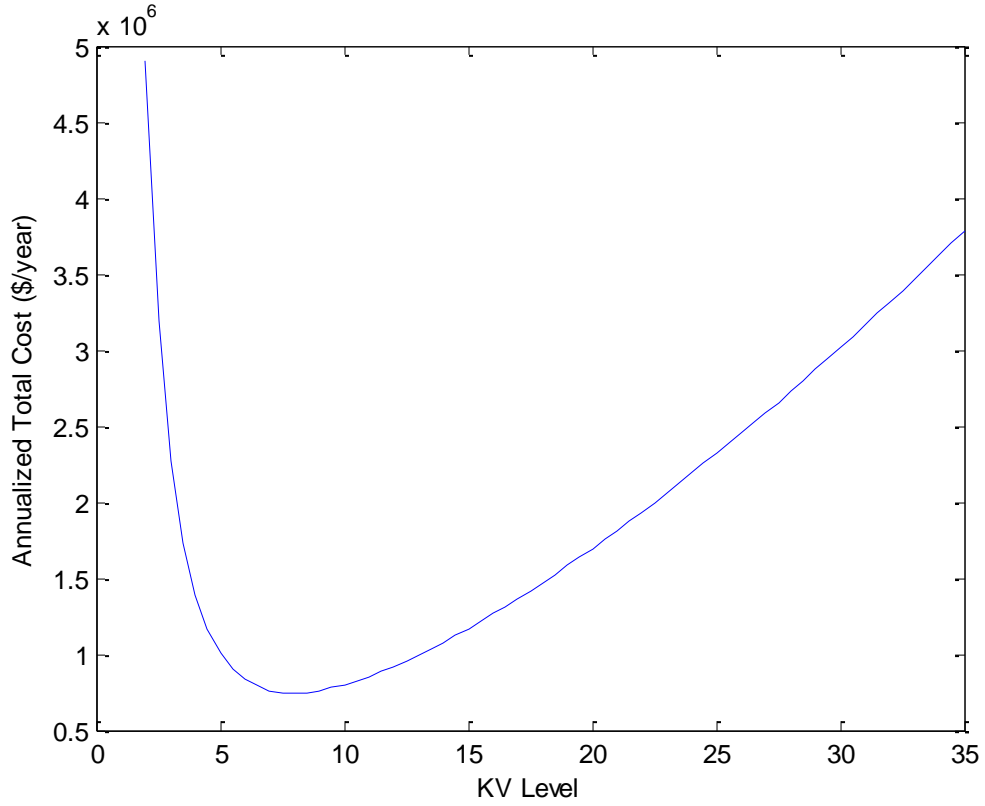


Figure 5.7.2: Annualized Total Cost of Configuration 7

**Step 4:** From Figure 5.7.2, it can be found that the minimum point of the annualized total cost is at kV level = 7kV, when the annualized total cost = 0.75 million \$/year.

This provides the optimal kV level  $V_{1N}=7$  kV. The reason that the optimal kV level is smaller than that of Configuration 1 and 2 is that the acquisition cost of this configuration is larger than Configuration 1 and 2, since more electronic devices are added to achieve the in-farm DC transmission.

## 5.8 kV Levels, Equipment Ratings and Wind Farm Cost Analysis of Configuration 8

In this subsection, Configuration 8 is analyzed for the kV levels, equipment ratings, and cost. The configuration is shown in Figure 5.8.1.

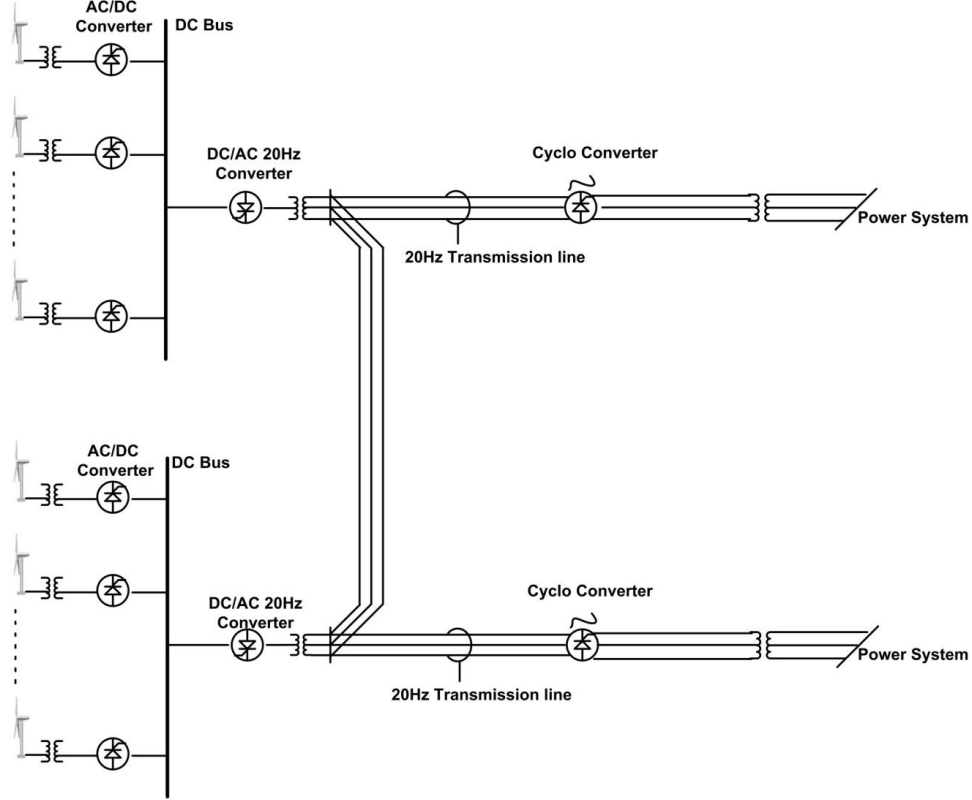


Figure 5.8.1: Alternative Wind Farm Configuration 8

### 5.8.1 Formulation of Operating Cost

The operating cost is formulated for Configuration 8 as below.

Operating Cost

$$= \int_0^{365 \cdot 24} [k(t) \cdot \text{Total Power Loss}(t)] dt = \int_0^{365 \cdot 24} \left[ k(t) \cdot P^2(t) \cdot \left[ m \cdot n \cdot \left( \frac{r_2}{V_{1N}^2} \right) \right] \right] dt = \left[ m \cdot n \cdot \left( \frac{r_2}{V_{1N}^2} \right) \right] \cdot \int_0^{365 \cdot 24} [k(t) \cdot P^2(t)] dt \quad (5.8.1)$$

### 5.8.2 Formulation of Acquisition Cost

The main components of the wind farm are:

1. Wind turbine and generator: cost  $C_1$ , expected economic life  $N_1$

2. Power Electronics: cost  $C_2$ , expected economic life  $N_2$
3. Power Circuits: cost  $C_3$ , expected economic life  $N_3$
4. Switchgear at the point of common coupling: cost  $C_4$ , expected economic life  $N_4$

For this specific wind farm with  $n_1$  wind turbine/generators,  $n_2$  power electronics,  $n_3$  power circuits, and  $n_4$  switchgear at the point of common coupling, the annualized acquisition cost, AAC, is:

$$AAC = \sum_{i=1}^4 [n_i \cdot AAC_i] = \sum_{i=1}^4 [n_i \cdot \frac{r \cdot (1+r)^{N_i}}{(1+r)^{N_i} - 1} \cdot C_i] \quad (5.8.2)$$

### 5.8.3 Formulation of Total Cost as a Function of kV Level

Similar as (5.1.10), the annualized total cost, ATC, is formulated by summing (5.8.1) and (5.8.2). As discussed in the subsections above, the maintenance cost is not to be considered.

$$ATC = \left[ m \cdot n \cdot \left( \frac{r_2}{V_{1N}^2} \right) \right] \cdot \int_0^{365 \cdot 24} [k(t) \cdot P^2(t)] dt + \sum_{i=1}^4 [n_i \cdot \frac{r \cdot (1+r)^{N_i}}{(1+r)^{N_i} - 1} \cdot C_i] \quad (5.8.3)$$

### 5.8.4 Example Case of Finding the Optimal kV Level – Configuration 8

In this subsection, a 30 wind turbine example is provided to show the process of finding the optimal kV level of Configuration 8.

The assumed parameters of Configuration 8 are:

- a) Number of buses:  $m = 3$ ;
- b) Number of wind turbines connecting to each bus:  $n = 10$ ;
- c) Rating of wind turbines: 2.2MVA at 25kV;
- d) The distance from the last turbine to the bus is 500 ft;
- e) The interest rate is 5%, which means,  $r = 0.05$ ;
- f)  $k(t)$  is assumed to be a stable factor,  $k(t) = \$0.1/\text{kwh}$ ;
- g) Based on assumption f),

$$\int_0^{365 \cdot 24} [k(t) \cdot P^2(t)] dt = \int_0^{365 \cdot 24} [0.1 \cdot P^2(t)] dt = 0.1 \cdot \int_0^{365 \cdot 24} [P^2(t)] dt$$

It is in further assumed that  $\int_0^{365 \cdot 24} [P^2(t)] dt = 2 \cdot 10^{10} (\text{kw})^2 \cdot h$ , which is based on the typical distribution of  $P$  over a year. Therefore,

$$\int_0^{365 \cdot 24} [k(t) \cdot P^2(t)] dt = \frac{\$0.1}{\text{kwh}} \cdot 2 \cdot 10^{10} (\text{kw})^2 \cdot h = 2 \cdot 10^9 \text{kw}$$

**h)** The life time of the components in years:

Wind turbine and generator:  $N_1=30$

Power Electronics:  $N_2=20$

Power Circuits:  $N_3=40$

Switchgear at the point of common coupling:  $N_4=20$

The analysis process is provided as below.

**Step 1:** Calculate the current range of the cable:  $\frac{2.2MVA}{25kV} = 88A$

**Step 2:** Select the cable size and get the resistance value: 105.5 kcm aluminum cable is selected. The resistance value of a 105.5 kcm aluminum cable is obtained: 0.07 ohm/1000ft. Therefore,;

$$r_2 = \frac{0.07ohm}{1000ft} \cdot 500ft = 0.035 ohm$$

**Step 3:** Add the operating cost and annualized acquisition cost to form the annualized total cost: from (5.8.3), the curve is plotted as shown in Figure 5.8.2.

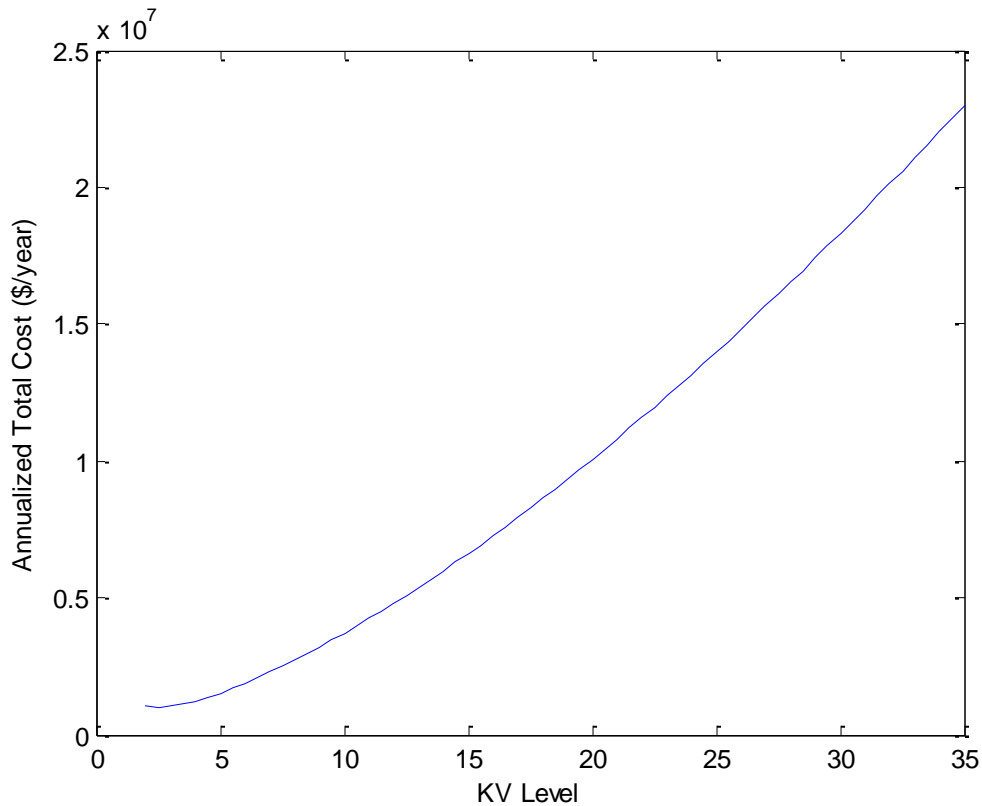


Figure 5.8.2: Annualized Total Cost of Configuration 8

**Step 4:** From Figure 5.8.2, it can be found that the minimum point of the annualized total cost is hard to be determined based on the minimum of the total cost. The kV level is selected to be the lowest value in the accepted range, *i.e.*, 2kV in this case. The annualized total cost is approximately 1.25 million \$/year.

This provides the optimal kV level  $V_{1N}=2$  kV. The reason that the optimal kV level is much smaller than that of most of the other configurations is that the acquisition cost of this configuration is much larger, while the operating cost is much lower.

## 5.9 Summary and Conclusions

Section 5 provides the mathematical formulation of the method to obtain the optimal kV level for the alternative wind farm configurations. The optimal kV level is derived based on the minimum of the annual total cost. For each configuration, the annual total cost is formulated, and a 30 wind turbine example is studied. Table 5.9.1 provides the summary of the kV level selection results from the case studies of the 8 configurations.

Table 5.9.1: Summary of kV Level Selection Results of the 8 Configurations

Configuration	kV Level Selection	Minimum Annualized Total Cost (M\$/year)
1	12	0.48
2	10	0.50
3	8	0.52
4	2	1.05
5	18	1.20
6	4	0.82
7	7	0.75
8	2	1.25

## 6 Operational Studies – Power Transfer Capability

This section provides the maximum power transfer capability (MPTC) of the alternative transmission configurations that involve AC transmission or LFAC transmission (with three-phase, six-pulse cycloconverters). Power transfer capability is the quantitative analysis of the ability of interconnected electric systems to transfer electrical power from one place to another under operational constraints. The operational constraints are the physical and electrical limitations to assure robust and secure operation of systems [43]. Here, we consider several constraints such as operational margins of converters interconnecting transmission systems between wind farms and load center and voltage-drop margins on transmission lines. The maximum power transfer capability is decided under the most restrictive one among the several constraints.

### 6.1 Technical Approach of Power Transfer Capability Study

The study of the power transfer capability is performed using two transmission systems, which interconnect a wind farm and a load center as shown in Figure 6.1.1: . Type 1 is a general transmission system to transfer 60 Hz electrical power and Types 2 is a LFAC transmission system using converters. The type 1 consists of three-phase overhead transmission lines and a three-phase step-up transformer, and the type 2 is composed of three-phase overhead transmission line, a three-phase step-up transformer, a three-phase PWM inverter, and a three-phase, six-pulse cycloconverter.

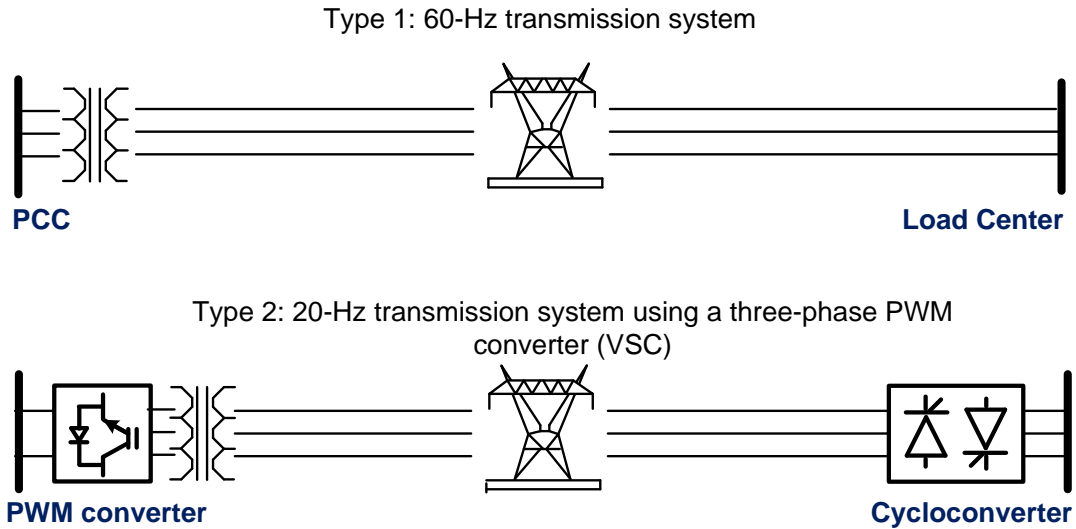


Figure 6.1.1: Two Types of Transmission Configurations for Case Studies

The models are first developed in steady state, since the MPTC study is quantitative analysis: frequency-domain overhead transmission lines and three-phase transformers, and frequency-domain converter models in averaging concepts. Since the overhead

transmission line and the three-phase transformer are used for both transmission systems, the models have to support the operations in variable frequencies, and converter models have to support 20 Hz operation. The three-phase PWM inverter has the ability to control DC-voltage level and reactive power at the three-phase side, and the cycloconverter controls the three-phase voltages at low-frequency side. Note that the three-phase PWM inverter is automatically synchronized to the voltages generated by the cycloconverter.

For the MPTC study, we consider three constraints: voltage limit, and DC-voltage limit, and modulation-index limits of both converters. The mathematical notations are as follows:

$$MPTC = \text{minimum}\{AC\text{-voltage limit, DC-voltage limit, modulation index limits, etc.}\}$$

The maximum power transfer capability is the maximum power that satisfies all the constraints. That is, the maximum power transfer capability is decided under the most restrictive one among the three constraints [43].

## 6.2 Methodology for Simulation Models in Steady State

The study of the MPTC is based on computer analysis in steady state. For the purpose, the federal and efficiency models for the proposed configurations are needed. Here, we introduce quadratic models of converters, transformers, and transmission lines. In this method, the state equations of the each device are reformulated as a set of linear and quadratized equations, in which highest order is not greater than two, by introducing additional state variables. The advantage of this formulation is that quadratic models can easily be denoted by a combination of either linear or quadratic equations and the quadratic equations have demonstrated the superior convergence to exact solutions with the application of Newton's method, one of the iterative methods. The Newton's method is ideally suited for solution of quadratic equations. The modeling process is as follows:

- Step 1:** Represent the state equations of each device in phasor representation;
- Step 2:** Reformulate the state equations into quadratized equations;
- Step 3:** Merge each devices into a network system using Kirchhoff's current law;
- Step 4:** Solve the network systems using the Newton's method.

The quadratization method can be easily used for nonlinear components without assumptions such as linearization of nonlinear equations. Therefore, the quadratization method has demonstrated as the federal and efficiency simulation method for steady-state models with nonlinear equations, such as converters and saturable transformers.

### 6.2.1 Frequency Domain Model: Transformer and Transmission Line

Three-phase transformer and transmission-line models are presented in this subsection as shown in Figure 6.2.1 and Figure 6.2.2 The frequency-domain models of the transformer and the transmission line are represented under steady-state, balanced conditions. The

formulation and solution methods of the frequency-domain models are important for reliable and efficiency modeling. The formulation of the frequency-domain models is based on two concepts: (1) the mathematical models characterizing the devices are represented in polar forms, which may contain either linear equations or nonlinear equations, and (2) The nonlinear equations are reformulated into quadratized equations of highest order 2. In the general compact form of each device, the linear and quadratized equations are denoted as follows:

$$\begin{bmatrix} I_r \\ I_i \\ 0 \end{bmatrix} = y_{eq} \begin{bmatrix} V_r \\ V_i \\ y \end{bmatrix} + \begin{bmatrix} x^T \cdot f_{eq1} \cdot x \\ x^T \cdot f_{eq1} \cdot x \\ \vdots \\ 0 \end{bmatrix} - b_{eq}, \quad \text{Where: } x = \begin{bmatrix} V_r \\ V_i \\ y \end{bmatrix}, \quad (6.2.1)$$

$x$  is the state variable,  $y_{eq}$  is a matrix form for linear parts,  $f_{eq}$  is a matrix form for nonlinear parts, and  $b_{eq}$  is previous data, control references, etc..

To solve the network system, all components, which are represented by the general compact form, are merged based on Kirchhoff's current law. In this process, the through variables, which might be currents at nodes in the models, become zero and the state variables, which might be internal and external states, are left in the general compact form for the entire network system. Since the general compact form contains nonlinear components, the network system cannot be solved in explicit calculations and iterative method is needed. Here we use Newton's method to solve the network system. Note that the convergence characteristics of the quadratized equations are superior, compared with other methods.



Copy Print Help

### 3-Phase Transformer

Transformer (2-Winding, 3-Phase)

**Side 1 Bus**

NEWBUS1

115.0 kV

☒ Delta ☐ Wye

**Side 2 Bus**

NEWBUS2

25.0 kV

☐ Delta ☒ Wye

**Phase Connection**

☒ Standard ☐ Alternate

Transformer Rating (MVA)	100.0	Tap Setting (pu)	1.0
Winding Resistance (pu)	0.01	Minimum (pu)	1.0
Leakage Reactance (pu)	0.1	Maximum (pu)	1.0
Nominal Core Loss (pu)	0.005	Number of Taps	1
Nominal Magnetizing Current (pu)	0.005	Circuit Number	1

WinIGS-F - Form: IGS\_M104 - Copyright ?A. P. Meliopoulos 1998-2011

Figure 6.2.1: Three-Phase Transformer

### 3-Phase Overhead Transmission Line

3-Phase Overhead Transmission Line

**Phase Conductors**

Type: ACSR  
Size: JOREE

**Shields/Neutrals**

Type: HS  
Size: 5/16HS

**Tower/Pole**

Type: 101A  
Circuit Number: 1

Structure Name: N/A

**Tower/Pole Ground Impedance (Ohms)**

R = 25.0 X = 0.0

Get From GIS

Line Length (miles): 10.0  
Line Span Length (miles): 0.1  
Soil Resistivity (Ohm-Meters): 100.0

GA Power H-Frame Wood Pole TOWER

**Bus Name, Side 1**

NEWBUS2

**Circuit Number**

1

**Bus Name, Side 2**

NEWBUS3

**Failure & Repair Rates**

Failure Rate (per year): 1.0

Repair Rate (per year): 1.0

☐ Insulated Shields  
☐ Transposed Phases  
☐ Transposed Shields

Read GPS Coordinates

**Operating Voltage (kV)**

100.0

**Insulation Levels (kV)**

FOW (Front of Wave): 100.0  
BIL (Basic Insulation Level): 100.0  
AC (AC Withstand): 100.0

WinIGS-F - Form: IGSF\_M102 - Copyright ?A. P. Meliopoulos 1998-2011

Figure 6.2.2: Three-Phase Overhead Transmission Line

**Three-phase transformer:** The frequency-domain three-phase transformer is derived from combining three single-phase transformer models. The single-phase model is based on the equivalent circuit illustrated in Figure 6.2.3. Note  $Y_l$  and  $Y_2$  are winding leakage admittances and  $Y_m$  is magnetic leakage admittance in the figure.

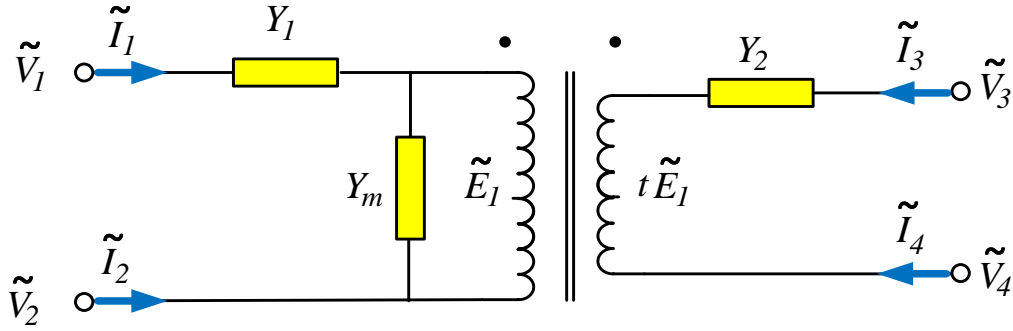


Figure 6.2.3: The Equivalent Circuit of a Single-Phase Transformer

Based on the equivalent circuit, the single-phase transformer is written by state equations (over Cartesian coordinates), and the nonlinear terms can be quadratized. After modeling a single-phase transformer, three single-phase transformers are combined by using standard Kirchhoff's laws to form a three-phase transformer according to appropriate phase connections, such as *Wye-Wye*, *Wye-Delta*, *Delta-Wye*, and *Delta-Delta*.

**Overhead transmission line:** Three-phase overhead transmission line is exactly represented the combination of voltages and currents with uniformly distributed parameters. However, for the familiarity and simplicity of engineers with circuits, an alternative representation of the transmission line can be formulated as pi-equivalent circuit as shown in Figure 6.2.4.

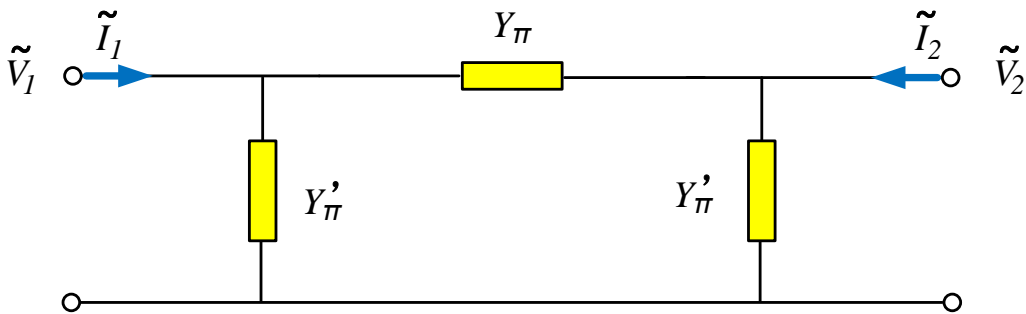


Figure 6.2.4: The PI-Equivalent Circuit of a Single Phase Line

To introduce the pi-equivalent circuit, a conductor line can be first represented in the ABC parameter model as follows:

$$\tilde{I}_1 = \frac{A}{B}\tilde{V}_1 - \frac{1}{B}\tilde{V}_2 \quad (6.2.2)$$

$$\tilde{I}_2 = -\frac{1}{B}\tilde{V}_1 + \frac{A}{B}\tilde{V}_2 \quad (6.2.3)$$

where:  $I_1$ , and  $V_1$  is the current and voltage at the sending terminal of the two-port circuit,  $I_2$ , and  $V_2$  is the current and voltage at the receiving terminal of the two-port

circuit,  $A = \cosh(p\ell)$ ,  $B = Z_0 \sinh(p\ell)$ ,  $p = \sqrt{zy}$ ,  $Z_0 = \sqrt{\frac{z}{y}}$ ,  $\ell$  is the length of the conductor line,  $z = r + j\omega L$ , and  $y = G + j\omega C$ .

Note that the  $p$  is the line propagation constant, and  $Z_0$  is the characteristic impedance of the conductor line. The ABC parameter model can be denoted by the general form for pi-equivalent circuit as follows:

$$\tilde{I}_1 = (Y_\pi + Y'_\pi)\tilde{V}_1 - Y_\pi\tilde{V}_2 \quad (6.2.4)$$

$$\tilde{I}_2 = -Y_\pi\tilde{V}_1 + (Y_\pi + Y'_\pi)\tilde{V}_2 \quad (6.2.5)$$

where  $Y_\pi = \frac{1}{B}$ , and  $Y'_\pi = \frac{A-1}{B}$ .

Since a three-phase line can be composed of three single-phase lines by means of the symmetrical component transformation, the extension to three-phase lines will be omitted in this technical report. However, we present three-phase pi-equivalent circuits of three different transmission lines (of 115kV, 230kV, and 345kV) as shown from Figure 6.2.5 to Figure 6.2.7. The length of the lines is 100-miles in the figures. Note that despite the same conduction-line, the parameters of three-phase pi-equivalent circuits vary according to the lengths of transmission lines and operational frequencies.

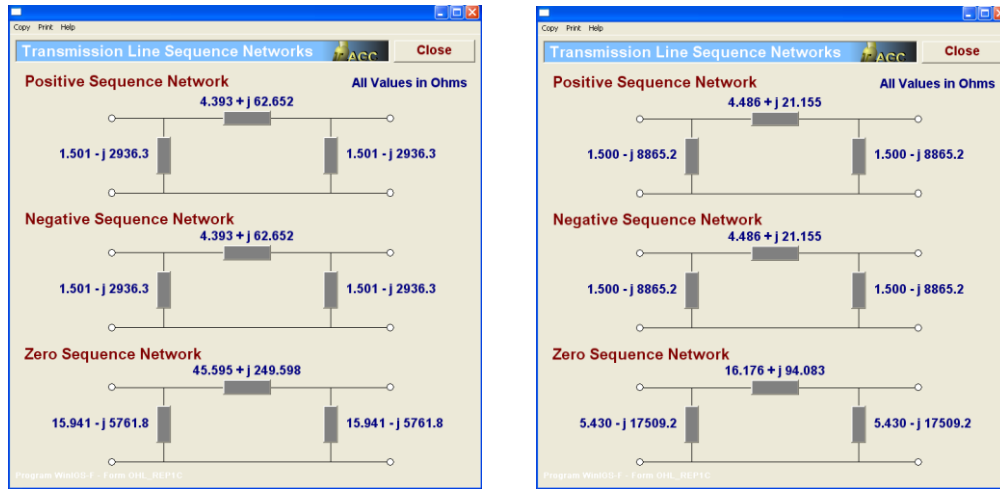


Figure 6.2.5: 115-kV Overhead Transmission Line: Left figure: equivalent circuit at 60 Hz. Right figure: equivalent circuit at 20 Hz.

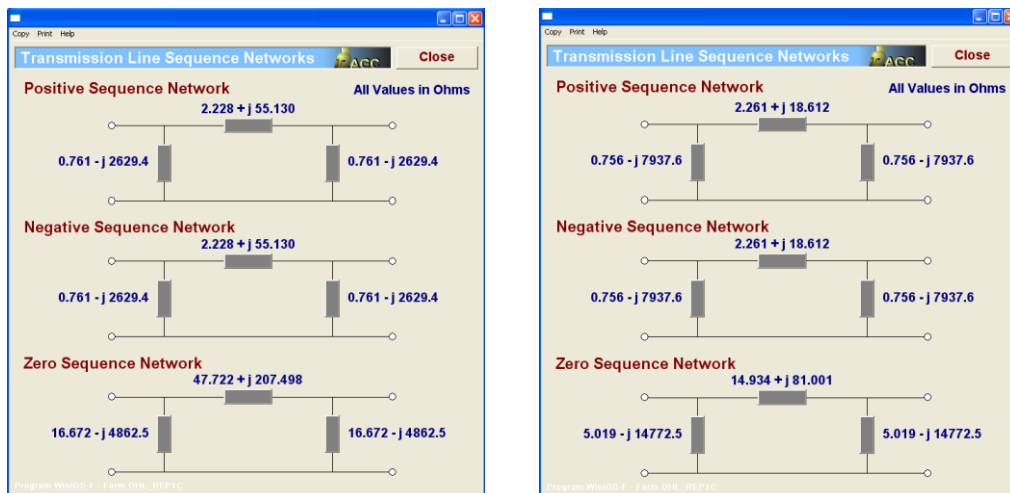


Figure 6.2.6: 230-kV Overhead Transmission Line: Left figure: equivalent circuit at 60 Hz. Right figure: equivalent circuit at 20 Hz.

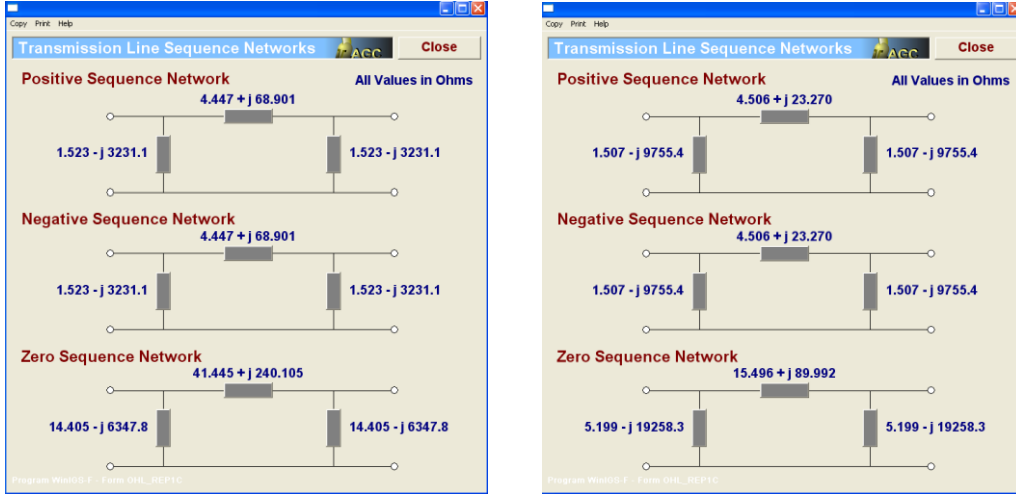


Figure 6.2.7: 345-kV Overhead Transmission Line: Left figure: equivalent circuit at 60 Hz. Right figure: equivalent circuit at 20 Hz.

## 6.2.2 Averaging Model: Converters

A method for modeling converters, which is named as averaging method, is presented in this subsection. The averaging method is based on the steady-state analysis and the equivalent relationship between input and output (two-port network analysis). In these averaging concepts, the voltage and current ripples are averaged and harmonics at three-phase side(s) are ignored. Note that the dynamic behaviors, such as switching operation and transient phenomena, are not in consideration for the averaging converter models. However, this method has the distinct advantages to quantitative analysis such as power transfer capability, total operational losses, and optimal kV-level studies of networks.

Here, we develop three converters: a phase-controlled six-pulse converter, a phase-controlled cycloconverter, and a PWM converter as shown in Figure 6.2.8. For averaging models of the three converters, some assumptions are needed: (1) the voltages and currents at the three-phase side(s) are assumed to be pure sinusoids and to be balanced, (2) each converter is controlled by a specific control algorithm, and (3) inductance and resistance are considered with approximate values. Note that the inductance is derived from limiting current circuits and filter inductances and the resistance can be approximated by the sum in electrical losses in snubber circuits, current limiting circuits, and electrical switches.

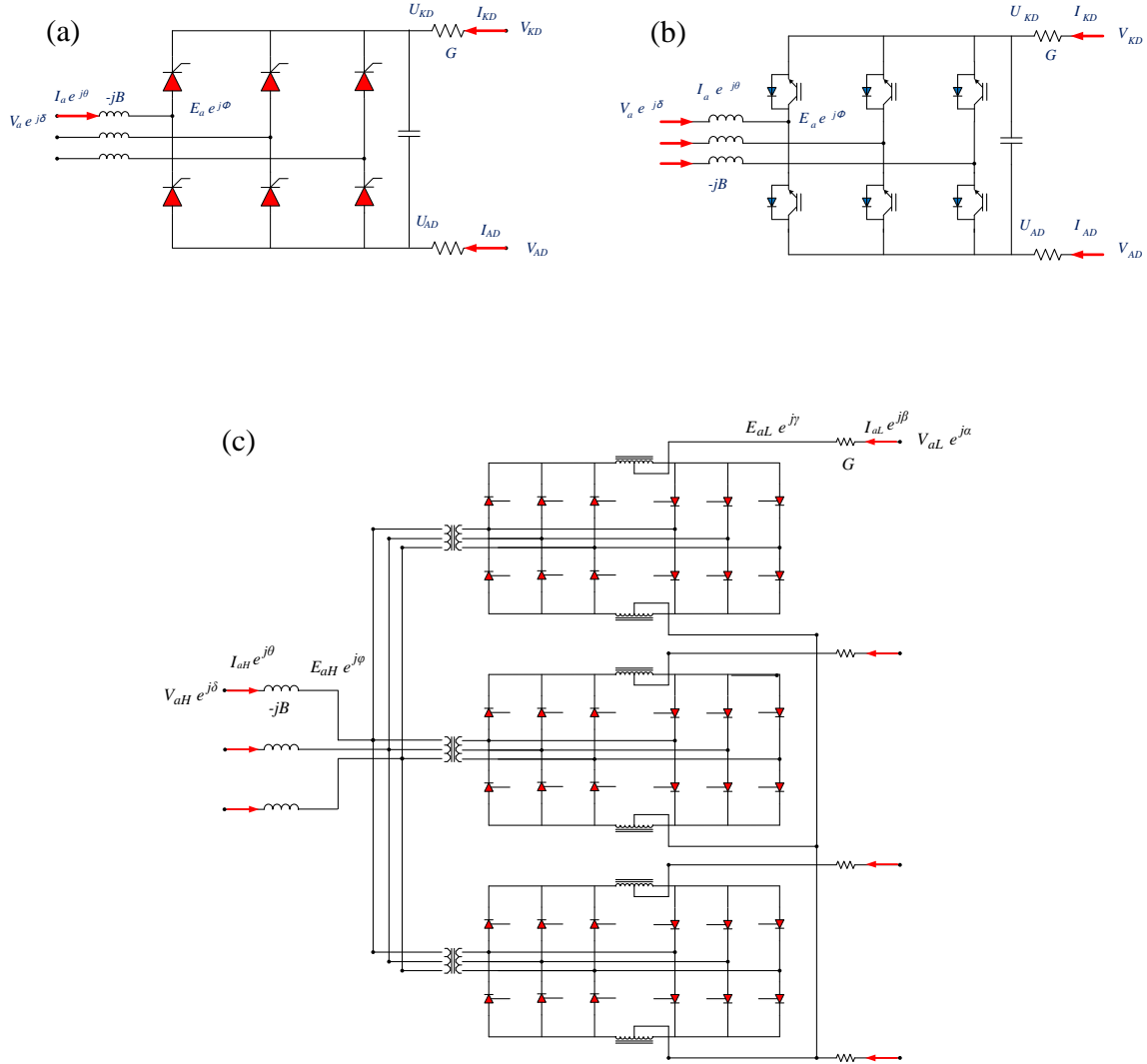


Figure 6.2.8: Power Electronic Systems (a) Three-Phase, Six-Pulse Converter, (b) Three-Phase, PWM Converter, and (c) Three-Phase, Six-Pulse Cycloconverter

The proposed averaging converters are modeled in the following details.

**Six-pulse converter:** The three-phase, six-pulse converter is based on an equidistant-firing control. The firing pulses for thyristors are generated at equal intervals of  $60^\circ$ , and all firings are delayed by equal delay angle  $\alpha$ . In the control algorithm, the voltage relationship can be denoted as follows:

$$V_{dc} = \frac{3\sqrt{2}}{\pi} v_{LL} \cos \alpha \text{ or } V_{dc} = \frac{3\sqrt{2}}{\pi} v_{LL} \cos \gamma, \quad (6.2.6)$$

where  $V_{LL}$  is the RMS value of the line-to-line voltage,  $V_{dc}$  is the DC-voltage, and  $\gamma$  is extinction angle that used for the inverter mode of the six-pulse converter.

As seen in the equation above, the DC-voltage can be controlled by the combination of the Line-to-Line voltage and the firing delay angle. Even though the DC-voltage or real power of the six-pulse converter can be easily controlled by regulating the firing delay angle, the reactive power cannot be controlled (but the imaginary power can be roughly controlled by the combination of transformer's tap control and firing angle control). That is why the system needs FACTS devices to compensate the imaginary power at three-phase lines.

**PWM converter:** The three-phase PWM converter is based on the Space-vector modulation (SVM) control algorithm, since the converter connected to PCC is a grid side converter (GSC). In this control algorithm, the voltage relationship can be presented by the combinations of the modulation index ( $m$ ) and the DC-voltage as follows:

$$\sqrt{2} \cdot V_{LL} = V_{dc} \cdot m \quad (6.2.7)$$

where  $V_{LL}$  is the RMS value of the line-to-line voltage,  $V_{dc}$  is the DC voltage, and  $m$  is modulation index. Note the modulation index can be regulated between 0 and 1.

Here, we develop two control modes: a real-power and reactive-power control mode (PQ-control mode) and a DC-voltage and reactive control mode (VQ-control mode). Generally, the GSC is controlled by using the VQ-control mode, since the GSC has to support the DC-voltage level at the PCC; and the stator-side converters (SSC) are controlled by using the PQ-control mode, since the SSCs have to support maximum power extraction from wind turbines. Also, the PWM converter has the controllability to regulate reactive power at three-phase lines, which is the main difference from the six-pulse converter.

**Six-pulse cycloconverter:** The three-phase, six-pulse cycloconverter in this technical report is based on the two concepts: (1) The converter is operated in the circulating current-free mode, and (2) the control algorithm is assumed to be the cosine-wave crossing method. The cycloconverter model is more complicate compared to previous models, since the reactive power at the both sides is not the same as the each other. So, the power factor has to be computed using the relationship between the input current and the output current. The relationship is denoted as follows:

$$I_p = 6 \frac{r\sqrt{3}}{2\pi} I_o \cos \phi_o \quad (6.2.8)$$

$$I_q = 6 \frac{2\sqrt{3}}{\pi^2} I_o \sum_{n=0}^{n=\infty} \frac{-a_{1_{2n}} \cos 2n\phi_o}{(2n-1)(2n+1)} \quad (6.2.9)$$

where  $I_o$  is the RMS current at output,  $\cos \phi_o$  is the power factor at output, and  $r$  is the modulation index that is computed as  $r = \frac{V_{a-output}}{V_{LL-input} \cdot \cos 30^\circ}$ .

The  $I_p$  and  $I_q$  are the in-phase current and the lagging quadrature current at the input side of the cycloconverter, respectively. Using the two currents, the displacement factor at the input can be computed as follows:

$$\cos \phi_i = \frac{I_p}{\sqrt{I_p^2 + I_q^2}} \quad (6.2.10)$$

where  $\cos \phi_i$  is the displacement factor at input.

The cycloconverter can control the voltage level and reactive power at output side by regulating control references (voltage magnitude and phase angle at the output side). However, the reactive power at the input side cannot be controlled and can be only automatically regulated according to the modulation index and the displacement factor at the output side. For example, while the modulation index is 1 and the displacement factor at output is 1, the displacement angle at the input side is  $34.5^\circ$ . Note that the displacement angle at input always exists between  $34.5^\circ$  and  $145.5^\circ$  [44]. Since the cycloconverter cannot control the imaginary power at input, the three-phase lines at input need a FACTS device as the six-pulse converter.

### 6.3 Case Studies of Power-Transfer Capability

The study of the maximum power transfer capability is based on computer analysis. The quantity of the power transfer is a scalar parameter which can be varied in the computer model. The amount of transfer is gradually increased from the minimum quantity to the maximum quantity of transfer power under operational constraints, and the maximum quantity is recorded according to distances. Since the maximum power transfer capability is the function of the operating voltage, the operating frequency, and the transmission distances varying in the test systems shown in Figure 6.1.1: . The MPTC is recorded according to these three parameters. For the studies, we present three cases based on three different operating-voltages as shown in Table 6.3.1. Note that the operating voltages are selected at 1/3 of nominal voltages of 115-kV, 230-kV, and 345-kV, since one of the advantages by introducing LFAC transmission systems is that one can use the devices (of the same V/H operating value) that have generally used in nominal frequency such as transmission lines, transformers, and protection relays.

Table 6.3.1: Operating Voltages for Power Transfer Studies

	Case 1	Case 2	Case 3
Operating Frequency of 60Hz	38-kV	76-kV	115-kV
Operating Frequency of 20Hz	38kV	76-kV	115-kV



To determine the maximum transmission capability, we checked the maximum transmitted power from the PCC to the load center according to the transmission distance, while the voltage drop between sending terminal and receiving terminal of the transmission lines is remained between -5% and 5% of the operating voltage. Also, the modulation indexes of converters are checked whether the converters are working in reasonable limits of the modulation indexes (around 0.93-0.85). Since the inverter in the LFAC systems have to support DC-voltage for the rectifiers which are connected to wind turbines, the DC-voltage level is important for the reliable operation of the LFAC system. Here, we present simulation results in tables and graphs representing the maximum power transfer capability according to the distance from 10 to 200 miles.

Case 1: Rated Power Line Voltage: 38 kV (line-to-line).

Table 6.3.2: Maximum Transmission Capability at the Operation Voltage 38kV

	Capability of Power Transmission (MW)										
Distance (miles)	10	30	50	70	90	100	120	140	160	180	200
Transfer Capability (MW) at 60Hz	64.0	23.05	13.94	9.96	7.73	6.95	6.05	5.29	4.89	4.59	4.40
Transfer Capability (MW) at 20Hz	124.7	65.44	41.40	29.68	23.07	20.39	17.36	14.23	11.72	9.49	7.24

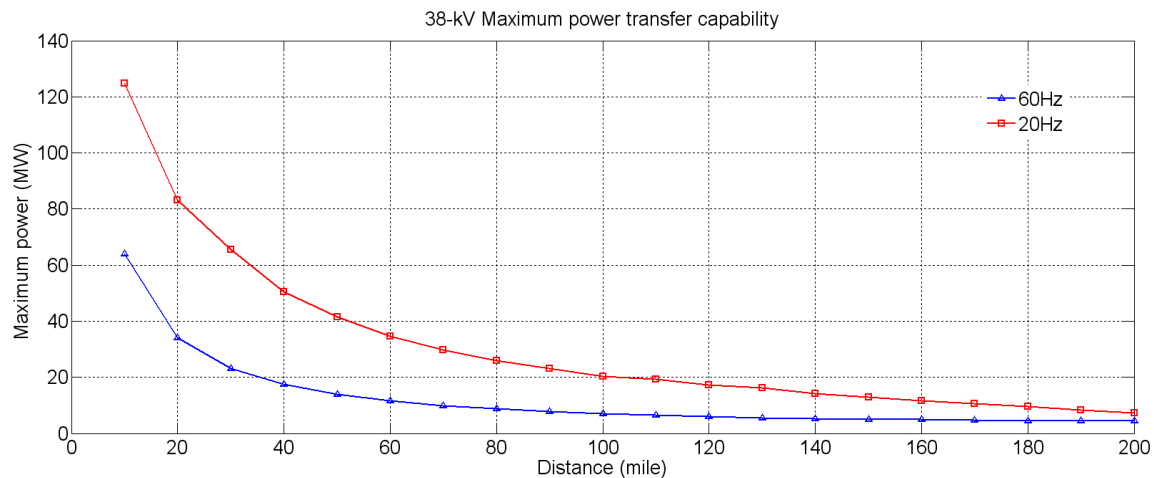


Figure 6.3.1: Power Transmission Capability of the Operation Voltage 38-kV

Case 2: Rated Power Line Voltage: 76 kV (line-to-line).

Table 6.3.3: Maximum Transmission Capability at the Operation Voltage 76kV

	Capability of Power Transmission (MW)										
Distance (miles)	10	30	50	70	90	100	120	140	160	180	200
Transfer Capability (MW) at 60Hz	180.3	82.8	57.54	44.17	36.78	34.31	30.56	27.98	26.19	24.84	23.38
Transfer Capability (MW) at 20Hz	225.3	141.3	106.1	86.28	73.49	68.29	60.19	54.27	49.22	45.21	41.96

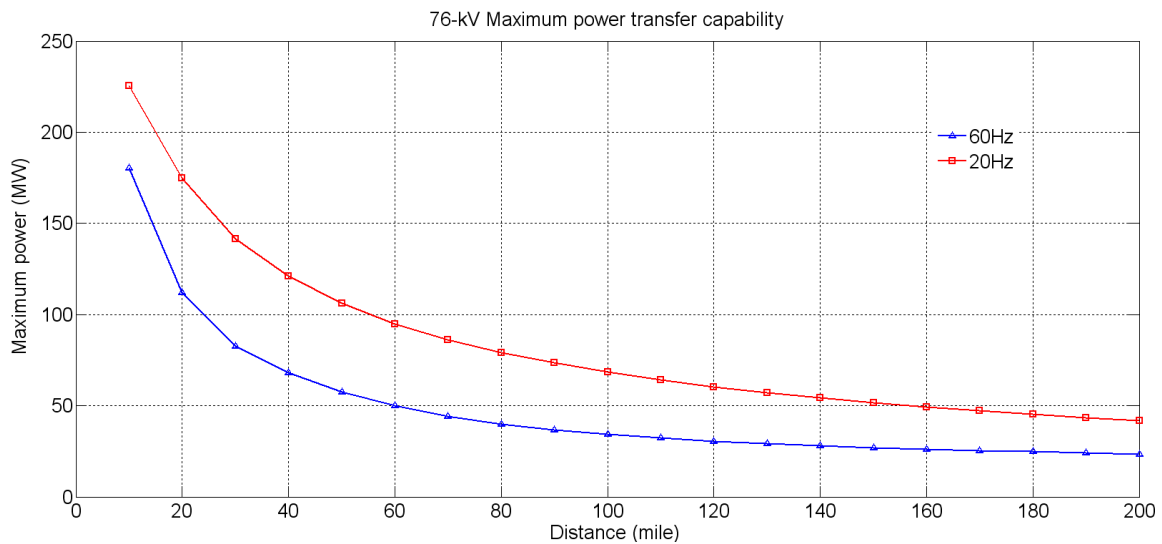


Figure 6.3.2: Power Transmission Capability of the Operation Voltage 76-kV

Case 3: Rated Power Line Voltage: 115 kV (line-to-line).

Table 6.3.4: Maximum Transmission Capability at the Operation Voltage 115kV

Distance (miles)	Capability of Power Transmission (MW)										
	10	30	50	70	90	100	120	140	160	180	200
Transfer Capability (MW) at 60Hz	301.4	147.8	101.8	79.21	66.44	61.54	55.60	51.14	48.01	45.62	43.98
Transfer Capability (MW) at 20Hz	401.5	264.9	202.8	169.0	143.8	135.7	120.7	108.1	98.69	91.16	84.60

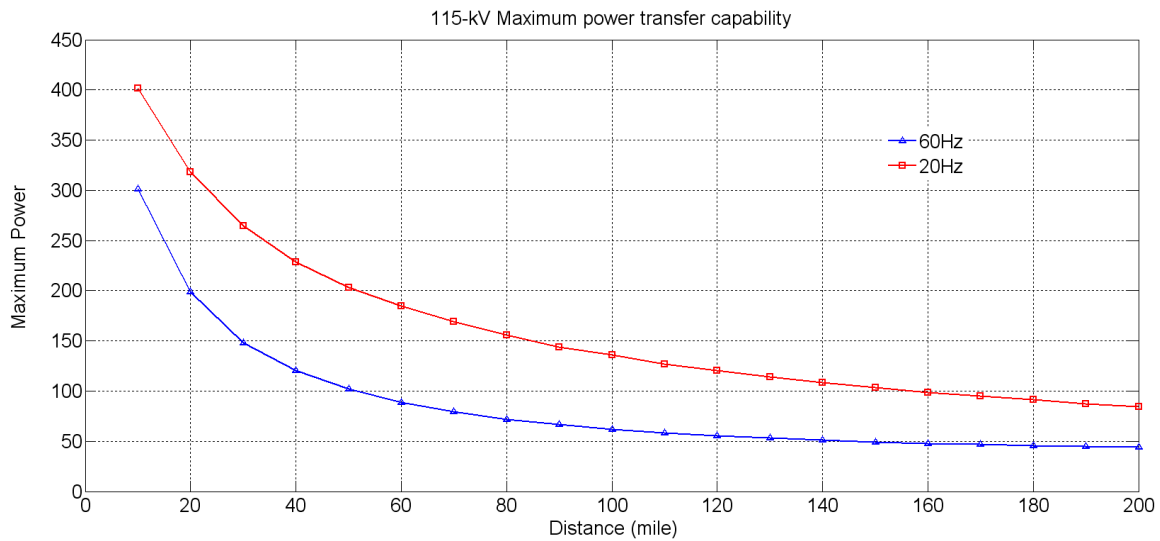


Figure 6.3.3: Power Transmission Capability of the Operation Voltage 115-kV

## 7 Transient Stability Studies

This section presents transient stability studies of alternative transmission systems using a three-phase, six-pulse cycloconverter. Power systems are subjected to frequent disturbances which might be small or large [44]. The small disturbances in LFAC transmission systems should be the state variations of electrical switches, transformer tap changes, load changes, etc. These small disturbances occur continuously and must be managed appropriately in power systems for secure system operation. However, the large disturbances, such as a short circuit on transmission systems and loss of a large generator, result in fluctuation of system voltages, and eventually lead to severe damages to power systems. The transient stability study in this section provides the ability of power systems using LFAC transmission systems to maintain steady voltages from transient conditions.

### 7.1 Description and Technical Approach of Transient Stability Studies

Voltage stability and voltage recovery have been recognized to be of paramount importance for secure system operation. As well-known, slow voltage recovery after disturbance causes significant damages, in which voltage collapse and blackout can be caused by power system instability, in power system [46]. Recently, power systems are highly stressed with the interconnection of weak-synchronous wind systems, and a knowledge and understanding of the impacts of the interconnected wind systems to power system are forced for the reliable and secure operation of power system. In the past, wind farms could be disconnected from power system during excessive voltage-instability since the total capacity of wind-energy generation was small compared to that of other sources. However, the penetration of wind energy in the grid is rapidly increasing and the transmission capacity from wind farms may be a substantial portion of the overall generation. So, the recent grid requirement demands continuing operation of wind farm during and after contingencies [47]. Therefore, voltage-ride-through (VRT) capability on wind-power systems is essential for stable operation of power system. The VRT capability requirement on wind power systems are described by NERC standard. Table 7.1.1 and Figure 7.1.1 provide voltage profiles which the wind-power systems should sustain in the voltage requirement during system disturbances [48].

Table 7.1.1: NERC PRC-024-1 Voltage-Ride-Through Requirement

HVRT DURATION		LVRT DURATION	
Time (second)	Voltage (pu)	Time (second)	Voltage (pu)
0.20	1.200	0.15	0.000
0.50	1.175	0.30	0.450
1.00	1.150	2.00	0.650
4.00	1.100	3.00	0.750
		4.00	0.900

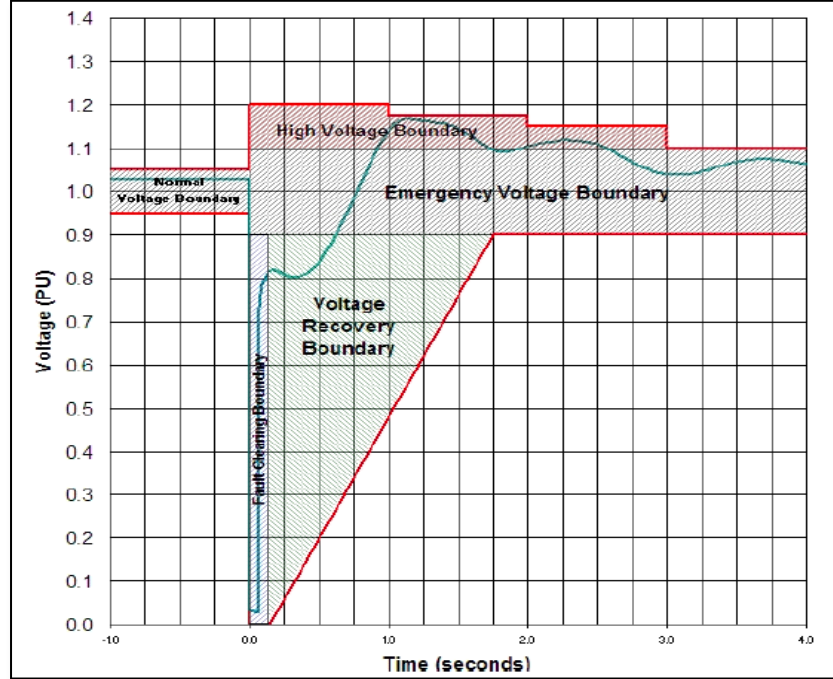


Figure 7.1.1: NERC PRC-024-1 Voltage-Ride-Through Requirement Curve

Note upper-limit is high-voltage-ride-through (HVRT) and the lower-limit is low-voltage-ride-through (LVRT).

For the purpose of stability studies, a comprehensive modeling method is required. Earlier attempts to model wind-generation systems were performed in steady state. However, the excessive simplicity, in which the dynamics in power system are neglected, leads erroneous assessment of system stability. So, a comprehensive modeling method is required for the stability analysis. Here, we introduce a new approach to model power devices composing the LFAC transmission systems. All models in power system are modeled in quasi-steady state, but the modeling concepts are the similar to those in the steady state. For example, the converters are modeled in averaging modeling concepts in phasor representation; however, the continuous power flow and control constraints in converters are allowed to vary in dynamics in each time step. Therefore, the power systems modeled in quasi-steady state are desirable in voltage stability and voltage recovery phenomena, while avoiding the either excessive modeling or simulation in full-time domain. Note that the details are omitted in this subsection, since the modeling processes in quasi-steady state are almost the same to those in steady state.

The methodology for stability study is based on computer simulations with case configurations with LFAC transmission systems. While the LFAC transmission systems are operating in steady state, a disturbance (fault) occur on a specific point, which might be in wind farm, transmission systems, and grid systems. After the disturbance is cleared, the case configurations are observed whether the case configurations can support

continuing operation over grid-cord requirement. Here we present two case-configurations and some possible scenarios are made for the proposed case-studies.

## 7.2 Case Studies of Voltage-Stability Study

Here, we introduce two wind farm configurations for voltage-stability study as follows:

Configuration 1: A LFAC transmission system connecting 20 Hz series wind farm;

Configuration 2: Network fashion of a LFAC transmission connecting DC wind farm.

The two wind farm configurations are used for the simulation analyses of the voltage-ride-through requirement. Each configuration is tested with its own scenarios according to fault positions, disturbance type, and clearing time after a fault, etc.

Configuration 1: A LFAC transmission system connecting 20 Hz series wind farm

This configuration 1 presents an example of 20 Hz wind farm with a LFAC transmission system connected to a power grid, as shown in Figure 7.2.1. The wind farm consists of tens of wind-turbines and full-size inverters/converters. The each wind-turbine generates 5MW electrical power with 2.5-kV rating voltage and series connected to each other with 300-meter spacing. The distance of the LFAC transmission system is 25-mile with rating voltage of 35-kV. At the point a cycloconverter converts the 20 Hz AC-power into 60 Hz AC-power and step-up transformer boost the voltage to 115-kV, 60 Hz transmission at that point.

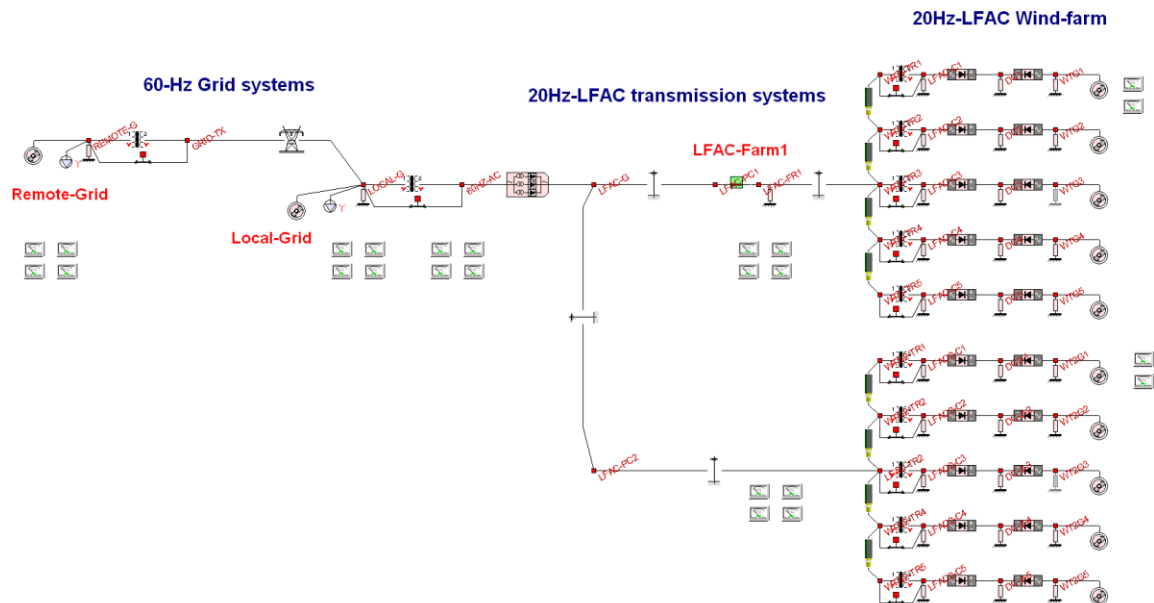


Figure 7.2.1: Single-Line Diagram of a LFAC Transmission System Connecting a Series LFAC Wind Farm to the Main Grid

Scenario 1: In this example study, the wind farm transmits 50-MW electrical power into grid systems, a three-phase fault is generated at the remote grid (at the point of REMOT-GRID in Figure 7.2.1), and the three-phase fault is cleared after 0.15 seconds from the initial fault. The simulation results are represented in Figure 7.2.2. Note the three-phase fault starts at 0.1 seconds and is cleared at 0.25 seconds. The graph (A) represents the magnitude of phase-A voltage at the remote grid, and the graph (B) and the graph (C) show the magnitude of phase-A voltage magnitude at the local grid and before the cycloconverter, respectively. Note that the voltages are recovered and the frequency and real-power are swing at equilibrium points as shown in Figure 7.2.3.

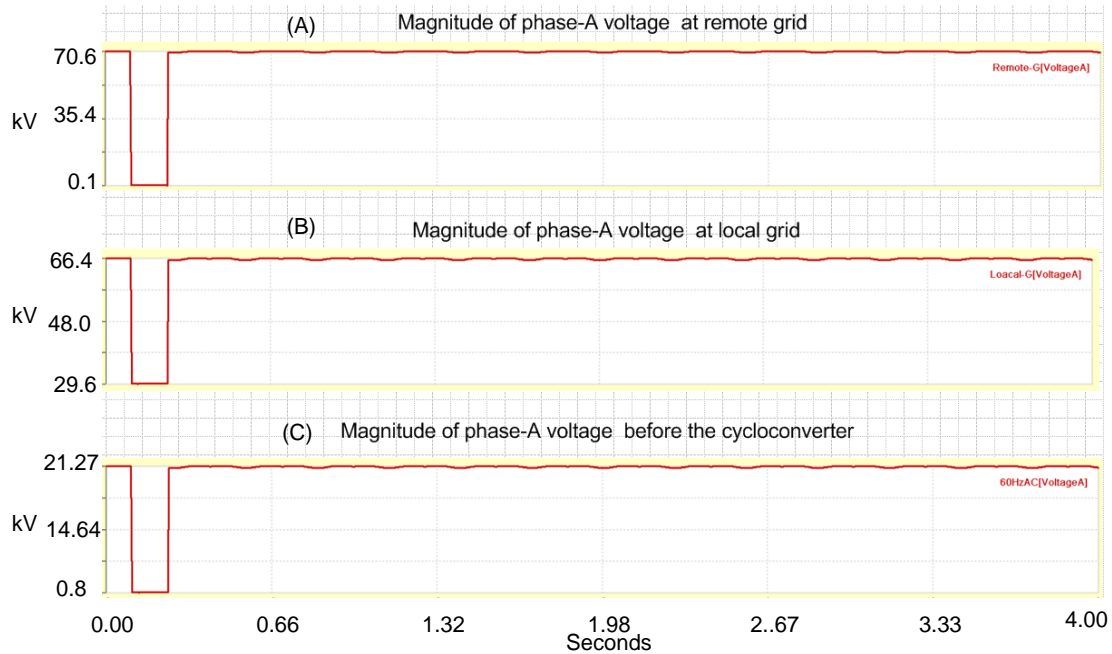


Figure 7.2.2: Configuration 1: Voltage Magnitude of Phase A at (A) Remote Grid and (B) Local Grid, and (C) Before the Cycloconverter during a Three-Phase Fault at Remote Grid

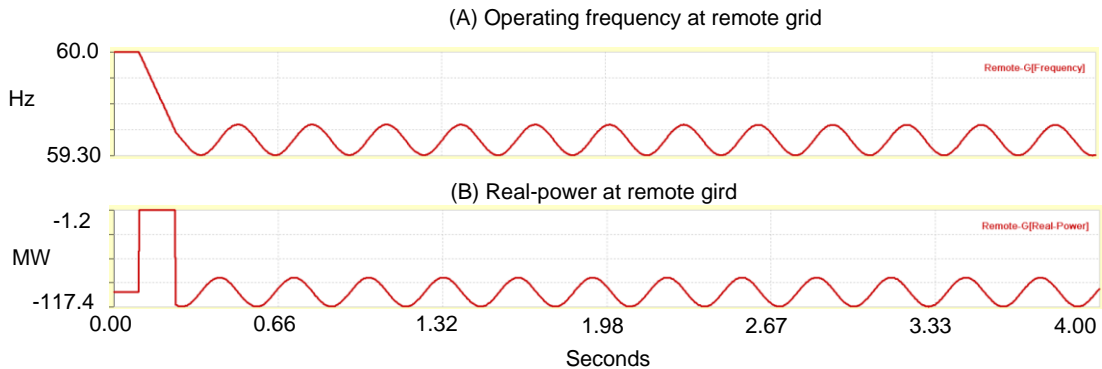


Figure 7.2.3: Configuration 1: (A) Operating Frequency and (B) Real Power at Remote Grid during a Three-Phase Fault at Remote Grid

Scenario 2: The wind farm transmits 50-MW electrical power into grid systems in steady state, and a three-phase breaker opens at 0.1 seconds and reclose at 0.25 seconds at PCC of wind farm 1 (at the point of LFAC-FARM1 in Figure 7.2.1). The simulation results are represented in Figure 7.2.4. The graph (A) represents the magnitude of phase-A voltage at the remote grid, and the graph (B) and the graph (C) show the magnitude of phase-A voltage magnitude at the local grid and before the cycloconverter, respectively. Note that the voltages are in bound of the VRT requirement and the frequency and real-power are swing at equilibrium points.

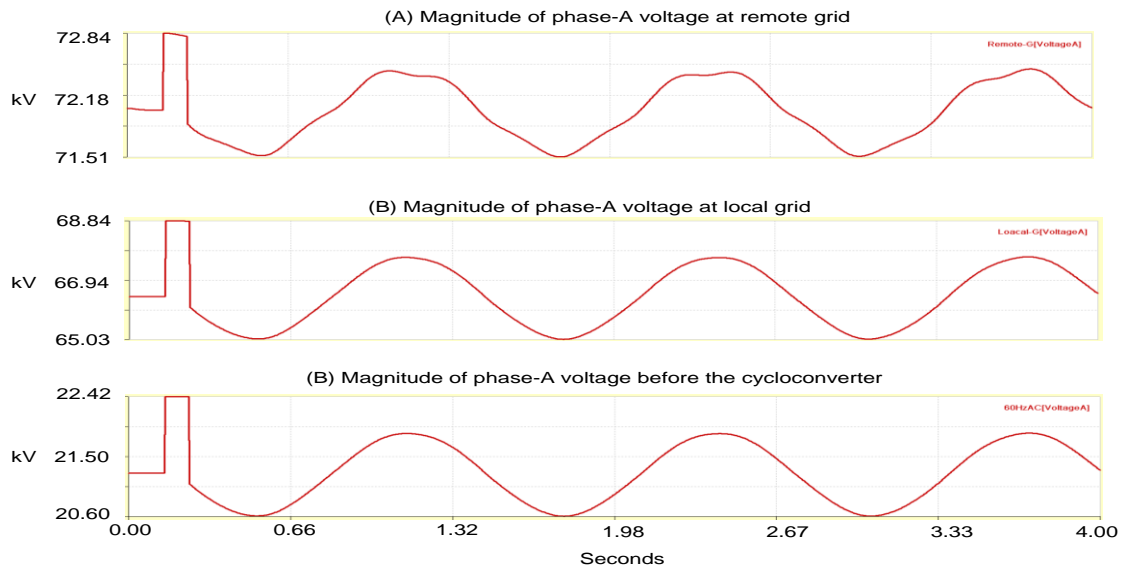


Figure 7.2.4: Configuration 1: Voltage Magnitude of Phase A at (A) Remote Grid, (B) Local Grid, and (C) Before the Cycloconverter during the Recloser Operation

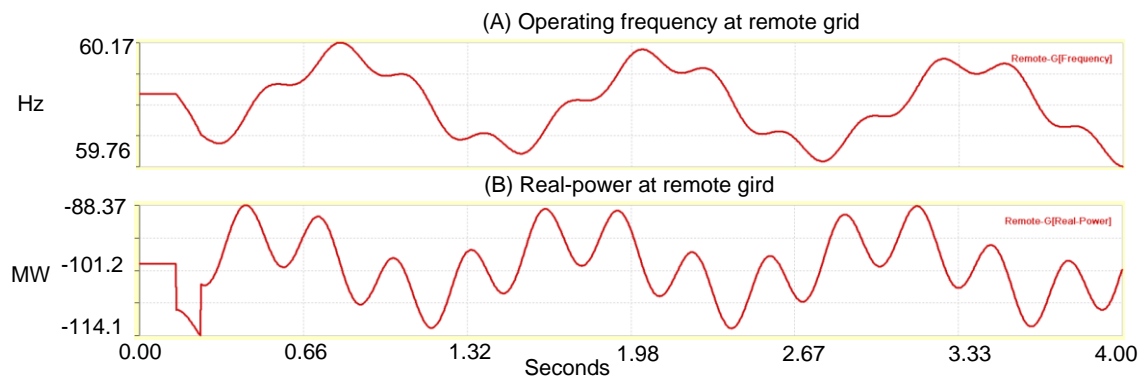


Figure 7.2.5: Configuration 1: (A) Operating Frequency and (B) Real Power at Remote Grid during the Recloser Operation

Scenario 3: The wind farm transmits 50-MW electrical power into grid systems, a three-phase fault is generated at the local grid (at the point of LOCAL-GRID in Figure 7.2.1),



and the three-phase fault is cleared after 0.15 seconds from the initial fault. The simulation results are represented in Figure 7.2.6. When the three-phase fault generates at local grid, the cycloconverter loses synchronism and the wind farm system is in instability.

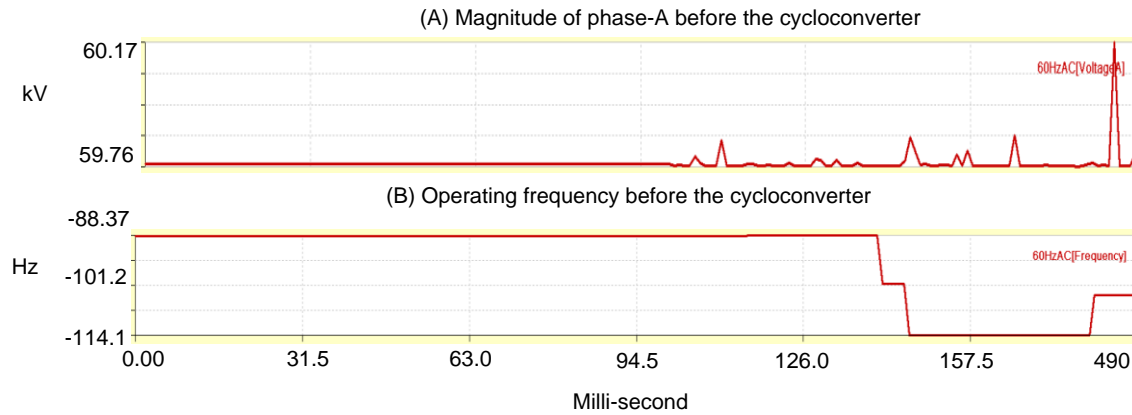


Figure 7.2.6: Configuration 1: (A) Voltage Magnitude of Phase A and (B) Operating Frequency during the Three-Phase Fault at Local Grid

Configuration 2: A LFAC transmission system connecting 20 Hz series wind farm

This configuration 2 presents an example of series DC wind farm with network-fashion of two LFAC-transmission systems connected to a power grid, as shown in Figure 7.2.7. The wind farm consists of tens of wind-turbines in series DC-connection. The each wind-turbine generates 5MW electrical power with 2.5-kV rating voltage and series connected to each other with 300-meter spacing. The distance of the LFAC transmission system is 25-mile with rating voltage of 35-kV. At the point a cycloconverter converts the 20 Hz AC-power into 60 Hz AC-power and step-up transformer boost the voltage to 115-kV, 60 Hz transmission at that point.

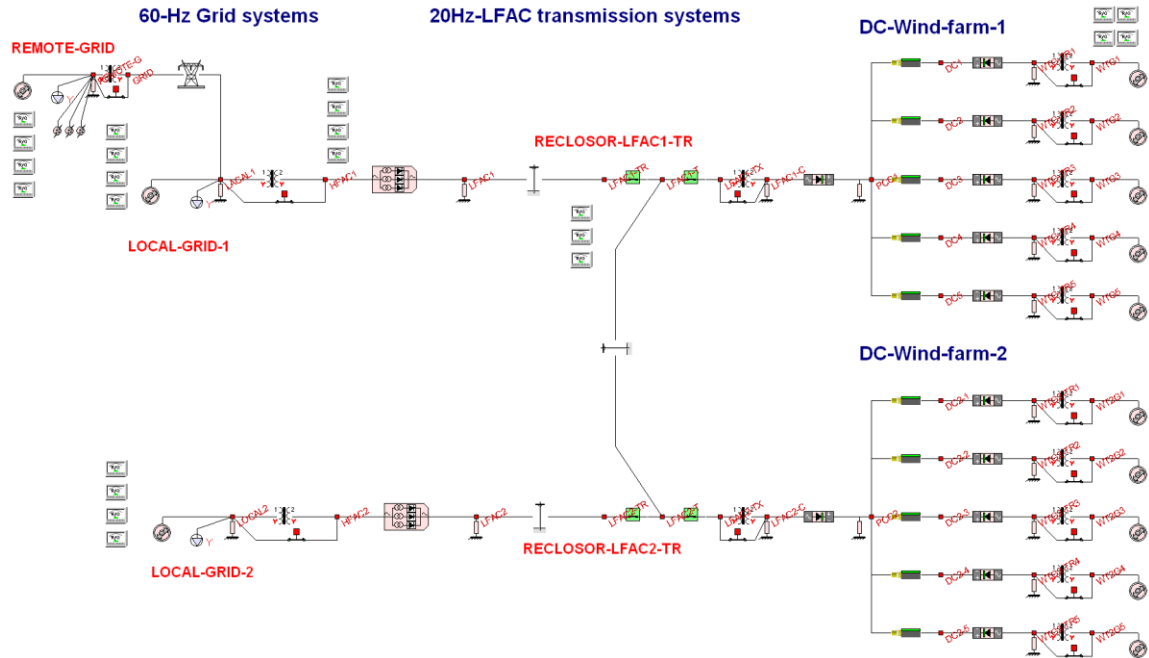


Figure 7.2.7: Single-Line Diagram of LFAC Transmission Network Connecting a Series DC Wind Farm

Scenario 1: In this example study, the wind farm transmits 50-MW electrical power into grid systems, a three-phase fault is generated at the remote grid (at the point of REMOTE-GRID in Figure 7.2.7), and the three-phase fault is cleared after 0.15 seconds from the initial fault. The simulation results are represented in Figure 7.2.8. Note the three-phase fault starts at 0.1 seconds and is cleared at 0.25 seconds. As shown in Figure 7.2.8, the graphs (A) represent the magnitude of phase-A voltage at the remote grid, and the graph (B) and the graph (C) show the magnitude of phase-A voltage magnitude at the local grid 1 and before the cycloconverter, respectively. Note that the voltages are recovered and the frequency and real-power are swing at equilibrium points as shown in Figure 7.2.9. Since the VRT requirement is satisfied, the configuration 2 is stable with three-phase fault at remote grid.

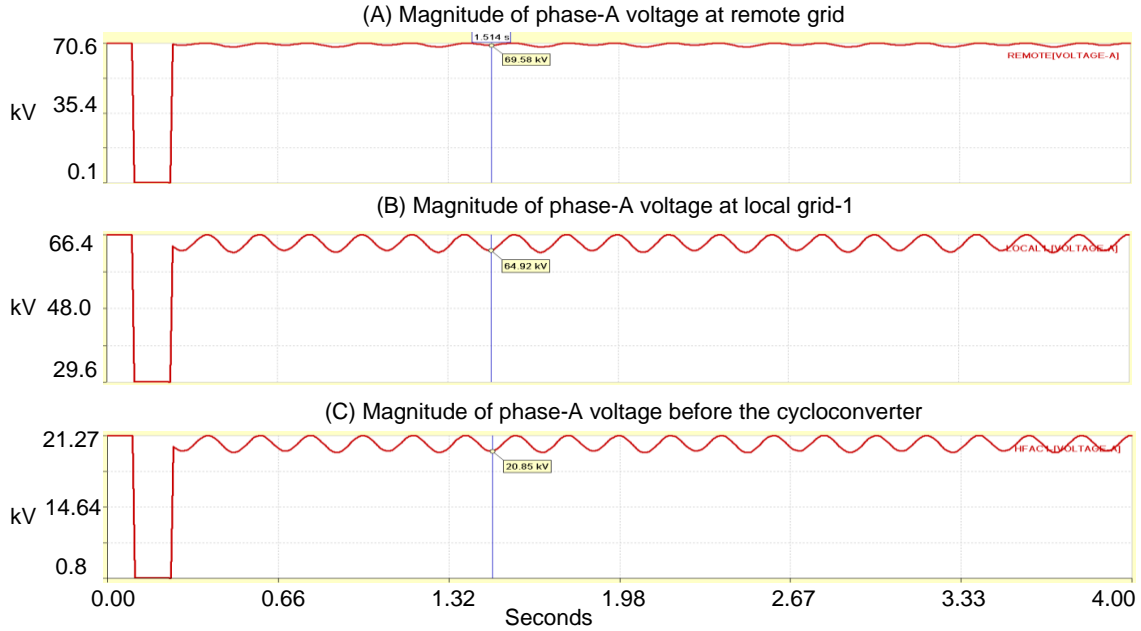


Figure 7.2.8: Configuration 2: Voltage Magnitude of Phase A (A) at Remote Grid, (B) at Local Grid 1, and (C) Before the Cycloconverter during a Three-Phase Fault at Remote Grid

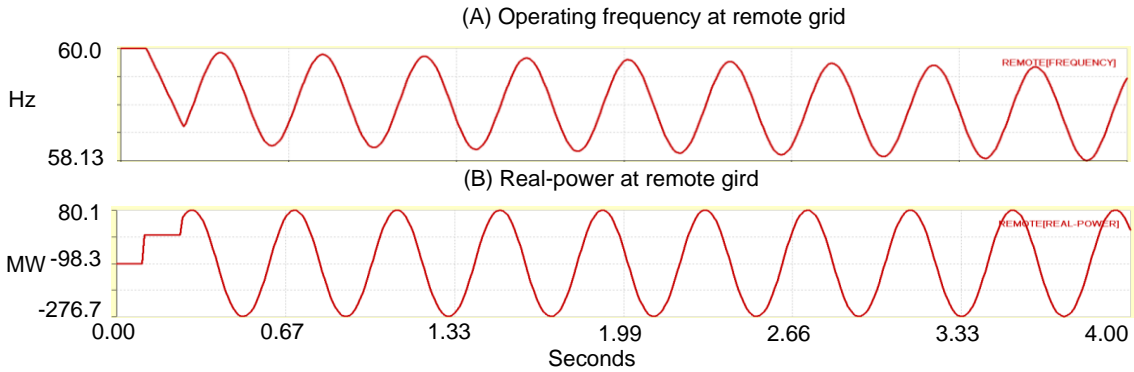


Figure 7.2.9: Configuration 2: (A) Operating Frequency and (B) Real Power at Remote Grid during a Three-Phase Fault at Remote Grid

Scenario 2: The wind farm transmit 50-MW electrical power into grid systems, a three-phase fault is generated at the local-grid 1 (at the point of LOCAL-GRID-1 in Figure 7.2.7), and the three-phase fault is cleared after 0.15 seconds from the initial fault. The simulation results are represented in Figure 7.2.8. Note the three-phase fault starts at 0.1 seconds and is cleared at 0.25 seconds. As shown in Figure 7.2.10, the graphs (A) and (B) represent the magnitude of phase-A voltage at the remote grid and at local grid 1, the graphs (C) and (D) are the real-power and operating frequency at remote grid. Note that the voltages are recovered and the frequency and real-power are swing at equilibrium

points as shown in Figure 7.2.8. However, the phase-A voltage at remote grid oscillates and is smaller than the VRT requirement. So, the configuration 2 is instable during the three-phase fault at local grid 1.

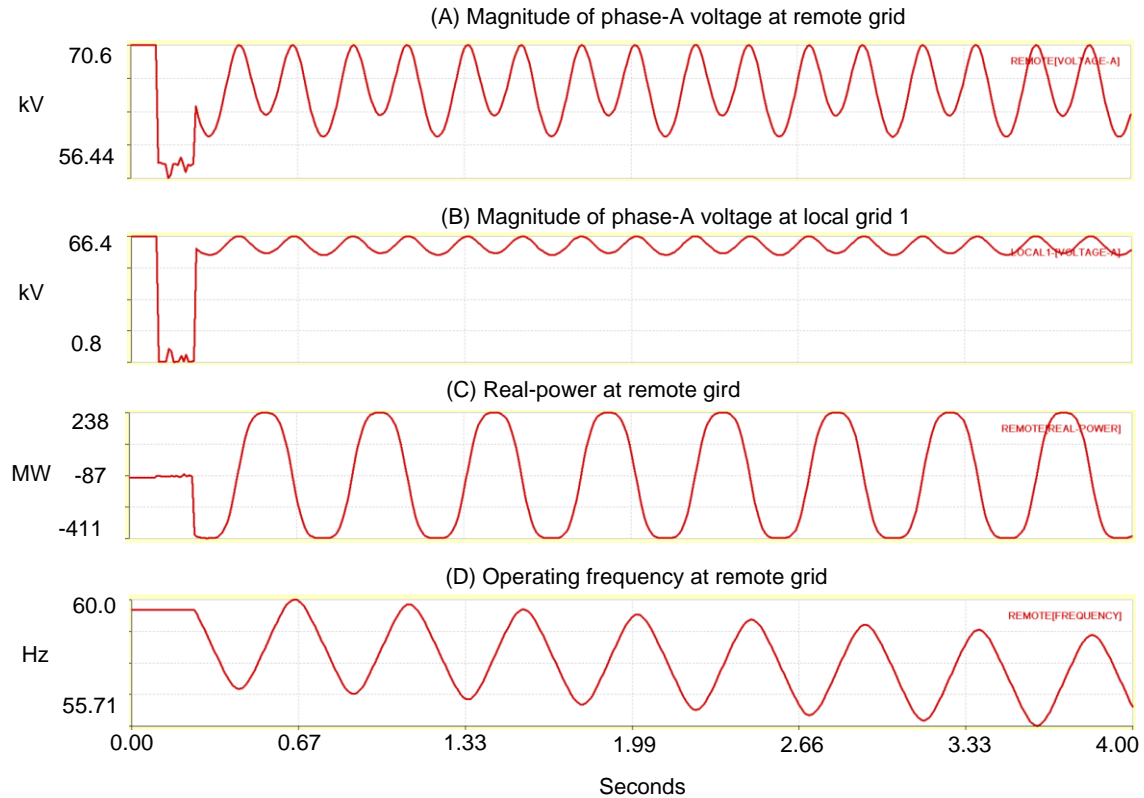


Figure 7.2.10: Configuration 2: Magnitude of Phase A Voltages at (A) Remote Grid and (B) Local Grid 1, and (C) Real Power and Operating Frequency at Remote Grid during a Three-Phase Fault at Local Grid 1

Scenario 3: The wind farm transmits 50-MW electrical power into grid systems in steady state, and a three-phase breaker opens at 0.5 seconds and reclose at 0.65 seconds at the point (RECLOSOR-LFAC2-TR in Figure 7.2.7). The simulation results are represented in Figure 7.2.11. The graph (A) represents the magnitude of phase-A voltage at the remote grid and the graph (B) show the magnitude of phase-A voltage magnitude at the local grid 1. Note that the voltages are in bound of the VRT requirement.

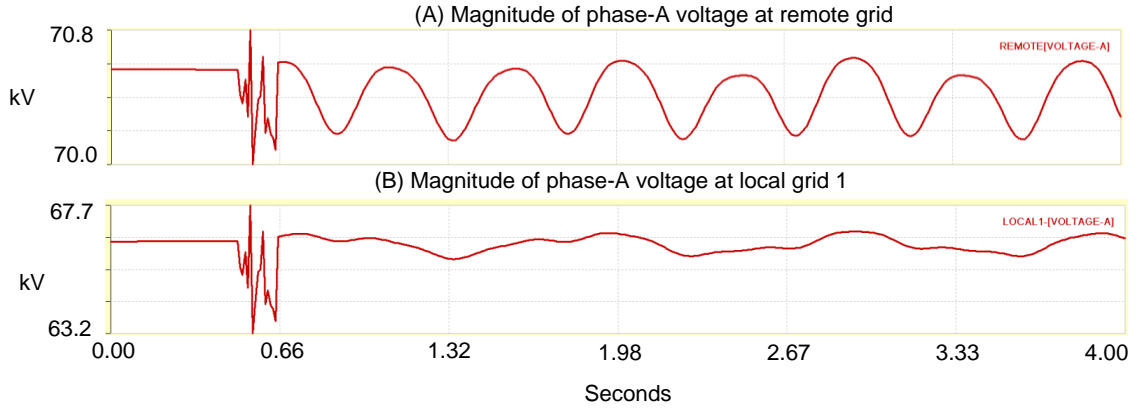


Figure 7.2.11: Configuration 2: Magnitude of Phase A voltages at (A) Remote Grid and (B) Local Grid 1 during Recloser Operation at RECLOSOR-LFAC2-TR

Scenario 4: The wind farm transmits 50-MW electrical power into grid systems in steady state, and a three-phase breaker opens at 0.5 seconds and reclose at 0.65 seconds at the point (RECLOSOR-LFAC1-TR in Figure 7.2.7). That is, the wind farms and local-grid 2 are disconnected from the main grid. The simulation results are represented in Figure 7.2.12. The graph (A) represents the magnitude of phase-A voltage at the remote grid, and the graph (B) show the magnitude of phase-A voltage magnitude at the local grid 1. Note that since the phase-A voltage at local-grid 1 is not satisfied by the VRT requirement, the configuration 2 is instable while the main-grid is disconnected from the wind farms and local-grid 2.

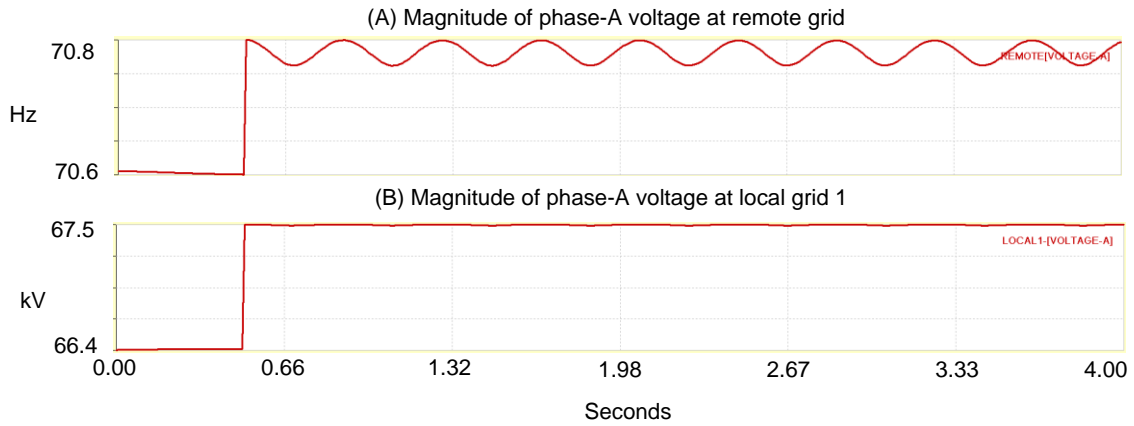


Figure 7.2.12: Configuration 2: Magnitude of Phase A Voltages at (A) Remote Grid and (B) Local Grid 1 during Recloser Operation at RECLOSOR-LFAC1-TR

## 8 Time-Domain Studies-I

This section presents time domain modeling and analysis of the general configurations.

### 8.1 System Configuration and Control

An example of the proposed LFAC transmission system is shown in Figure 8.1.1: At the sending end, a medium-voltage dc collection bus is formed by rectifying the ac output power of series-connected wind turbines. A dc current source  $I_w$  represents the total power delivered from the wind turbines. A dc/ac 12-pulse thyristor-based inverter is used to generate low-frequency (20 Hz) ac power. It is connected to a three-winding transformer that raises the voltage to a higher level, for transmission. AC filters are used to suppress the 11th, 13th, and higher-order ( $\geq 23$ rd) current harmonics, and to supply reactive power to the converter. A smoothing reactor ( $R-L$ ) is connected at the inverter's dc terminals. At the receiving end, a three-phase bridge (6-pulse) cycloconverter with 36 thyristors is used as an interface between the low-frequency transmission line and the 60 Hz power grid.  $L_f-C_f$  is the cycloconverter's filter at the low-frequency side. At the grid side, AC filters are used to suppress odd current harmonics, and to supply reactive power to the cycloconverter.

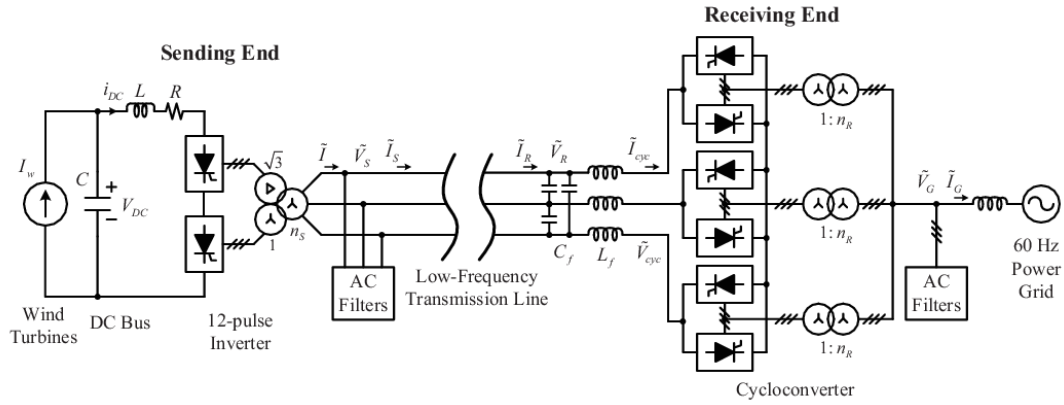


Figure 8.1.1: Configuration of the Proposed LFAC Transmission System

### 8.2 Sending End Control

The control structure for the sending-end inverter is shown in Figure 8.2.1. The controller regulates the dc bus voltage  $V_{DC}$  by adjusting the voltage  $V$  at the inverter terminals. The cosine wave crossing method [30] is applied to determine the firing angle  $\alpha_s$ , which is

$$\alpha_s = \arccos \frac{V^*}{V_P} \quad (8.2.1)$$

where  $V_p$  is the peak value of the cosine wave. Note that  $V^* < 0$  and  $90^\circ < \alpha_s < 180^\circ$  (using common notation), since the converter is in the inverter mode of operation [31].  $V$  and  $V_s$  (line-to-neutral, rms) are related by [32]:

$$V = \frac{6\sqrt{6}V_s}{\pi n_s} \cos \alpha_s \quad (8.2.2)$$

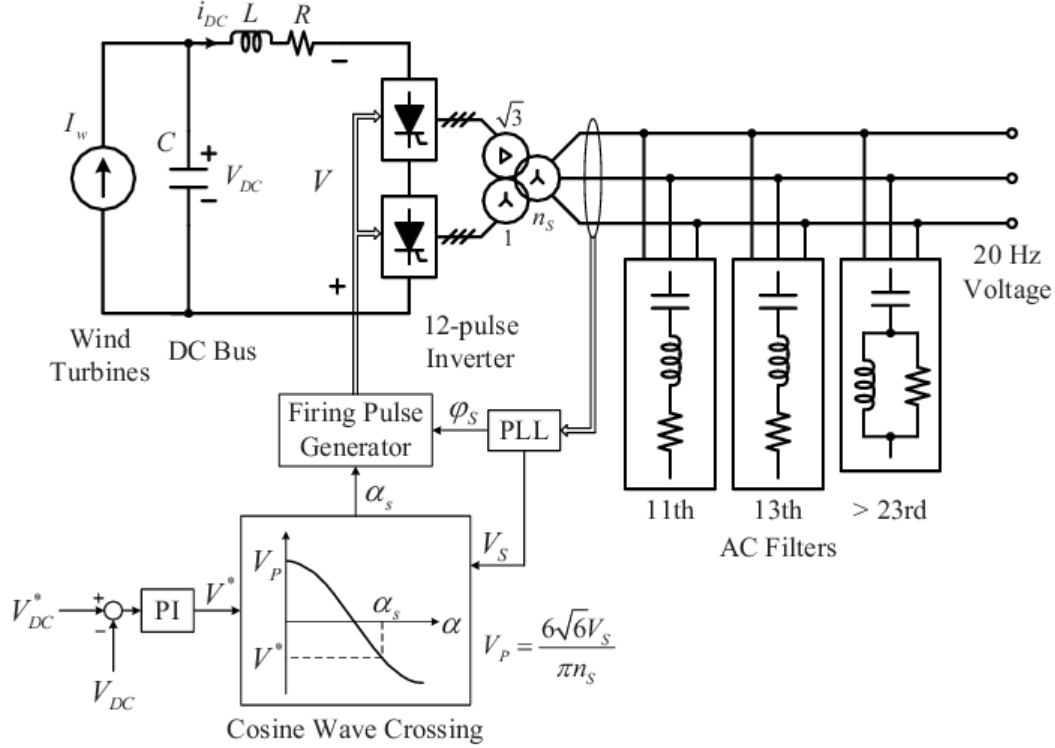


Figure 8.2.1: Sending End DC/AC Inverter Control

A phase-locked loop (PLL) provides the angular position of the ac side voltage, which is necessary for generating the firing pulses of the thyristors. It also outputs the rms value of the fundamental component of the voltage, which is used in the firing angle calculation.

### 8.3 Receiving End Control

The structure of the cycloconverter controller at the receiving end is illustrated in Figure 8.3.1:. The goal is to provide a constant 20 Hz voltage of given rms value  $V_R^*$  (line-to-neutral) at the receiving end. The fundamental component of the receiving end voltage  $V_R$  is obtained with the signal conditioning logic depicted in Figure 8.3.2.

The firing angles are determined with the cosine wave crossing method, as shown in Figure 8.3.3:, which uses phase- $a$  as an example.  $\alpha_{aP}$  and  $\alpha_{aN}$  are the firing angles of

the phase- $a$  positive and negative converter, respectively (denoted as ‘ $aP$ ’ and ‘ $aN$ ’ in Figure 8.3.1:). For the positive converter, the average voltage at the 20 Hz terminals is given by [32]:

$$V_{aP} = \frac{3\sqrt{6}V_G}{\pi n_R} \cos \alpha_{aP} \quad (8.3.1)$$

where  $V_G$  is the rms value of the line-to-neutral voltage at the grid side, and  $n_R$  is the turns ratio of the transformers. The condition  $\alpha_{aP} + \alpha_{aN} = \pi$  ensures that average voltages with the same polarity are generated from the positive and negative converter at the 20 Hz terminals [34]. However, the firing pulses  $S_{aP}$  and  $S_{aN}$  are not simultaneously applied to both converters, in order to obtain a non-circulating current mode of operation. This functionality is embedded in the ‘Bank Selector’ block of Figure 8.3.1:, which operates based on the filtered current  $\hat{i}_{cyc,abc}$ . Note (for later use) that the maximum line-to-neutral rms value of the 20 Hz cycloconverter voltage is [30]:

$$V_{cyc}^{max} = \frac{3\sqrt{3}V_G}{\pi n_R} \quad (8.3.2)$$

and that a voltage ratio is defined as

$$r = \frac{V_{cyc}}{V_{cyc}^{max}} \quad (8.3.3)$$

In practice, the theoretical maximum value  $r = 1$  cannot be achieved, due to the transformers’ leakage inductance, which was ignored in the analysis.



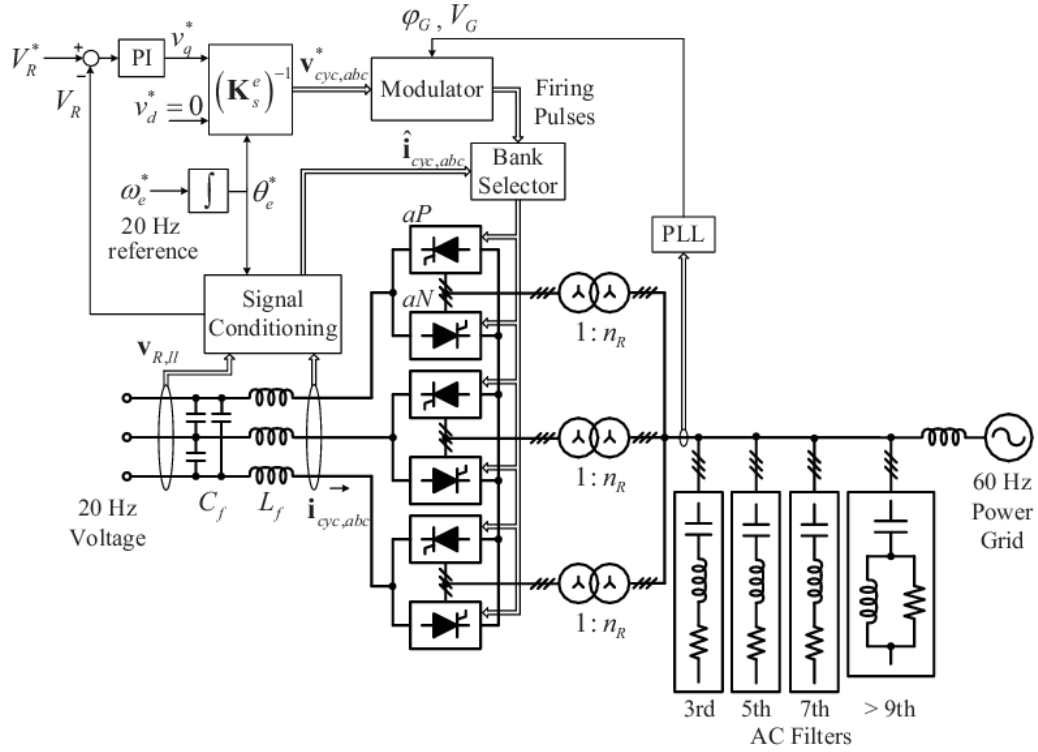


Figure 8.3.1: Receiving End Cycloconverter Control (The reference frame transformation matrix  $K_s^e$  is defined in [33], and transforms variables from the stationary to the synchronous reference frame.)

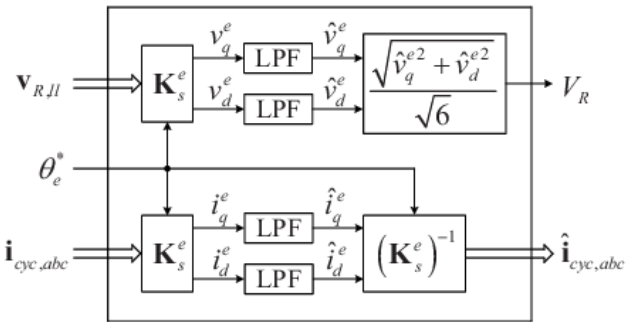


Figure 8.3.2: Details of the Signal Conditioning Block(LPF = low-pass filter; the time constants are 0.05 s and 0.01 s for the voltage and current respectively.)

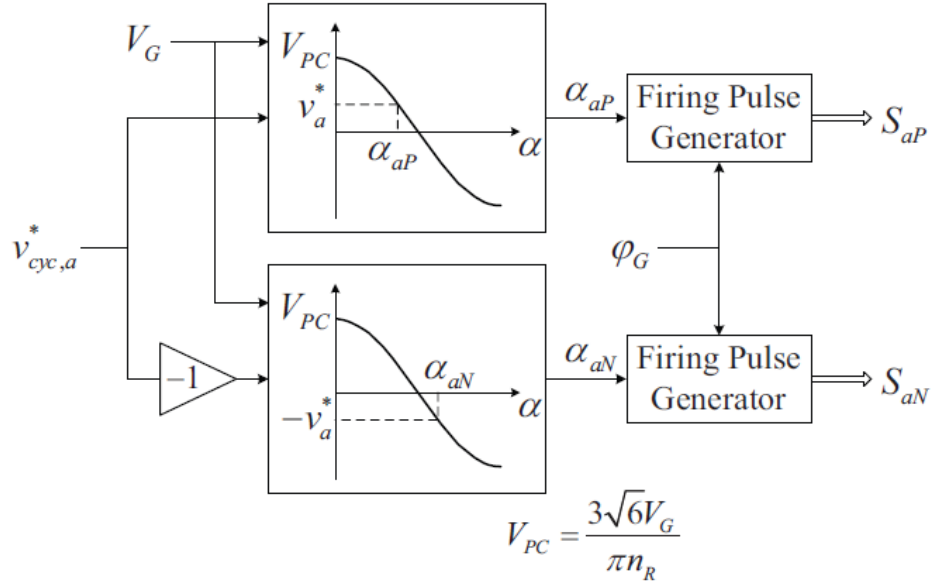


Figure 8.3.3: Modulator for Phase A

## 8.4 System Design

### 8.4.1 Main Power Components

The main power components are selected based on a steady-state analysis of the LFAC transmission system shown in Figure 8.1.1: under the following assumptions:

- Only fundamental components of voltages and currents are considered. The receiving end is modeled as a 20 Hz voltage source of nominal magnitude.
- The power losses of the reactor, thyristors, filters, and transformers are ignored.
- The resistances and leakage inductances of transformers are neglected.
- The AC filters are represented by an equivalent capacitance corresponding to the fundamental frequency.
- The design is based on rated operating conditions (*i.e.*, maximum power output).

At the steady state, the average value of the DC current  $I_{DC}$  is equal to  $I_w$ , so the power delivered from the wind turbines is

$$P_w = V_{DC} I_{DC} = V_{DC} I_w. \quad (8.4.1)$$

For the 12-pulse converter, the rms value of the current at the transmission side is [32]:

$$I = \frac{2\sqrt{6} I_{DC}}{\pi n_S} = \frac{2\sqrt{6} I_w}{\pi n_S}. \quad (8.4.2)$$

Hence, (8.4.2) can be written as

$$I = MP_w, \quad (8.4.3)$$

with

$$M = \frac{2\sqrt{6}}{\pi n_S V_{DC}}. \quad (8.4.4)$$

Let  $\tilde{V}_S = V_S \angle 0^\circ$  and  $\tilde{I}$  denote phasors of the line-to-neutral voltage and line current, respectively. Since  $-\tilde{I}$  lags  $\tilde{V}_S$  by  $\alpha_S$  [32], it follows that  $\tilde{I} = I \angle (180^\circ - \alpha_S)$ . So, the active power delivered by the 12-pulse inverter is given by

$$P_S = P_w = 3V_S I \cos (\alpha_S - 180^\circ) = -3V_S I \cos \alpha_S > 0. \quad (8.4.5)$$

Substitution of (8.4.3) into (8.4.5) yields

$$\cos \alpha_S = -\frac{1}{3MV_S} \quad (8.4.6)$$

and

$$\sin \alpha_S = \sqrt{1 - \frac{1}{9M^2 V_S^2}}. \quad (8.4.7)$$

The reactive power generated from the 12-pulse inverter is

$$Q_S = 3V_S I \sin (\alpha_S - 180^\circ) = -3V_S I \sin \alpha_S. \quad (8.4.8)$$

From (8.4.5)–(8.4.8), it follows that

$$Q_S = P_S \tan \alpha_S = -P_S \sqrt{9M^2 V_S^2 - 1}. \quad (8.4.9)$$

The negative sign in (8.4.8) and (8.4.9) indicates that the 12-pulse inverter always absorbs reactive power. Equation (8.4.9) shows that  $Q_S$  can be expressed as a function  $Q_S = f(P_S, V_S)$ . Based on the above analysis, the steady-state single-phase equivalent

circuit of the LFAC transmission system is shown in Figure 8.4.1:  $C_{eq}$  is the equivalent capacitance of the sending-end AC filters at fundamental frequency. The transmission line is modeled by a  $\Pi$ -equivalent (positive-sequence) circuit using lumped parameters. The well-known hyperbolic trigonometric expressions for  $Z'$  and  $\frac{Y'}{2}$  are used [35]. Given a power rating of a wind power plant  $P_{\text{rated}}$ , the maximum reactive power that is absorbed by the 12-pulse inverter can be estimated according to (8.4.9), which yields

$$Q_{\text{rated}} = P_{\text{rated}} \sqrt{3M^2 V_o^2 - 1}, \quad (8.4.10)$$

where  $V_o$  is the nominal transmission voltage level (line-to-line rms). Here, it is assumed that the sending-end AC filters supply the rated reactive power to the inverter. Therefore,

$$C_{eq} = \frac{Q_{\text{rated}}}{\omega_e V_o^2}, \quad (8.4.11)$$

where  $\omega_e = 2\pi 20$  rad/s. In addition, the apparent power rating of the transformer at the sending end  $S_{ts}$  should satisfy

$$S_{ts} > \sqrt{P_{\text{rated}}^2 + Q_{\text{rated}}^2} = \sqrt{3} P_{\text{rated}} M V_o. \quad (8.4.12)$$

At the 60 Hz grid side, the reactive power capacity of the AC filters and the apparent power rating of the transformers depend on the cycloconverter's voltage ratio  $r$ , which is a design parameter, and the 20 Hz side power factor [34], which can be estimated as follows.

For a given transmission cable, the voltage ratings (nominal and maximum voltage), the current rating, and the distributed cable parameters (resistance, inductance, and capacitance per unit length) are known. Here, it is assumed that a power cable is chosen to transmit the rated wind power plant power  $P_{\text{rated}}$  without violating the cable's voltage and current ratings. (The relationship between active power through the cable and maximum transmission distance, given a certain cable, will be discussed later.) For simplicity, it is further assumed that the rms value of line-to-line voltage at both sending and receiving ends is  $V_o$  and the current through  $Z'$  and  $L_f$  is approximately equal to the current rating of the cable  $I_{\text{rated}}$ .

Since the AC filters are designed to supply all reactive power to the 12-pulse inverter at the sending end, the reactive power injected into the cycloconverter's 20 Hz side can be estimated using

$$Q_{\text{cyc}}^{20} \approx \text{Im}\{Y'\} V_o^2 + \omega_e 3C_f V_o^2 - 3I_{\text{rated}}^2 \text{Im}\{Z'\} - 3I_{\text{rated}}^2 \omega_e L_f, \quad (8.4.13)$$

where the first two terms represent the reactive power generated from the cable and the  $LC$  filter's capacitor, and the last two terms represent the reactive power consumed by the cable and the  $LC$  filter's inductor. The active power injected into the cycloconverter from the 20 Hz side can be estimated using

$$P_{cyc}^{20} \approx P_{rated} - \text{Re}\{Y'\}V_o^2 - 3I_{rated}^2\text{Re}\{Z'\}, \quad (8.4.14)$$

where the last two terms represent the power loss of the cable. Thus, the 20 Hz side power factor can be estimated according to (8.4.13) and (8.4.14).

Now the 60 Hz side power factor  $PF^{60}$  at the transformers' grid-side terminals can be obtained using the method presented in [34]. Then the apparent power rating of each out of the three receiving-end transformers  $S_{tR}$  should satisfy

$$S_{tR} > \frac{P_{cyc}^{20}}{(3)(PF^{60})}. \quad (8.4.15)$$

Also, it is assumed that the grid-side AC filters are designed to supply the rated amount of reactive power to the cycloconverter.

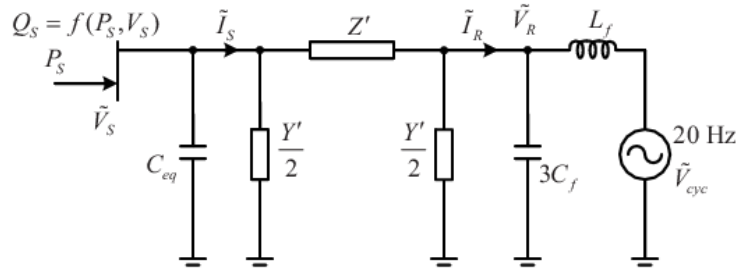


Figure 8.4.1: Equivalent Circuit of 20 Hz Transmission System

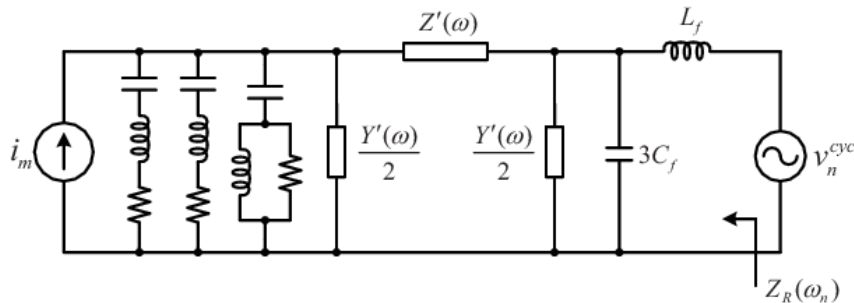


Figure 8.4.2: Equivalent Circuit of 20 Hz Transmission System for Harmonic Analysis

### 8.4.2 Filter Design

At the sending end, the 12-pulse inverter produces harmonics of order  $m = 12k \pm 1$ ,  $k = 1, 2, \dots$ , and can be represented as a source of harmonic currents ( $i_m$  in Figure 8.4.2:). These current harmonics are filtered by two single-tuned filters for the 11th and 13th harmonics, and one damped filter for higher-order harmonics ( $\geq 23$ rd). Generally, the filter design is dependent on the reactive power that the filter supplies at fundamental frequency (also known as the filter size) and the required quality factor  $Q$  [36]. The total reactive power requirement of these filters can be estimated based on (8.4.10). Here, it is assumed that the total reactive power requirement is divided equally among the three filters. The quality factor for each filter can be determined using the method presented in 36. A high quality factor ( $Q = 100$ ) is used for the single-tuned filters, and a low quality factor ( $Q = 1$ ) is used for the high-pass damped filter. Finally, with the capacitance and quality factor known, the inductance and resistance of each filter can be determined. With such filter design, the 12-pulse-related current harmonics originating at the sending end are essentially absent from the transmission line.

At the receiving end, there are two groups of filters which include the AC filters at the 60 Hz side and the  $LC$  filter at the 20 Hz side. At the 60 Hz side, if the cycloconverter generates exactly  $60/3 = 20$  Hz, it can be shown [34] that the line current has only odd harmonic components, *i.e.*, 3rd, 5th, 7th,  $\dots$ . Here, three single-tuned filters and one damped filter are used to prevent these harmonic currents from being injected into the 60 Hz power grid. These filters are designed with a procedure similar to that for the ac filters at the sending end.

At the 20 Hz side, the line-to-neutral voltage has harmonics of order 3, 5, 7,  $\dots$  [34]. However, the harmonic components of order equal to integer multiples of three are absent in the line-to-line voltage. Therefore, as seen from the 20 Hz side, the cycloconverter acts as a source of harmonic voltages of orders  $n = 6k \pm 1, k = 1, 2, \dots$  ( $v_n^{cyc}$  in Figure 8.4.2:). The design of the  $LC$  filter has two objectives:

- 1) to decrease the amplitudes of the voltage harmonics generated by the cycloconverter;
- 2) to increase the equivalent harmonic impedance magnitudes seen from the receiving end, indicated by  $Z_R(\omega_n)$  in Figure 8.4.2:.

The design procedure presented here takes into account the voltage harmonics of order 5, 7, 11, and 13. For cycloconverters, the amplitude of the voltage harmonics only depends on the voltage ratio  $r$  and the fundamental power factor at the 20 Hz side, under the assumption of sinusoidal output current [34], which is sufficient for design purposes. Generally, the voltage harmonics tend to become worse with decreasing  $r$ . Here, we set  $r = 0.9$ . Figure 8.4.3: illustrates the relationship between the per unit amplitudes of the voltage harmonics under consideration (5th, 7th, 11th, and 13th) and the power factor angle  $\phi$ , computed based on formulas in [34]. Apparently, for the 5th and 7th voltage harmonics, the amplitudes are symmetric with respect to  $\phi = 0^\circ$ , and positive  $\phi$  (*i.e.*, reactive power consumption by the cycloconverter) can result in reduced amplitudes of

the 11th and 13th voltage harmonics. At  $\phi \approx 85^\circ$ , minimum amplitudes are obtained. However, this value is unacceptably low, so  $\phi = 35^\circ$  is selected (for operation at rated power). After  $\phi$  has been determined, it follows from (8.4.13) and (8.4.14) that there is a linear relation between  $L_f$  and  $C_f$ , as in  $C_f = aL_f + b$ , since  $\tan \phi = Q_{cyc}^{20}/P_{cyc}^{20}$ . However, any  $(L_f, C_f)$  pair determined based on this equation should only be used as an initial guess. These initial parameters might not yield the required power factor angle ( $\phi = 35^\circ$ ) due to the simplifying assumptions made in the analysis. The proper  $LC$  filter parameters can be obtained by solving the circuit shown in Figure 8.4.1:<sup>1</sup>. For example, given a value for  $L_f$ , the capacitance  $C_f$  that leads to the right power factor angle can be found by searching around its initial guess value. Therefore, if  $L_f$  varies within a certain range, a number of  $(L_f, C_f)$  pairs can be obtained. Among these  $(L_f, C_f)$  candidates, a selection is made such that the magnitudes  $|Z_R(\omega_n)|$  for  $n = 5, 7, 11, 13$  are deemed to be adequately large. A numerical example will be provided in the next section.

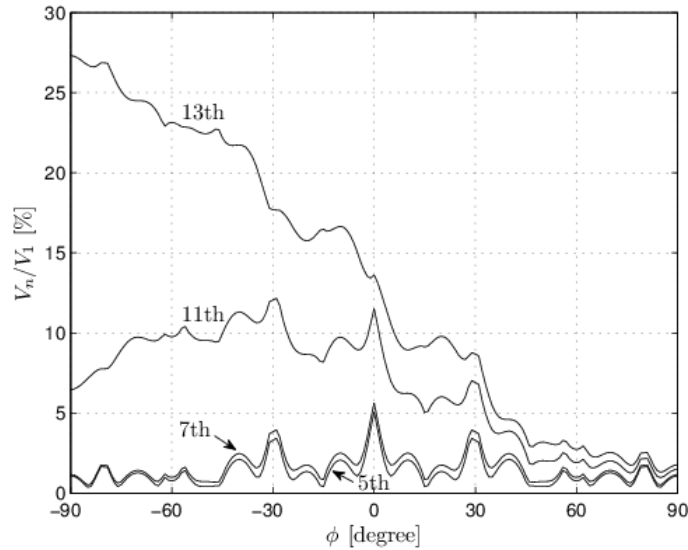


Figure 8.4.3: Harmonic Voltage Amplitudes Generated by the Cycloconverter at the 20 Hz Side

## 8.5 Case Study

In this section, a design case study of a 20 Hz LFAC transmission system is presented. The transmission voltage level is chosen as 132 kV. An appropriate submarine three-core XLPE power cable is selected (nominal voltage: 132 kV, maximum voltage: 145 kV, rated current: 825 A, cross section: 1000 mm<sup>2</sup>, copper conductor). The cable's

<sup>1</sup>The circuit can be solved by formulating this as a three-bus power flow problem, where the sending end is a  $PQ$ -type bus. Since  $Q_S = f(P_S, V_S)$ , the power flow is solved for a range of  $Q_S$  values, until the computed  $V_S$  provides the correct value of  $Q_S$ , when substituted in  $f(\cdot)$ .

resistance, inductance, and capacitance per km are 17.6 mΩ/km, 0.35 mH/km, and 0.25 μF/km, respectively [37, 38].

The LFAC system is compared to a conventional 60 Hz HVAC transmission system that uses the same power cable, with a steady-state single-phase equivalent circuit shown in Figure 8.5.1.  $X_{sc}$  represents the short-circuit level of the 60 Hz power grid. Shunt reactive compensation ( $X_S$  and  $X_R$  in Fig. 2) is connected at both ends to improve the active power transmission capability, especially for long transmission distances [39]. The power grid voltage is 132 kV line-to-line. The short-circuit level is  $S_{sc} = 5,000$  MVA, which is a typical value for a 132-kV system [40]. At the sending end, unity power factor is assumed ( $Q_S = 0$ ), in order to calculate the maximum possible transmissible active power through the cable. Two cases are considered:

- 1) No shunt reactive compensation, *i.e.*,  $X_S = X_R = 0$ . This case is denoted as ‘60 Hz 0/0’.
- 2) Shunt reactive compensation split equally between the two ends. This case is denoted as ‘60 Hz 50/50’. The total amount of reactive compensation is  $Q_X = \text{Im}\{Y'\}V_o^2$ , so  $X_S = X_R = 2V_o^2/Q_X$ .

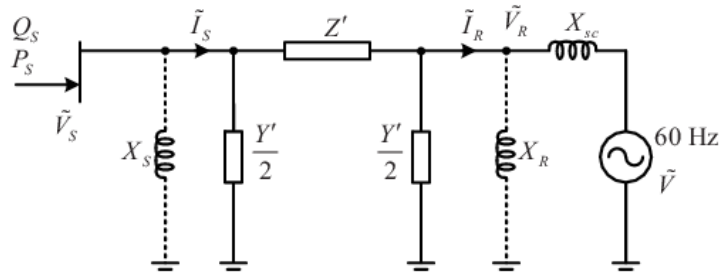


Figure 8.5.1: Equivalent Circuit of 60 Hz Transmission System

The relationship between sending end active power  $P_S$  and maximum transmission distance is calculated using the circuit of Figure 8.5.1, and plotted in Figure 8.5.2. The maximum transmission distance is obtained whenever the current or the voltage rating of the power cable is reached. In this case study, the cable’s rated apparent power is 188 MVA. The maximum distance for transmitting 180 MW is 45 km without shunt compensation, and 70 km with shunt compensation.

The 20 Hz LFAC system is designed to transmit 180 MW over 160 km. At the sending end, the DC bus voltage level is chosen as 30 kV. A 214-MVA, 132/13.2 kV ( $n_s = 10$ ), 20 Hz phase-shift transformer is used. With the 20 Hz rated frequency, this transformer would have larger volume compared to 60 Hz transformers. This is a drawback of the proposed LFAC system. The total size of the AC filters at the sending end is 115 MVar.



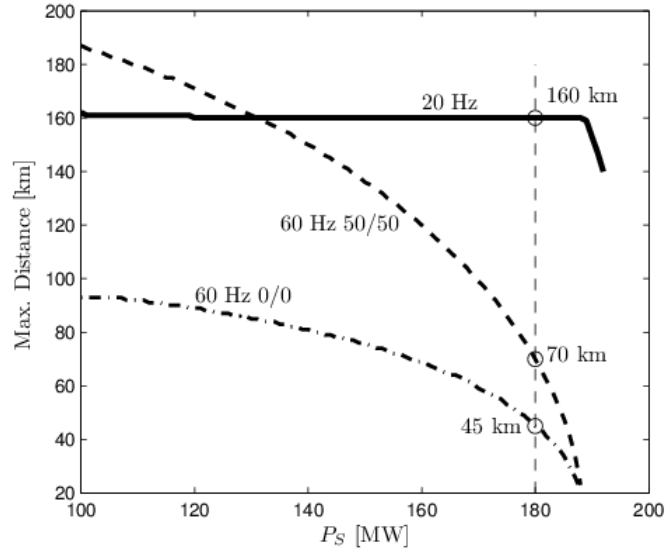


Figure 8.5.2: Sending End Active Power vs. Max. Transmission Distance

For the cycloconverter, the voltage (line-to-line) generated at the 20 Hz side is 132 kV. The voltage ratio is selected as  $r = 0.9$ , and the 20 Hz side power factor angle is designed to be  $\phi = 35^\circ$ . According to (8.3.2) and (8.3.4), the transformer ratio is  $n_R = 1.5$ , and the 60 Hz side power factor is  $\text{PF}^{60} \approx 0.68$  [34]. Based on the analysis of Section 8.2.1 and equation (8.4.15), the apparent power rating of each cycloconverter transformer is chosen to be 100 MVA. The total size of AC filters at the 60 Hz side is 200 MVar.

Figure 8.5.3: depicts the approximate linear relation between  $L_f$  and  $C_f$  by a dashed line. The more accurate capacitance values that yield the required power factor angle are represented by the solid curve. A solution is found for  $L_f$  between 7 mH and 63 mH. Note that a solution can be obtained for  $L_f$  outside this range as well; however, in this case, either the current or the voltage rating of the power cable are violated. Figure 8.5.4: shows the variation of  $|Z_R(\omega_n)|$  corresponding to the feasible  $(L_f, C_f)$  pairs. It can be seen that the  $LC$  filter with  $L_f = 63$  mH and  $C_f = 8.7 \mu\text{F}$  gives the maximum impedance magnitudes for the 5th, 11th, and 13th harmonics.

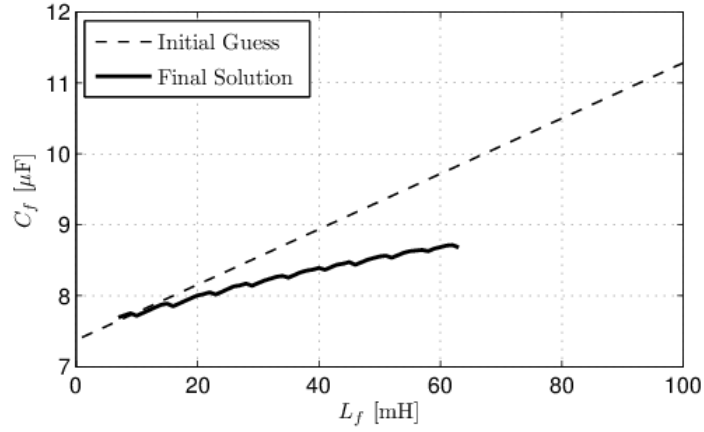


Figure 8.5.3:  $LC$  Filter Design

Finally, based on the above system parameters, the relationship between sending-end active power and maximum transmission distance for the 20 Hz LFAC system is calculated and superimposed in Figure 8.5.2. It can be observed that the proposed LFAC system is a feasible option for delivering the rated power over a distance ca. 2-3 times further than the HVAC solution. Typically, for distances longer than 100 km, HVDC systems are the preferred solution 41, but an LFAC system could be an alternative transmission technology for the 100-200 km range, at least from a technical standpoint.

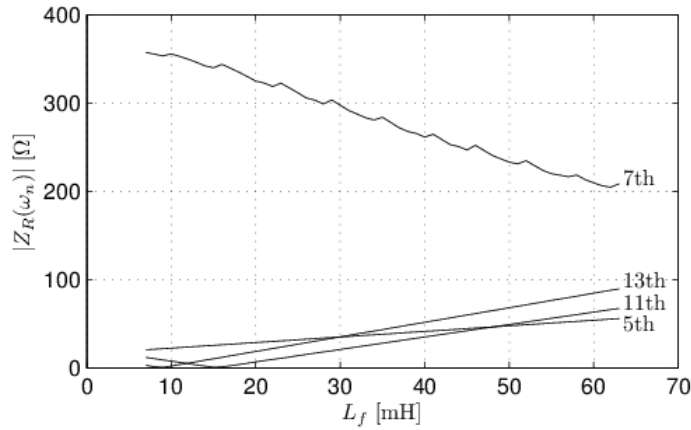


Figure 8.5.4: Equivalent Impedance Magnitude Seen from the Receiving End  
( $n = 5, 7, 11, 13$ )

## 8.6 Simulation Results

To demonstrate the validity of the proposed LFAC system, simulations have been carried out using Matlab/Simulink and the Piecewise Linear Electrical Circuit Simulation (PLECS) toolbox. The wind power plant is rated at 180 MW, and the transmission distance is 160 km. The system parameters are listed in Table 8.6.1:. The parameters of

the PI controllers in Figure 8.2.1: and Figure 8.3.1: are listed in Table 8.6.2. The transmission power cable is modeled by cascading 20 identical  $\Pi$  sections.

Table 8.6.1: LFAC System Simulation Parameters

Sending End			
DC Bus Capacitor		$C = 1000 \mu\text{F}$	
Smoothing Inductor		$L = 0.1 \text{ H}, R = 1 \text{ m}\Omega$	
20 Hz Phase-shift Transformer			
Rated Power	214 MVA	Voltage	132/13.2 kV
Winding Resistance	0.001 p.u.	Leakage Reactance	0.05 p.u.
Magnetizing Resistance	1000 p.u.	Magnetizing Reactance	200 p.u.
AC Filters (115 MVar, 132 kV, 20 Hz)			
	R ( $\Omega$ )	L (mH)	C ( $\mu\text{F}$ )
11 th	0.41	29.7	17.6
13 th	0.35	21.3	17.6
> 23 rd	19.7	6.8	17.6
Transmission Power Cable (132 kV)			
Resistance	17.6 m $\Omega$ /km	Inductance	0.35 mH/km
Capacitance	0.25 $\mu\text{F}$ /km	Rated Current	825 A
Receiving End			
LC Filter		$L_f = 63 \text{ mH}, C_f = 8.7 \mu\text{F}$	
Transformers			
Rated Power	100 MVA	Voltage	132/88 kV
Winding Resistance	0.001 p.u.	Leakage Reactance	0.05 p.u.
Magnetizing Resistance	1000 p.u.	Magnetizing Reactance	200 p.u.
AC Filters (200 MVar, 132 kV, 60 Hz)			
	R ( $\Omega$ )	L (mH)	C ( $\mu\text{F}$ )
3 rd	1.16	102.7	7.6
5 th	0.70	37.0	7.6
7 th	0.50	18.9	7.6
> 9 th	38.7	11.4	7.6

Table 8.6.2: Parameters of PI Controllers with Transfer Function  $K(1 + \frac{1}{\tau s})$

	Sending end	Receiving end
$K$	1	0.125
$\tau$	0.4	0.05

Figure 8.6.1: shows the steady-state line-to-line voltage and current waveforms at the sending end, the receiving end, the 20 Hz side of the cycloconverter, and the 60 Hz power grid side under rated power conditions. The 20 Hz voltage generated from the cycloconverter has significant harmonic distortion (THD is 16.4%). Due to the  $LC$  filter, the voltages at the receiving end and the sending end have reduced THD values (3.2% and 2.2%, respectively). The measured fundamental power factor angle  $\phi$  at the 20 Hz side of the cycloconverter is  $33^\circ$ , which is close to the design requirement.

Figure 8.6.2: depicts the results of a transient simulation where the power from wind turbines  $P_w$  ramps from 170 MW to 180 MW, at 10 MW/s. Shown are the transient responses of the active power injected into the 60 Hz power grid, the DC bus voltage at the sending end, and the magnitude of the fundamental component of the 20 Hz voltage at the receiving end.

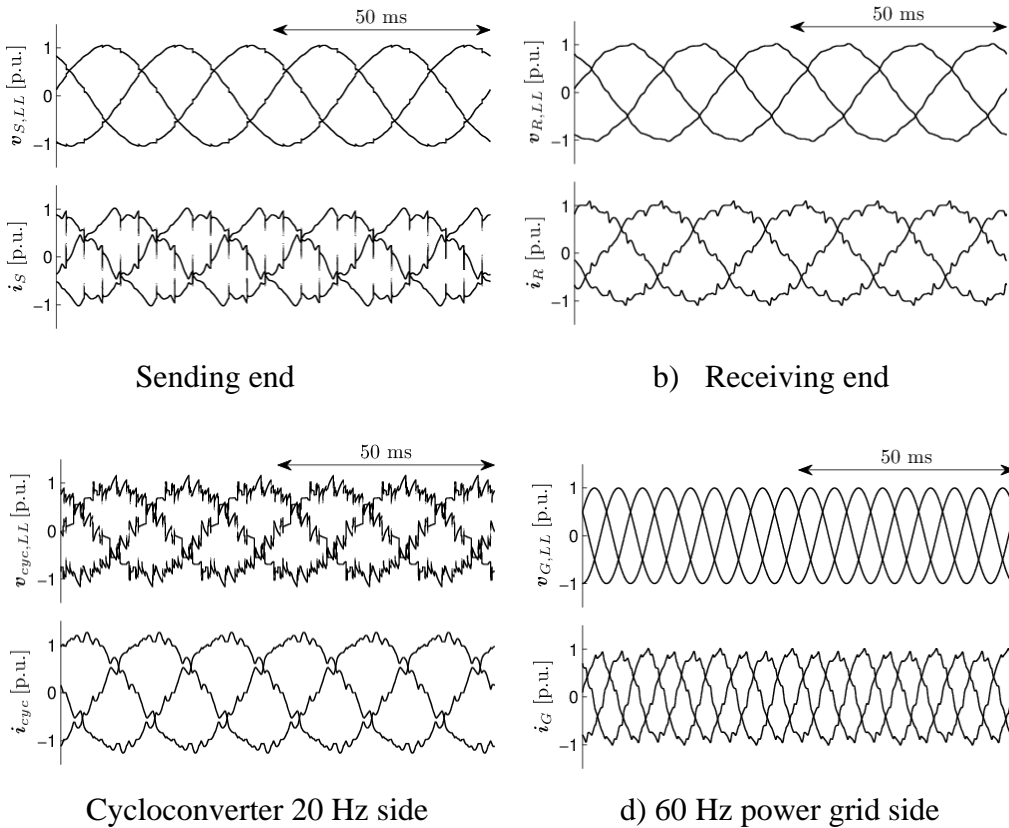


Figure 8.6.1: Simulated Voltage and Current Waveforms

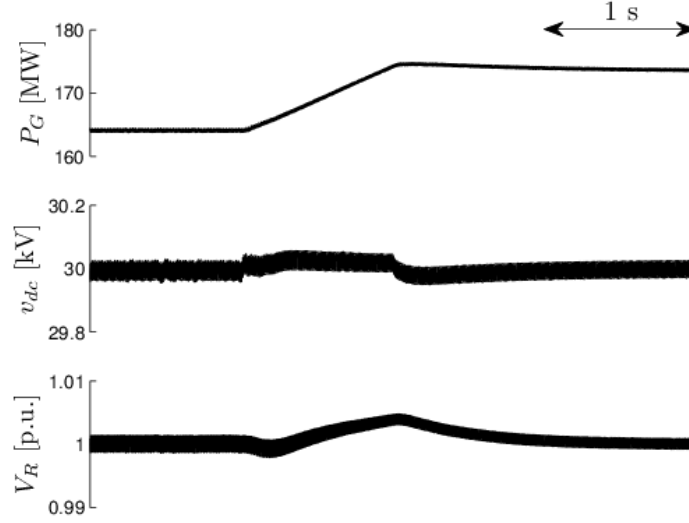


Figure 8.6.2: Transient Waveforms

## 8.7 Conclusion

A low-frequency AC transmission system has been proposed. The methodology to design the system's components and control strategies has been discussed. The use of low frequency can improve the transmission capability of submarine power cables due to low cable charging current. The proposed LFAC system appears to be a feasible solution for the integration of offshore wind power plants over long distances. Technically, it could be used to substitute HVDC systems. Furthermore, it is easier to establish a low-frequency AC network to transmit bulk power from multiple plants.

In order to help the wind energy industry to make a better-informed decision for the transmission type for offshore wind power, it is of significance to perform a complete technical and economic comparison among HVAC, HVDC, and LFAC, *e.g.*, transmission efficiency, transient stability, and investment evaluation. The above are subjects of ongoing work.

## 9 Time-Domain Studies-II

This section presents time-domain studies of alternative-transmission systems using a three-phase, six-pulse cycloconverter. Time-domain simulation is utilized for better understanding of the dynamic behavior of the alternative transmission systems. Alternative-transmission systems employ phase-controlled converters and PWM converters, and the converters using electrical switches are well-known harmonic sources. Harmonic pollution in power system causes several problems: heat problem in transformer and electrical machines, aging problem of isolation of power-system devices, malfunction of dynamic-control systems, and inductive interference over communication networks. Harmonics should be mitigated in power systems and the voltages and currents at every point should be near pure sine-waves; the harmonics should be within allowable limits. So, understanding the harmonic content from alternative systems is necessary to design the harmonic filters for the alternative-transmission systems for high power quality.

Since power consumption from electrical load varies in real time, the flexible control of an amount of the transfer power from wind farms can allow continuing operation of electrical systems. Since the alternative-transmission systems consist of several converters, operating voltage, operating frequency, and real- and reactive-power can be controlled by changing their control references. However, inappropriate control algorithm or control parameters become the direct reason of switching malfunctions. Eventually, the voltage spikes and current spikes can occur and the electrical switches should be damaged physically. Power-transient studies can allow the optimal design of control systems of alternative transmissions and the knowledge to support continuing operation of the LFAC transmission systems.

### 9.1 Technical Approach of Time-Domain Studies

The time-domain studies are performed using two LFAC-transmission systems interconnecting a wind farm and grid systems as shown in Figure 9.1.1 and Figure 9.1.2. For the LFAC-transmission systems, variable-speed wind-turbine systems (type-3 and type-4 wind generation units) are considered, since variable-speed wind-generation systems are attractive for increasing energy capture and reducing mechanical-fatigue damage. The variable-speed wind-turbine systems cannot be directly connected to grid systems and converters are used to connect systems with different frequency. In the proposed wind farm configurations, three-phase PWM converters and a three-phase six-pulse cycloconverter are used to interconnect systems with different frequency. The three-phase PWM converters interconnect wind farms and a LFAC transmission system while the three-phase cycloconverter interconnect the LFAC transmission system and nominal-frequency grid systems. Also, each converter performs its own roles: the cycloconverter controls operating frequency at the LFAC transmission system and allows voltage synchronization for the three-phase PWM inverters; the three-phase PWM inverters should support DC-voltage level and the controllability of reactive power of the

LFAC transmission systems; and the three-phase PWM rectifiers allow the power tracking to extract maximum power from wind turbines.

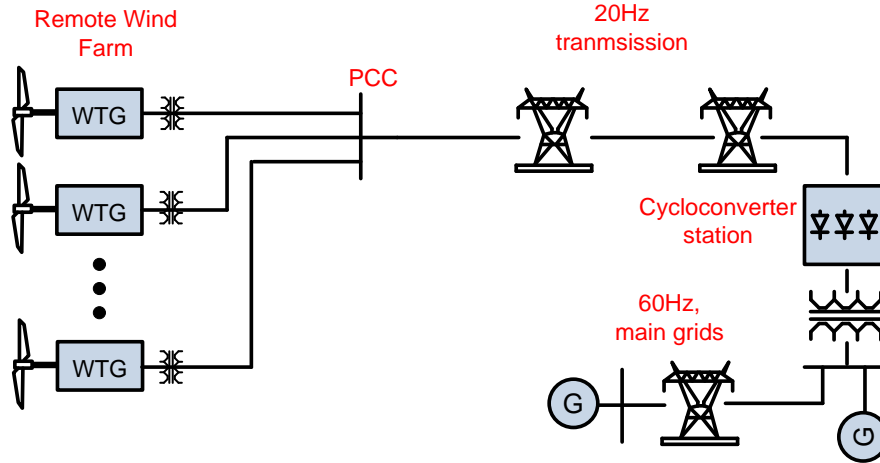


Figure 9.1.1: Wind Farm Configuration: LFAC Wind Farm and LFAC Transmission

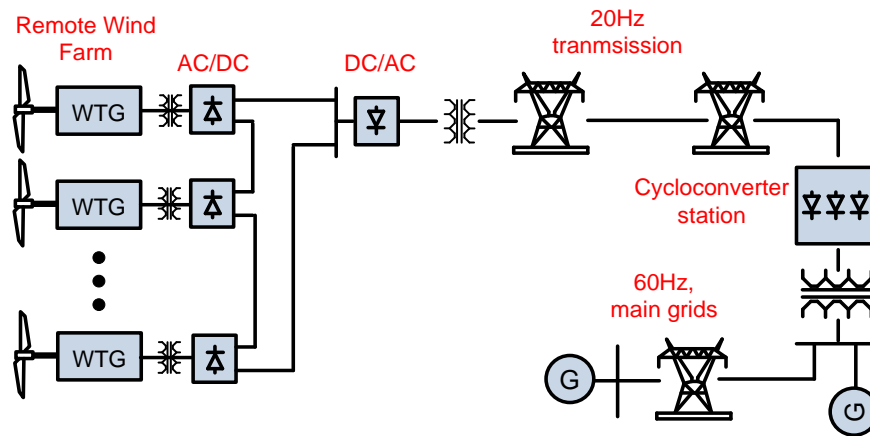


Figure 9.1.2: Wind Farm Configuration: Series DC Wind Farm and LFAC Transmission

For the realistic models of the wind farm configurations, each device (containing the LFAC transmission systems) has to be modeled in realistic manners. For the purpose, we use quadratic integration method and Kirchhoff's current law. Since mathematical models of physical components in power systems are generally modeled by state equations, these equations cannot be solved exactly in explicit calculations. So, approximate methods are necessary to model power systems and the quadratic integration method is introduced as the approximate method. As soon as all devices are model, the devices are merged to form an entire network system using Kirchhoff's current law. More details are presented in next subsection.

Using the realistic network systems, power-transient studies and harmonics studies are performed. For the power-transient study, power step changes (the required power-order)

suddenly occur while the LFAC transmission systems are operating in steady state. Also, harmonics studies are performed according to the control modes (partial- and full-circulating current modes) and modulation indexes of the cycloconverter. Since the cycloconverter is directly connected to grid systems, we present harmonic contents of voltages and currents before and after the cycloconverter.

## **9.2 Methodology for Simulation Models in Time-Domain**

Time-domain studies are based on computer analysis in time-domain. For the purpose, the reliable and realistic models for alternative transmission systems connecting wind farms are needed. Here, we introduce an advanced time-domain method, which is named as quadratic-integration method. The quadratic integration has demonstrated the superior properties compared to pre-dominant methods (such as backward Euler's method and trapezoidal integration method). Especially, the quadratic integration is a powerful simulation method for nonlinearities and switching systems, since the method is totally free from artificial numerical oscillations that are not natural phenomena from systems instability but fictitious phenomena from simulation methods themselves. The basic concepts and advantages of the quadratic integration are in Appendix C.

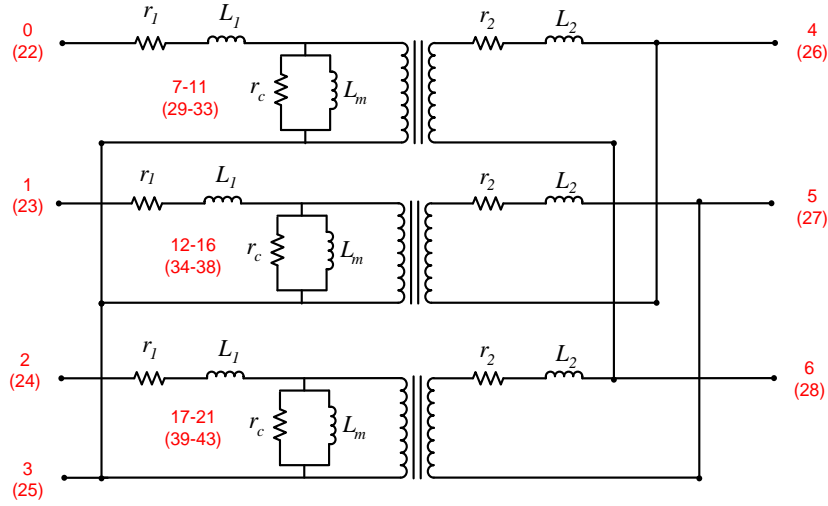
The detailed modeling methodology of time-domain models is presented based on the application of the quadratic integration method and standard nodal analysis. The modeling process for time-domain models is performed: (1) each component constructing a power device is written in state equations, (2) the quadratic integration is applied to the state equations to derive the algebraic-companion form (ACF) of the each component, and (3) the ACF of the power device is constructed by merging the ACF of all components in the power device. With the modeling process above, power devices composing alternative-transmission systems are modeled. Here we present a three-phase transformer model, a three-phase, six-pulse, cycloconverter, and a three-phase PWM converter, since the models are essential for the alternative transmission systems.

### **9.2.1 Three-Phase Transformer**

Modeling of the three-phase isolation transformer can be modeled using three single-phase transformers. First, a single-phase transformer is written as state equations and the quadratic integration method is applied to the state equations for algebraic-companion forms. Finally, the algebraic companion forms are interconnected to provide the topology of the three-phase transformer. Here, we only introduce a wye-delta connected three-phase transformer, even though all the combinations of connections can be modeled. Figure 9.2.1 shows (A) the three-phase isolation transformer, and (B) a single-phase transformer.



(A)



(B)

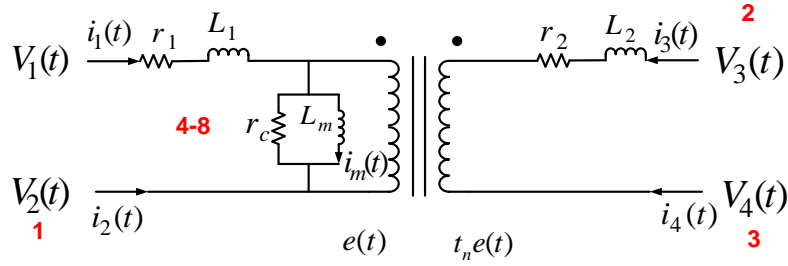


Figure 9.2.1: (A) Three-Phase Y-Δ Isolation Transformer and (B) Single Phase Transformer

The differential equations and algebraic equations describing the single-phase transformer model are written in state-space form. There are two sets of equations: external equations and internal equations. The external equations consist of the node currents of the single phase transformer and the internal equations are derived with internal states. The state-space model is given as follows:

$$i_1(t) = i_{1L}(t) \quad (9.2.1)$$

$$i_2(t) = -i_{1L}(t) \quad (9.2.2)$$

$$i_3(t) = i_{3L}(t) \quad (9.2.3)$$

$$i_4(t) = -i_{3L}(t) \quad (9.2.4)$$

$$0 = -r_c i_{1L}(t) - r_c t i_{3L}(t) + r_c i_m(t) + e(t) \quad (9.2.5)$$

$$0 = L_m i_m(t) - \lambda(t) \quad (9.2.6)$$

$$0 = v_1(t) - v_2(t) - e(t) - r_1 i_{1L}(t) - L_1 \frac{d}{dt} i_{1L}(t) \quad (9.2.7)$$

$$0 = v_3(t) - v_4(t) - t e(t) - r_2 i_{3L}(t) - L_2 \frac{d}{dt} i_{3L}(t) \quad (9.2.8)$$

$$0 = e(t) - \frac{d}{dt} \lambda(t) \quad (9.2.9)$$

where  $\lambda$  is magnetic flux linkage.

The compact matrix form is also given as follows:

$$\vec{I}(t) = M \cdot \vec{V}(t) + N \cdot \frac{d}{dt} \vec{V}(t) \quad (9.2.10)$$

where:

$$M = \begin{bmatrix} 0 & 0 & 0 & 0 & 0 & 0 & 0 & 1 & 0 \\ 0 & 0 & 0 & 0 & 0 & 0 & 0 & -1 & 0 \\ 0 & 0 & 0 & 0 & 0 & 0 & 0 & 0 & 1 \\ 0 & 0 & 0 & 0 & 0 & 0 & 0 & 0 & -1 \\ 0 & 0 & 0 & 0 & r_c & 1 & 0 & -r_c & -r_c t \\ 0 & 0 & 0 & 0 & L_m & 0 & -1 & 0 & 0 \\ 1 & -1 & 0 & 0 & 0 & -1 & 0 & -r_1 & 0 \\ 0 & 0 & 1 & -1 & 0 & -t & 0 & 0 & -r_2 \\ 0 & 0 & 0 & 0 & 0 & 1 & 0 & 0 & 0 \end{bmatrix}, \quad N = \begin{bmatrix} 0 & 0 & 0 & 0 & 0 & 0 & 0 & 0 & 0 \\ 0 & 0 & 0 & 0 & 0 & 0 & 0 & 0 & 0 \\ 0 & 0 & 0 & 0 & 0 & 0 & 0 & 0 & 0 \\ 0 & 0 & 0 & 0 & 0 & 0 & 0 & 0 & 0 \\ 0 & 0 & 0 & 0 & 0 & 0 & 0 & 0 & 0 \\ 0 & 0 & 0 & 0 & 0 & 0 & 0 & 0 & 0 \\ 0 & 0 & 0 & 0 & 0 & 0 & 0 & -L_1 & 0 \\ 0 & 0 & 0 & 0 & 0 & 0 & 0 & 0 & -L_2 \\ 0 & 0 & 0 & 0 & 0 & 0 & -1 & 0 & 0 \end{bmatrix}$$

$$\vec{I}(t) = [i_1(t) \quad i_2(t) \quad i_3(t) \quad i_4(t) \quad 0 \quad 0 \quad 0 \quad 0 \quad 0]^T,$$

$$\vec{V}(t) = [v_1(t) \quad v_2(t) \quad v_3(t) \quad v_4(t) \quad i_m(t) \quad e(t) \quad \lambda(t) \quad i_{L1}(t) \quad i_{L3}(t)]^T$$

The compact matrix form of the single-phase transformer is reformulated into algebraic-companion form applying quadratic integration. The transformer algebraic-companion form (ACF) at each time step  $[t-h, t]$  is:

$$A \cdot \begin{bmatrix} \vec{I}(t) \\ \vec{I}(t_m) \end{bmatrix} = B \cdot \begin{bmatrix} \vec{V}(t) \\ \vec{V}(t_m) \end{bmatrix} - C \cdot \vec{V}(t-h) - D \cdot \vec{I}(t-h) \quad (9.2.11)$$

where:

$$A = \begin{bmatrix} -\frac{h}{24}A_s & \frac{h}{3}A_s \\ \frac{h}{6}A_s & \frac{2h}{3}A_s \end{bmatrix}, \quad B = \begin{bmatrix} -\frac{h}{24}M & \frac{h}{3}M + N \\ \frac{h}{6}M + N & \frac{2h}{3}M \end{bmatrix}, \quad C = \begin{bmatrix} -\frac{5h}{24}M + N \\ -\frac{h}{6}M + N \end{bmatrix}, \quad D = \begin{bmatrix} \frac{5h}{24}A_s \\ \frac{h}{6}A_s \end{bmatrix},$$

$$\vec{I}(t_m) = [i_1(t_m) \quad i_2(t_m) \quad i_3(t_m) \quad i_4(t_m) \quad 0 \quad 0 \quad 0 \quad 0 \quad 0]^T,$$

$$\vec{V}(t_m) = [v_1(t_m) \quad v_2(t_m) \quad v_3(t_m) \quad v_4(t_m) \quad i_m(t_m) \quad e(t_m) \quad \lambda(t_m) \quad i_{L1}(t_m) \quad i_{L3}(t_m)]^T,$$

$A_s = \text{diag}(1, 1, 1, 1, 0, 0, 0, 0, 0)$ , and  $t_m$  is the mid-point of the integration time step.

The algebraic-companion forms of the three single-phase transformers are merged to form the algebraic companion form of a three-phase isolation transformer. For this purpose it is noted that each single-phase transformer is connected to specific nodes of the three-phase isolation transformer. The connectivity of each single-phase transformer is defined in terms of the order of the corresponding states. Figure 9.2.1 shows the node numbers on specific nodes. Table 9.2.1 provides the connectivity pointers of the single phase transformers. The merging of these models into an overall model of the three-phase transformer is achieved by writing the Kirchhoff's current law at each internal node of the three-phase transformer substituting the appropriate equations. This process is achieved with the algorithm below:

DO WHILE ( *itrans* < Number of 1- $\Phi$  transformers)

DO WHILE ( *i* < Number of ROW<sub>1- $\Phi$</sub> )

*i1* = Valve Pointer [ *i* ][ *itrans* ]

DO WHILE ( *j* < Number of Column<sub>1- $\Phi$</sub> )

*j1* = Valve Pointer [ *j* ][ *itrans* ]

$A_{3\Phi}[i1][j1] = A_{1\Phi}[i][j]$

$B_{3\Phi}[i1][j1] = B_{1\Phi}[i][j]$

$C_{3\Phi}[i1][j1] = C_{1\Phi}[i][j]$

$D_{3\Phi}[i1][j1] = D_{1\Phi}[i][j]$

END DO

END DO

END DO

where  $i = 1, 2, \dots$ , number of row of each matrix,  
 $j = 1, 2, \dots$ , number of column of each matrix, and  
 $itrans = 1, 2, \dots$ , number of 1- $\Phi$  transformers.

Table 9.2.1: Connectivity Pointer of Three Single-Phase Transformers

# 1- $\Phi$ transformer		Connective Node in the Three-phase Transformer								
1	t	0	3	4	6	7	8	9	10	11
	t <sub>m</sub>	22	25	26	28	29	30	31	32	33
2	t	1	3	5	4	12	13	14	15	16
	t <sub>m</sub>	23	25	27	26	34	35	36	37	38
3	t	2	3	6	5	17	18	19	20	21
	t <sub>m</sub>	24	25	28	27	39	40	41	42	43

The end result is the algebraic-companion form of the overall three-phase transformer given by the following equation:

$$A_{3\Phi} \cdot \begin{bmatrix} \bar{I}(t) \\ \bar{I}(t_m) \end{bmatrix} = B_{3\Phi} \cdot \begin{bmatrix} \bar{V}(t) \\ \bar{V}(t_m) \end{bmatrix} - C_{3\Phi} \cdot \bar{V}(t-h) - D_{3\Phi} \cdot \bar{I}(t-h) \quad (9.2.12)$$

where  $A_{3\Phi}$  and  $B_{3\Phi}$  are 44 by 44 matrices, and  $C_{3\Phi}$ , and  $D_{3\Phi}$  are 44 by 22 matrices, which are automatically built with the computer algorithm above.

### 9.2.2 Three-Phase Six-Pulse Cycloconverter

The three-phase six-pulse cycloconverter consists of three physical components as shown in Figure 9.2.2: three-phase isolation transformers, electrical switches (thyristors), and circulating-current circuits. Furthermore, a controller is needed to generate switching sequences for the thyristors on both converters. The cycloconverter controller controls the magnitude and frequency of output voltages by controlling the timing (phase) of the thyristor firing pulses. To control the output voltages, many control algorithms have been proposed and studied for the control of the three-phase six-pulse cycloconverter. Cosine-wave crossing method is elected among the control algorithms, since this method has been proven to have the unique property of minimum total harmonic distortion on output voltage waveform [44][49].

The three-phase six-pulse cycloconverter requires electrical isolation between the inputs to the individual six-pulse bridges, since the three-phase six-pulse cycloconverter doesn't have any common connected points between the input and output [44]. Three-phase isolation transformers offer electrical isolation and magnetic interconnection. However, the modeling process of the three-phase isolation transformer is omitted in this subsection, since the physical structure of the three-phase isolation transformer is the same to that of

the three-phase transformer in subsection A of this chapter. Only, the modeling process of the electrical valve and the circulating-current circuit is presented for the equivalent circuit of the three-phase, six-pulse cycloconverter.

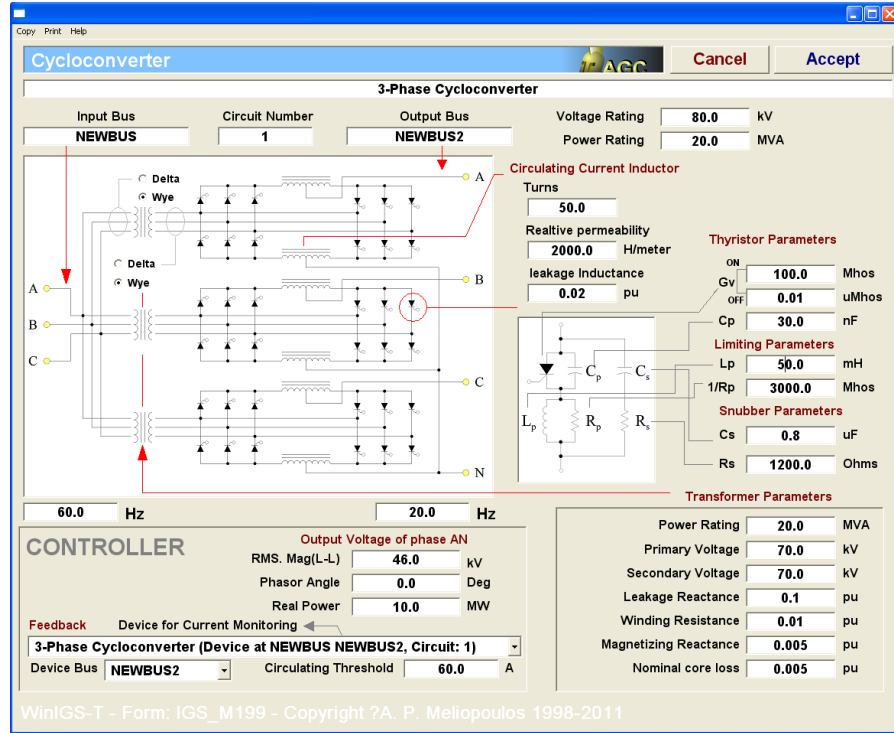


Figure 9.2.2: Three-Phase, Six-Pulse Cycloconverter

The electrical valve consists of an electrical switch (thyristor) and protection circuits (a snubber circuit and a limiting current circuit) as shown in Figure 9.2.3. The protection circuits are to reduce the electrical stress placed on the three-phase six-pulse cycloconverter by state changes of switches [50].

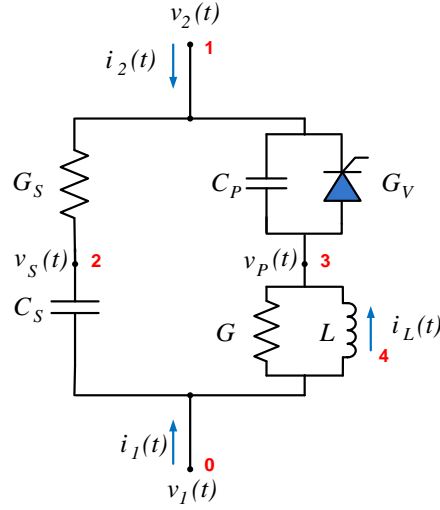


Figure 9.2.3: Electrical Valve

The differential equations and algebraic equations describing the electrical-valve model are written in state-space form. There are two sets of equations: external equations and internal equations. The external equations consist of the node currents of the electrical valve and the internal equations are derived with internal states. The state-space model is given as follows:

$$i_1(t) = G \cdot [v_1(t) - v_P(t)] + G_S [v_S(t) - v_2(t)] + i_L(t) \quad (9.2.13)$$

$$i_2(t) = G \cdot [v_P(t) - v_1(t)] + G_S [v_2(t) - v_S(t)] - i_L(t) \quad (9.2.14)$$

$$0 = G_S \cdot [v_S(t) - v_2(t)] + C_S \frac{d}{dt} [v_S(t) - v_1(t)] \quad (9.2.15)$$

$$0 = G_V \cdot [v_P(t) - v_2(t)] + C_P \frac{d}{dt} [v_P(t) - v_2(t)] + G \cdot [v_P(t) - v_1(t)] - i_L(t) \quad (9.2.16)$$

$$0 = -v_1(t) + v_P(t) + L \frac{d}{dt} i_L(t) \quad (9.2.17)$$

A compact matrix form can be easily written using equations from state-space equations above, and the algebraic companion form is yielded by the application of the quadratic integration method to the compact matrix form. All processes are the same as in the case of the single-phase transformer model in subsection A in this chapter.

The discontinuous transactions between positive and negative converter valves generate abnormal distortions of output-currents. Here, circulating-current circuits are introduced to avoid abnormal distortions on output-currents, since the circulating-current circuits can

support continuous conduction of both converters. Figure 9.2.4 shows the equivalent circuit of the circulating-current circuit.

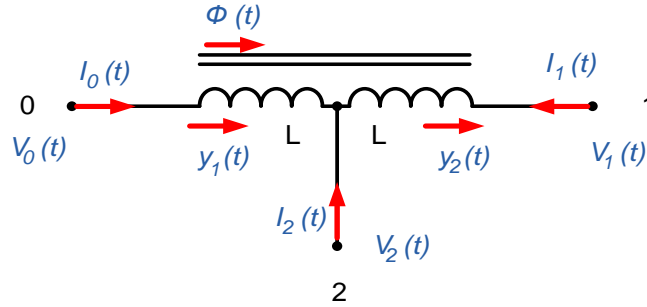


Figure 9.2.4: Circulating Current Circuit Model

The differential equations and algebraic equations describing the circulating-current model are written in state-space form. There are two sets of equations: external equations and internal equations. The state-space model of the circulating-current circuit is given as follows:

$$i_0(t) = y_1(t) \quad (9.2.18)$$

$$i_1(t) = -y_2(t) \quad (9.2.19)$$

$$i_2(t) = -y_1(t) + y_2(t) \quad (9.2.20)$$

$$0 = N_1 y_1(t) + N_2 y_2(t) - \Re \phi(t) \quad (9.2.21)$$

$$0 = v_0(t) - v_2(t) - \frac{dN_1 \phi(t)}{dt} - L_l \frac{d}{dt} y_1(t) \quad (9.2.22)$$

$$0 = v_2(t) - v_1(t) - \frac{dN_2 \phi(t)}{dt} - L_l \frac{d}{dt} y_2(t) \quad (9.2.23)$$

where:  $\Re$  is reluctance,  $L_l$  is the leakage inductance, and  $\phi$  is magnetic flux on core.

A compact-matrix form can be easily written using the state-space equations above and the algebraic-companion form is derived by the application of the quadratic integration method to the compact matrix form. All processes are the same with the case of the single-phase transformer model in subsection A of this chapter.

The algebraic-companion forms of three three-phase isolation transformers, thirty-six valves, and six circulating-current circuits are merged to form the three-phase six-pulse cycloconverter algebraic-companion form. For this purpose it is noted that each

component is connected to specific nodes of the cycloconverter as in case of three-phase transformer. The merging of these models into an overall model of the three-phase six-pulse cycloconverter is achieved by applying the Kirchhoff's current law at each internal node of the three-phase six-pulse cycloconverter substituting the appropriate equations.

### 9.2.3 Controller Design of the Three-Phase, Six-Pulse Cycloconverter

The cycloconverter controller controls the magnitude and frequency of output-voltages by controlling the timing (phase) of the thyristor firing pulses. To control the output-voltages, many control algorithms have been proposed and studied for the control of the three-phase six-pulse cycloconverter. Cosine-wave crossing method is elected among the control algorithms, since the method has been proven to have the unique property of minimum total distortion on output voltage waveform among phase-control algorithms for the three-phase six-pulse cycloconverter [44][49]. The implementation of the control scheme consists of two steps. In the first step, an estimation method is applied to determine the control references. The control references consist of two parameters at the input side (the magnitude and phase angle of positive, fundamental voltage,  $v_{ab}(t)$ ) and two parameters at the output side (the magnitude of positive fundamental voltage,  $v_{an}(t)$  and the real power). In the second step, cosine-wave crossing method is implemented in partial or full circulating current mode.

The control references are needed to update the switching time of the electrical-valves. For cosine-wave crossing method, the magnitude and phase angle of input voltage ( $v_{ab}$ ), the magnitude of output voltage ( $v_{an}$ ), and the output power are estimated. However, since converters are well-known harmonic sources, the references need to take distortion into consideration. Here, the positive-sequence fundamental voltages ( $v_{ab}$  and  $v_{an}$ ) at both input and output sides, and the positive-sequence fundamental output current are extracted from real-time voltages and currents via a Digital Signal Processor (DSP). To extract the positive-sequence fundamental output-values, two processes are applied to real-time values: discrete Fourier-series analysis for the fundamental values and modal decomposition for the positive-sequence values.

The discrete Fourier-series representation of  $v_{ab}(t)$  is defined as follows:

$$v_{ab}(t) = \sum_{k=1}^{\infty} [a_{ABk} \cos k(\omega t) + b_{ABk} \sin k(\omega t)] \quad (9.2.24)$$

The Fourier-coefficient representations of the fundamental component of  $v_{ab}(t)$  are defined as follows:

$$a_{AB1} = \frac{2}{m} \left[ \sum_{j=1}^m v_{ab}(t_j) \cos(\omega t_j) \right] \text{ and } b_{AB1} = \frac{2}{m} \left[ \sum_{j=1}^m v_{ab}(t_j) \sin(\omega t_j) \right],$$

where  $j = 1, 2, \dots, m$ .



At each time step, the quantities  $a_{AB1}$ ,  $a_{BC1}$ ,  $a_{CA1}$ ,  $b_{AB1}$ ,  $b_{BC1}$ , and  $b_{CA1}$  of three Line-to-Line voltages are estimated. With the extracted Fourier coefficient, the polar coordinates of the fundamental frequency components can be expressed as follows:

$$\tilde{V}_{AB1} = V_{AB1} \angle \phi_{AB1}, \quad (9.2.25)$$

$$\tilde{V}_{BC1} = V_{BC1} \angle \phi_{BC1}, \quad (9.2.26)$$

$$\tilde{V}_{CA1} = V_{CA1} \angle \phi_{CA1} \quad (9.2.27)$$

where:  $V_{k1} = \sqrt{a_{k1}^2 + b_{k1}^2}$ ,  $\phi_{k1} = \tan^{-1}\left(-\frac{b_{k1}}{a_{k1}}\right)$ , and  $k1$  is the sequence of  $AB1$ ,  $BC1$ , and  $CA1$ .

The calculated three voltages can be unbalanced and contain negative and zero sequence components. To use the positive sequence of fundamental component as reference voltage, modal decomposition is used as the following representation.

$$\begin{bmatrix} \tilde{V}_1 \\ \tilde{V}_2 \\ \tilde{V}_0 \end{bmatrix} = \frac{1}{3} \begin{bmatrix} 1 & a & a^2 \\ 1 & a^2 & a \\ 1 & 1 & 1 \end{bmatrix} \begin{bmatrix} \tilde{V}_{AB1} \\ \tilde{V}_{BC1} \\ \tilde{V}_{CA1} \end{bmatrix} \quad (9.2.28)$$

$\tilde{V}_1$ ,  $\tilde{V}_2$ , and  $\tilde{V}_0$  are the positive, negative, and zero sequence components of line-to-line voltages, and  $a = e^{j2\pi/3}$ . Therefore, the positive-sequence, fundamental voltage,  $\tilde{V}_{abl}$ , obtained from the Fourier analysis and the modal decomposition, can be expressed as follows:

$$v_{abl}(t) = V_{abl} \cos(\omega t + \phi_{V_{abl}}) \quad (9.2.29)$$

$$\text{where: } V_{abl} = \frac{1}{3} \cdot \sqrt{V_X^2 + V_Y^2}, \quad \phi_{abl} = \tan^{-1}\left(-\frac{V_Y}{V_X}\right),$$

$$V_X = \left[ V_{AB1} \cos(\phi_{AB1}) + V_{BC1} \cos\left(\phi_{BC1} + \frac{2\pi}{3}\right) + V_{CA1} \cos\left(\phi_{CA1} + \frac{4\pi}{3}\right) \right], \text{ and}$$

$$V_Y = \left[ V_{AB1} \sin(\phi_{AB1}) + V_{BC1} \sin\left(\phi_{BC1} + \frac{2\pi}{3}\right) + V_{CA1} \sin\left(\phi_{CA1} + \frac{4\pi}{3}\right) \right].$$

Based on the same procedure, the positive-sequence fundamental output-voltage  $v_{anl}(t)$  and output-current  $i_{al}(t)$  are computed, and output power is also computed using the positive-sequence fundamental output voltage and current.

Cosine-wave crossing method is a popular scheme, since it minimizes the total harmonic distortion (THD) of output-voltages [44][49] and it is a simple method to be implemented for the three-phase six-pulse cycloconverter. Since the three-phase six-pulse cycloconverter interconnects a low-frequency system (16.66/20Hz) with normal power grids (50/60Hz), harmonic distortion is an important power quality issue, and harmonic filter size depends on it. For minimizing the impacts from harmonics, a sophisticated control algorithm is needed for the three-phase six-pulse cycloconverter, and the cosine-wave crossing method with full- or partial-circulating currents is proposed in this chapter.

In cosine-wave crossing method, the firing pulses for thyristors are generated at crossing points of cosine-wave (which is named wanted output-voltage) and estimated-voltage references that are emulated by the reference voltage,  $v_{abl}(t)$ . The whole processes are shown in Figure 9.2.5.

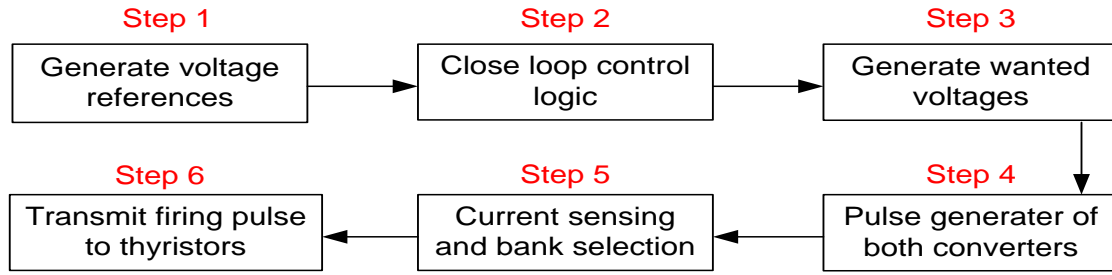


Figure 9.2.5: Control Algorithm for the Cycloconverter

In Step 1, the positive-sequence fundamental input-voltages are generated based on the positive-sequence fundamental input-voltage  $V_{abl}(t)$ . Note that  $V_{abl}(t)$  is the estimated value from DSP. The reference voltages are computed as follows:

$$V_{ab}(t) = V_{abl} \cos(w_i t + \phi_{V_{abl}}) \quad (9.2.30)$$

$$V_{ac}(t) = V_{abl} \cos(w_i t + \phi_{V_{abl}} - 60^\circ) \quad (9.2.31)$$

$$V_{bc}(t) = V_{abl} \cos(w_i t + \phi_{V_{abl}} - 120^\circ) \quad (9.2.32)$$

$$V_{ba}(t) = V_{abl} \cos(w_i t + \phi_{V_{abl}} - 180^\circ) \quad (9.2.33)$$

$$V_{ca}(t) = V_{abl} \cos(w_i t + \phi_{V_{abl}} - 240^\circ) \quad (9.2.34)$$

$$V_{cb}(t) = V_{abl} \cos(w_i t + \phi_{V_{abl}} - 300^\circ) \quad (9.2.35)$$

where  $w_i$  is angular velocity at high-frequency side.

Since the output-voltages at the low-frequency side are not the same to the wanted voltages (output-voltages are normally bigger than wanted voltages), a closed-loop controller is used to regulate the wanted voltages and equate the output-voltages and the voltage order. Here, we use two closed-loop controllers for magnitude and phase angle of the wanted voltage. Since the closed-loop controller for the magnitude is almost the same to that of the phase angle, the closed-loop controller for the phase angle of wanted voltage is only presented in this report. The process is implemented in Step 2 and the closed-loop controller for the phase angle is shown in Figure 9.2.6. Note that the phase angle is used to control the output power.

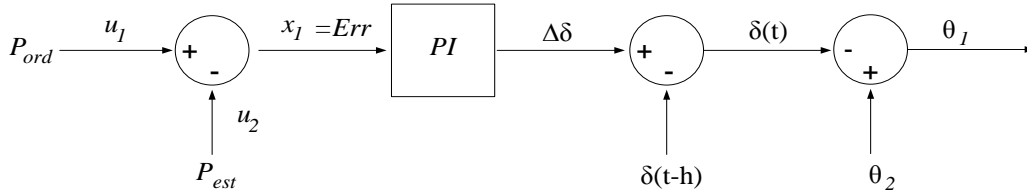


Figure 9.2.6: Close Loop Control Algorithm for (a) Magnitude of Voltage and (b) Output Power

The state-space equations of the control algorithm are represented as follows:

$$0 = x_1(t) - u_1(t) + u_2(t) \quad (9.2.36)$$

$$k_p \dot{x}_1 - \dot{x}_2 = -k_f x_1 \quad (9.2.37)$$

$$0 = x_2(t) - x_3(t) - u_3(t) \quad (9.2.38)$$

$$0 = x_3(t) - x_4(t) - u_4(t) \quad (9.2.39)$$

$$\text{where: } u = [u_1 \quad u_2 \quad u_3 \quad u_4]^T = [p_{ord} \quad p_{est} \quad \delta(t-h) \quad \theta_2]^T,$$

$x = [x_1 \quad x_2 \quad x_3 \quad x_4]^T = [Err \quad \Delta\delta \quad \delta \quad \theta_1]^T$ , and  $P_{ord}$  is power order,  $P_{est}$  is the estimated power from the DSP,  $\theta_1$  is the phase angle at output voltage ( $v_{an}$ ) of the cycloconverter,  $\theta_2$  is the phase angle at loads, and  $\delta = \theta_1 - \theta_2$ .

Note that the algebraic-companion form of the power controller can be also calculated upon application of the quadratic integration, and the algebraic companion-form of the controller can be integrated to the three-phase six-pulse cycloconverter. The process is the same to the modeling process of the single-phase transformer in subsection A in this chapter.

In Step 3, the wanted voltages are computed, based on the outputs of the closed-loop controllers. The wanted voltages can be computed as follows:

$$V_{wa}(t) = V_{want} \cos(w_o t + \theta_1) \quad (9.2.40)$$

$$V_{wb}(t) = V_{want} \cos(w_o t + \theta_1 - 120^\circ) \quad (9.2.41)$$

$$V_{wc}(t) = V_{want} \cos(w_o t + \theta_1 - 240^\circ) \quad (9.2.42)$$

where  $w_o$  is angular velocity at low frequency side, and  $V_{want}$  and  $\theta_1$  are the magnitude and phase angle from closed-loop controllers.

In step 4, firing pulses for thyristors can be generated at the point  $V_w(t) = V_T(t)$  for both positive converter and negative converter.  $V_T$  is the average values of two adjacent estimated input-voltages from the DSP. For an example, assuming that  $V_{ab}(t)$  and  $V_{ac}(t)$  are the adjacent input voltages, then  $V_T(t) = \frac{V_{ab}(t) + V_{ac}(t)}{2}$ .

In Step 5, the magnitudes of the output currents can be sensed, and the values can be used to select either the positive or the negative converters. Assuming that the output-current  $I_a(t)$  is bigger than circulating threshold current  $-I_T$ , the positive converters are activated, and assuming that the output-current is smaller than  $I_T$ , the negative converters are activated. In circulating mode ( $|I_a(t)| \leq I_T$ ), both converters are activated. Note that the circulating threshold current is a determined value from system operators.

In Step 6, the firing pulses are transmitted to the proper converter bank(s). Assuming that the cycloconverter is working in the full circulating mode, firing pulses are transmitted to both converters, and the sum of the firing angles for both converters is always  $180^\circ$ . Otherwise, the firing pulses have to be transmitted to the proper converter bank(s), according to the output currents and circulating threshold currents..

Note that the control algorithm is repeated at every time-step, until the simulation is over.

#### 9.2.4 Three-Phase PWM Converter

In this subsection, the modeling methodology for the three-phase pulse-width modulation (PWM) converter is presented. The three-phase PWM converter is used for the alternative-transmission systems, since phase-controlled converters are impractical for weak-synchronous systems and induction machines for wind farms. Also, the three-phase PWM converters have demonstrated several superior properties including: (a) bi-directional power flow control, (b) low-harmonic distortion of AC-line currents, and (c) flexible imaginary power control [51]. These converters have to support maximum power capturing from wind-turbine systems and offer constant output-voltage frequency from variable speed wind [52]. The three-phase PWM converter consists of six electrical-valves and a smoothing capacitor as shown in Figure 9.2.7. Furthermore, controllers are needed to generate switching sequences for on/off-controllable switches of the three-phase PWM converter. The controllers are based on direct power control algorithm using

space vectors, since the controllers have demonstrated rapid dynamic response with simple structure [53].

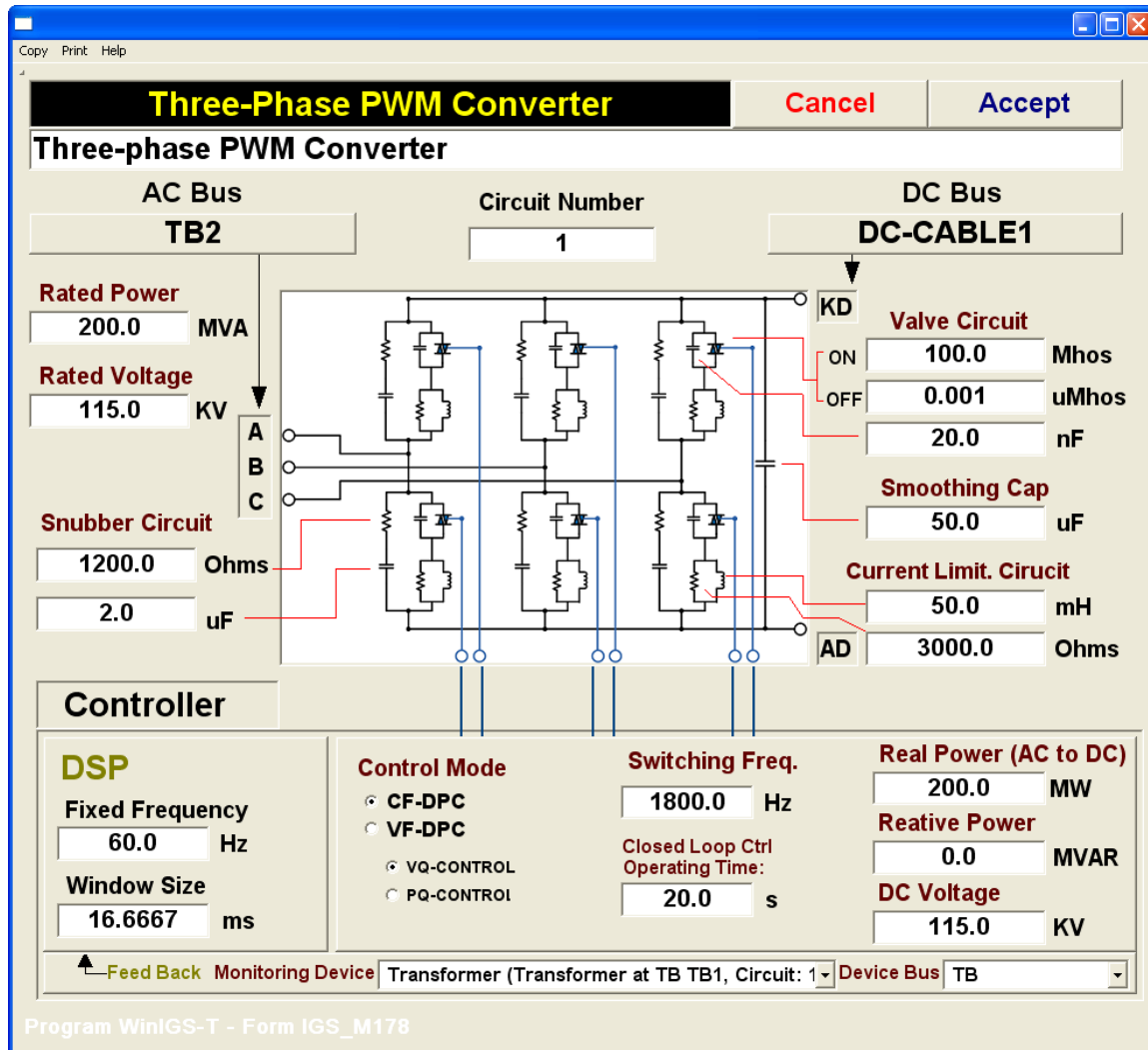


Figure 9.2.7: Three-Phase PWM Converter

The electrical-valves in the three-phase PWM converter are the same to those in the three-phase six-pulse cycloconverter, except that the electrical switches are on/off-controllable switches. Even though the physical structure of the electrical-valves in the three-phase PWM converter is different from those of the electrical-valves in the cycloconverter, the mathematical equations for the valve are equivalent to each other. So, the electrical-valve model is omitted in this subsection and a smoothing capacitor model is presented for the three-phase PWM converter. The equivalent circuit of the smoothing capacitor is shown in Figure 9.2.8.

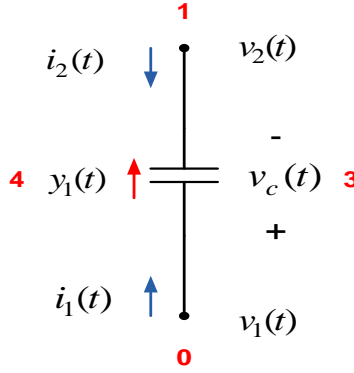


Figure 9.2.8: Three-Phase PWM Converter

The differential equations and algebraic equations describing a smoothing capacitor model are written in state-space form. There are two sets of equations: external equations and internal equations. The state-space model of the smoothing capacitor is given as follows:

$$i_1(t) = Cy_1(t) \quad (9.2.43)$$

$$i_2(t) = -i_1(t) \quad (9.2.44)$$

$$\frac{dv_c(t)}{dt} = y_1(t) \quad (9.2.45)$$

$$0 = v_c(t) - v_1(t) + v_2(t) \quad (9.2.46)$$

A compact-matrix form can be easily written using the state-space equations above and the algebraic-companion form is derived by the application of the quadratic integration method to the compact matrix form. All processes are the same with the case of the single-phase transformer model in subsection A of this chapter.

### 9.2.5 Controller Design of the PWM Converter

To control the proposed three-phase PWM converters, direct-power control (DPC) algorithm is used, since the control algorithm has demonstrated several outstanding characteristics such as: simple algorithm, superior dynamic response, and steady-state performance [54]. The control algorithm can be modeled for both (1) constant-frequency applications and (2) variable-frequency applications. Generally, the three-phase PWM converter with the constant-frequency control-algorithm, which is named as grid-side converter (GSC), is directly connected to the grid systems and the GSC supports constant DC-voltage and reactive-power controllability for grid connected systems. Otherwise, the PWM converter with variable-frequency control algorithm, which is named as machine-side converter (MSC), is directly connected to the wind turbines and the MSC support

maximum power capturing from wind turbine systems and reactive-power controllability to them. Note that MSC is directly connected to the rotor of a doubly-fed induction generator (DFIG) in Type-3 wind-generation unit and the stator of a permanent-magnet synchronous generator (PMSG) in Type-4 wind-generation unit. Since the control algorithms of the three-phase PWM converter are very diverse according the control purpose and controlled devices, all cannot be considered in this section. So, we present two general control algorithms for both a constant-frequency controller and a variable-frequency controller as shown in Figure 9.2.9 and Figure 9.2.10. Note we only present the modeling process of the constant-frequency controller since the space to describe both controllers is not enough as well as the DPC algorithms for Type-4 wind-generation unit are easily found in previous researches form [54] to [56].

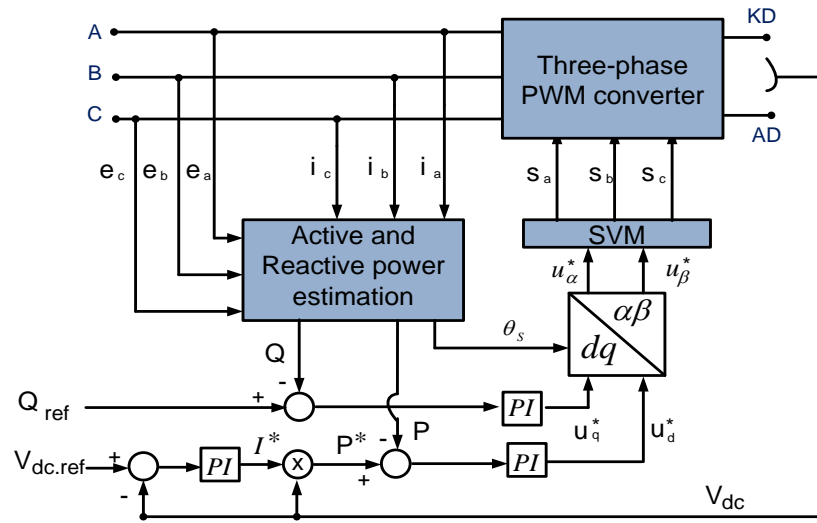


Figure 9.2.9: Constant-Frequency Controller using Direct-Power Algorithm with Space-Vector Modulation

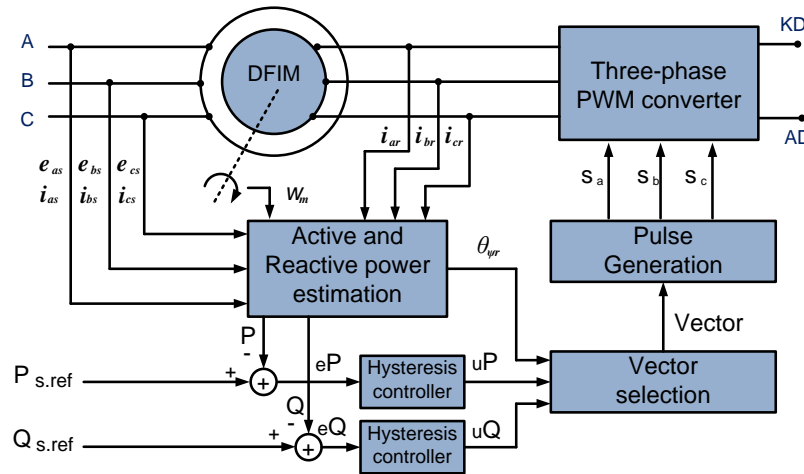


Figure 9.2.10: Variable-Frequency Controller using Direct-Power Algorithm with Hysteresis Controllers

Figure 9.2.9 shows a constant-frequency control algorithm and it is based on direct-power control algorithm with space vector modulation (DPC-SVM). The control algorithm can be modeled based on the following three steps:

**Step 1:** Active and real power (P and Q), and synchronous position angle ( $\theta_s$ ) estimation

**Step 2:** Voltage-reference estimation in  $\alpha\beta$ -coordination

**Step 3:** Switching sequence estimation from SVM algorithm

In Step 1 active- and real-power and synchronous-position angle are estimated with the same processes of the reference-estimation part in subsection C in this chapter. First the positive-sequence fundamental three-phase voltages and three-phase currents are computed and the three references are calculated as follows:

$$P = \frac{3}{2} V_{a1} I_{a1} \cos(\phi_{v_{a1}} - \phi_{i_{a1}}) \quad (9.2.47)$$

$$Q = \frac{3}{2} V_{a1} I_{a1} \sin(\phi_{v_{a1}} - \phi_{i_{a1}}) \quad (9.2.48)$$

The voltages in  $\alpha\beta$ -coordination are computed using *Clarke direct transformation* as follows:

$$\begin{bmatrix} v_\alpha \\ v_\beta \end{bmatrix} = \frac{2}{3} \cdot \begin{bmatrix} 1 & -\frac{1}{2} & -\frac{1}{2} \\ 0 & \frac{\sqrt{3}}{2} & -\frac{\sqrt{3}}{2} \end{bmatrix} \cdot \begin{bmatrix} V_{a1} \\ V_{b1} \\ V_{c1} \end{bmatrix} \quad (9.2.49)$$

Using the two voltages in  $\alpha\beta$ -coordination, the synchronous angle-position ( $\theta_s$ ) is computed. Therefore, the result is:

$$\theta_s = \text{atan}\left(\frac{v_\beta}{v_\alpha}\right) \quad (9.2.50)$$

In step 2, direct power control algorithm is modeled in state-space equations to compute the reference voltages in  $\alpha\beta$ -coordination. DPC algorithm is two-state algorithm in which DC-voltage and reactive-power can be decoupled to each other and controlled separately. As shown in Figure 9.2.11, three PI-controllers are used to compute the reference voltages in  $\alpha\beta$ -coordination.



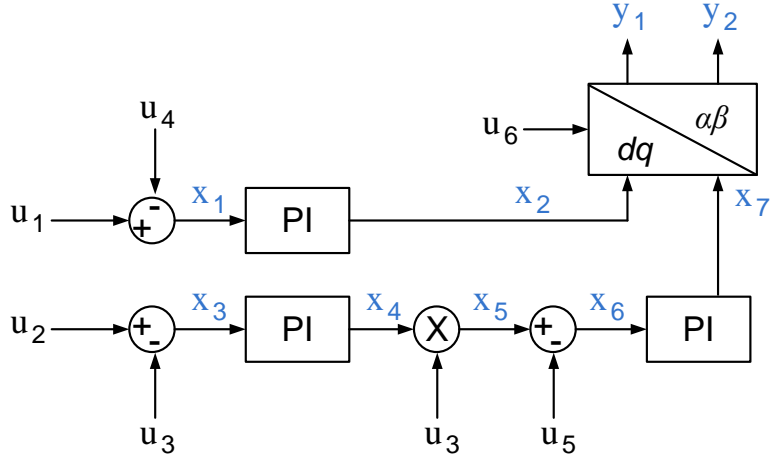


Figure 9.2.11: Block Diagram of DPC Control Algorithm

Here, we represent the control algorithm into state-space equations. Note  $U$  and  $X$  is input vector and state vector of the DPC, respectively, and the vectors are denoted as following equations in mathematic representation.

$$U = [u_1 \quad u_2 \quad u_3 \quad u_4 \quad u_5 \quad u_6]^T = [Q_{ref} \quad V_{dc.ref} \quad V_{dc} \quad Q \quad P \quad \theta_s]^T$$

$$X = [x_1 \quad x_2 \quad x_3 \quad x_4 \quad x_5 \quad x_6 \quad x_7]^T = [Q_{ref} - Q \quad U_q^* \quad V_{dc.ref} - V_{dc} \quad I^* \quad P^* \quad P^x - P \quad U_d^*]^T$$

The state-equations of the DPC are:

$$0 = x_1(t) - u_1(t) + u_4(t) \quad (9.2.51)$$

$$-k_{p1} \cdot \dot{x}_1(t) + \dot{x}_2(t) = k_{I1} \cdot x_1(t) \quad (9.2.52)$$

$$0 = x_3(t) - u_2(t) + u_3(t) \quad (9.2.53)$$

$$-k_{p2} \cdot \dot{x}_3(t) + \dot{x}_4(t) = k_{I2} \cdot x_3(t) \quad (9.2.54)$$

$$0 = u_3(t)x_4(t) - x_5(t) \quad (9.2.55)$$

$$0 = x_5(t) - x_6(t) - u_5(t) \quad (9.2.56)$$

$$-k_{p3} \cdot \dot{x}_6(t) + \dot{x}_7(t) = k_{I3} \cdot x_6(t) \quad (9.2.57)$$

In the compact matrix form of the state-space equations, the DPC is represented as follows:

$$A \cdot \dot{X} = B \cdot X + C \cdot U \quad (9.2.58)$$

where:

$$A = \begin{bmatrix} 0 & 0 & 0 & 0 & 0 & 0 & 0 \\ -k_{p1} & 1 & 0 & 0 & 0 & 0 & 0 \\ 0 & 0 & 0 & 0 & 0 & 0 & 0 \\ 0 & 0 & -k_{p2} & 1 & 0 & 0 & 0 \\ 0 & 0 & 0 & 0 & 0 & 0 & 0 \\ 0 & 0 & 0 & 0 & 0 & 0 & 0 \\ 0 & 0 & 0 & 0 & 0 & -k_{p3} & 1 \end{bmatrix}, B = \begin{bmatrix} 1 & 0 & 0 & 0 & 0 & 0 & 0 \\ k_{I1} & 0 & 0 & 0 & 0 & 0 & 0 \\ 0 & 0 & 1 & 0 & 0 & 0 & 0 \\ 0 & 0 & k_{I2} & 0 & 0 & 0 & 0 \\ 0 & 0 & 0 & u_3(t) & -1 & 0 & 0 \\ 0 & 0 & 0 & 0 & 1 & -1 & 0 \\ 0 & 0 & 0 & 0 & 0 & k_{I3} & 0 \end{bmatrix}, \text{ and}$$

$$C = \begin{bmatrix} -1 & 0 & 0 & 1 & 0 & 0 \\ 0 & 0 & 0 & 0 & 0 & 0 \\ 0 & -1 & 1 & 0 & 0 & 0 \\ 0 & 0 & 0 & 0 & 0 & 0 \\ 0 & 0 & 0 & 0 & 0 & 0 \\ 0 & 0 & 0 & 0 & -1 & 0 \\ 0 & 0 & 0 & 0 & 0 & 0 \end{bmatrix}.$$

Note  $k_{pj}$  and  $k_{Ij}$  are constant values for PI controllers and  $j$  is integers from 1 to 3.

Using the quadratic integration, the ACF of the DPC can be calculated in the same modeling processes of the single-phase transformer in subsection A of this chapter. Since the state variables of  $x_2$  and  $x_7$  are the reference voltages ( $u_q^*$  and  $u_d^*$ ) in  $dq$ -coordination, the voltages in  $dq$ -coordination are transformed into those in  $\alpha\beta$ -coordination. Finally, the reference voltages for SVM are computed as follows:

$$\begin{bmatrix} u_\alpha^* \\ u_\beta^* \end{bmatrix} = \begin{bmatrix} \cos u_6 & -\sin u_6 \\ \sin u_6 & \cos u_6 \end{bmatrix} \begin{bmatrix} x_7 \\ x_2 \end{bmatrix} \quad (9.2.59)$$

In step 3, the SVM diagram in Figure 9.2.12 is used to calculate on- and off-switching times of the electrical-switches. The SVM is one of digital control algorithms for the three-phase PWM converter connected to constant-frequency systems. According to the reference voltage on the diagram, switching times and switching sequence are decided. First, the reference voltage on the SVM diagram can be calculated using the reference voltages ( $u_\alpha^*$  and  $u_\beta^*$ ) from the DPC algorithm as follows:

$$\vec{V}_{svm,ref} = |V_{svm,ref}| \angle \theta_\alpha, \quad (9.2.60)$$

$$\text{where } |V_{svm.ref}| = \sqrt{(u_\alpha^*)^2 + (u_\beta^*)^2} \quad \text{and} \quad \theta_\alpha = \text{atan}\left(\frac{u_\beta^*}{u_\alpha^*}\right).$$

The dwelling time (pulse-width) that denotes switching time is calculated based on *volt-second balancing* principle as follows. Note  $T_a$ ,  $T_b$ , and  $T_c$  are the dwelling times of the three legs of *phase A*, *phase B*, and *phase C*, respectively.

$$T_a = T_s m_a \sin\left(\frac{\pi}{3} - \theta\right), \quad (9.2.61)$$

$$T_b = T_s m_a \sin(\theta), \text{ and} \quad (9.2.62)$$

$$T_0 = T_s - T_a - T_b \quad (9.2.63)$$

where:  $m_a = \frac{\sqrt{3}V_{ref}}{V_{dc}}$ ,  $\theta = \theta_\alpha - (n-1)\frac{\pi}{3}$ , and  $n$  is the section number in the SVM diagram. Note the modulation index  $m_a$  is in the range of  $0 \leq m_a \leq 1$ .

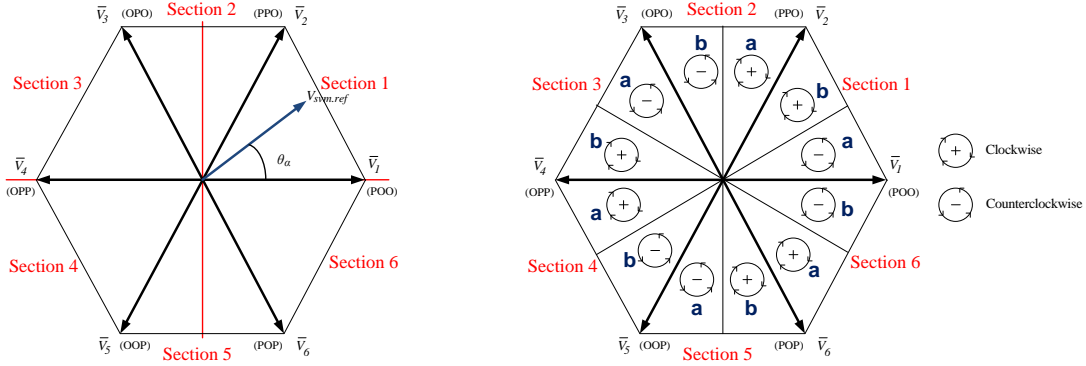


Figure 9.2.12: (A) SVM Diagram and (B) Mirror Image in SVM Diagram

After the dwelling times are computed, the switching sequence is arranged for the three-legs based on *seven-segment* arrangement and *even-order harmonics* elimination method. We select the switching sequence in the following requirements [57]:

- During the transition from one state to another state, only two switches in the same leg have to be involved.
- During the transition from one section to another section in the SVM diagram, none or minimum number of switching is required.

As well known, waveforms of half-wave symmetry should not contain any even-order harmonics. To achieve the half-wave symmetry, two regions facing each other in the SVM diagram can be arranged in a mirror image. Note that the switching sequences rotate clockwise or counterclockwise as shown in (B) of Figure 9.2.12 and the line-to-line voltages are achieved in half-wave symmetrical forms.

### **9.3 Power-Transient Studies of LFAC Transmission Systems**

For the power-transient studies, we introduce two wind farm configurations using the LFAC transmission system. The first wind farm configuration is using a parallel low-frequency wind farm and a low-frequency radial AC transmission system as shown in Figure 9.3.1, and the second configuration is using a series DC wind farm and a low-frequency radial AC transmission system as shown in Figure 9.3.5. Using the two wind farm configurations, the power transient studies are performed. In this simulation, the power step change suddenly occurs while the LFAC transmission system is operating in steady state.

#### **Case 1: Wind Farm configuration: LFAC wind farm and LFAC transmission system**

This Case 1 presents simulation results on an example wind farm with a LFAC transmission system connected to a power grid, as shown in Figure 9.3.1. The wind farm consists of many wind-turbine systems - the example system includes three of them. The wind generated power is rectified to DC and then it is converted to 20 Hz AC power. A transformer boosts the voltage to 46-kV. A LFAC line operated at 46-kV transmits the power over a distance of 100-km to the nearest power grid substation. At that point a cycloconverter converts the 20 Hz AC-power into 60 Hz AC-power and another transformer boost the voltage to 115-kV for the interconnection. The transformer is connected to the power grid which is a 115-kV, 60 Hz transmission at that point. The three-phase six-pulse cycloconverter is operating in a full circulating-current mode and the control algorithm for generating the switching pulses is the cosine-wave crossing

method.

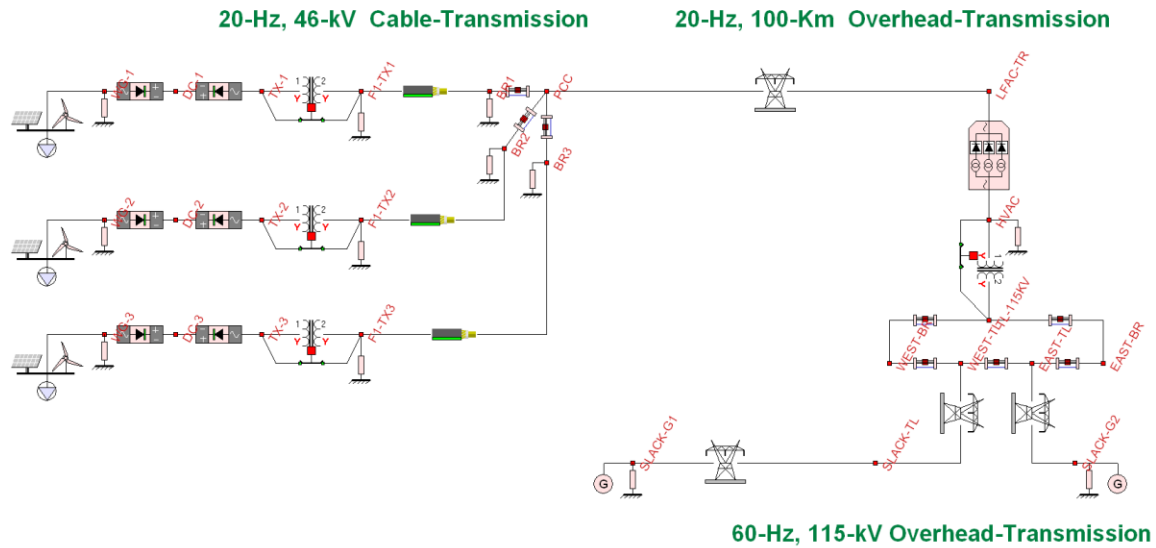


Figure 9.3.1: Wind Farm Configuration: LFAC Wind Farm and LFAC Transmission

Each wind turbine/generator system consists of a wind-turbine, full-rectifier and full-inverter that converts the power into 20 Hz AC power and a transformer that boost the voltage to 46 kV. The power from all wind turbine/generator systems are collected to a common point and the total power is transmitted via a LFAC transmission line to the interconnection point with the power grid. The interconnection is achieved with the cycloconverter and the step-up transformer. The LFAC system was simulated in a transient condition. Specifically, while the system is operating with 4 MW through the LFAC line, suddenly the wind power changes to the point that requires the LFAC line to transmit 9 MW.

Figure 9.3.2 represents three-phase (a) line-to-line voltages and (d) currents at the 60Hz AC transmission system connected to the three-phase six-pulse cycloconverter, three phase (c) voltages and (b) currents at the LFAC transmission system connected to the three-phase six-pulse cycloconverter, and the (e) real power from wind farm and the (f) RMS voltage at LFAC, while power demand suddenly changes 4MW into 9MW at 3 second. Figure 9.3.3 shows the results during the transient condition from 2.80 to 3.40 (seconds) - zoom-in view, and Figure 9.3.4 represents the results during steady state from 6.75 to 7.00 (seconds). Note that the output power can be automatically regulated by controlling the power angle  $\delta$ . The transient conditions last shorter than 0.15 seconds.

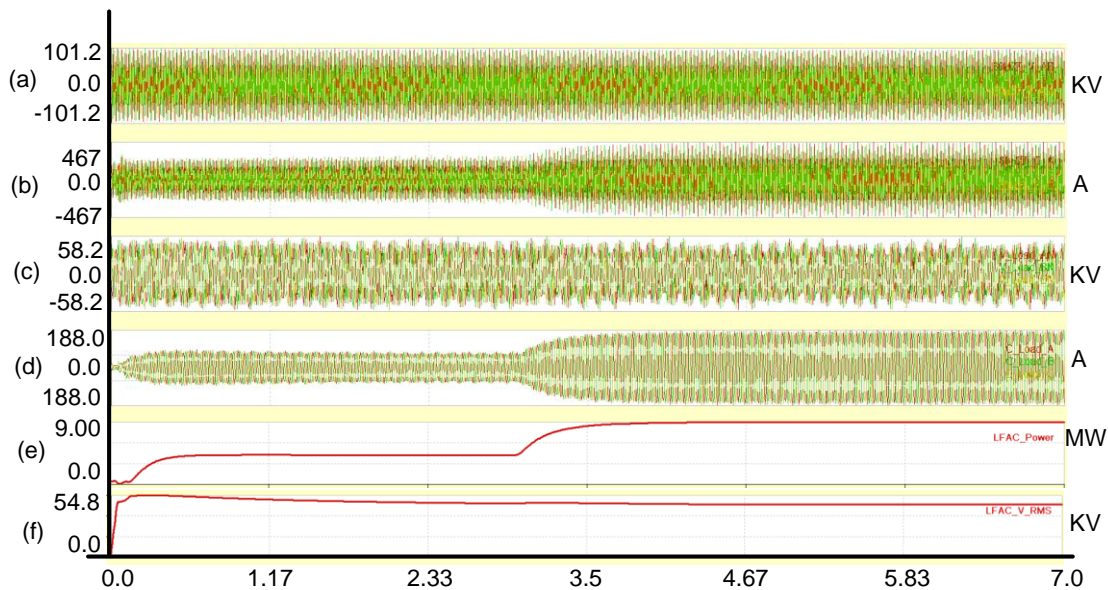


Figure 9.3.2: Three-Phase (a) Line-to-Line Voltages and (d) Currents at 60Hz AC Transmission Connected to the Cycloconverter; Three-Phase (c) Voltages and (b) Currents at LFAC Transmission Connected to the Cycloconverter; and (e) Real Power from Wind Farm and (f) RMS Voltage at the LFAC from 0.0 to 7.0 Seconds

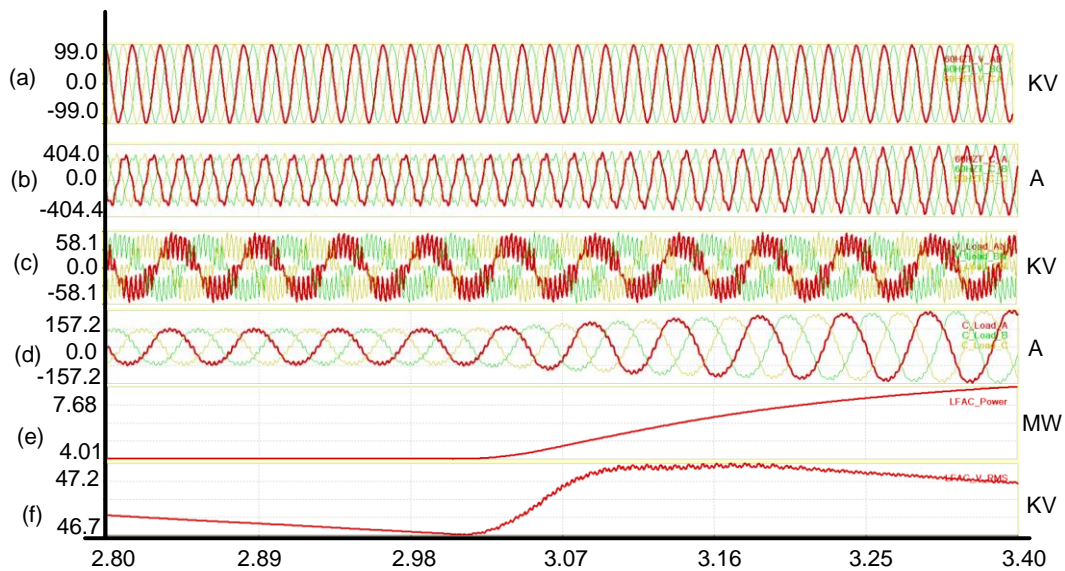


Figure 9.3.3: Three-Phase (a) Line-to-Line Voltage and (d) Currents at 60Hz AC Transmission Connected to the Cycloconverter; Three-Phase (c) Voltages and (b) Currents at LFAC Transmission Connected to the Cycloconverter; and (e) Real Power from Wind Farm and (f) RMS Voltage at the LFAC from 2.8 to 3.4 Seconds

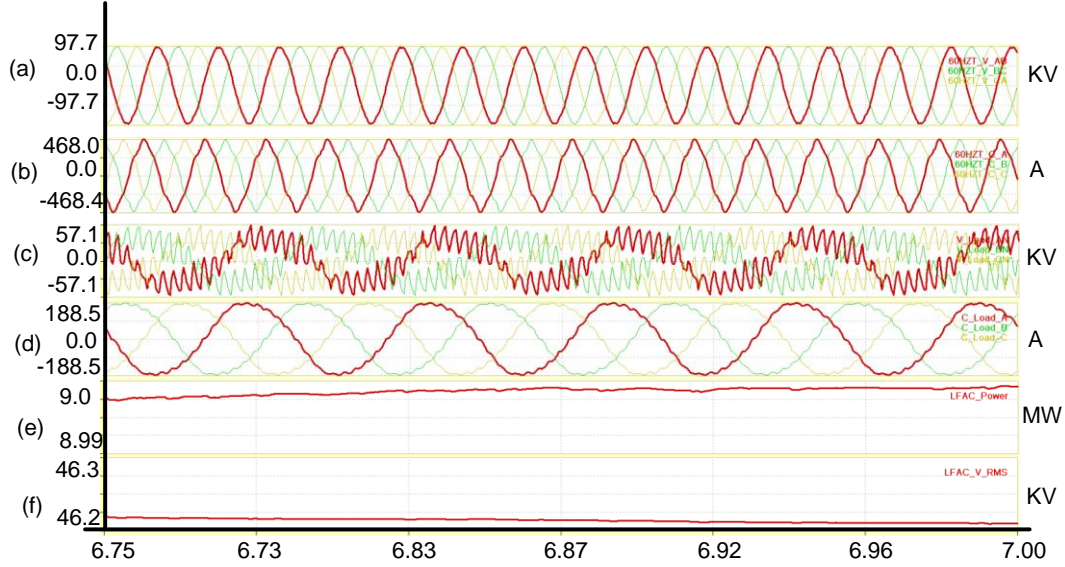


Figure 9.3.4: Three-Phase (a) Line-to-Line Voltage and (d) Current at 60Hz AC Transmission Connected to the Cycloconverter; Three-Phase (c) Voltages and (b) Currents at LFAC Transmission Connected to the Cycloconverter; and (e) Real Power from Wind Farm and (f) RMS Voltage at the LFAC from 6.75 to 7.0 Seconds

#### Case 2: Wind Farm configuration: DC wind farm and LFAC transmission system

This case study presents simulation results on an example wind farm with a LFAC-transmission system connected to a power grid, as shown in Figure 9.3.5. The wind farm consists of many wind turbine systems - the example system includes three of them. The wind-turbine systems are connected in series after the wind generated power is rectified to DC, and the DC-power is converted to 20 Hz AC-power using an inverter. A transformer boosts the voltage to 46-kV. A LFAC line operated at 46-kV transmits the power over a distance of 80-Km to the nearest power grid substation. At that point a cycloconverter converts the LFAC power into 60 Hz AC-power for the interconnection and another transformer boost the voltage to 115 kV. The transformer is connected to the power grid which is a 115-kV, 60 Hz-transmission at that point.



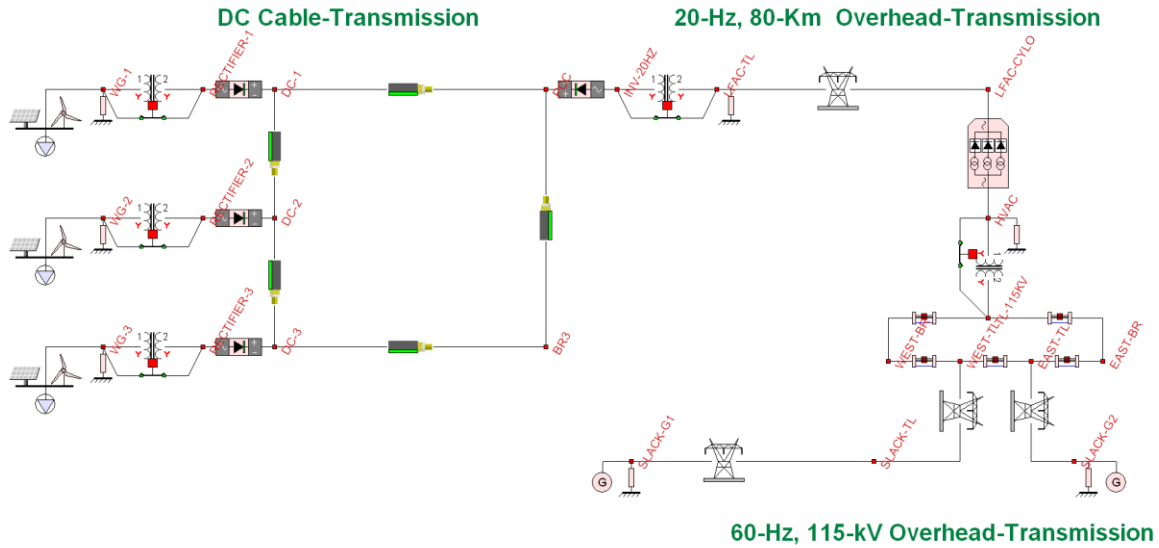


Figure 9.3.5: Single-Line Diagram of a Power Transient Test System

The results illustrate the operation of the wind farm transmission system by using a three-phase six-pulse cycloconverter. The three-phase six-pulse, cycloconverter is operating in a partial circulating current mode and the control algorithm for generating switching pulses is the cosine-wave crossing method.

Figure 9.3.6 represents three-phase (a) line-to-line voltages and (b) currents at the 60Hz AC transmission system connected to the three-phase six-pulse cycloconverter; three-phase (c) voltages and (d) currents at the LFAC-transmission system connected to the three-phase, six-pulse cycloconverter; and the (e) real power from wind farm and the (f) RMS voltage at LFAC during 10 seconds. In this simulation, the power demand changes 6MW into 10MW at 5 second.

Figure 9.3.7 and Figure 9.3.8 represent three-phase (a) line-to-line voltages and (b) currents at the 60Hz AC transmission system connected to the three-phase, six-pulse cycloconverter, and three-phase (c) voltages and (d) currents at the LFAC- transmission system connected to the three-phase, six-pulse cycloconverter in steady state. In Figure 9.3.7, the power demand is 6-MW and the operation mode is a partial circulating-current mode of 0.7-pu of the phase currents at the LFAC side. The Figure 9.3.8 shows the results with following conditions: the power demand is 10MW and the operation mode is a partial circulating-current mode of 0.4-pu of the phase current at the LFAC side.



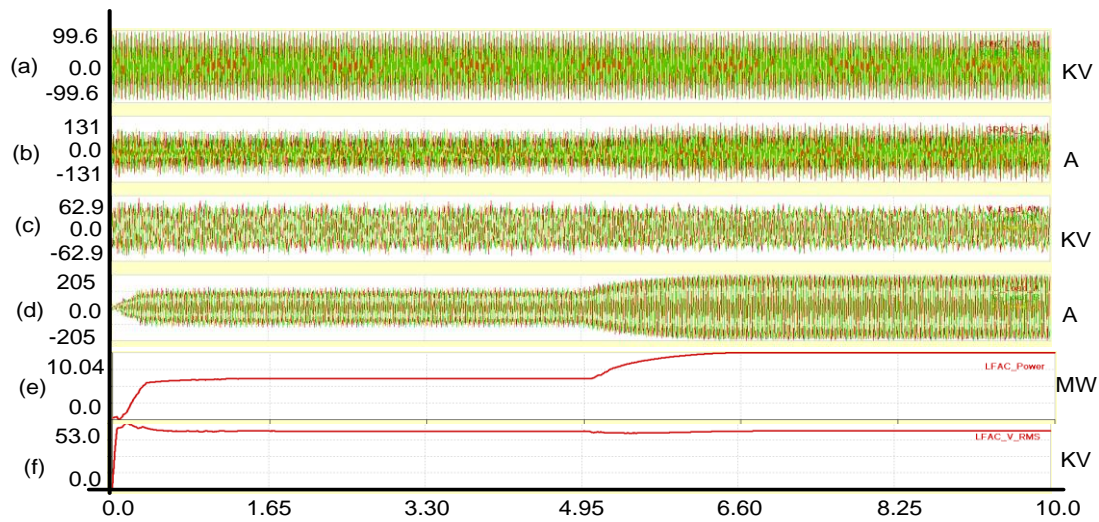


Figure 9.3.6: (a) Three-Phase Line-to-Line Voltages and (b) Three-Phase Currents at 60Hz AC Transmission Connected to the Cycloconverter; Three-Phase (c) Voltages and (b) Currents at LFAC Transmission Connected to the Cycloconverter; and (e) Real Power from Wind Farm and (f) RMS Voltage at the LFAC from 0.0 to 8.0 Seconds

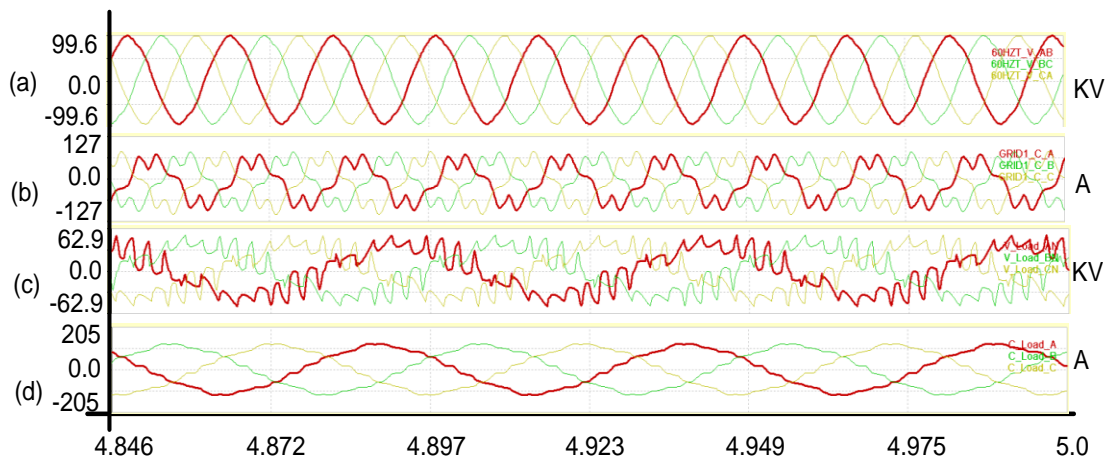


Figure 9.3.7: (a) Three-Phase Line-to-Line Voltages and (b) Three-Phase Currents at 60Hz AC Transmission Connected to the Cycloconverter; and Three-Phase (c) Voltages and (b) Currents at LFAC Transmission Connected to the Cycloconverter during Steady State from 4.846 to 5.0 Seconds

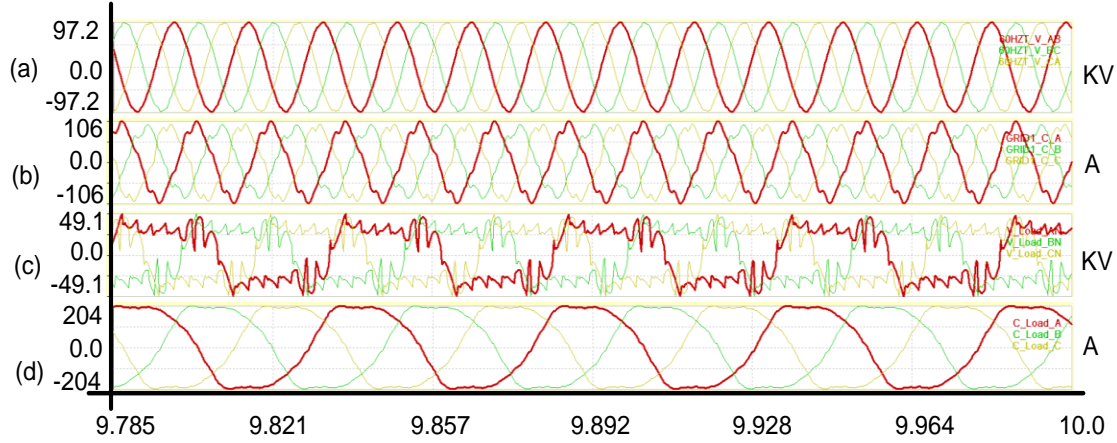


Figure 9.3.8: (a) Three-Phase Line-to-Line Voltages and (b) Three-Phase Currents at 60Hz AC Transmission Connected to the Cycloconverter; Three-Phase (c) Voltages and (b) Currents at LFAC Transmission Connected to the Cycloconverter during Steady State from 9.785 to 8.0 Seconds

Figure 9.3.9 and Figure 9.3.10 represent the results in transient conditions: (a) three-phase currents at the 60Hz AC- transmission system connected to the three-phase, six-pulse cycloconverter, three-phase (b) voltages and (c) currents at the LFAC-transmission system connected to the three-phase, six-pulse cycloconverter. Figure 9.3.9 shows the initial transient condition from 0.0 to 0.5 seconds. The cycloconverter is operated in a full circulating-current mode while the maximum currents at the LFAC side are smaller than 80 A, and otherwise, the cycloconverter is operated in a partial circulating-current mode. In Figure 9.3.10, the power demand suddenly changes 6MW to 10MW at 5.0 second. Note that the output power can be automatically regulated by controlling the power angle  $\delta$ . The transient conditions last longer than 1.0 second.

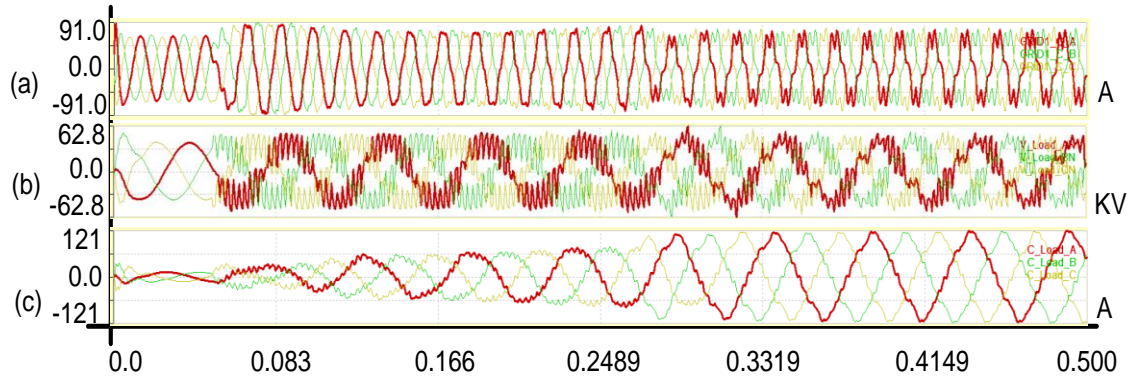


Figure 9.3.9: (a) Three-Phase Currents at 60Hz AC Transmission Connected to the Cycloconverter; and Three-Phase (b) Voltages and (c) Currents at LFAC Transmission Connected to the Cycloconverter during Steady State from 0.0 to 0.500 Seconds.

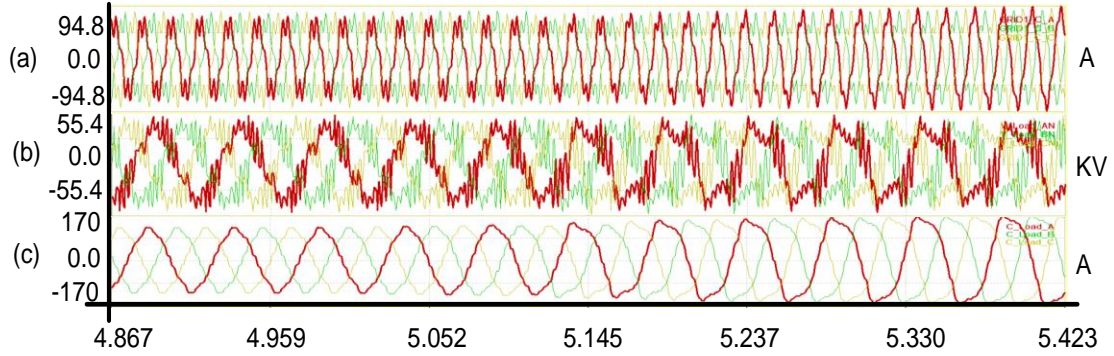


Figure 9.3.10: (a) Three-Phase Currents at 60Hz AC Transmission Connected to the Cycloconverter; and Three-Phase (b) Voltages and (c) Currents at LFAC Transmission Connected to the Cycloconverter during Steady State from 4.867 to 5.423 Seconds

#### 9.4 Harmonics Study of LFAC Transmission Systems

The wind farm configuration in Figure 9.3.1 is used for harmonics study. The operating voltage at high-frequency side is 70-kV (RMS) and the operating voltage at low-frequency side is changed to regulate the modulation index of the three-phase six-pulse converter since the harmonics depend on the modulation index. The electrical power of 10 MW is transmitted from wind farm to grid systems. Note that the modulation index ( $r$ ) is computed as following equation:

$$r = \frac{V_{a-output}}{V_{LL-input} \cdot \cos 30^\circ} \quad (9.3.1)$$

where  $V_{a-output}$  is the phase voltage at the low-frequency side and  $V_{LL-input}$  is the line-to-line voltage at the high-frequency side.

Figure 9.4.1 shows the simulation results in modulation index 1.0 in full circulating-current mode: (A) the line-to-line voltage between phase A and phase B and (B) the current at phase A; and (C) the phase-voltage and (D) the phase-current at phase A. The harmonics are computed using *Fourier-series* analysis and the harmonic spectrums are presented in logarithmic scale for the currents and voltages at both sides of the cycloconverter as shown in Figure 9.4.2. Note that the harmonic order is computed as follows:

$$\text{Harmonic order} = \frac{\text{high frequency}}{\text{fundamental frequency}} \quad (9.3.2)$$

where the fundamental frequency is 60 Hz at the HFAC side and 20 Hz at the LFAC side.

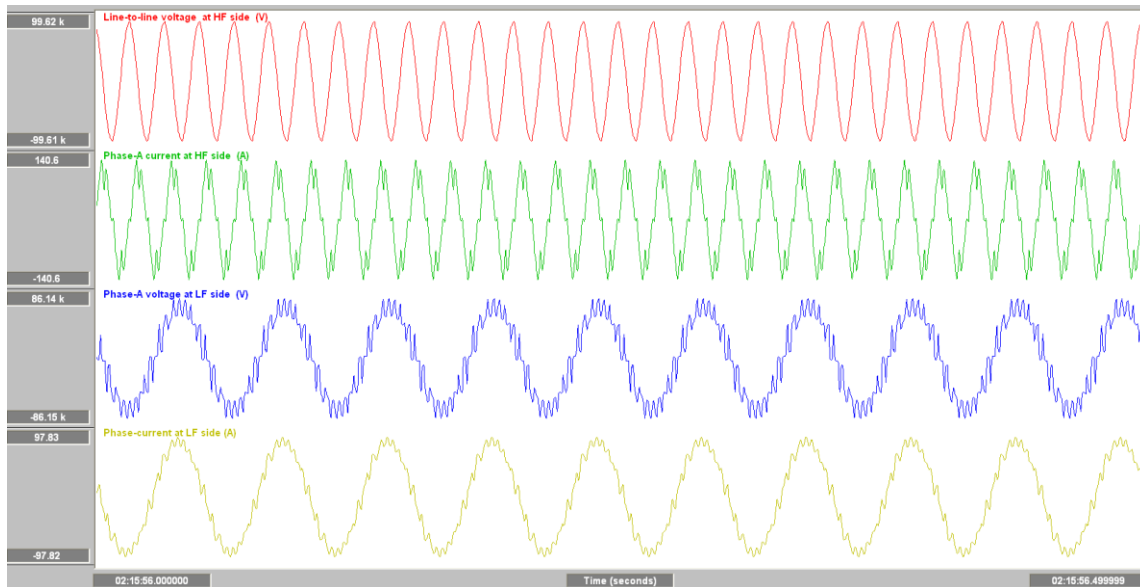
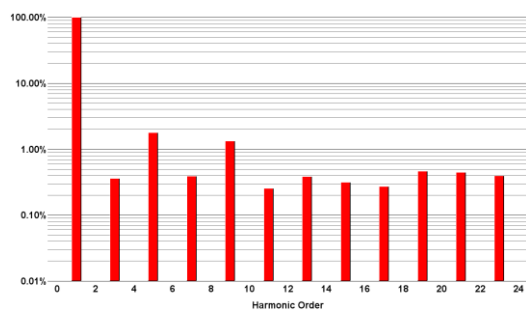
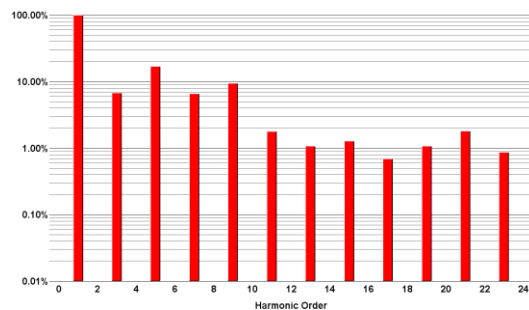


Figure 9.4.1: (A) Line-to-Line Voltage between Phase A and Phase B; (B) Current at Phase A; (C) Phase Voltage and (D) Phase Current at Phase A

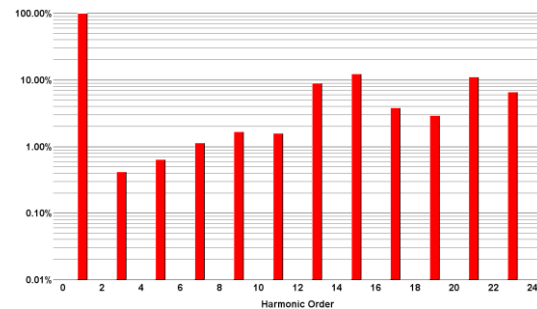
(A) Harmonic spectrums of line-to-line voltage at the HF side



(B) Harmonic spectrums of phase-current at the HF side



(C) Harmonic spectrums of Phase-voltage at the LF side



(D) Harmonic spectrums of phase-current at the LF side

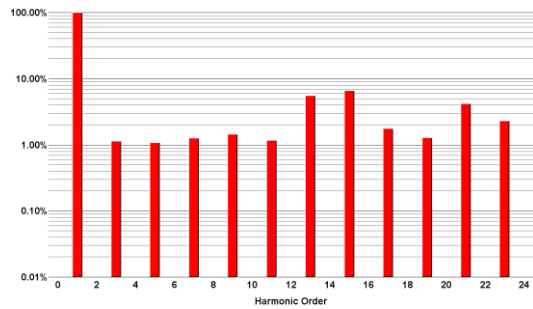


Figure 9.4.2: Harmonic Spectrums: (A) Line-to-Line Voltage between Phase A and Phase B, (B) Current at Phase A, (C) Phase Voltage at Phase A, and (D) Phase Current at Phase A

Table 9.4.1 presents numerical values of the harmonic spectrums of the phase-voltage at the low-frequency side of the cycloconverter and Figure 9.4.3 shows the graphs of the numerical values. In this study, the modulation index is changed from 0.38 to 1.0 and the harmonics is recorded according to the modulation index. As shown in Table 9.4.1 and Figure 9.4.3, the modulation index is an important parameter since the harmonic contents depend on it. While the modulation index approaches zero, the THDs are substantially increasing; otherwise, while the modulation index approaches one, the THDs are decreasing. Therefore, the modulation index between 0.75 and 1.00 assures the small filter size for the cycloconverter.

Table 9.4.1: Numerical Values of Harmonic Contents of the Phase Voltage at LFAC

Modulation Index $m_a$	Harmonic Order										
	3	5	7	9	11	13	15	17	19	21	THDs
1.00	0.41	0.62	1.2	1.8	1.7	8.9	8.3	3.8	2.9	8.1	20.1
0.88	1.4	1.6	1.8	0.87	0.8	6.3	8.7	3.3	4	8.3	22.52
0.75	2	1.8	2.1	0.51	1.1	4.6	8.7	8.1	8.4	8.3	26.43
0.63	3.9	3.3	1.8	0.22	0.69	3	8.6	20	22	8.1	33.78
0.50	8	3	1	0.77	2.5	8.9	8.9	31	30	6.5	42.14
0.38	17	4.8	3.7	1.4	1.2	0.4	0.04	39	37	2.4	48.87

Unit: percentage (%)

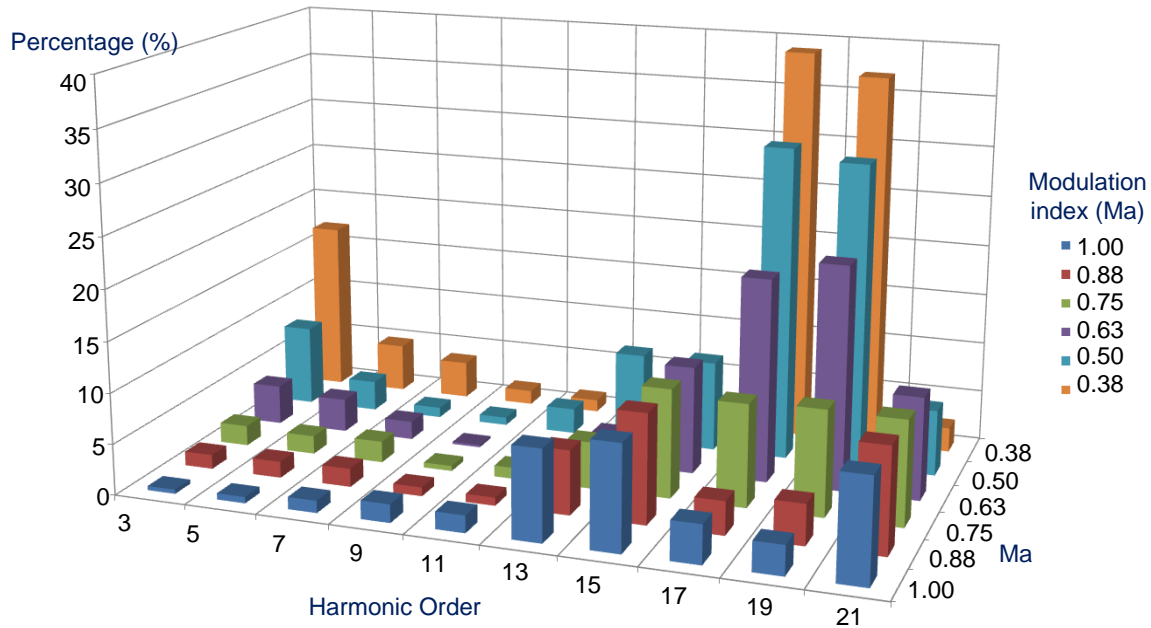


Figure 9.4.3: Harmonic Spectrums of the Phase Voltage at the LFAC Side



Next test presents the harmonics comparison between full- and partial- circulating current modes. For the purpose, the same modulation index is used for both cases. The modulation index is 0.38 and the magnitude of threshold current ( $I_T$ ) is the half of the maximum value of the phase-current at the LFAC side of the cycloconverter. Table 9.4.2 presents the numerical values of the harmonics contents and Figure 9.4.4 graphically represents the harmonic spectrums for both modes. As shown in Table 9.4.2 and Figure 9.4.4, the full-circulating current mode presents a smaller total harmonic distortion of the phase-voltage at the LFAC side than that from the partial-circulating current mode.

Table 9.4.2: Numerical Values of Harmonic Contents of the Phase Voltage at LFAC Side in Both Full- and Fifty Percent-Circulating Current Modes

Circulating Mode	Harmonic Order										
	3	5	7	9	11	13	15	17	19	21	THDs
Full	17	4.8	3.7	1.4	1.2	0.4	0.04	39	37	2.4	48.87
50%	39	17	12	11	4.1	7.9	28	39	29	19	59.67

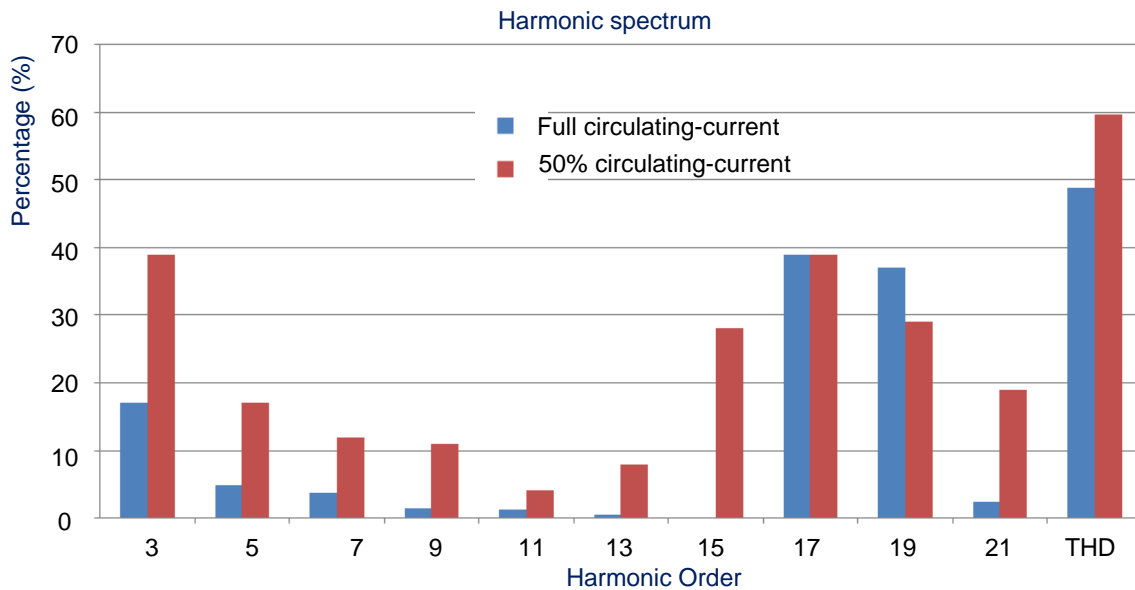


Figure 9.4.4: Harmonic Spectrums of the Phase Voltage at the LFAC Side: (Blue) Full Circulating-Current Mode and (Red) 50% Circulating-Current Mode

## 10 Reliability Analysis of Wind Farm Configurations

This section describes the reliability analysis of the 8 configurations listed in Chapter 4 of the report. Alternative transmission configurations have been formed by the combination of AC transmission at nominal power frequency, HVDC transmission, and low frequency AC transmission. Chapter 4 describes the 8 alternative configurations. These configurations will be compared from the reliability point of view in this chapter.

The general formulation of the reliability approach is provided in subsection 10.1, followed by the individual analysis of each of the 8 alternate configurations. For each configuration, the reliability analysis model is developed first, considering both the structural reliability model (full capacity model) and wind variability model. In addition, for each alternative configuration, a 30 wind turbine example is also provided. The reliability parameters used in each of the examples were assumed since actual reliability data are not available. The assumed parameters are shown in Appendix F.

### 10.1 Approach Description

The reliability analysis of any wind farm configuration is performed by assuming that each component of the configuration has a Monte Carlo model. In other words, each component is characterized with two basic parameters: failure rate and repair rate. Assumed values for these parameters are shown in Appendix F. Using these models for each component, the overall reliability of the wind farm is computed. In order to separate and quantify the effect of equipment failures from the variability of the wind energy resource, the overall problem of reliability analysis is separated into two sub-problems: (a) structural reliability model (full capacity model), and (b) wind variability model. The definition and relationship between these two models is provided below.

**Structural Reliability Model:** This model assumes that the wind energy is 100% reliable. This means that if the wind farm equipments are available, the output of the wind farm will be equal to the full capacity of the wind farm. For this reason, we shall also refer to this model as full capacity model.

**Wind Variability Model:** This model includes the wind variability as well as the structural reliability model of the wind farm.

The cost analysis of the configurations is provided in Section 5 of the report. The calculation results of the annual cost of each of the configurations are provided in the case study part of each subsection, as a reference for the evaluation of reliability. Most of the time the cost is increasing with reliability, *i.e.*, the configuration with a higher reliability indices normally accounts for a higher cost, such as connecting in parallel is more reliable than connecting in series, but requires more acquisition cost. Therefore, the selection of wind farm is not entirely based on the maximum of reliability or the minimum of cost, but the optimal combination of both.

### 10.1.1 Structural Reliability Model - Full Capacity Model

In this case, wind speed variation is not considered. This is achieved by assuming that all wind turbines will generate their full capacity, *e.g.*, a WTS V80-2MW will always generate 2MW, if available. Generally speaking, the generation capacity of the wind turbines is denoted as  $G$  in the following analysis, and some assumptions are made:

- a) All wind turbines are identical, *i.e.*, they have the same generation capacity;
- b) All components in the configurations are 2-states components, *i.e.*, they can only be either “up” or “down” states.
- c) Storage components are not considered in the reliability analysis.
- d) No transmission constraints are considered.

For each configuration, the specific formulation of reliability analysis calculation is shown in the following sections. Based on the assumptions above, the reliability analysis in full capacity case of each configuration will follow the procedure as:

- a) Component identification and classification of the configuration;
- b) Reliability modeling of each component
- c) Reliability modeling of connections, *e.g.*, parallel or series lines
- d) Generation capacity probabilistic distribution at PCC
- e) Reliability indices calculation

Formulations of reliability calculation will be provided after the analysis, and a 30 wind turbine case study will be provided in each section as an example.

### 10.1.2 Wind Variability Model

In this case, wind speed is considered so that the wind turbines are generating at whatever wind power is available. The reliability index will consider the wind speed distribution.

Wind speed is an important factor that influences the reliability indices especially the adequacy assessment result of the wind farm. The output of a wind turbine is essentially influenced by the wind speed. This subsection provides a general description of the analysis procedure for calculating reliability indices when considering wind speed.

Reference [27] has provided a good analysis of the relationship of wind speed and wind turbine output power. A typical probability distribution of wind speeds is shown in Figure 10.1.1 created from historical hourly wind data, and a typical WTS power output curve as a function of wind speed is shown in Figure 10.1.2 for a WTS V80-2MW. Since wind speed is continuously changing, a probabilistic way is used to assess it and to calculate the expected value.



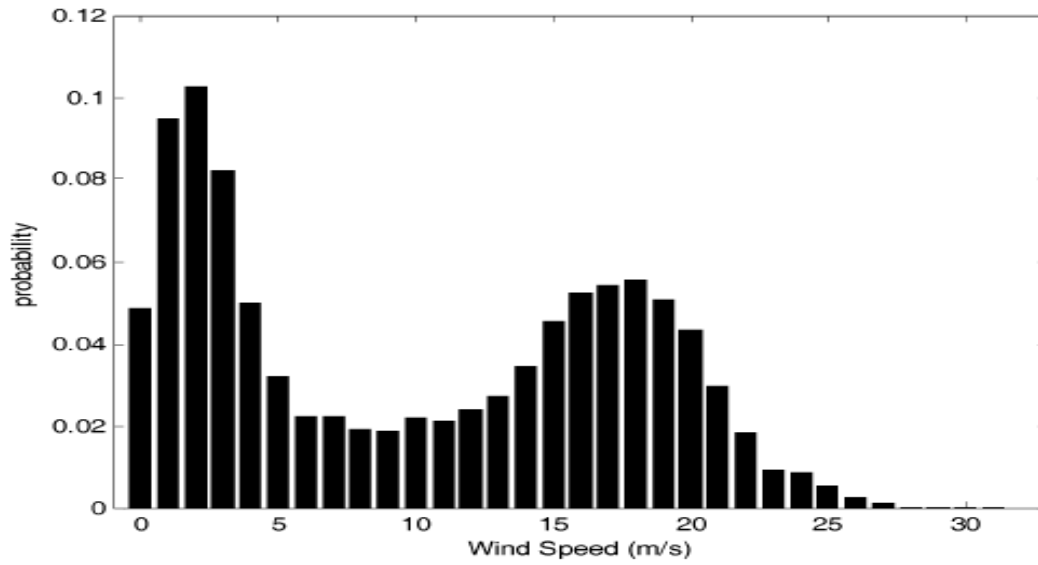


Figure 10.1.1: Wind Speed Probabilistic Distribution [27]

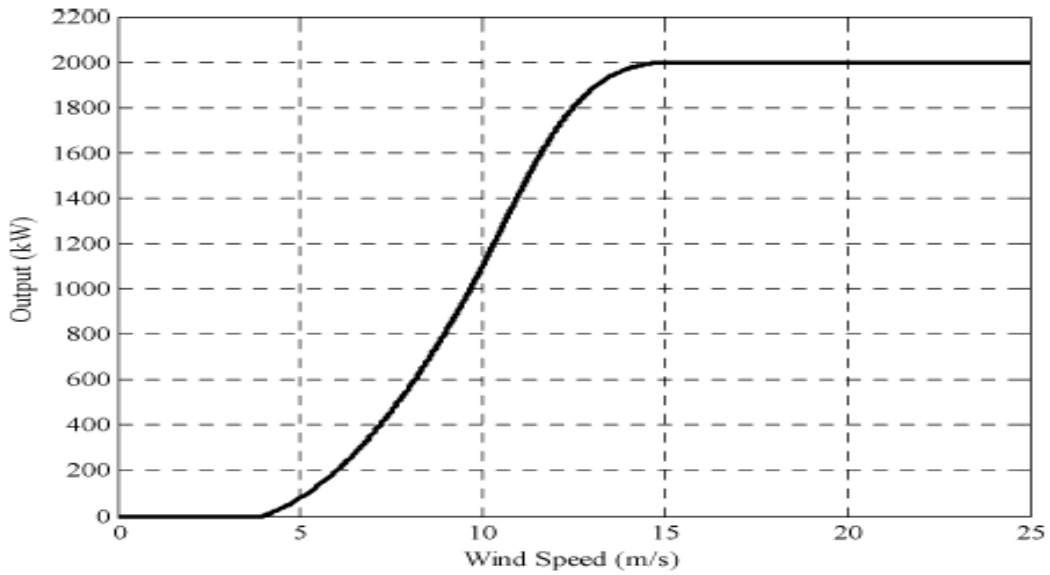


Figure 10.1.2: A Typical Wind Turbine Output Considering Wind Speed Variation [27]

Figure 10.1.2 provides the output of wind turbine as a function of the wind speed. When the turbine/generator is in its “up” state, the specific output of the turbine/generator,  $G(v)$ , is provided from the mapping shown in Figure 10.1.2, *i.e.*, from the wind speed. For each speed  $v$ , its probability  $P(v)$  is as shown in Figure 10.1.1.

The expected value of the output of a single turbine is:

$$E(G) = \int_v [G(v) \cdot P(v)] \quad (10.1.1)$$

In case of discrete wind speed data, the integral becomes the summation:

$$E(G) = \sum_v [G(v) \cdot P(v)] \quad (10.1.2)$$

The relationship shown in Figure 10.1.2 can be simplified by approximating the given function with a piecewise linear function, *i.e.*, after cut-in point and before cut-out point of wind speed, the output power of a wind turbine is almost a linear function of the speed, which results in the expression of output function:

$$G(v) = \begin{cases} 0 & v < 5 \\ 200(v - 5) & 5 \leq v \leq 15 \\ 2000 & v > 15 \end{cases} \quad (10.1.3)$$

which is then used in the evaluation of the integral (10.1.1) or summation (10.1.2) above.

Using the single turbine generating system analysis, the effect of wind speed variation is modeled as a modification to the constant generation capacity  $G$  in the full capacity case, *i.e.*,  $G$  is substitute by  $E(G)$  provided by (10.1.1) or (10.1.2) in wind variable model.

In the following sections, the wind speed variation case is analyzed for every configuration, provided after the full capacity case.

## 10.2 Reliability Analysis of Wind Farm Configuration 1

In this subsection, Configuration 1 is analyzed from the reliability point of view. This analysis is provided as an example of the analysis of all the 8 configurations, and is therefore explained in detail. In the subsequent subsections, the reliability analysis of Configuration 2 to 8 is performed in the similar way as shown in this subsection for Configuration 1.

Configuration 1 is shown in Figure 10.2.1. In this configuration, the wind turbine systems (WTS) generate AC at variable frequency dictated by the wind speed. This is a simple configuration, without low frequency transmission taken into account.

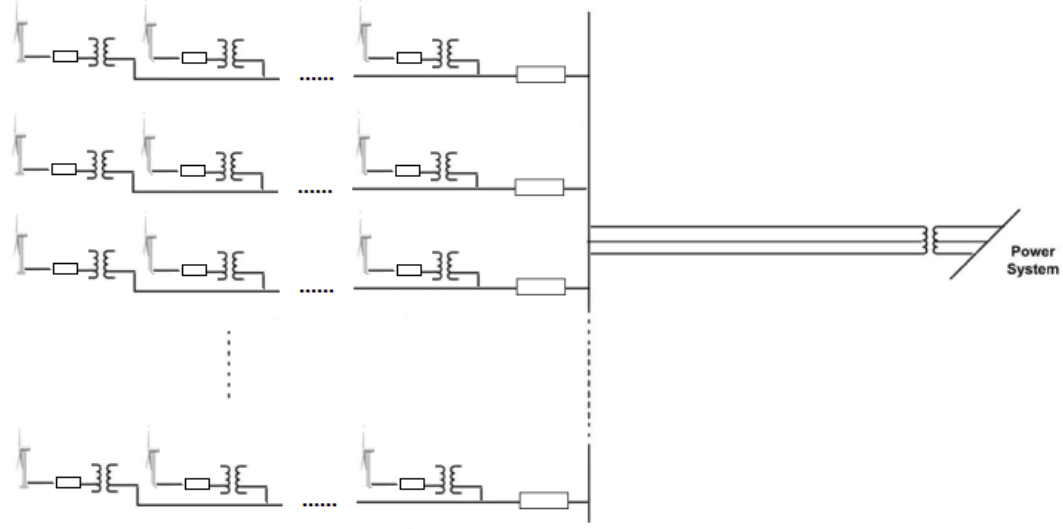


Figure 10.2.1: Wind Farm Configuration 1


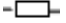






In this configuration example 1, there are  $m$  parallel circuits of wind generators, each consisting of  $n_1, n_2, \dots, n_m$  series wind turbines respectively. The wind generator output is AC and all the wind generators in a line are connected in series.

This section describes the reliability analysis of wind farm configuration 1 assuming the wind turbines are working in full capacity condition and in wind speed variation condition. The full capacity case refers to the situation that wind is blowing all the time so that the wind turbines are generating at their full capacity. The wind speed variation case refers to the situation that the wind turbines generate capacity based on the wind speed variation.

The reliability analysis in full capacity case is provided first. The objective of reliability analysis is to provide the probability distribution function of power supply at the point of common coupling (PCC) assuming that the availability of wind energy is 100%. The end result will be in the form of a cumulative probability function of the available power at PCC. This result can be served as the planning and operation index of the power system operator. The wind speed variation case is provided after the full capacity case.

A list of components in Configuration 1 and their quantities is shown in Table 10.2.1:

Table 10.2.1: Components and their Quantities in Configuration 1

	Icon	Component	Total Number of Component
1		Wind Turbine	$N = n_1 + n_2 + \dots + n_m$
2		Small Switch	$N = n_1 + n_2 + \dots + n_m$
3		Small Transformer	$N = n_1 + n_2 + \dots + n_m$
4		In Farm AC Transmission Line	$N = n_1 + n_2 + \dots + n_m$
5		Large Switch	$m$
6		AC Bus	1
7		60Hz AC Transmission Line	1
8		Large Substation Transformer	1

In order to simplify the presentation, the following assumptions are made: (a) all the elements of the same component type are identical, *i.e.*, have the same attributes and parameters. For example, there are  $N = n_1 + n_2 + \dots + n_m$  wind turbines in the configuration, and the assumption is that they have identical failure rates and repair rates; (b) every component is assumed to be a two-state element, which means it only has “up” and “down” states. “Up” state represents the successfully working state while the “down” state represents the failure state of the component; and (c) no transmission constraints are taken into account. It should be understood that these assumptions are not necessary in the computer model and analysis.

The reliability parameters of all the components, which include the failure rate and the repair rate, are listed in Appendix F. The full capacity of each wind turbine is denoted as  $G$ .

In each parallel circuit, a number of components are connected in series. The components are “dependent” on each other’s success state from the reliability point of view, *i.e.*, if anyone in the line fails, that line will fail.

Each of the parallel circuits performs “independently” from the others. If one circuit fails, the other circuits will still be able to operate. At the AC collection bus and subsequent transmission part, the components are connected in series. These components are “essential” to the transmission system of the wind farm. If any of the components fails, the wind farm will not be able to transmit any energy to the power grid. The calculation of generation capacity levels and their corresponding probabilities are provided as below.

### 10.2.1 Formulation of Reliability Analysis of Configuration 1 in Full Capacity Case

**Single Component Probabilistic Model:** For component  $i$ , the duration of success is  $\frac{1}{\lambda_i}$  and the duration of failure is  $\frac{1}{\mu_i}$ . The probabilities of this component's being success and failure are:

$$P_i(\text{Success}) = \frac{\frac{1}{\lambda_i}}{\frac{1}{\lambda_i} + \frac{1}{\mu_i}} = \frac{\mu_i}{\lambda_i + \mu_i} \quad (10.2.1)$$

$$P_i(\text{Failure}) = \frac{\frac{1}{\mu_i}}{\frac{1}{\lambda_i} + \frac{1}{\mu_i}} = \frac{\lambda_i}{\lambda_i + \mu_i} \quad (10.2.2)$$

**Probabilistic Model of Circuit  $i$ :** The  $i$ th circuit (of the  $m$  parallel circuits) is considered. The  $i$ th circuit will be successful in transmitting energy only when all the components in the line are in their “up” state due to that all generators are serially connected through each parallel line. Therefore, the states of the  $i$ th circuit and the power transmitted in each state are shown in Table 10.2.2:

Table 10.2.2: States of the  $i$ th Circuit and Power Transmitted in Configuration 1

State	Power Transmitted	Component Status	Probability
Up	$n_i \cdot G$	All components “up”	$P_{line\ i}(Up)$
Down	0	At least one “down”	$P_{line\ i}(Down)$

Line up and line down probabilities can be easily obtained by multiplying the up state probabilities of the components which are connected in series. The success and failure probabilities of each component can be computed from following formula, in the format of (10.2.1) and (10.2.2).

$$\text{Wind Turbine: } (WT\ up) = \frac{\mu_{WT}}{\lambda_{WT} + \mu_{WT}} ; \quad P(WT\ down) = \frac{\lambda_{WT}}{\lambda_{WT} + \mu_{WT}}$$

$$\text{Small Switch: } (sSW\ up) = \frac{\mu_{sSw}}{\lambda_{sSw} + \mu_{sSw}} ; \quad P(WT\ down) = \frac{\lambda_{sSw}}{\lambda_{sSw} + \mu_{sSw}}$$

$$\text{Small Transformer: } (sT\ up) = \frac{\mu_{sT}}{\lambda_{sT} + \mu_{sT}} ; \quad P(T_k\ down) = \frac{\lambda_{sT}}{\lambda_{sT} + \mu_{sT}}$$

$$\text{In Farm AC Transmission Line: } (FAC\ up) = \frac{\mu_{FAC}}{\lambda_{FAC} + \mu_{FAC}} ; P(WT\ down) = \frac{\lambda_{FAC}}{\lambda_{FAC} + \mu_{FAC}}$$

$$\text{Large Switch: } P(lSW\ up) = \frac{\mu_{lSw}}{\lambda_{lSw} + \mu_{lSw}} ; \quad P(WT\ down) = \frac{\lambda_{lSw}}{\lambda_{lSw} + \mu_{lSw}}$$

Therefore the probability of up state and down state of the  $i$ th line can be computed from formulas shown below.

$$P_{line\ i}(Up) = [(P(WT\ up) \cdot P(sSw\ up) \cdot P(sT\ up) \cdot P(FAC\ up))]^{n_i} \cdot P(lSW\ up) \quad (10.2.3)$$

$$P_{line\ i}(Down) = 1 - P_{line\ i}(Up) \quad i = 1, 2, \dots, m \quad (10.2.4)$$

which can be easily obtained by putting the same factors together assuming that in each category components have the same failure rate of  $\lambda$  and the same repair rate of  $\mu$ .

The complete expressions of the probability of the states of the  $i$ th line are:

$$\begin{aligned} P_{line\ i}(Up) &= [(P(WT\ up) \cdot P(sSw\ up) \cdot P(sT\ up) \cdot P(FAC\ up))]^{n_i} \cdot P(lSW\ up) \\ &= \left[ \frac{\mu_{WT}}{\lambda_{WT} + \mu_{WT}} \cdot \frac{\mu_{sSw}}{\lambda_{sSw} + \mu_{sSw}} \cdot \frac{\mu_{sT}}{\lambda_{sT} + \mu_{sT}} \cdot \frac{\mu_{FAC}}{\lambda_{FAC} + \mu_{FAC}} \right]^{n_i} \cdot \frac{\mu_{lSW}}{\lambda_{lSW} + \mu_{lSW}} \end{aligned} \quad (10.2.5)$$

$$P(\text{line } i \text{ down}) = 1 - \left[ \frac{\mu_{WT}}{\lambda_{WT} + \mu_{WT}} \cdot \frac{\mu_{sSw}}{\lambda_{sSw} + \mu_{sSw}} \cdot \frac{\mu_{sT}}{\lambda_{sT} + \mu_{sT}} \cdot \frac{\mu_{FAC}}{\lambda_{FAC} + \mu_{FAC}} \right]^{n_i} \cdot \frac{\mu_{lSW}}{\lambda_{lSW} + \mu_{lSW}} \quad (10.2.6)$$

**Probabilistic Model of  $m$  Parallel Circuits:** Since the  $m$  circuits are in parallel, the total generating states depend on the success or failure status of each line. For example, if it is the case that  $\mathbf{n}_1 = \mathbf{n}_2 = \dots = \mathbf{n}_m = \mathbf{n}$ , the generation capacity states of the  $m$  lines are shown in Table 10.2.3.

Table 10.2.3: States of the  $m$  Parallel Circuits (Lines)

State	Generation Capacity	Probability
1	0	$P_{parallel\_0}$
2	$1 \cdot n \cdot G$	$P_{parallel\_1nG}$
3	$2 \cdot n \cdot G$	$P_{parallel\_2nG}$
...	...	...
$m$	$(m - 1) \cdot n \cdot G$	$P_{parallel\_ (m-1)nG}$
$m+1$	$m \cdot n \cdot G$	$P_{parallel\_ mnG}$

The probability of the states is calculated using combinatorial analysis. The  $(j+1)$  state, which has the generation capacity of  $j \cdot n \cdot G$ , has the probability:

$$P_{parallel\_jng} = C_m^j \cdot P_{line\ i}^j(up) \cdot P_{line\ i}^{m-j}(down) \quad (10.2.7)$$

where  $C_m^j = \frac{m!}{j!(m-j)!}$  is the combinatorial number;  $P_{line\ i}(Up)$  and  $P_{line\ i}(Down)$  are the values calculated in (10.2.5) and (10.2.6).

**Probabilistic Model of the Entire Configuration:** Given the probabilistic model of the generating section above, *i.e.*, the  $m$  parallel circuits (lines), the states of the whole configuration are determined by the generating section in series with the transmission section. As an example, the states and corresponding probability when  $\mathbf{n}_1 = \mathbf{n}_2 = \dots = \mathbf{n}_m = \mathbf{n}$  are shown in Table 10.2.4.

Table 10.2.4: States of Entire Configuration and Probabilities

State	Generation Capacity	Probability
1	0	$P_{\text{system}_0}$
2	$1 \cdot n \cdot G$	$P_{\text{system}_{1nG}}$
3	$2 \cdot n \cdot G$	$P_{\text{system}_{2nG}}$
...	...	...
$m$	$(m-1) \cdot n \cdot G$	$P_{\text{system}_{(m-1)nG}}$
$m+1$	$m \cdot n \cdot G$	$P_{\text{system}_{mnG}}$

The success and failure probabilities of components in transmission section can be computed from the following formula, in the format of (10.2.1) and (10.2.2).

$$\text{AC Bus: } P(\text{ACB up}) = \frac{\mu_{ACB}}{\lambda_{ACB} + \mu_{ACB}} ; \quad P(\text{ACB down}) = \frac{\lambda_{ACB}}{\lambda_{ACB} + \mu_{ACB}}$$

$$60 \text{ Hz AC Transmission Line: } (60AC \text{ up}) = \frac{\mu_{60AC}}{\lambda_{60AC} + \mu_{60AC}} ; \quad P(WT \text{ down}) = \frac{\lambda_{60AC}}{\lambda_{60AC} + \mu_{60AC}}$$

$$\text{Large Substation Transformer: } (lT \text{ up}) = \frac{\mu_{lT}}{\lambda_{lT} + \mu_{lT}} ; \quad P(lT \text{ down}) = \frac{\lambda_{lT}}{\lambda_{lT} + \mu_{lT}}$$

When  $j \neq 0$ , the probability of the  $(j+1)$ th state, which is the probability of transmitting power of  $j \cdot n \cdot G$ , is:

$$\begin{aligned}
P_{\text{system}_{jnG}} &= P_{\text{parallel}_{jnG}} \cdot P(\text{ACB up}) \cdot P(60AC \text{ up}) \cdot P(lT \text{ up}) \\
&= P_{\text{parallel}_{jnG}} \cdot \frac{\mu_{ACB}}{\lambda_{ACB} + \mu_{ACB}} \cdot \frac{\mu_{60AC}}{\lambda_{60AC} + \mu_{60AC}} \cdot \frac{\mu_{lT}}{\lambda_{lT} + \mu_{lT}} \\
&= C_m^j \cdot P_{\text{line } i}^j(\text{up}) \cdot P_{\text{line } i}^{m-j}(\text{down}) \cdot \frac{\mu_{ACB}}{\lambda_{ACB} + \mu_{ACB}} \cdot \frac{\mu_{60AC}}{\lambda_{60AC} + \mu_{60AC}} \cdot \frac{\mu_{lT}}{\lambda_{lT} + \mu_{lT}} \\
&= \frac{m!}{j!(m-j)!} \cdot \left\{ \left[ \frac{\mu_{WT}}{\lambda_{WT} + \mu_{WT}} \cdot \frac{\mu_{sSw}}{\lambda_{sSw} + \mu_{sSw}} \cdot \frac{\mu_{sT}}{\lambda_{sT} + \mu_{sT}} \cdot \frac{\mu_{fAC}}{\lambda_{fAC} + \mu_{fAC}} \right]^{n_i} \cdot \frac{\mu_{lSw}}{\lambda_{lSw} + \mu_{lSw}} \right\}^j \cdot \left\{ 1 - \left[ \frac{\mu_{WT}}{\lambda_{WT} + \mu_{WT}} \cdot \frac{\mu_{sSw}}{\lambda_{sSw} + \mu_{sSw}} \cdot \frac{\mu_{sT}}{\lambda_{sT} + \mu_{sT}} \cdot \frac{\mu_{fAC}}{\lambda_{fAC} + \mu_{fAC}} \right]^{n_i} \cdot \frac{\mu_{lSw}}{\lambda_{lSw} + \mu_{lSw}} \right\}^{m-j} \cdot \frac{\mu_{ACB}}{\lambda_{ACB} + \mu_{ACB}} \cdot \frac{\mu_{60AC}}{\lambda_{60AC} + \mu_{60AC}} \cdot \frac{\mu_{lT}}{\lambda_{lT} + \mu_{lT}} \quad (10.2.8)
\end{aligned}$$

This probability is denoted as  $P(j+1)$ , for all  $j \neq 0$ .

When  $j = 0$ , the probability  $P(0+1)=P(1)$  can be calculated as:

$$P(1) = 1 - \sum_{w=1}^m P(w + 1) \quad (10.2.9)$$

where  $P(w+1)$  is determined by (10.2.8)

Therefore in this simple case, the energy levels of the configuration shown in Figure 10.2.1 at the coupling point with the power grid have a list of states and corresponding probability shown in Table 10.2.5.

Table 10.2.5: States and Corresponding Probabilities

State	Generation Capacity	Probability
1	0	$P(1)$
2	$1 \cdot n \cdot G$	$P(2)$
3	$2 \cdot n \cdot G$	$P(3)$
...	...	...
$m$	$(m-1) \cdot n \cdot G$	$P(m)$
$m+1$	$m \cdot n \cdot G$	$P(m+1)$

where the probabilities are determined by (10.2.8) and (10.2.9).

**Expected Generated Wind Energy (EGWE):** In this part, the reliability index of EGWE is calculated given the probability analysis as above. EGWE is the essential index to be considered for this configuration. Some of other indices that are important are shown in next part.

Generally, if we know the output states and the probability of each state such as in Table 10.2.5, EGWE is the expectation of the probabilistic output (in one hour):

$$EGWE = \sum_{i=1}^{number\ of\ states} G_i \cdot P(i) \quad (10.2.10)$$

where  $G_i$  is the generation capacity of the  $i$ th state.

Note here that EGWE is in term of energy (MWh), and (10.2.10) gives the result in term of power. Since operating time is easy to be measured, the required EGWE can be determined by multiplying (10.2.10) by the operating time (in hours).

For the general case, the assumption of  $n_1 = n_2 = \dots = n_m = n$  should be removed; each of the  $m$  parallel circuits has two states: (a) either transmitting full capacity or (b) 0. For line  $i$ , the expected transmitted capacity to the collector AC bus is:

$$EGWE_{line\ i} = n_i \cdot G \cdot P_{line\ i}(up) + 0 \cdot P_{line\ i}(down) = n_i \cdot G \cdot P_{line\ i}(up) \quad (10.2.11)$$

The total expected available energy at point of common coupling is the index of EGWE:



$$\begin{aligned}
EGWE &= \left[ \sum_{i=1}^m n_i \cdot G \cdot P_{line\ i}(up) \right] \cdot P(ACB\ up) \cdot P(60AC\ up) \cdot P(IT\ up) + 0 \\
&= \left[ \sum_{i=1}^m n_i \cdot G \cdot P_{line\ i}(up) \right] \cdot P(ACB\ up) \cdot P(60AC\ up) \cdot P(IT\ up) \\
&= \left( \sum_{i=1}^m \{ n_i \cdot G \cdot \left[ \frac{\mu_{WT}}{\lambda_{WT} + \mu_{WT}} \cdot \frac{\mu_{SSw}}{\lambda_{SSw} + \mu_{SSw}} \cdot \frac{\mu_{ST}}{\lambda_{ST} + \mu_{ST}} \cdot \frac{\mu_{FAC}}{\lambda_{FAC} + \mu_{FAC}} \right]^{n_i} \cdot \frac{\mu_{ISw}}{\lambda_{ISw} + \mu_{ISw}} \} \right) \cdot \frac{\mu_{ACB}}{\lambda_{ACB} + \mu_{ACB}} \cdot \frac{\mu_{60AC}}{\lambda_{60AC} + \mu_{60AC}} \cdot \frac{\mu_{IT}}{\lambda_{IT} + \mu_{IT}} \quad (10.2.12)
\end{aligned}$$

### 10.2.2 Reliability Analysis of Configuration 1 Considering Wind Speed

Using the single turbine generating system analysis, the effect of wind speed variation is modeled as a modification to the constant generation capacity  $G$  in the full capacity case.

The total output expectation at a certain point of time is still in the form of

$$\begin{aligned}
EGWE &= \left( \sum_{i=1}^m \{ n_i \cdot G \cdot \left[ \frac{\mu_{WT}}{\lambda_{WT} + \mu_{WT}} \cdot \frac{\mu_{SSw}}{\lambda_{SSw} + \mu_{SSw}} \cdot \frac{\mu_{ST}}{\lambda_{ST} + \mu_{ST}} \cdot \frac{\mu_{FAC}}{\lambda_{FAC} + \mu_{FAC}} \right]^{n_i} \cdot \frac{\mu_{ISw}}{\lambda_{ISw} + \mu_{ISw}} \} \right) \\
&\quad \cdot \frac{\mu_{ACB}}{\lambda_{ACB} + \mu_{ACB}} \cdot \frac{\mu_{60AC}}{\lambda_{60AC} + \mu_{60AC}} \cdot \frac{\mu_{IT}}{\lambda_{IT} + \mu_{IT}}
\end{aligned}$$

as in equation (10.2.12), but  $G$  is changed into  $G(v)$  at that time point as the function of the wind speed. For a given period of time with the wind speed probability distribution as Figure 10.2.1, the expectation of output energy will be:

$$\begin{aligned}
EGWE = E(G) &= \sum_v [G(v) \cdot P(v)] \cdot \left( \sum_{i=1}^m \{ n_i \cdot \left[ \frac{\mu_{WT}}{\lambda_{WT} + \mu_{WT}} \cdot \frac{\mu_{SSw}}{\lambda_{SSw} + \mu_{SSw}} \cdot \frac{\mu_{ST}}{\lambda_{ST} + \mu_{ST}} \cdot \frac{\mu_{FAC}}{\lambda_{FAC} + \mu_{FAC}} \right]^{n_i} \cdot \frac{\mu_{ISw}}{\lambda_{ISw} + \mu_{ISw}} \} \right) \\
&\quad \cdot \frac{\mu_{ACB}}{\lambda_{ACB} + \mu_{ACB}} \cdot \frac{\mu_{60AC}}{\lambda_{60AC} + \mu_{60AC}} \cdot \frac{\mu_{IT}}{\lambda_{IT} + \mu_{IT}} \quad (10.2.13)
\end{aligned}$$

It is shown from (10.2.13) that the influence of wind speed on the calculation of the expectation is simply a modification by substituting the constant turbine output by the expectation of that turbine output.

The expected value of the total output is the index of EGWE in a single second. This index is an averaging assessment of the output power of the wind farm, which can be used as reference for power system planning and operation control. The next section will include the calculation of most of the other indices.

### 10.2.3 Reliability Indices Calculation

This section describes the calculation method of most reliability indices associated with the wind farm, taking configuration 1 as the analysis objective. The definition and the formula of these indices, including EGWE, are shown in Table 10.2.6.

Table 10.2.6: Definition and Expression of Reliability indices

<i>Reliability Index</i>	<i>Expression</i>
Installed Wind Power (IWP)	$IWP = \sum \text{nominal power of turbines in wind farm}$
Installed Wind Energy (IWE)	$IWE = \text{Installed Capacity} \cdot \text{Number of Operating Hours}$
Expected Available Wind Energy (EAWWE)	$EAWWE = \sum \text{Energy produced by turbines}$ Note: components' possible failure is not included
Expected Generated Wind Energy (EGWE)	$EGWE = \sum \text{Energy effectively available by turbines}$ Note: components's failure is considered
Capacity Factor (CF)	$CF = EGWE / IWE$
Generation Ratio (GR)	$GR = \text{power delivered to PCC} / IWP$ wind speed and failure of components are considered.

**Expected Generated Wind Energy (EGWE) and Expected Available Wind Energy (EAWWE):**

In this part, the reliability indices of EGWE and EAWWE will be calculated.

EGWE is discussed much in detail in the sections above, including the calculation methods both in full capacity case and wind speed variation case. Formula (10.2.12) and (10.2.13) have provided the expression of EGWE.

EAWWE stands for *Expected Available Wind Energy*, which is the index to evaluate the available wind power, *i.e.*, the available wind energy in a second. Commonly, wind speed variation is considered.

$$EAWWE = \sum \text{Energy produced by turbines} = N \cdot E(G) \quad (10.2.14)$$

where  $E(G)$  is the expected turbine output determined by (10.1.1) or (10.1.2). In this case, the wind speed variation is considered, but the transmission failure due to the failure of components is not considered. This is how EAWWE is different from EGWE.

Installed Wind Power (IWP), Installed Wind Energy(IWE), Capacity Factor (CF), and Generation Ratio (GR):

**In this part, the reliability indices of IWP, IWE, CF and GR are calculated based on the result of EGWE and the probability analysis provided above.**

Given the definitions and expressions in Table 10.2.6, the indices are calculated for configuration 1 as:

$$IWP = \sum \text{nominal power of turbines in wind farm} = N \cdot G \quad (10.2.15)$$

where  $N = n_1 + n_2 + \dots + n_m$  is the total number of wind turbines in the farm, and  $G$  is the nominal capacity of a single wind turbine in full capacity case.

$$IWE = \sum \text{Installed Capacity} \cdot \# \text{ of Operating Hours} = IWP \cdot t = N \cdot G \cdot t \quad (10.2.16)$$

where  $t$  is the number of operating time in hours.

$$CF = EGWE / IWE \quad (10.2.17)$$

$$GR = (EGWE/t) / IWP \quad (10.2.18)$$

where  $EGWE$  is the index calculated by (10.2.8) with both wind speed variation and transmission failure considered.

#### 10.2.4 Case Study: A 30 WT Case of Configuration 1

An example reliability analysis is shown in this section, using the configuration in Figure 10.2.1. The parameters of the configuration are: (a) Number of parallel lines:  $m=3$ ; (b) Number of wind turbines in each Line:  $n_1 = n_2 = n_3 = 10$ ; (c) Generating Capacity of each Turbine:  $G = 2\text{MW}$ . Wind speed distribution and the wind turbine output function are shown in Figures 10.1.1 and 10.1.2. The configuration in this case study is shown in Figure 10.2.2.

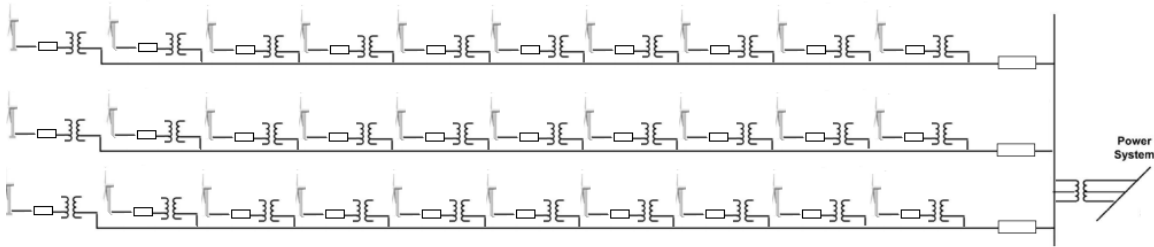


Figure 10.2.2: A 30 WT Case Study Configuration for Configuration 1

Reliability parameters used for this example calculation is shown in Appendix F.

**Full Capacity Case:** In full capacity case, the calculation result of the output probabilistic distribution is shown in Table 10.2.7. The essential reliability index  $EGWE = 49.42 \text{ MWh}$  in one hour.

Table 10.2.7: Case Study Output States and Probabilities

State	Generation Capacity(MW)	Probability
1	0	0.06291222
2	8	0.00861636
3	16	0.08026351
4	24	0.33229952
5	32	0.51590836

The other reliability indices are calculated as:

$$EAW E = \sum \text{Energy produced by turbines} = N \cdot E(G) = 30 \cdot 2 = 60\text{MW in one hour.}$$

Note here the indices of EGWE and EAW E is calculated in one hour basis. In order to get the indices within a certain period, the operating time should be multiplied. For example, if the indices for a year is needed, the calculation of EGWE and EAW E should be  $25.8374\text{MW} \cdot 8760 \text{ hours}$  and  $60\text{MW} \cdot 8760 \text{ hours}$  respectively.

$$IWP = \sum \text{nominal power of turbines in wind farm} = N \cdot G = 30 \cdot 2 = 60\text{MW}$$

$$IWE = IWP \cdot t = N \cdot G \cdot t = 60\text{MW} \cdot t = 60 \text{ MWh in one hour}$$

where t is the number of operating time in hours.

$$CF = EGWE / IWE = 0.824$$

$$GR = EGWE / IWP = 49.42/60 = 82.4\%$$

**Wind Speed Variation Case:** When wind speed is considered, the single wind turbine output function is shown in (10.1.1). From the wind speed probability distribution, the expected output of a single wind turbine becomes  $EGWE = \sum_v [G(v) \cdot P(v)] = 0.93 \text{ MWh}$ . From (10.2.13),  $EGWE = \sum_v [G(v) \cdot P(v)] \cdot \sum_{i=1}^m [n_i \cdot \left( \prod_{k=1}^4 \frac{\mu_k}{\lambda_k + \mu_k} \right)^{n_i} \cdot \frac{\mu_5}{\lambda_5 + \mu_5}] \cdot \prod_{q=6}^{12} \frac{\mu_q}{\lambda_q + \mu_q} = 22.98\text{MWh}$ , which is the reliability index EGWE in one hour.

The result shows the expected generation capacity that can be transmitted to the point of common coupling. This expected value can be used for system planning and operation.

$$EAW E = \sum \text{Energy produced by turbines} = N \cdot E(G) = 30 \cdot 0.93 = 27.9 \text{ MWh in one hour.}$$

$$IWP = \sum \text{nominal power of turbines in wind farm} = N \cdot G = 30 \cdot 2 = 60MW$$

$IWE = IWP \cdot t = N \cdot G \cdot t = 60MW \cdot t = 60MWh$  in one hour, where t is the number of operating hours.

$$CF = EGWE / IWE = 22.98/60 = 0.383$$

$$GR = EGWE / IWP = 22.98/60 = 38.3\%$$

The results of the reliability analysis for alternate configuration 1 are summarized in Table 10.2.8.

Table 10.2.8: Summary of Reliability Indices for Alternate Configuration 1

<i>Reliability Index</i>	<i>Computed Value</i>
Installed Wind Power (IWP)	60 MW
Installed Wind Energy (IWE)	60 MWh in one hour
Expected Available Wind Energy (EAWE)	27.9 MWh in one hour
Expected Generated Wind Energy (EGWE)	22.98MWh in one hour
Capacity Factor (CF)	0.383
Generation Ratio (GR)	38.3 %

### 10.3 Reliability Analysis of Wind Farm Configuration 2

This section provides the reliability analysis and case study result for configuration 2.

Figure 10.3.1 shows configuration 2. Configuration 2 has AC Wind Farm and DC Transmission.

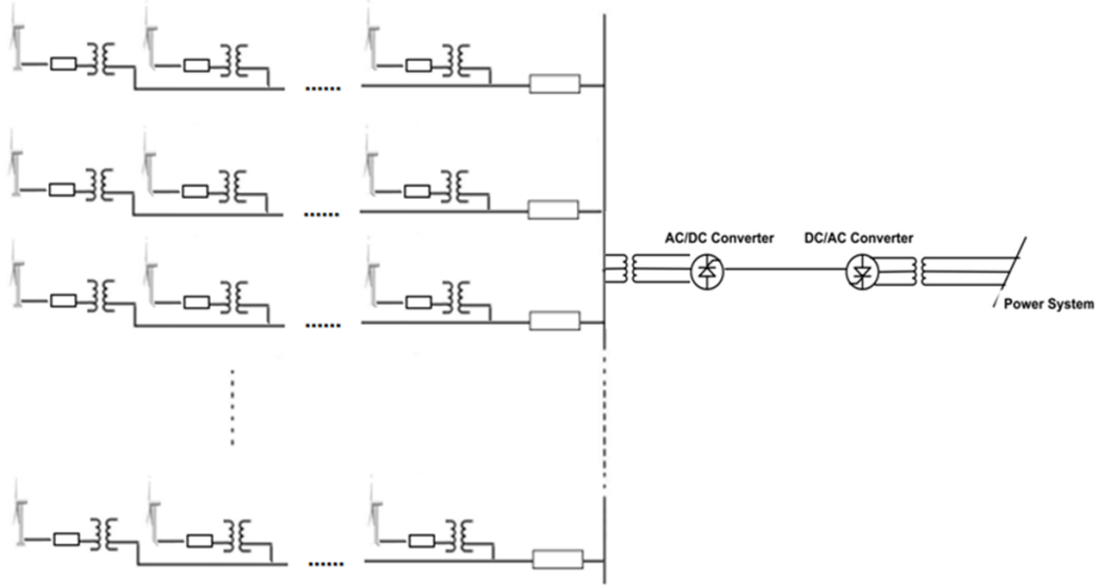


Figure 10.3.1: Wind Farm Configuration 2

The formulation of the reliability analysis for this configuration is as below. The probabilistic methods used for this formulation are exactly the ones shown in the analysis of configuration 1.

### 10.3.1 Probabilistic Model of Circuit $i$

This configuration has  $m$  parallel lines, each line consisting of  $n$  wind turbines. The probability of the states of each line is provided as below.

$$\begin{aligned}
 P_{line\ i}(Up) &= [P_{WT}^{n_i}(up) \cdot P_{SSW}^{n_i}(up) \cdot P_{ST}^{n_i}(up) \cdot P_{FAC}^{n_i}(up)] \cdot P_{LSW}(up) \\
 &= \left[ \frac{\mu_{WT}}{\lambda_{WT} + \mu_{WT}} \cdot \frac{\mu_{SSW}}{\lambda_{SSW} + \mu_{SSW}} \cdot \frac{\mu_{ST}}{\lambda_{ST} + \mu_{ST}} \cdot \frac{\mu_{FAC}}{\lambda_{FAC} + \mu_{FAC}} \right]^{n_i} \cdot \frac{\mu_{LSW}}{\lambda_{LSW} + \mu_{LSW}} \\
 P_{line\ i}(Down) &= 1 - P_{line\ i}(Up) \\
 &= 1 - \left[ \frac{\mu_{WT}}{\lambda_{WT} + \mu_{WT}} \cdot \frac{\mu_{SSW}}{\lambda_{SSW} + \mu_{SSW}} \cdot \frac{\mu_{ST}}{\lambda_{ST} + \mu_{ST}} \cdot \frac{\mu_{FAC}}{\lambda_{FAC} + \mu_{FAC}} \right]^{n_i} \cdot \frac{\mu_{LSW}}{\lambda_{LSW} + \mu_{LSW}}
 \end{aligned}$$

### 10.3.2 Probabilistic Model of $m$ Parallel Circuits

The  $m$  lines are in parallel, and the probability of having  $j$  lines up is shown as below.

$$P_{parallel\_jng} = C_m^j \cdot P_{line\ i}^j(up) \cdot P_{line\ i}^{m-j}(down)$$

where  $C_m^j = \frac{m!}{j!(m-j)!}$  is the combinatorial number.

### 10.3.3 Probabilistic Model of the Entire Configuration

The output states at the point of common coupling (PCC) are similar to the ones in configuration 1. At PCC, there are  $m+1$  states, the delivered capacity of which is similar to that in the analysis of Configuration 1. The 1<sup>st</sup> state represents the situation when there is no capacity successfully delivered.

When  $j \neq 0$ , the probability of the  $(j+1)$ th state, which is the probability of transmitting power of  $j \cdot n \cdot G$ , is:

$$\begin{aligned}
P_{system\_jnG} &= P_{parallel\_jnG} \cdot P(ACB \text{ up}) \cdot P(IT \text{ up}) \cdot P(IAC/DC \text{ up}) \cdot P(DC \text{ up}) \cdot P(DC/AC \text{ up}) \\
&\quad \cdot P(IT \text{ up}) \\
&= P_{parallel\_jnG} \cdot \frac{\mu_{ACB}}{\lambda_{ACB} + \mu_{ACB}} \cdot \frac{\mu_{IT}}{\lambda_{IT} + \mu_{IT}} \cdot \frac{\mu_{IAC/DC}}{\lambda_{IAC/DC} + \mu_{IAC/DC}} \cdot \frac{\mu_{DC}}{\lambda_{DC} + \mu_{DC}} \cdot \frac{\mu_{DC/AC}}{\lambda_{DC/AC} + \mu_{DC/AC}} \cdot \frac{\mu_{IT}}{\lambda_{IT} + \mu_{IT}} \\
&= C_m^j \cdot P_{line\ i}^j(up) \cdot P_{line\ i}^{m-j}(down) \cdot \frac{\mu_{ACB}}{\lambda_{ACB} + \mu_{ACB}} \cdot \frac{\mu_{IT}}{\lambda_{IT} + \mu_{IT}} \cdot \frac{\mu_{IAC/DC}}{\lambda_{IAC/DC} + \mu_{IAC/DC}} \cdot \frac{\mu_{DC}}{\lambda_{DC} + \mu_{DC}} \\
&\quad \cdot \frac{\mu_{DC/AC}}{\lambda_{DC/AC} + \mu_{DC/AC}} \cdot \frac{\mu_{IT}}{\lambda_{IT} + \mu_{IT}} \\
&= \frac{m!}{j!(m-j)!} \cdot \left\{ \left[ \frac{\mu_{WT}}{\lambda_{WT} + \mu_{WT}} \cdot \frac{\mu_{SSW}}{\lambda_{SSW} + \mu_{SSW}} \cdot \frac{\mu_{ST}}{\lambda_{ST} + \mu_{ST}} \cdot \frac{\mu_{FAC}}{\lambda_{FAC} + \mu_{FAC}} \right]^{n_i} \cdot \frac{\mu_{LSW}}{\lambda_{LSW} + \mu_{LSW}} \right\}^j \cdot \{1 \\
&\quad - \left[ \frac{\mu_{WT}}{\lambda_{WT} + \mu_{WT}} \cdot \frac{\mu_{SSW}}{\lambda_{SSW} + \mu_{SSW}} \cdot \frac{\mu_{ST}}{\lambda_{ST} + \mu_{ST}} \cdot \frac{\mu_{FAC}}{\lambda_{FAC} + \mu_{FAC}} \right]^{n_i} \cdot \frac{\mu_{LSW}}{\lambda_{LSW} + \mu_{LSW}} \}^{m-j} \\
&\quad \cdot \frac{\mu_{ACB}}{\lambda_{ACB} + \mu_{ACB}} \cdot \frac{\mu_{IT}}{\lambda_{IT} + \mu_{IT}} \cdot \frac{\mu_{IAC/DC}}{\lambda_{IAC/DC} + \mu_{IAC/DC}} \cdot \frac{\mu_{DC}}{\lambda_{DC} + \mu_{DC}} \cdot \frac{\mu_{DC/AC}}{\lambda_{DC/AC} + \mu_{DC/AC}} \cdot \frac{\mu_{IT}}{\lambda_{IT} + \mu_{IT}}
\end{aligned}$$

This probability is denoted as  $P(j+1)$ , for all  $j \neq 0$ .

When  $j = 0$ , the probability  $P(0+1)=P(1)$  can be calculated as:

$$P(1) = 1 - \sum_{w=1}^m P(w+1)$$

### 10.3.4 Expected Generated Wind Energy (EGWE)

The total expected available energy at point of common coupling is the index of EGWE:

$$\begin{aligned}
EGWE &= \left[ \sum_{i=1}^m n_i \cdot G \cdot P_{line\ i}(up) \right] \cdot P(ACB \text{ up}) \cdot P(IT \text{ up}) \cdot P(IAC/DC \text{ up}) \cdot P(DC \text{ up}) \\
&\quad \cdot P(DC/AC \text{ up}) \cdot P(IT \text{ up}) + 0
\end{aligned}$$

$$\begin{aligned}
&= \left[ \sum_{i=1}^m n_i \cdot G \cdot P_{line\ i}(up) \right] \cdot P(ACB\ up) \cdot P(IT\ up) \cdot P(lAC/DC\ up) \cdot P(DC\ up) \cdot P(DC/AC\ up) \\
&\quad \cdot P(IT\ up) \\
&= \left( \sum_{i=1}^m \{ n_i \cdot G \cdot \left[ \frac{\mu_{WT}}{\lambda_{WT} + \mu_{WT}} \cdot \frac{\mu_{sSw}}{\lambda_{sSw} + \mu_{sSw}} \cdot \frac{\mu_{sT}}{\lambda_{sT} + \mu_{sT}} \cdot \frac{\mu_{FAC}}{\lambda_{FAC} + \mu_{FAC}} \right]^{n_i} \cdot \frac{\mu_{lSw}}{\lambda_{lSw} + \mu_{lSw}} \} \right) \cdot \frac{\mu_{ACB}}{\lambda_{ACB} + \mu_{ACB}} \\
&\quad \cdot \frac{\mu_{IT}}{\lambda_{IT} + \mu_{IT}} \cdot \frac{\mu_{lAC/DC}}{\lambda_{lAC/DC} + \mu_{lAC/DC}} \cdot \frac{\mu_{DC}}{\lambda_{DC} + \mu_{DC}} \cdot \frac{\mu_{DC/AC}}{\lambda_{DC/AC} + \mu_{DC/AC}} \cdot \frac{\mu_{IT}}{\lambda_{IT} + \mu_{IT}}
\end{aligned}$$

### 10.3.5 Case Study

A 30 turbine case is also studied for configuration 2. The parameters of the connection in the configuration are:

- 1) m=3, which means there are 3 parallel lines;
- 2) n=10, which means there are 10 turbines in each line.

The formulation of the calculation is as below.

$$\begin{aligned}
EGWE &= \left[ \sum_{i=1}^m n_i \cdot G \cdot P_{line\ i}(up) \right] \cdot P(ACB\ up) \cdot P(IT\ up) \cdot P(lAC/DC\ up) \cdot P(DC\ up) \\
&\quad \cdot P(DC/AC\ up) \cdot P(IT\ up) + 0 \\
&= \left[ \sum_{i=1}^m n_i \cdot G \cdot P_{line\ i}(up) \right] \cdot P(ACB\ up) \cdot P(IT\ up) \cdot P(lAC/DC\ up) \cdot P(DC\ up) \cdot P(DC/AC\ up) \\
&\quad \cdot P(IT\ up) \\
&= \left( \sum_{i=1}^m \{ n_i \cdot G \cdot \left[ \frac{\mu_{WT}}{\lambda_{WT} + \mu_{WT}} \cdot \frac{\mu_{sSw}}{\lambda_{sSw} + \mu_{sSw}} \cdot \frac{\mu_{sT}}{\lambda_{sT} + \mu_{sT}} \cdot \frac{\mu_{FAC}}{\lambda_{FAC} + \mu_{FAC}} \right]^{n_i} \cdot \frac{\mu_{lSw}}{\lambda_{lSw} + \mu_{lSw}} \} \right) \cdot \frac{\mu_{ACB}}{\lambda_{ACB} + \mu_{ACB}} \\
&\quad \cdot \frac{\mu_{IT}}{\lambda_{IT} + \mu_{IT}} \cdot \frac{\mu_{lAC/DC}}{\lambda_{lAC/DC} + \mu_{lAC/DC}} \cdot \frac{\mu_{DC}}{\lambda_{DC} + \mu_{DC}} \cdot \frac{\mu_{DC/AC}}{\lambda_{DC/AC} + \mu_{DC/AC}} \cdot \frac{\mu_{IT}}{\lambda_{IT} + \mu_{IT}} \\
&= 24.1052 \cdot G
\end{aligned}$$

$$IWP = 30 \cdot G = 60 \text{ MW}$$

$$IWE = 30 \cdot G \cdot t = 60 \text{ MW} \cdot t = 60 \text{ MWh in an hour.}$$

In full capacity case,

$$EGWE = 48.21 \text{ MWh in an hour}$$



EAWWE = 60 MWh in an hour

$$CF = \frac{EGWE}{IWE} = \frac{48.21}{60} = 0.8035$$

$$GR = \frac{\frac{EGWE}{t}}{IWP} = \frac{48.21}{60} = 80.35\%$$

In wind speed variation case,

EGWE=22.42 MWh in an hour

EAWWE = 27.9 MWh in an hour

$$CF = \frac{EGWE}{IWE} = 0.3736$$

$$GR = \frac{\frac{EGWE}{t}}{IWP} = \frac{22.42}{60} = 37.36\%$$

The results of the reliability analysis for alternate configuration 2 are summarized in Table 10.3.1.

Table 10.3.1: Summary of Reliability Indices for Alternate Configuration 2

<i>Reliability Index</i>	<i>Computed Value</i>
Installed Wind Power (IWP)	60 MW
Installed Wind Energy (IWE)	60 MWh in one hour
Expected Available Wind Energy (EAWWE)	27.9 MWh in one hour
Expected Generated Wind Energy (EGWE)	22.42MWh in one hour
Capacity Factor (CF)	0.374
Generation Ratio (GR)	37.4%

#### 10.4 Reliability Analysis of Wind Farm Configuration 3

This section describes the reliability analysis and case study result for configuration 3.

Figure 10.4.1 shows configuration 3. Configuration 3 has DC Series Wind Farm and AC Transmission.

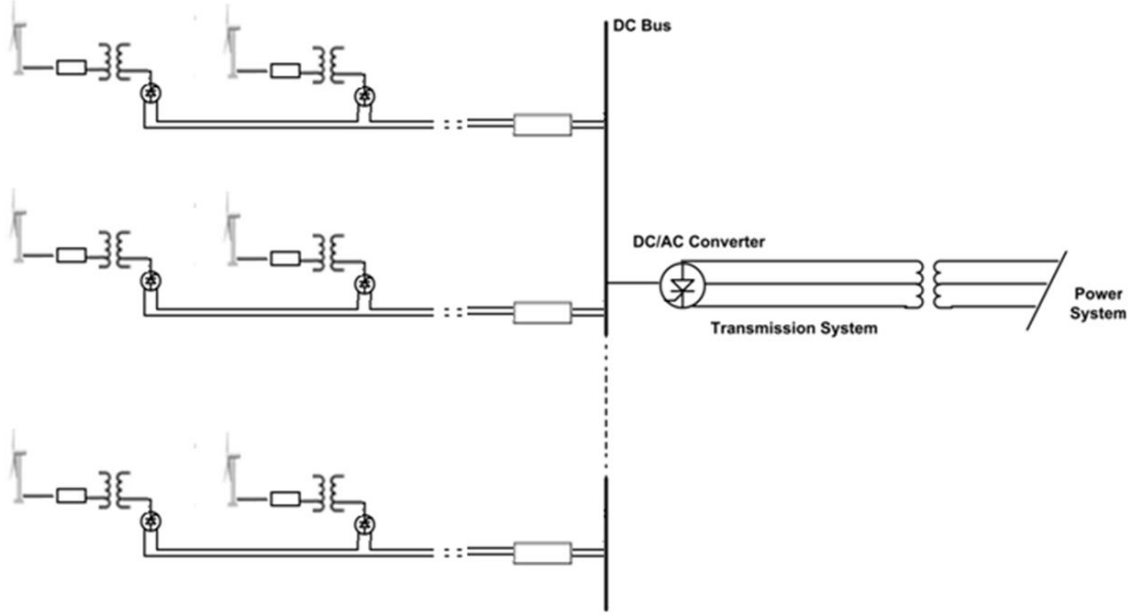


Figure 10.4.1: Wind Farm Configuration 3

The formulation of the reliability analysis for this configuration is as below. The probabilistic methods used for this formulation is exactly the ones shown in the analysis of configuration 1.

#### 10.4.1 Probabilistic Model of Circuit $i$

This configuration has  $m$  parallel lines, each line consisting of  $n$  wind turbines. The probability of the states of each line is provided as below.

$$P_{line\ i}(Up) = \left[ P_{WT}^{n_i}(up) \cdot P_{sSW}^{n_i}(up) \cdot P_{sST}^{n_i}(up) \cdot P_{sAC/DC}^{n_i}(up) \cdot P_{FDC}^{n_i}(up) \right] \cdot P_{LSW}(up)$$

$$= \left[ \frac{\mu_{WT}}{\lambda_{WT} + \mu_{WT}} \cdot \frac{\mu_{sSW}}{\lambda_{sSW} + \mu_{sSW}} \cdot \frac{\mu_{sT}}{\lambda_{sT} + \mu_{sT}} \cdot \frac{\mu_{sAC/DC}}{\lambda_{sAC/DC} + \mu_{sAC/DC}} \cdot \frac{\mu_{FDC}}{\lambda_{FDC} + \mu_{FDC}} \right]^{n_i} \cdot \frac{\mu_{LSW}}{\lambda_{LSW} + \mu_{LSW}}$$

$$P_{line\ i}(Down) = 1 - P_{line\ i}(Up)$$

$$= 1 - \left[ \frac{\mu_{WT}}{\lambda_{WT} + \mu_{WT}} \cdot \frac{\mu_{sSW}}{\lambda_{sSW} + \mu_{sSW}} \cdot \frac{\mu_{sT}}{\lambda_{sT} + \mu_{sT}} \cdot \frac{\mu_{AC/DC}}{\lambda_{AC/DC} + \mu_{AC/DC}} \cdot \frac{\mu_{FDC}}{\lambda_{FDC} + \mu_{FDC}} \right]^{n_i} \cdot \frac{\mu_{LSW}}{\lambda_{LSW} + \mu_{LSW}}$$

#### 10.4.2 Probabilistic Model of $m$ Parallel Circuits

The  $m$  lines are in parallel, and the probability of having  $j$  lines up is shown as below.

$$P_{parallel\_jnG} = C_m^j \cdot P_{line\ i}^j(up) \cdot P_{line\ i}^{m-j}(down)$$

where  $C_m^j = \frac{m!}{j!(m-j)!}$  is the combinatorial number

### 10.4.3 Probabilistic Model of the Entire Configuration

The output states at the point of common coupling (PCC) are similar to the ones in configuration 1. At PCC, there are  $m+1$  states, the delivered capacity of which is similar to that in the analysis of Configuration 1. The 1<sup>st</sup> state represents the situation when there is no capacity successfully delivered.

When  $j \neq 0$ , the probability of the  $(j+1)$ th state, which is the probability of transmitting power of  $j \cdot n \cdot G$ , is:

$$\begin{aligned} P_{system\_jnG} &= P_{parallel\_jnG} \cdot P(DCB\ up) \cdot P(DC/AC\ up) \cdot P(60AC\ up) \cdot P(lT\ up) \\ &= P_{parallel\_jnG} \cdot \frac{\mu_{DCB}}{\lambda_{DCB} + \mu_{DCB}} \cdot \frac{\mu_{DC/AC}}{\lambda_{DC/AC} + \mu_{DC/AC}} \cdot \frac{\mu_{60AC}}{\lambda_{60AC} + \mu_{60AC}} \cdot \frac{\mu_{lT}}{\lambda_{lT} + \mu_{lT}} \\ &= C_m^j \cdot P_{line\ i}^j(up) \cdot P_{line\ i}^{m-j}(down) \cdot \frac{\mu_{DCB}}{\lambda_{DCB} + \mu_{DCB}} \cdot \frac{\mu_{DC/AC}}{\lambda_{DC/AC} + \mu_{DC/AC}} \cdot \frac{\mu_{60AC}}{\lambda_{60AC} + \mu_{60AC}} \cdot \frac{\mu_{lT}}{\lambda_{lT} + \mu_{lT}} \\ &= \frac{m!}{j!(m-j)!} \cdot \left\{ \left[ \frac{\mu_{WT}}{\lambda_{WT} + \mu_{WT}} \cdot \frac{\mu_{sSw}}{\lambda_{sSw} + \mu_{sSw}} \cdot \frac{\mu_{sT}}{\lambda_{sT} + \mu_{sT}} \cdot \frac{\mu_{sAC/DC}}{\lambda_{sAC/DC} + \mu_{sAC/DC}} \cdot \frac{\mu_{FDC}}{\lambda_{FDC} + \mu_{FDC}} \right]^{n_i} \cdot \frac{\mu_{lSw}}{\lambda_{lSw} + \mu_{lSw}} \right\}^j \cdot \left\{ 1 - \right. \\ &\quad \left. \left[ \frac{\mu_{WT}}{\lambda_{WT} + \mu_{WT}} \cdot \frac{\mu_{sSw}}{\lambda_{sSw} + \mu_{sSw}} \cdot \frac{\mu_{sT}}{\lambda_{sT} + \mu_{sT}} \cdot \frac{\mu_{sAC/DC}}{\lambda_{sAC/DC} + \mu_{sAC/DC}} \cdot \frac{\mu_{FDC}}{\lambda_{FDC} + \mu_{FDC}} \right]^{n_i} \cdot \frac{\mu_{lSw}}{\lambda_{lSw} + \mu_{lSw}} \right\}^{m-j} \cdot \frac{\mu_{DCB}}{\lambda_{DCB} + \mu_{DCB}} \cdot \frac{\mu_{DC/AC}}{\lambda_{DC/AC} + \mu_{DC/AC}} \cdot \frac{\mu_{60AC}}{\lambda_{60AC} + \mu_{60AC}} \cdot \frac{\mu_{lT}}{\lambda_{lT} + \mu_{lT}} \end{aligned}$$

This probability is denoted as  $P(j+1)$ , for all  $j \neq 0$ .

When  $j = 0$ , the probability  $P(0+1)=P(1)$  can be calculated as:

$$P(1) = 1 - \sum_{w=1}^m P(w+1)$$

### 10.4.4 Expected Generated Wind Energy (EGWE)

The total expected available energy at point of common coupling is the index of EGWE:

$$\begin{aligned} EGWE &= \left[ \sum_{i=1}^m n_i \cdot G \cdot P_{line\ i}(up) \right] \cdot P(DCB\ up) \cdot P(DC/AC\ up) \cdot P(60AC\ up) \cdot P(lT\ up) + 0 \\ &= \left[ \sum_{i=1}^m n_i \cdot G \cdot P_{line\ i}(up) \right] \cdot P(DCB\ up) \cdot P(DC/AC\ up) \cdot P(60AC\ up) \cdot P(lT\ up) \end{aligned}$$

$$= \left( \sum_{i=1}^m \{n_i \cdot G \cdot \left[ \frac{\mu_{WT}}{\lambda_{WT} + \mu_{WT}} \cdot \frac{\mu_{sSw}}{\lambda_{sSw} + \mu_{sSw}} \cdot \frac{\mu_{sT}}{\lambda_{sT} + \mu_{sT}} \cdot \frac{\mu_{sAC/DC}}{\lambda_{sAC/DC} + \mu_{sAC/DC}} \cdot \frac{\mu_{FDC}}{\lambda_{FDC} + \mu_{FDC}} \right]^{n_i} \cdot \frac{\mu_{lSw}}{\lambda_{lSw} + \mu_{lSw}} \} \right) \cdot \frac{\mu_{DCB}}{\lambda_{DCB} + \mu_{DCB}} \cdot \frac{\mu_{DC/AC}}{\lambda_{DC/AC} + \mu_{DC/AC}} \cdot \frac{\mu_{60AC}}{\lambda_{60AC} + \mu_{60AC}} \cdot \frac{\mu_{lT}}{\lambda_{lT} + \mu_{lT}}$$

### 10.4.5 Case Study

A 30 turbine case is also studied for configuration 3. The parameters of the connection in the configuration are:

- 1) m=3, which means there are 3 parallel lines;
- 2) n=10, which means there are 10 turbines in each line.

The formulation of the calculation is as below.

$$\begin{aligned} EGWE &= \left[ \sum_{i=1}^m n_i \cdot G \cdot P_{line\ i}(up) \right] \cdot P(DCB\ up) \cdot P(DC/AC\ up) \cdot P(60AC\ up) \cdot P(lT\ up) + 0 \\ &= \left[ \sum_{i=1}^m n_i \cdot G \cdot P_{line\ i}(up) \right] \cdot P(DCB\ up) \cdot P(DC/AC\ up) \cdot P(60AC\ up) \cdot P(lT\ up) \\ &= \left( \sum_{i=1}^m \{n_i \cdot G \cdot \left[ \frac{\mu_{WT}}{\lambda_{WT} + \mu_{WT}} \cdot \frac{\mu_{sSw}}{\lambda_{sSw} + \mu_{sSw}} \cdot \frac{\mu_{sT}}{\lambda_{sT} + \mu_{sT}} \cdot \frac{\mu_{sAC/DC}}{\lambda_{sAC/DC} + \mu_{sAC/DC}} \cdot \frac{\mu_{FDC}}{\lambda_{FDC} + \mu_{FDC}} \right]^{n_i} \cdot \frac{\mu_{lSw}}{\lambda_{lSw} + \mu_{lSw}} \} \right) \cdot \frac{\mu_{DCB}}{\lambda_{DCB} + \mu_{DCB}} \cdot \frac{\mu_{DC/AC}}{\lambda_{DC/AC} + \mu_{DC/AC}} \cdot \frac{\mu_{60AC}}{\lambda_{60AC} + \mu_{60AC}} \cdot \frac{\mu_{lT}}{\lambda_{lT} + \mu_{lT}} \\ &= 22.3897G \end{aligned}$$

$$IWP = 30 \cdot G = 60 \text{ MW}$$

$$IWE = 30 \cdot G \cdot t = 60 \text{ MW} \cdot t = 60 \text{ MWh in an hour.}$$

In full capacity case,

$$EGWE = 44.77 \text{ MWh in an hour}$$

$$EAW = 60 \text{ MWh in an hour}$$

$$CF = \frac{EGWE}{IWE} = \frac{44.77}{60} = 0.7462$$

$$GR = \frac{\frac{EGWE}{t}}{IWP} = \frac{44.77}{60} = 74.62\%$$

In wind speed variation case,

$$\text{EGWE} = 20.82 \text{ MWh in an hour}$$

$$\text{EAWWE} = 27.9 \text{ MWh in an hour}$$

$$\text{CF} = \frac{\text{EGWE}}{\text{IWE}} = 0.347$$

$$\text{GR} = \frac{\frac{\text{EGWE}}{t}}{\text{IWP}} = \frac{22.42}{60} = 34.7\%$$

The results of the reliability analysis for alternate configuration 3 are summarized in Table 10.4.1.

Table 10.4.1: Summary of Reliability Indices for Alternate Configuration 3

<i>Reliability Index</i>	<i>Computed Value</i>
Installed Wind Power (IWP)	60 MW
Installed Wind Energy (IWE)	60 MWh in one hour
Expected Available Wind Energy (EAWWE)	27.9 MWh in one hour
Expected Generated Wind Energy (EGWE)	20.82MWh in one hour
Capacity Factor (CF)	0.347
Generation Ratio (GR)	34.7%

## 10.5 Reliability Analysis of Wind Farm Configuration 4

This section provides the reliability analysis and case study result for configuration 4.

Figure 10.5.1 shows configuration 4. Configuration 4 has DC Parallel Wind Farm and AC Transmission.

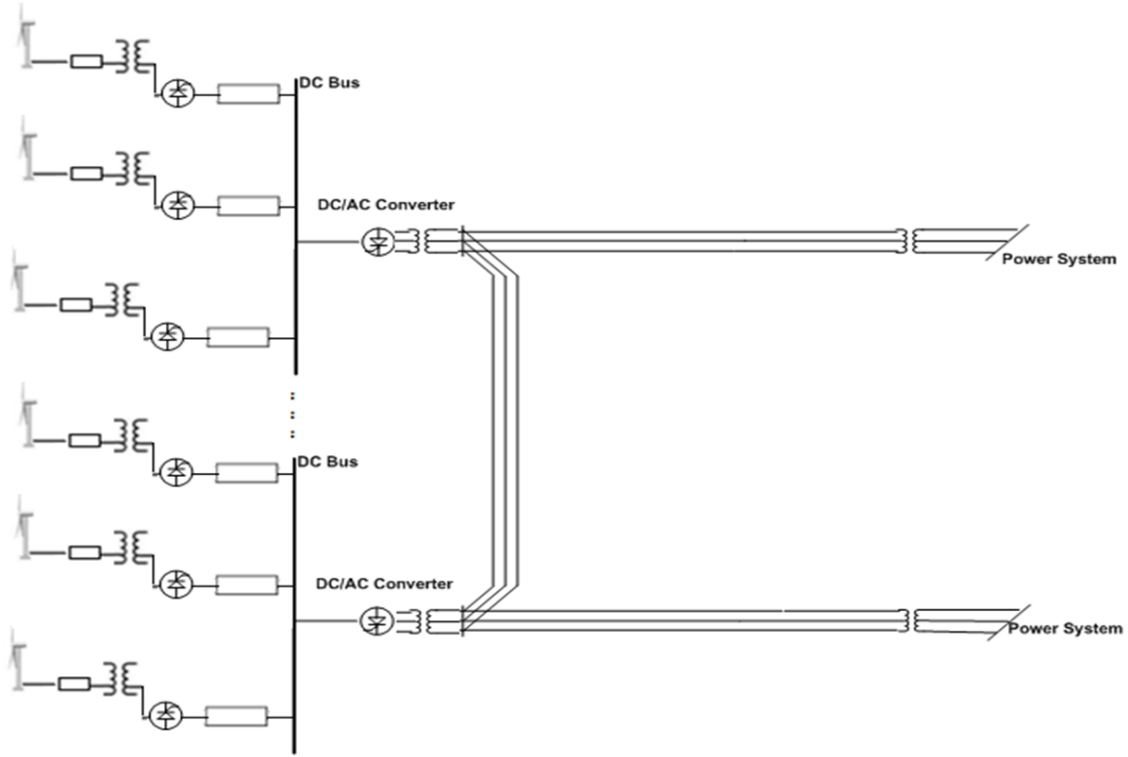


Figure 10.5.1: Wind Farm Configuration 4

The formulation of the reliability analysis for this configuration is as below. The probabilistic methods used for this formulation is exactly the ones shown in the analysis of configuration 1.

### 10.5.1 Probabilistic Model of Circuit $i$

In this configuration, there are assumed to be  $m$  DC buses, each bus consist of  $n$  parallel connected wind turbines.

$$P_{line\ i}(Up) = P(WT\ up) \cdot P(sSw\ up) \cdot P(sT\ up) \cdot P(sAC/DC\ up) \cdot P(FDC\ up) \cdot P_{lSw}(up)$$

$$= \frac{\mu_{WT}}{\lambda_{WT} + \mu_{WT}} \cdot \frac{\mu_{sSw}}{\lambda_{sSw} + \mu_{sSw}} \cdot \frac{\mu_{sT}}{\lambda_{sT} + \mu_{sT}} \cdot \frac{\mu_{sAC/DC}}{\lambda_{sAC/DC} + \mu_{sAC/DC}} \cdot \frac{\mu_{FDC}}{\lambda_{FDC} + \mu_{FDC}} \cdot \frac{\mu_{lSw}}{\lambda_{lSw} + \mu_{lSw}}$$

$$P_{line\ i}(Down) = 1 - P_{line\ i}(Up)$$

$$= 1 - \frac{\mu_{WT}}{\lambda_{WT} + \mu_{WT}} \cdot \frac{\mu_{sSw}}{\lambda_{sSw} + \mu_{sSw}} \cdot \frac{\mu_{sT}}{\lambda_{sT} + \mu_{sT}} \cdot \frac{\mu_{sAC/DC}}{\lambda_{sAC/DC} + \mu_{sAC/DC}} \cdot \frac{\mu_{FDC}}{\lambda_{FDC} + \mu_{FDC}} \cdot \frac{\mu_{lSw}}{\lambda_{lSw} + \mu_{lSw}}$$

### 10.5.2 Probabilistic Model of $m$ Buses

$$P_{parallel\_jng} = C_{mn}^j \cdot P_{line\ i}^j(up) \cdot P_{line\ i}^{mn-j}(down)$$

where  $C_{mn}^j = \frac{mn!}{j!(mn-j)!}$  is the combinatorial number.

### 10.5.3 Probabilistic Model of the Entire Configuration

The configuration contains  $m$  buses and each bus contains  $n$  wind turbines. This case is more complicated than the previous configurations.

Some assumptions need to be made.

- 1) Transmission Constraints are not considered.
- 2) All DC buses are identical.
- 3) All inter-transmission lines, which are the lines connecting the transmission lines, are identical.
- 4) All transmission lines, which are the lines connecting the DC bus with the point of common coupling, are identical.

With these assumptions, the probability of a wind turbine generation's successful transmitting to point of common coupling (PCC), is the multiplication of the probability of its successful transmitting to the DC bus with its successful transmitting from DC bus to PCC. In addition, the probability of the successful transmission for each turbine is identical.

The successful transmission from a DC bus to PCC contains many cases. However, the unsuccessful transmission from a DC bus to PCC, is limited to 2 cases: a) all transmission lines fail, and b) the transmission line connected to this DC bus fails, and at the same time, the inter-transmission lines connected to this DC bus fail.

Therefore, the power reaches the transmission line can be delivered to the power system unless all of the transmission is not successful.

The probability of at least one transmission line works is

$$P_{Tran}(up) = 1 - (1 - P(60AC\ up) \cdot P(IT\ up))^m$$

The probability of the DC bus, converter and 20Hz transformer will work is

$$P_{DCT}(up) = P(DCB\ up) \cdot P(Conv\ up) \cdot P(T\ up)$$

$$P_{DCT}(down) = 1 - P(DCB\ up) \cdot P(Conv\ up) \cdot P(T\ up)$$

For the convenience of computation, the probability of the internal transmission line that can deliver the power to transmission line is:

$$P_{Intel60}(up) = \frac{\mu_{Inter60}}{\lambda_{Inter60} + \mu_{Inter60}}$$

So the probability of the right part of this configuration will work is

$$P_{right} = P_{Tran}(up) \cdot P_{Intel}(up)$$

For  $0 < j \leq n$

$$\begin{aligned} P_{system\_inG} = P_{right} \cdot [ & C_m^m \cdot P_{DCT}^m(up) \cdot C_{mn}^j \cdot P_{line\ i}^j(up) \cdot P_{line\ i}^{mn-j}(down) \\ & + C_m^{m-1} \cdot P_{DCT}^{m-1}(up) \cdot P_{DCT}^1(down) \cdot C_{(m-1)n}^j \cdot P_{line\ i}^j(up) \\ & \cdot P_{line\ i}^{mn-j}(down) + \dots + C_m^1 \cdot P_{DCT}^1(up) \cdot P_{DCT}^{m-1}(down) \cdot C_n^j \cdot P_{line\ i}^j(up) \\ & \cdot P_{line\ i}^{mn-j}(down) ] \end{aligned}$$

For  $n < j \leq n + n$

For  $(m-1)n < j \leq mn$

$$P_{system\_inG} = P_{right} \cdot [C_m^m \cdot P_{DCT}^m(up) \cdot C_{mn}^j \cdot P_{line\ i}^j(up) \cdot P_{line\ i}^{mn-j}(down)]$$

#### 10.5.4 Expected Generated Wind Energy (EGWE)

$$EGWE = \sum_{i=1}^{number\ of\ states} G_i \cdot P(i)$$

For the general case, each of the  $mn$  parallel circuits has two states: (a) either transmitting full capacity or (b) 0. For line  $i$ , the expected transmitted capacity to the collector AC bus is:

$$EGWE_{line\ i} = G \cdot P_{line\ i}(up) + 0 \cdot P_{line\ i}(down) = G \cdot P_{line\ i}(up)$$

The total expected available energy at point of common coupling is the index of EGWE:

$$\begin{aligned} EGWE &= mn * G \cdot P_{line\ i}(up) \cdot P(DCT\ up) \cdot P(right\ up) + 0 \\ &= mn * G \cdot P_{line\ i}(up) \cdot P(DCB\ up) \cdot P(Conv\ up) \cdot P(T\ up) \cdot P_{Intel60}(up) \cdot [1 - (1 - \\ &P(60AC\ up) \cdot P(IT\ up))^m] \\ &= mn \cdot G \cdot \frac{\mu_{WT}}{\lambda_{WT} + \mu_{WT}} \cdot \frac{\mu_{sSw}}{\lambda_{sSw} + \mu_{sSw}} \cdot \frac{\mu_{sT}}{\lambda_{sT} + \mu_{sT}} \cdot \frac{\mu_{sAC/DC}}{\lambda_{sAC/DC} + \mu_{sAC/DC}} \cdot \frac{\mu_{FDC}}{\lambda_{FDC} + \mu_{FDC}} \cdot \frac{\mu_{lSw}}{\lambda_{lSw} + \mu_{lSw}} \cdot \frac{\mu_{DCB}}{\lambda_{DCB} + \mu_{DCB}} \cdot \\ &\frac{\mu_{DC/AC}}{\lambda_{DC/AC} + \mu_{DC/AC}} \cdot \frac{\mu_{IT}}{\lambda_{IT} + \mu_{IT}} \cdot \frac{\mu_{Inter60}}{\lambda_{Inter60} + \mu_{Inter60}} \cdot \left[ 1 - \left( 1 - \frac{\mu_{60AC}}{\lambda_{60AC} + \mu_{60AC}} \cdot \frac{\mu_{IT}}{\lambda_{IT} + \mu_{IT}} \right)^m \right] \end{aligned}$$

#### 10.5.5 Case Study

A 30 turbine case is also studied for configuration 4. The parameters of the connection in the configuration are:

- 1)  $m=3$ , which means there are 3 buses;



2) n=10, which means there are 10 turbines on each bus.

The formulation of the calculation is as below.

$$\begin{aligned}
 EGWE &= mn * G \cdot P_{line\ i}(up) \cdot P(DCT\ up) \cdot P(right\ up) + 0 \\
 &= mn * G \cdot P_{line\ i}(up) \cdot P(DCB\ up) \cdot P(Conv\ up) \cdot P(T\ up) \cdot P_{Intel60}(up) \cdot [1 \\
 &\quad - (1 - P(60AC\ up) \cdot P(IT\ up))^m] \\
 &= mn \cdot G \cdot \frac{\mu_{WT}}{\lambda_{WT} + \mu_{WT}} \cdot \frac{\mu_{sSw}}{\lambda_{sSw} + \mu_{sSw}} \cdot \frac{\mu_{sT}}{\lambda_{sT} + \mu_{sT}} \cdot \frac{\frac{\mu_{sAC}}{DC}}{\lambda_{sAC} + \frac{\mu_{sAC}}{DC}} \cdot \frac{\mu_{FDC}}{\lambda_{FDC} + \mu_{FDC}} \cdot \frac{\mu_{lSw}}{\lambda_{lSw} + \mu_{lSw}} \\
 &\quad \cdot \frac{\mu_{DCB}}{\lambda_{DCB} + \mu_{DCB}} \cdot \frac{\frac{\mu_{DC}}{AC}}{\lambda_{DC} + \frac{\mu_{DC}}{AC}} \cdot \frac{\mu_{IT}}{\lambda_{IT} + \mu_{IT}} \cdot \frac{\mu_{Inter60}}{\lambda_{Inter60} + \mu_{Inter60}} \\
 &\quad \cdot \left[ 1 - \left( 1 - \frac{\mu_{60AC}}{\lambda_{60AC} + \mu_{60AC}} \cdot \frac{\mu_{IT}}{\lambda_{IT} + \mu_{IT}} \right)^m \right] \\
 &= 28.1884G
 \end{aligned}$$

$$IWP = 30 \cdot G = 60 \text{ MW}$$

$$IWE = 30 \cdot G \cdot t = 60 \text{ MW} \cdot t = 60 \text{ MWh in an hour.}$$

In full capacity case,

$$EGWE = 56.37 \text{ MWh in an hour}$$

$$EAW = 60 \text{ MWh in an hour}$$

$$CF = \frac{EGWE}{IWE} = \frac{56.37}{60} = 0.9396$$

$$GR = \frac{\frac{EGWE}{t}}{IWP} = \frac{56.37}{60} = 93.96\%$$

In wind speed variation case,

$$EGWE = 26.22 \text{ MWh in an hour}$$

$$EAW = 27.9 \text{ MWh in an hour}$$

$$CF = \frac{EGWE}{IWE} = 0.437$$

$$GR = \frac{\frac{EGWE}{t}}{IWP} = \frac{26.22}{60} = 43.7\%$$

The results of the reliability analysis for alternate configuration 4 are summarized in Table 10.5.1.

Table 10.5.1: Summary of Reliability Indices for Alternate Configuration 4

<i>Reliability Index</i>	<i>Computed Value</i>
Installed Wind Power (IWP)	60 MW
Installed Wind Energy (IWE)	60 MWh in one hour
Expected Available Wind Energy (EAWWE)	27.9 MWh in one hour
Expected Generated Wind Energy (EGWE)	26.22MWh in one hour
Capacity Factor (CF)	0.437
Generation Ratio (GR)	43.7%

## 10.6 Reliability Analysis of Wind Farm Configuration 5

This section provides the reliability analysis and case study result for configuration 5.

Figure 10.6.1 gives out configuration 5. Configuration 5 has DC Series Wind Farm and LFAC Transmission (single branch).

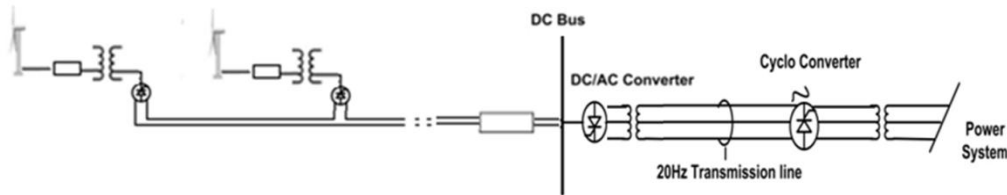


Figure 10.6.1: Wind Farm Configuration 5

The formulation of the reliability analysis for this configuration is as below. The probabilistic methods used for this formulation is exactly the ones shown in the analysis of configuration 1.

### 10.6.1 Probabilistic Model of the Entire Configuration

Since the generators are in series, the system won't be up unless all the components are up. Therefore, the number of wind turbine power that is delivered successfully,  $j$ , is either 0 or  $m$ .

When  $j = m$ , the probability of the state is:

$$P_{system\_jnG} = [P_{WT}^{mn}(up) \cdot P_{SSW}^{mn}(up) \cdot P_{SST}^{mn}(up) \cdot P_{SAC/DC}^{mn}(up) \cdot P_{FDC}^{mn}(up)] \cdot P(ISW\ up) \cdot P(DCB\ up) \cdot P(DC/AC\ up) \cdot P(20T\ up) \cdot P(20AC\ up) \cdot P(Conv\ up) \cdot P(lT\ up)$$

$$= \left[ \frac{\mu_{WT}}{\lambda_{WT} + \mu_{WT}} \cdot \frac{\mu_{sSw}}{\lambda_{sSw} + \mu_{sSw}} \cdot \frac{\mu_{sT}}{\lambda_{sT} + \mu_{sT}} \cdot \frac{\mu_{sAC}}{\lambda_{sAC} + \mu_{sAC}} \cdot \frac{\mu_{FDC}}{\lambda_{FDC} + \mu_{FDC}} \right]^{mn} \cdot \frac{\mu_{ISw}}{\lambda_{ISw} + \mu_{ISw}} \cdot \frac{\mu_{DCB}}{\lambda_{DCB} + \mu_{DCB}} \cdot \frac{\mu_{DC}}{\lambda_{DC} + \mu_{DC}} \cdot \frac{\mu_{20T}}{\lambda_{20T} + \mu_{20T}} \cdot \frac{\mu_{20AC}}{\lambda_{20AC} + \mu_{20AC}} \cdot \frac{\mu_{Conv}}{\lambda_{Conv} + \mu_{Conv}} \cdot \frac{\mu_{IT}}{\lambda_{IT} + \mu_{IT}}$$

When  $j = 0$ , the probability  $P(0+I)=P(I)$  can be calculated as:

$$P(1) = 1 - \sum_{w=1}^m P(w + 1)$$

### 10.6.2 Expected Generated Wind Energy (EGWE)

The total expected available energy at point of common coupling is the index of EGWE:

$$EGWE = mn \cdot G \cdot \left[ P_{WT}^{mn}(up) \cdot P_{sSw}^{mn}(up) \cdot P_{sT}^{mn}(up) \cdot P_{sAC}^{mn}(up) \cdot P_{FDC}^{mn}(up) \right] \cdot P(ISW up) \cdot P(DCB up) \cdot P\left(\frac{DC}{AC} up\right) \cdot P(20T up) \cdot P(20AC up) \cdot P(Conv up) \cdot P(IT up)$$

$$= mn \cdot G \cdot \left[ \frac{\mu_{WT}}{\lambda_{WT} + \mu_{WT}} \cdot \frac{\mu_{sSw}}{\lambda_{sSw} + \mu_{sSw}} \cdot \frac{\mu_{sT}}{\lambda_{sT} + \mu_{sT}} \cdot \frac{\mu_{sAC}}{\lambda_{sAC} + \mu_{sAC}} \cdot \frac{\mu_{FDC}}{\lambda_{FDC} + \mu_{FDC}} \right]^{mn} \cdot \frac{\mu_{ISw}}{\lambda_{ISw} + \mu_{ISw}} \cdot \frac{\mu_{DCB}}{\lambda_{DCB} + \mu_{DCB}} \cdot \frac{\mu_{DC/AC}}{\lambda_{DC/AC} + \mu_{DC/AC}} \cdot \frac{\mu_{20T}}{\lambda_{20T} + \mu_{20T}} \cdot \frac{\mu_{20AC}}{\lambda_{20AC} + \mu_{20AC}} \cdot \frac{\mu_{Conv}}{\lambda_{Conv} + \mu_{Conv}} \cdot \frac{\mu_{IT}}{\lambda_{IT} + \mu_{IT}}$$

### 10.6.3 Case Study

A 30 turbine case is also studied for configuration 5. The parameters of the connection in the configuration are:

- 1)  $m=1$ , which means there are 1 parallel lines;
- 2)  $n=30$ , which means there are 30 turbines in each line.

The formulation of the calculation is as below.

$$EGWE = mn \cdot G \cdot \left[ P_{WT}^{mn}(up) \cdot P_{sSw}^{mn}(up) \cdot P_{sT}^{mn}(up) \cdot P_{sAC}^{mn}(up) \cdot P_{FDC}^{mn}(up) \right] \cdot P(ISW up) \cdot P(DCB up) \cdot P\left(\frac{DC}{AC} up\right) \cdot P(20T up) \cdot P(20AC up) \cdot P(Conv up) \cdot P(IT up)$$

$$= mn \cdot G \cdot \left[ \frac{\mu_{WT}}{\lambda_{WT} + \mu_{WT}} \cdot \frac{\mu_{sSw}}{\lambda_{sSw} + \mu_{sSw}} \cdot \frac{\mu_{sT}}{\lambda_{sT} + \mu_{sT}} \cdot \frac{\mu_{sAC}}{\lambda_{sAC} + \mu_{sAC}} \cdot \frac{\mu_{FDC}}{\lambda_{FDC} + \mu_{FDC}} \right]^{mn} \cdot \frac{\mu_{ISw}}{\lambda_{ISw} + \mu_{ISw}} \cdot \frac{\mu_{DCB}}{\lambda_{DCB} + \mu_{DCB}} \cdot \frac{\mu_{DC}}{\lambda_{DC} + \mu_{DC}} \cdot \frac{\mu_{20T}}{\lambda_{20T} + \mu_{20T}} \cdot \frac{\mu_{20AC}}{\lambda_{20AC} + \mu_{20AC}} \cdot \frac{\mu_{Conv}}{\lambda_{Conv} + \mu_{Conv}} \cdot \frac{\mu_{IT}}{\lambda_{IT} + \mu_{IT}}$$

$$= 13.2399G$$

$$IWP = 30 \cdot G = 60 \text{ MW}$$

$$IWE = 30 \cdot G \cdot t = 60\text{MW} \cdot t = 60 \text{ MWh in an hour.}$$

In full capacity case,

$$EGWE=26.47 \text{ MWh in an hour}$$

$$EAW E = 60 \text{ MWh in an hour}$$

$$CF = \frac{EGWE}{IWE} = \frac{26.47}{60} = 0.4413$$

$$GR = \frac{\frac{EGWE}{t}}{IWP} = \frac{26.47}{60} = 44.13\%$$

In wind speed variation case,

$$EGWE=12.31 \text{ MWh in an hour}$$

$$EAW E = 27.9 \text{ MWh in an hour}$$

$$CF = \frac{EGWE}{IWE} = 0.205$$

$$GR = \frac{\frac{EGWE}{t}}{IWP} = \frac{22.42}{60} = 20.5\%$$

The results of the reliability analysis for alternate configuration 5 are summarized in Table 13.6.1.

Table 10.6.1: Summary of Reliability Indices for Alternate Configuration 5

<i>Reliability Index</i>	<i>Computed Value</i>
Installed Wind Power (IWP)	60 MW
Installed Wind Energy (IWE)	60 MWh in one hour
Expected Available Wind Energy (EAW E)	27.9 MWh in one hour
Expected Generated Wind Energy (EGWE)	12.31MWh in one hour
Capacity Factor (CF)	0.205
Generation Ratio (GR)	20.5%

## 10.7 Reliability Analysis of Wind Farm Configuration 6

This section provides the reliability analysis and case study result for configuration 6.

Figure 10.7.1 gives out configuration 6. Configuration 6 has DC Parallel Wind Farm, and LFAC Transmission (single branch).

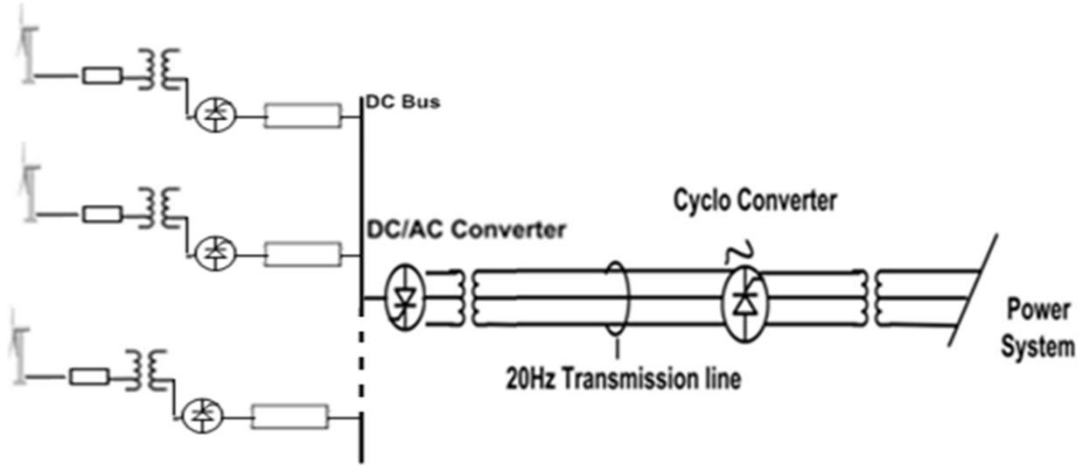


Figure 10.7.1: Wind Farm Configuration 6

The formulation of the reliability analysis for this configuration is as below. The probabilistic methods used for this formulation is exactly the ones shown in the analysis of configuration 1.

### 10.7.1 Probabilistic Model of Circuit $i$

The probabilities of the states of the  $i$ th circuit are developed.

$$P_{line\ i}(Up) = P(WT\ up) \cdot P(sSw\ up) \cdot P(sT\ up) \cdot P(sAC/DC\ up) \cdot P(FDC\ up) \cdot P_{ISW}(up)$$

$$= \frac{\mu_{WT}}{\lambda_{WT} + \mu_{WT}} \cdot \frac{\mu_{sSw}}{\lambda_{sSw} + \mu_{sSw}} \cdot \frac{\mu_{sT}}{\lambda_{sT} + \mu_{sT}} \cdot \frac{\mu_{sAC/DC}}{\lambda_{sAC/DC} + \mu_{sAC/DC}} \cdot \frac{\mu_{FDC}}{\lambda_{FDC} + \mu_{FDC}} \cdot \frac{\mu_{ISW}}{\lambda_{ISW} + \mu_{ISW}}$$

$$P_{line\ i}(Down) = 1 - P_{line\ i}(Up)$$

$$= 1 - \frac{\mu_{WT}}{\lambda_{WT} + \mu_{WT}} \cdot \frac{\mu_{sSw}}{\lambda_{sSw} + \mu_{sSw}} \cdot \frac{\mu_{sT}}{\lambda_{sT} + \mu_{sT}} \cdot \frac{\mu_{sAC/DC}}{\lambda_{sAC/DC} + \mu_{sAC/DC}} \cdot \frac{\mu_{FDC}}{\lambda_{FDC} + \mu_{FDC}} \cdot \frac{\mu_{ISW}}{\lambda_{ISW} + \mu_{ISW}}$$

### 10.7.2 Probabilistic Model of m Parallel Circuits

$$P_{parallel\_jng} = C_m^j \cdot P_{line\ i}^j(up) \cdot P_{line\ i}^{m-j}(down)$$

where  $C_m^j = \frac{m!}{j!(m-j)!}$  is the combinatorial number.

### 10.7.3 Probabilistic Model of the Entire Configuration

The output states at the point of common coupling (PCC) are similar to the ones in configuration 1. At PCC, there are  $m+1$  states, the delivered capacity of which is similar to that in the analysis of Configuration 1. The 1<sup>st</sup> state represents the situation when there is no capacity successfully delivered.

When  $j \neq 0$ , the probability of the  $(j+1)$ th state, which is the probability of transmitting power of  $j \cdot n \cdot G$ , is:

$$\begin{aligned} P_{system\_jng} &= P_{parallel\_jng} \cdot P(DCB\ up) \cdot P(DC/AC\ up) \cdot P(20T\ up) \cdot P(20AC\ up) \cdot P(Conv\ up) \cdot \\ P(lT\ up) &= P_{parallel\_jng} \cdot \frac{\mu_{DCB}}{\lambda_{DCB} + \mu_{DCB}} \cdot \frac{\mu_{DC/AC}}{\lambda_{DC/AC} + \mu_{DC/AC}} \cdot \frac{\mu_{20T}}{\lambda_{20T} + \mu_{20T}} \cdot \frac{\mu_{20AC}}{\lambda_{20AC} + \mu_{20AC}} \cdot \frac{\mu_{Conv}}{\lambda_{Conv} + \mu_{Conv}} \cdot \frac{\mu_{lT}}{\lambda_{lT} + \mu_{lT}} \\ &= C_m^j \cdot P_{line\ i}^j(up) \cdot P_{line\ i}^{m-j}(down) \cdot \frac{\mu_{DCB}}{\lambda_{DCB} + \mu_{DCB}} \cdot \frac{\mu_{DC/AC}}{\lambda_{DC/AC} + \mu_{DC/AC}} \cdot \frac{\mu_{20T}}{\lambda_{20T} + \mu_{20T}} \cdot \frac{\mu_{20AC}}{\lambda_{20AC} + \mu_{20AC}} \cdot \frac{\mu_{Conv}}{\lambda_{Conv} + \mu_{Conv}} \cdot \frac{\mu_{lT}}{\lambda_{lT} + \mu_{lT}} \\ &= \frac{m!}{j!(m-j)!} \cdot \left\{ \frac{\mu_{WT}}{\lambda_{WT} + \mu_{WT}} \cdot \frac{\mu_{sSw}}{\lambda_{sSw} + \mu_{sSw}} \cdot \frac{\mu_{sT}}{\lambda_{sT} + \mu_{sT}} \cdot \frac{\mu_{sAC/DC}}{\lambda_{sAC/DC} + \mu_{sAC/DC}} \cdot \frac{\mu_{FDC}}{\lambda_{FDC} + \mu_{FDC}} \cdot \frac{\mu_{lSw}}{\lambda_{lSw} + \mu_{lSw}} \right\}^j \cdot \left\{ 1 - \frac{\mu_{WT}}{\lambda_{WT} + \mu_{WT}} \cdot \frac{\mu_{sSw}}{\lambda_{sSw} + \mu_{sSw}} \cdot \frac{\mu_{sT}}{\lambda_{sT} + \mu_{sT}} \cdot \frac{\mu_{sAC/DC}}{\lambda_{sAC/DC} + \mu_{sAC/DC}} \cdot \frac{\mu_{FDC}}{\lambda_{FDC} + \mu_{FDC}} \cdot \frac{\mu_{lSw}}{\lambda_{lSw} + \mu_{lSw}} \right\}^{m-j} \cdot \frac{\mu_{DCB}}{\lambda_{DCB} + \mu_{DCB}} \cdot \frac{\mu_{DC/AC}}{\lambda_{DC/AC} + \mu_{DC/AC}} \cdot \frac{\mu_{20T}}{\lambda_{20T} + \mu_{20T}} \cdot \frac{\mu_{20AC}}{\lambda_{20AC} + \mu_{20AC}} \cdot \frac{\mu_{Conv}}{\lambda_{Conv} + \mu_{Conv}} \cdot \frac{\mu_{lT}}{\lambda_{lT} + \mu_{lT}} \end{aligned}$$

This probability is denoted as  $P(j+1)$ , for all  $j \neq 0$ .

When  $j = 0$ , the probability  $P(0+1)=P(1)$  can be calculated as:

$$P(1) = 1 - \sum_{w=1}^m P(w+1)$$

### 10.7.4 Expected Generated Wind Energy (EGWE)

The total expected available energy at point of common coupling is the index of EGWE:

$$\begin{aligned} EGWE &= \left[ \sum_{i=1}^m n_i \cdot G \cdot P_{line\ i}(up) \right] \cdot P(DCB\ up) \cdot P(DC/AC\ up) \cdot P(20T\ up) \cdot P(20AC\ up) \cdot \\ &P(Conv\ up) \cdot P(lT\ up) + 0 \\ &= \left[ \sum_{i=1}^m n_i \cdot G \cdot P_{line\ i}(up) \right] \cdot P(DCB\ up) \cdot P(DC/AC\ up) \cdot P(20T\ up) \cdot P(20AC\ up) \cdot P(Conv\ up) \\ &\quad \cdot P(lT\ up) \end{aligned}$$



$$GR = \frac{\frac{EGWE}{t}}{IWP} = \frac{55.61}{60} = 92.7\%$$

In wind speed variation case,

EGWE=25.86 MWh in an hour

EAWWE = 27.9 MWh in an hour

$$CF = \frac{EGWE}{IWE} = 0.431$$

$$GR = \frac{\frac{EGWE}{t}}{IWP} = \frac{22.42}{60} = 43.1\%$$

The results of the reliability analysis for alternate configuration 6 are summarized in Table 10.7.1.

Table 10.7.1: Summary of Reliability Indices for Alternate Configuration 6

<i>Reliability Index</i>	<i>Computed Value</i>
Installed Wind Power (IWP)	60 MW
Installed Wind Energy (IWE)	60 MWh in one hour
Expected Available Wind Energy (EAWWE)	27.9 MWh in one hour
Expected Generated Wind Energy (EGWE)	25.86MWh in one hour
Capacity Factor (CF)	0.431
Generation Ratio (GR)	43.1%

## 10.8 Reliability Analysis of Wind Farm Configuration 7

This section provides the reliability analysis and case study result for configuration 7.

Figure 10.8.1 gives out configuration 7. Configuration 7 has DC Series Wind Farm, LFAC Transmission (multiple branches).



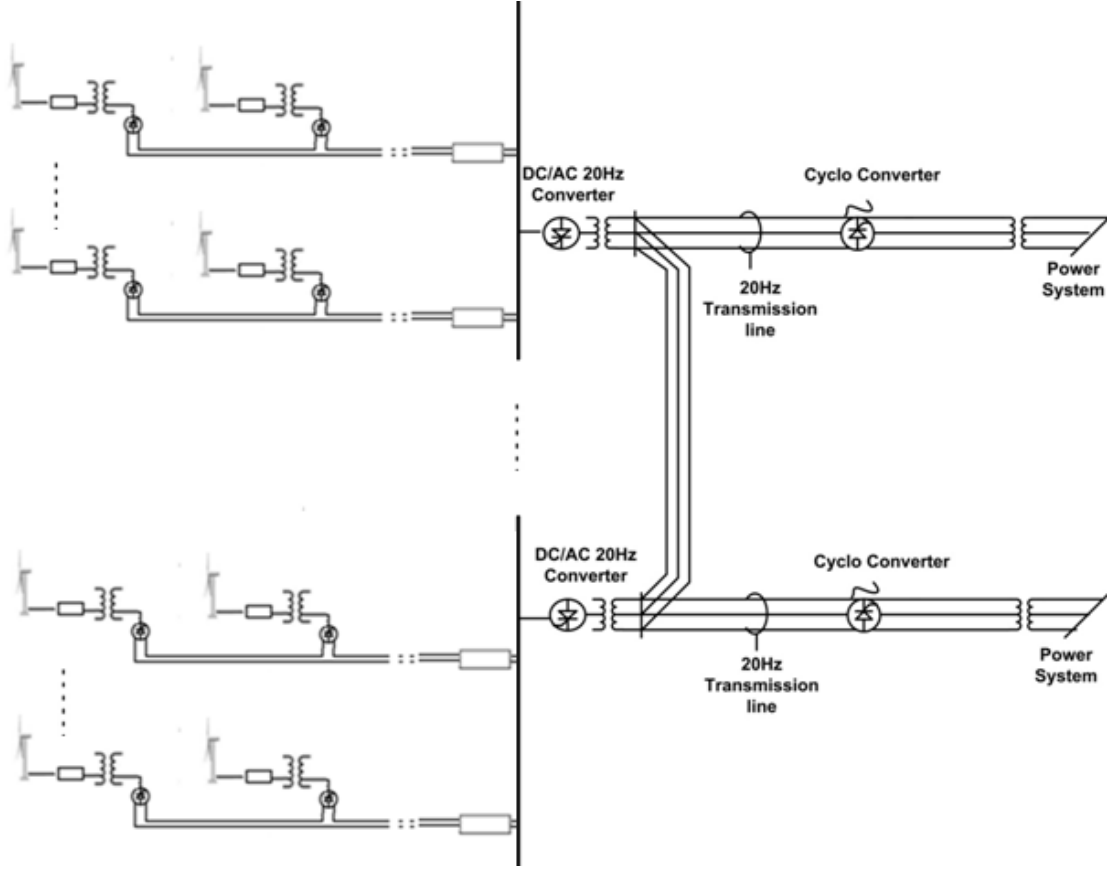


Figure 10.8.1: Wind Farm Configuration 7

The formulation of the reliability analysis for this configuration is as below. The probabilistic methods used for this formulation is exactly the ones shown in the analysis of configuration 1.

### 10.8.1 Probabilistic Model of Circuit $i$

$$P_{line\ i}(Up) = \left[ P_{WT}^{n_i}(up) \cdot P_{sSW}^{n_i}(up) \cdot P_{sST}^{n_i}(up) \cdot P_{sAC/DC}^{n_i}(up) \cdot P_{FDC}^{n_i}(up) \right] \cdot P_{LSW}(up)$$

$$= \left[ \frac{\mu_{WT}}{\lambda_{WT} + \mu_{WT}} \cdot \frac{\mu_{sSW}}{\lambda_{sSW} + \mu_{sSW}} \cdot \frac{\mu_{sT}}{\lambda_{sT} + \mu_{sT}} \cdot \frac{\mu_{sAC/DC}}{\lambda_{sAC/DC} + \mu_{sAC/DC}} \cdot \frac{\mu_{FDC}}{\lambda_{FDC} + \mu_{FDC}} \right]^{n_i} \cdot \frac{\mu_{LSW}}{\lambda_{LSW} + \mu_{LSW}}$$

$$P_{line\ i}(Down) = 1 - P_{line\ i}(Up)$$

$$= 1 - \left[ \frac{\mu_{WT}}{\lambda_{WT} + \mu_{WT}} \cdot \frac{\mu_{sSW}}{\lambda_{sSW} + \mu_{sSW}} \cdot \frac{\mu_{sT}}{\lambda_{sT} + \mu_{sT}} \cdot \frac{\mu_{sAC/DC}}{\lambda_{sAC/DC} + \mu_{sAC/DC}} \cdot \frac{\mu_{FDC}}{\lambda_{FDC} + \mu_{FDC}} \cdot \frac{\mu_{LSW}}{\lambda_{LSW} + \mu_{LSW}} \right]^{n_i} \cdot \frac{\mu_{LSW}}{\lambda_{LSW} + \mu_{LSW}}$$

### 10.8.2 Probabilistic Model of m Parallel Circuits

$$P_{parallel\_jng} = C_m^j \cdot P_{line\ i}^j(up) \cdot P_{line\ i}^{m-j}(down)$$

where  $C_m^j = \frac{m!}{j!(m-j)!}$  is the combinatorial number

### 10.8.3 Probabilistic Model of the Entire Configuration

This configuration has network transmission system. The probability method used to analyze the network is exactly the one to analyze a single branch. Since in the network transmission case, the variables related to the number of wind turbines are more than that of a single branch, by including the number of buses, the number of parallel circuits, and the number of turbines on a single circuit. This variability makes the formulation of the probability of this entire configuration complicated, by involving multiple combinatorial numbers. In this subsection, the single branch case is analyzed to provide the method that is to be used for more complex cases.

When the transmission system contains only one branch, the output states at the point of common coupling (PCC) are similar to the ones in configuration 1. At PCC, there are  $m+1$  states, the delivered capacity of which is similar to that in the analysis of Configuration 1. The 1<sup>st</sup> state represents the situation when there is no capacity successfully delivered.

When  $j \neq 0$ , the probability of the  $(j+1)$ th state, which is the probability of transmitting power of  $j \cdot n \cdot G$ , is:

$$\begin{aligned} P_{system\_jng} &= P_{parallel\_jng} \cdot P(DCB\ up) \cdot P(DC/AC\ up) \cdot P(20T\ up) \cdot P(20AC\ up) \cdot P(Conv\ up) \\ &\quad \cdot P(lT\ up) \\ &= P_{parallel\_jng} \cdot \frac{\mu_{DCB}}{\lambda_{DCB} + \mu_{DCB}} \cdot \frac{\mu_{DC/AC}}{\lambda_{DC/AC} + \mu_{DC/AC}} \cdot \frac{\mu_{20T}}{\lambda_{20T} + \mu_{20T}} \cdot \frac{\mu_{20AC}}{\lambda_{20AC} + \mu_{20AC}} \cdot \frac{\mu_{Conv}}{\lambda_{Conv} + \mu_{Conv}} \cdot \frac{\mu_{lT}}{\lambda_{lT} + \mu_{lT}} \\ &= C_m^j \cdot P_{line\ i}^j(up) \cdot P_{line\ i}^{m-j}(down) \cdot \frac{\mu_{DCB}}{\lambda_{DCB} + \mu_{DCB}} \cdot \frac{\mu_{DC/AC}}{\lambda_{DC/AC} + \mu_{DC/AC}} \cdot \frac{\mu_{20T}}{\lambda_{20T} + \mu_{20T}} \cdot \frac{\mu_{20AC}}{\lambda_{20AC} + \mu_{20AC}} \\ &\quad \cdot \frac{\mu_{Conv}}{\lambda_{Conv} + \mu_{Conv}} \cdot \frac{\mu_{lT}}{\lambda_{lT} + \mu_{lT}} \\ &= \frac{m!}{j!(m-j)!} \cdot \left\{ \left[ \frac{\mu_{WT}}{\lambda_{WT} + \mu_{WT}} \cdot \frac{\mu_{sSw}}{\lambda_{sSw} + \mu_{sSw}} \cdot \frac{\mu_{sT}}{\lambda_{sT} + \mu_{sT}} \cdot \frac{\mu_{sAC/DC}}{\lambda_{sAC/DC} + \mu_{sAC/DC}} \cdot \frac{\mu_{FDC}}{\lambda_{FDC} + \mu_{FDC}} \cdot \frac{\mu_{lSw}}{\lambda_{lSw} + \mu_{lSw}} \right]^{n_i} \cdot \frac{\mu_{lSw}}{\lambda_{lSw} + \mu_{lSw}} \right\}^j \cdot \\ &\quad \left\{ 1 - \left[ \frac{\mu_{WT}}{\lambda_{WT} + \mu_{WT}} \cdot \frac{\mu_{sSw}}{\lambda_{sSw} + \mu_{sSw}} \cdot \frac{\mu_{sT}}{\lambda_{sT} + \mu_{sT}} \cdot \frac{\mu_{sAC/DC}}{\lambda_{sAC/DC} + \mu_{sAC/DC}} \cdot \frac{\mu_{FDC}}{\lambda_{FDC} + \mu_{FDC}} \cdot \frac{\mu_{lSw}}{\lambda_{lSw} + \mu_{lSw}} \right]^{n_i} \cdot \frac{\mu_{lSw}}{\lambda_{lSw} + \mu_{lSw}} \right\}^{m-j} \cdot \frac{\mu_{DCB}}{\lambda_{DCB} + \mu_{DCB}} \cdot \\ &\quad \frac{\mu_{DC/AC}}{\lambda_{DC/AC} + \mu_{DC/AC}} \cdot \frac{\mu_{20T}}{\lambda_{20T} + \mu_{20T}} \cdot \frac{\mu_{20AC}}{\lambda_{20AC} + \mu_{20AC}} \cdot \frac{\mu_{Conv}}{\lambda_{Conv} + \mu_{Conv}} \cdot \frac{\mu_{lT}}{\lambda_{lT} + \mu_{lT}} \end{aligned}$$

This probability is denoted as  $P(j+1)$ , for all  $j \neq 0$ .

When  $j = 0$ , the probability  $P(0+1)=P(1)$  can be calculated as:

$$P(1) = 1 - \sum_{w=1}^m P(w + 1)$$

#### 10.8.4 Expected Generated Wind Energy (EGWE)

The total expected available energy at point of common coupling is the index of EGWE:

$$\begin{aligned} EGWE &= \left[ \sum_{i=1}^m n_i \cdot G \cdot P_{line\ i}(up) \right] \cdot P(DCB\ up) \cdot P(DC/AC\ up) \cdot P(20T\ up) \cdot P(20AC\ up) \cdot P(Conv\ up) \\ &\quad \cdot P(lT\ up) + 0 \\ &= \left[ \sum_{i=1}^m n_i \cdot G \cdot P_{line\ i}(up) \right] \cdot P(DCB\ up) \cdot P(DC/AC\ up) \cdot P(20T\ up) \cdot P(20AC\ up) \cdot P(Conv\ up) \\ &\quad \cdot P(lT\ up) \\ &= \left( \sum_{i=1}^m \{ n_i \cdot G \cdot \left[ \frac{\mu_{WT}}{\lambda_{WT} + \mu_{WT}} \cdot \frac{\mu_{sSw}}{\lambda_{sSw} + \mu_{sSw}} \cdot \frac{\mu_{sT}}{\lambda_{sT} + \mu_{sT}} \cdot \frac{\mu_{sAC/DC}}{\lambda_{sAC/DC} + \mu_{sAC/DC}} \cdot \frac{\mu_{FDC}}{\lambda_{FDC} + \mu_{FDC}} \right]^{n_i} \cdot \frac{\mu_{lSw}}{\lambda_{lSw} + \mu_{lSw}} \} \right) \cdot \\ &\quad \frac{\mu_{DCB}}{\lambda_{DCB} + \mu_{DCB}} \cdot \frac{\mu_{DC/AC}}{\lambda_{DC/AC} + \mu_{DC/AC}} \cdot \frac{\mu_{20T}}{\lambda_{20T} + \mu_{20T}} \cdot \frac{\mu_{20AC}}{\lambda_{20AC} + \mu_{20AC}} \cdot \frac{\mu_{Conv}}{\lambda_{Conv} + \mu_{Conv}} \cdot \frac{\mu_{lT}}{\lambda_{lT} + \mu_{lT}} \end{aligned}$$

#### 10.8.5 Case Study

A 30 turbine case is also studied for configuration 7. The parameters of the connection in the configuration are:

- 1) m=3, which means there are 3 parallel lines;
- 2) n=10, which means there are 10 turbines in each line.

The formulation of the calculation is as below.

$$\begin{aligned} GWE &= \left[ \sum_{i=1}^m n_i \cdot G \cdot P_{line\ i}(up) \right] \cdot P(DCB\ up) \cdot P(DC/AC\ up) \cdot P(20T\ up) \cdot P(20AC\ up) \cdot P(Conv\ up) \\ &\quad \cdot P(lT\ up) + 0 \\ &= \left[ \sum_{i=1}^m n_i \cdot G \cdot P_{line\ i}(up) \right] \cdot P(DCB\ up) \cdot P(DC/AC\ up) \cdot P(20T\ up) \cdot P(20AC\ up) \cdot P(Conv\ up) \\ &\quad \cdot P(lT\ up) \end{aligned}$$

$$= \left( \sum_{i=1}^m \{n_i \cdot G \cdot \left[ \frac{\mu_{WT}}{\lambda_{WT} + \mu_{WT}} \cdot \frac{\mu_{sSw}}{\lambda_{sSw} + \mu_{sSw}} \cdot \frac{\mu_{sT}}{\lambda_{sT} + \mu_{sT}} \cdot \frac{\mu_{sAC}}{\lambda_{sAC} + \mu_{sAC}} \cdot \frac{\mu_{FDC}}{\lambda_{FDC} + \mu_{FDC}} \right]^{n_i} \cdot \frac{\mu_{lSw}}{\lambda_{lSw} + \mu_{lSw}} \} \right) \cdot \frac{\mu_{DCB}}{\lambda_{DCB} + \mu_{DCB}} \cdot \frac{\mu_{DC}}{\lambda_{DC} + \mu_{DC}} \cdot \frac{\mu_{20T}}{\lambda_{20T} + \mu_{20T}} \cdot \frac{\mu_{20AC}}{\lambda_{20AC} + \mu_{20AC}} \cdot \frac{\mu_{Conv}}{\lambda_{Conv} + \mu_{Conv}} \cdot \frac{\mu_{lT}}{\lambda_{lT} + \mu_{lT}}$$

$$= 22.088G$$

$$IWP = 30 \cdot G = 60 \text{ MW}$$

$$IWE = 30 \cdot G \cdot t = 60 \text{ MW} \cdot t = 60 \text{ MWh in an hour.}$$

In full capacity case,

$$EGWE = 44.17 \text{ MWh in an hour}$$

$$EAW = 60 \text{ MWh in an hour}$$

$$CF = \frac{EGWE}{IWE} = \frac{44.17}{60} = 0.7362$$

$$GR = \frac{\frac{EGWE}{t}}{IWP} = \frac{44.17}{60} = 73.62\%$$

In wind speed variation case,

$$EGWE = 20.54 \text{ MWh in an hour}$$

$$EAW = 27.9 \text{ MWh in an hour}$$

$$CF = \frac{EGWE}{IWE} = 0.342$$

$$GR = \frac{\frac{EGWE}{t}}{IWP} = \frac{22.42}{60} = 34.2\%$$

The results of the reliability analysis for alternate configuration 7 are summarized in Table 10.8.1.

Table 10.8.1: Summary of Reliability Indices for Alternate Configuration 7

<i>Reliability Index</i>	<i>Computed Value</i>
Installed Wind Power (IWP)	60 MW
Installed Wind Energy (IWE)	60 MWh in one hour
Expected Available Wind Energy (EAWE)	27.9 MWh in one hour
Expected Generated Wind Energy (EGWE)	20.54MWh in one hour
Capacity Factor (CF)	0.342
Generation Ratio (GR)	34.2%

### 10.9 Reliability Analysis of Wind Farm Configuration 8

This section provides the reliability analysis and case study result for configuration 8.

Figure 10.9.1 gives out configuration 8. Configuration 8 has DC Parallel Wind Farm, LFAC Transmission (multiple branches).

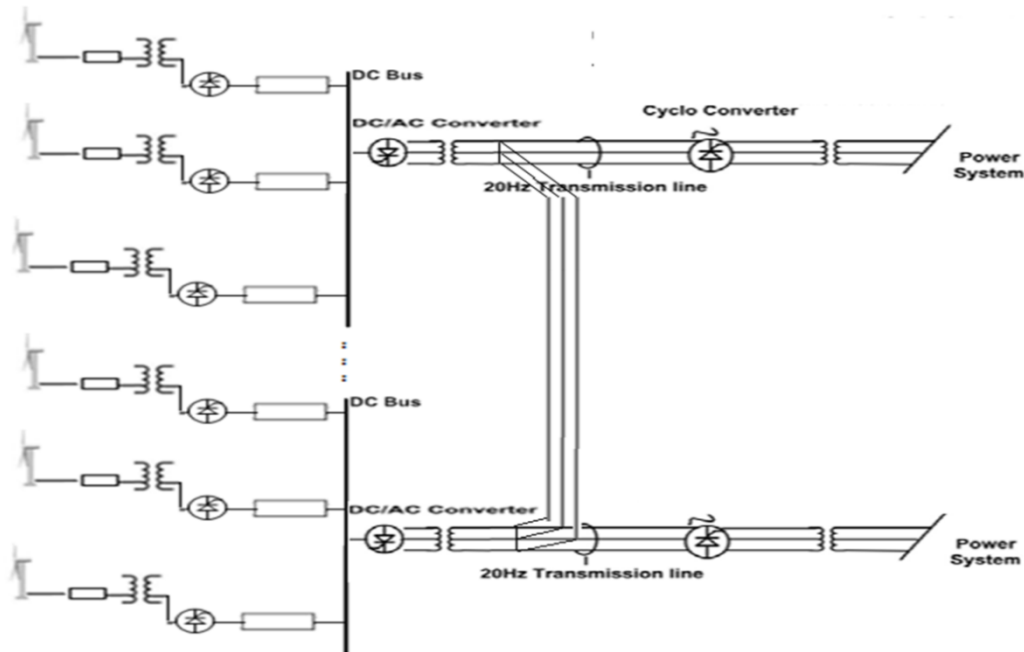


Figure 10.9.1: Wind Farm Configuration 8

The formulation of the reliability analysis for this configuration is as below. The probabilistic methods used for this formulation is exactly the ones shown in the analysis of configuration 1.

### 10.9.1 Probabilistic Model of Circuit $i$

The probabilities of the states of the  $i$ th circuit are provided.

$$P_{line\ i}(Up) = P(WT\ up) \cdot P(sSw\ up) \cdot P(sT\ up) \cdot P(sAC/DC\ up) \cdot P(FDC\ up) \cdot P_{lSw}(up)$$

$$= \frac{\mu_{WT}}{\lambda_{WT} + \mu_{WT}} \cdot \frac{\mu_{sSw}}{\lambda_{sSw} + \mu_{sSw}} \cdot \frac{\mu_{sT}}{\lambda_{sT} + \mu_{sT}} \cdot \frac{\mu_{sAC/DC}}{\lambda_{sAC/DC} + \mu_{sAC/DC}} \cdot \frac{\mu_{FDC}}{\lambda_{FDC} + \mu_{FDC}} \cdot \frac{\mu_{lSw}}{\lambda_{lSw} + \mu_{lSw}}$$

$$P_{line\ i}(Down) = 1 - P_{line\ i}(Up)$$

$$= 1 - \frac{\mu_{WT}}{\lambda_{WT} + \mu_{WT}} \cdot \frac{\mu_{sSw}}{\lambda_{sSw} + \mu_{sSw}} \cdot \frac{\mu_{sT}}{\lambda_{sT} + \mu_{sT}} \cdot \frac{\mu_{sAC/DC}}{\lambda_{sAC/DC} + \mu_{sAC/DC}} \cdot \frac{\mu_{FDC}}{\lambda_{FDC} + \mu_{FDC}} \cdot \frac{\mu_{lSw}}{\lambda_{lSw} + \mu_{lSw}}$$

### 10.9.2 Probabilistic Model of $m$ Parallel Circuits

$$P_{parallel\_jng} = C_{mn}^j \cdot P_{line\ i}^j(up) \cdot P_{line\ i}^{mn-j}(down)$$

where  $C_{mn}^j = \frac{mn!}{j!(mn-j)!}$  is the combinatorial number

### 10.9.3 Probabilistic Model of the Entire Configuration

The configuration contains  $m$  buses and each bus contains  $n$  wind turbines. This case is more complicated so that some assumptions need to be made. Firstly, a single AC transmission line is supposed to be able to transmit the whole capacity. Therefore, the power reaches the transmission line can be derived to the power system unless all of the transmission lines are broken down.

The probability of at least one transmission line works is

$$P_{Tran} = 1 - (1 - P(20AC\ up) \cdot P(Conv\ up) \cdot P(lT\ up))^m$$

The probability of the DC bus, converter and 20Hz transformer will work is

$$P_{DC\_Con\_T} = P(DCB\ up) \cdot P(Conv\ up) \cdot P(20T\ up)$$

$$P_{DCT}(down) = 1 - P(DCB\ up) \cdot P(Conv\ up) \cdot P(20T\ up)$$

For the convenience of computation, the probability of the internal transmission line that can deliver the power to transmission line is

$$P_{Intel20}(up) = \frac{\mu_{Inter20}}{\lambda_{Inter20} + \mu_{Inter20}}$$

So the probability of the right part of this configuration will work is

$$P_{right} = P_{Tran}(up) \cdot P_{Intel}(up)$$

For  $0 < j \leq n$

$$P_{\text{system\_inG}} = P_{\text{right}} \cdot [C_m^m \cdot P_{DCT}^m(\text{up}) \cdot C_{mn}^j \cdot P_{\text{line } i}^j(\text{up}) \cdot P_{\text{line } i}^{mn-j}(\text{down}) \\ + C_m^{m-1} \cdot P_{DCT}^{m-1}(\text{up}) \cdot P_{DCT}^1(\text{down}) \cdot C_{(m-1)n}^j \cdot P_{\text{line } i}^j(\text{up}) \cdot P_{\text{line } i}^{mn-j}(\text{down}) \\ + \dots + C_m^1 \cdot P_{DCT}^1(\text{up}) \cdot P_{DCT}^{m-1}(\text{down}) \cdot C_n^j \cdot P_{\text{line } i}^j(\text{up}) \cdot P_{\text{line } i}^{mn-j}(\text{down})]$$

For  $n < j \leq n + n$

For  $(m-1)n < j \leq mn$

$$P_{\text{system\_inG}} = P_{\text{right}} \cdot [C_m^m \cdot P_{DCT}^m(\text{up}) \cdot C_{mn}^j \cdot P_{\text{line } i}^j(\text{up}) \cdot P_{\text{line } i}^{mn-j}(\text{down})]$$

#### 10.9.4 Expected Generated Wind Energy (EGWE)

$$EGWE = \sum_{i=1}^{\text{number of states}} G_i \cdot P(i)$$

For the general case, each of the  $mn$  parallel circuits has two states: (a) either transmitting full capacity or (b) 0. For line  $i$ , the expected transmitted capacity to the collector AC bus is:

$$EGWE = mn * G \cdot P_{\text{line } i}(\text{up}) \cdot P(DCT \text{ up}) \cdot P(\text{right up}) + 0$$

$$= mn * G \cdot P_{\text{line } i}(\text{up}) \cdot P(DCB \text{ up}) \cdot P(Conv \text{ up}) \cdot P(T \text{ up}) \cdot P_{\text{Inter20}}(\text{up}) \cdot [1 - (1 - P(20AC \text{ up}) \cdot P(Conv \text{ up}) \cdot P(IT \text{ up}))^m]$$

$$= mn \cdot G \cdot \frac{\mu_{WT}}{\lambda_{WT} + \mu_{WT}} \cdot \frac{\mu_{SSW}}{\lambda_{SSW} + \mu_{SSW}} \cdot \frac{\mu_{ST}}{\lambda_{ST} + \mu_{ST}} \cdot \frac{\mu_{SAC/DC}}{\lambda_{SAC/DC} + \mu_{SAC/DC}} \cdot \frac{\mu_{FDC}}{\lambda_{FDC} + \mu_{FDC}} \cdot \frac{\mu_{LSW}}{\lambda_{LSW} + \mu_{LSW}} \\ \cdot \frac{\mu_{DCB}}{\lambda_{DCB} + \mu_{DCB}} \cdot \frac{\mu_{DC/AC}}{\lambda_{DC/AC} + \mu_{DC/AC}} \cdot \frac{\mu_{20T}}{\lambda_{20T} + \mu_{20T}} \cdot \frac{\mu_{Inter20}}{\lambda_{Inter20} + \mu_{Inter20}} \\ \cdot \left[ 1 - \left( 1 - \frac{\mu_{20AC}}{\lambda_{20AC} + \mu_{20AC}} \cdot \frac{\mu_{Conv}}{\lambda_{Conv} + \mu_{Conv}} \cdot \frac{\mu_{IT}}{\lambda_{IT} + \mu_{IT}} \right)^m \right]$$

#### 10.9.5 Case Study

A 30 turbine case is also studied for configuration 8. The parameters of the connection in the configuration are:

- 1)  $m=3$ , which means there are 3 parallel lines;
- 2)  $n=10$ , which means there are 10 turbines in each line.

The formulation of the calculation is as below.

$$EGWE = mn * G \cdot P_{\text{line } i}(\text{up}) \cdot P(DCT \text{ up}) \cdot P(\text{right up}) + 0$$

$$\begin{aligned}
&= mn * G \cdot P_{line i}(up) \cdot P(DCB up) \cdot P(Conv up) \cdot P(T up) \cdot P_{Intel20}(up) \cdot [1 - (1 - \\
&P(20AC up) \cdot P(Conv up) \cdot P(IT up))^m] \\
&= mn \cdot G \cdot \frac{\mu_{WT}}{\lambda_{WT} + \mu_{WT}} \cdot \frac{\mu_{sSw}}{\lambda_{sSw} + \mu_{sSw}} \cdot \frac{\mu_{sT}}{\lambda_{sT} + \mu_{sT}} \cdot \frac{\frac{\mu_{sAC}}{DC}}{\lambda_{sAC} + \frac{\mu_{sAC}}{DC}} \cdot \frac{\mu_{FDC}}{\lambda_{FDC} + \mu_{FDC}} \cdot \frac{\mu_{lSw}}{\lambda_{lSw} + \mu_{lSw}} \cdot \frac{\mu_{DCB}}{\lambda_{DCB} + \mu_{DCB}} \cdot \frac{\frac{\mu_{DC}}{AC}}{\lambda_{DC} + \frac{\mu_{DC}}{AC}} \cdot \\
&\frac{\mu_{20T}}{\lambda_{20T} + \mu_{20T}} \cdot \frac{\mu_{Inter20}}{\lambda_{Inter20} + \mu_{Inter20}} \cdot \left[ 1 - \left( 1 - \frac{\mu_{20AC}}{\lambda_{20AC} + \mu_{20AC}} \cdot \frac{\mu_{Conv}}{\lambda_{Conv} + \mu_{Conv}} \cdot \frac{\mu_{IT}}{\lambda_{IT} + \mu_{IT}} \right)^m \right] \\
&= 28.2625G
\end{aligned}$$

$$IWP = 30 \cdot G = 60 \text{ MW}$$

$$IWE = 30 \cdot G \cdot t = 60 \text{ MW} \cdot t = 60 \text{ MWh in an hour.}$$

In full capacity case,

$$EGWE = 56.53 \text{ MWh in an hour}$$

$$EAW = 60 \text{ MWh in an hour}$$

$$CF = \frac{EGWE}{IWE} = \frac{56.53}{60} = 0.942$$

$$GR = \frac{\frac{EGWE}{t}}{IWP} = \frac{56.53}{60} = 94.2\%$$

In wind speed variation case,

$$EGWE = 26.27 \text{ MWh in an hour}$$

$$EAW = 27.9 \text{ MWh in an hour}$$

$$CF = \frac{EGWE}{IWE} = 0.438$$

$$GR = \frac{\frac{EGWE}{t}}{IWP} = \frac{22.42}{60} = 43.8\%$$

The results of the reliability analysis for alternate configuration 8 are summarized in Table 10.9.1.



Table 10.9.1: Summary of Reliability Indices for Alternate Configuration 8

<i>Reliability Index</i>	<i>Computed Value</i>
Installed Wind Power (IWP)	60 MW
Installed Wind Energy (IWE)	60 MWh in one hour
Expected Available Wind Energy (EAWE)	27.9 MWh in one hour
Expected Generated Wind Energy (EGWE)	26.27MWh in one hour
Capacity Factor (CF)	0.438
Generation Ratio (GR)	43.8%

## 10.10 Summary and Conclusions

Section 10 provides the general reliability analysis methods for the configurations listed in Section 4. For each configuration, a specific modeling and analyzing process has been shown in a subsection, as provided above from Subsection 10.2 to Subsection 10.9. A 30 wind turbine case study is performed after the analysis of every configuration. The calculation results have been provided and compared. Table 10.8.1 provides the summary of the essential reliability indices results from the case studies of the 8 configurations.

Table 10.10.1: Summary of Reliability Indices for the 8 Alternate Configurations

Configuration	EGWE	IWP	CF
1	22.98	60	0.383
2	22.42	60	0.374
3	20.82	60	0.347
4	26.22	60	0.437
5	12.31	60	0.205
6	25.86	60	0.431
7	20.54	60	0.342
8	26.27	60	0.438

It can be understood that the decision of alternate wind farm or transmission technology selection is not completely based on the reliability analysis, but these results are of significant value as the assessment criteria.

## 11 Conclusions

Alternative transmission systems from remote wind farms to the main power grid using low-frequency AC (LFAC) technology are evaluated in this report and compared when appropriate to conventional AC transmission systems and DC transmission systems. The performance of LFAC is assessed from several points of view, *i.e.* total cost, reliability, power transfer capability, transient stability and electromagnetic transient performance. A methodology has been also developed for selection of optimal kV level, equipment rating and in general design of specific wind farms and transmission.

The methodologies have been demonstrated for the three different selections of transmission systems for connecting remote wind farms to the main power grid. Specifically, eight alternative configurations have been defined that incorporate the three transmission options (conventional AC, DC transmission and low frequency AC transmission). Each one of these configurations were analyzed with the listed criteria and the example results have been provided in the report. While the results are applicable to the example systems selected, the methodology is applicable to any specific site and can be utilized in the design procedure for these systems.

The results indicate that low frequency AC transmission has economic and performance advantages over conventional AC and DC transmission when the transmission distance is above 50 miles. Low frequency AC systems have greater power transfer performance, lower cost and high reliability. The related issue of existing technology for the easy implementation of low frequency AC transmission systems and wind generation at 20Hz/16.66Hz is quite achievable since these technologies already exist.

Wind energy is the most rapidly developing generating systems from all renewable resources and the forecast is that they may be forming a large percentage of the generation system. For this reason their performance is of paramount importance to the reliability of the power system of the near and far future. The models developed in this research project can be utilized to study other very important operational characteristics and capabilities of this system.

One main concern is that as the percentage of wind generating systems become very large (even 100% in some systems) what will be the operational challenges of these new systems from the stability, control, operation and protection point of view. For example since these systems can almost instantaneously (within a cycle) control voltage and frequency the traditional control schemes may not work for these systems since now frequency does not provide the same information (transient response of the system, frequency response, etc.). New paradigms must be developed for the control of systems with very large penetration of wind generation. In addition these systems limit fault currents. This property renders the present protection schemes, that depend on high separation between fault currents and load currents, ineffective. New protection paradigms and algorithms must be developed for these systems. Another important area is the behavior of these systems during faults. This has been recognized and new requirements have been formulated regarding the response of these systems during faults under the names, zero voltage ride through capability or disturbance ride through

capability. This capability should be integrated with the other issues that we have discussed earlier.

## References

1. X. Wang, H. Dai, and R. J. Thomas, "Reliability modeling of large wind farms and electric utility interface systems" *IEEE Transactions on Power Apparatus and Systems*, Vol. 103, no. 3, March, 1984, pp. 569-575.
2. Thomas, R.J., Phadke, A.G., Pottle, C, "Operational Characteristics of A Large Wind-Farm Utility- System with A Controllable AC/DC/AC Interface" *IEEE Transactions on Power Systems*, Vol. 3, No.1. February 1988.
3. An-Jen Shi, Thorp J., Thomas R., "An AC/DC/AC Interface Control Strategy to Improve Wind Energy Economics", *IEEE Transactions on Power Apparatus and Systems*, Vol. PAS-104, No. 12. December 1985.
4. T. Funaki, "Feasibility of the low frequency AC transmission," in *Proc. IEEE PES Winter Meeting*, Vol. 4, pp. 2693–2698, 2000.
5. W. Xifan, C. Chengjun, and Z. Zhichao, "Experiment on fractional frequency transmission system," *IEEE Trans. Power Syst.*, Vol. 21, No. 1, pp. 372–377, Feb. 2006.
6. N. Qin, S. You, Z. Xu, and V. Akhmatov, "Offshore wind farm connection with low frequency AC transmission technology," in *Proc. IEEE PES General Meeting*, Calgary, Alberta, Canada, 2009.
7. S. Lundberg, "Evaluation of wind farm layouts," in *Nordic Workshop on Power and Industrial Electronics (NORPIE 2004)*, Trondheim, Norway, 14-16 June, 2004.
8. S. Meier and P. C. Kjær, "Benchmark of Annual Energy Production for Different Wind Farm Topologies," in *Proc. 36th Annual Power Electronics Specialists Conference*, PESC '2005, Recife, Brazil, June 2005.
9. K. Macken, L. Driesen, and R. Belmans, "A DC bus system for connecting offshore wind turbines with the utility system," in *European Wind Energy Conference 2001*, Copenhagen, Denmark, 2-6 July 2001, pp. 1030 – 1035.
10. T. Ackermann, "Transmission systems for offshore wind farms," *Power Engineering Review, IEEE*, vol. 22, no. 12, pp. 23-27, Dec. 2002.
11. M. Hausler and F. Owman, "AC or DC for connecting offshore wind farms to the transmission grid?" in *Third International Workshop on Transmission Networks for Offshore Wind Farms*, Stockholm, Sweden, 11-12 April, 2002.
12. N. Kirby, L. Xu, M. Lockett, and W. Siepmann, "HVDC transmission for large offshore wind farms," *Power Engineering Journal*, vol. 16, no. 3, pp. 135 –141, June 2003.

13. O. Martander and J. Svensson, "Connecting offshore wind farms using DC cables," in *Wind Power for the 21st Century*, Kassel, Germany, 25-27 September 2000.
14. T. Schutte, M. Strom, and B. Gustavsson, "The use of low frequency AC for offshore wind power," in *Second International Workshop on Transmission Networks for Offshore Wind Farms*, Stockholm, Sweden, 30-31 March, 2001.
15. W. Siepmann, "AC transmission technology for offshore wind farms," in *Second International Workshop on Transmission Networks for Offshore Wind Farms*, Stockholm, Sweden, 30-31 March, 2001.
16. P. Bauer, S. de Haan, C. Meyl, and J. Pierik, "Evaluation of electrical systems for offshore windfarms," in *IEEE Industry Applications Conference 2000*, 8-12 Oct. 2000, pp. 1416 –1423 vol.3.
17. O. Martander and J. Svensson, "Connecting offshore wind farms using DC cables," in *Wind Power for the 21st Century*, Kassel, Germany, 25-27 September 2000.
18. F. Santjer, L.-H. Sobeck, and G. Gerdes, "Influence of the electrical design of offshore wind farms and of transmission lines on efficiency," in *Second International Workshop on Transmission Networks for Offshore Wind Farms*, Stockholm, Sweden, 30-31 March, 2001.
19. K. Smith and G. Hagerman, "The potential for offshore wind energy development in the United States," in *Second International Workshop on Transmission Networks for Offshore Wind Farms*, Stockholm, Sweden, 30-31 March, 2001.
20. M. Häusler and F. Owman, "AC or DC for connecting offshore wind farms to the transmission grid?" in *Third International Workshop on Transmission Networks for Offshore Wind Farms*, Stockholm, Sweden, 11-12 April, 2002.
21. C. Skaug and C. Stranne, "HVDC wind park configuration study," Diploma thesis, Chalmers University of Technology, Department of Electric Power Engineering, Göteborg, Sweden, October 1999.
22. R. Barthelmie and S. Pryor, "A review of the economics of offshore wind farms," *Wind engineering*, vol. 25, no. 3, pp. 203–213, 2001.
23. J. Svenson and F. Olsen, "Cost optimizing of large-scale offshore wind farms in the danish waters," in *1999 European Wind Energy Conference*, Nice, France, 1-5 March, 1999, pp. 294–299.
24. M. Zubiaga, G. Abad, J.A. Barrena, S. Aurtenetxea, A. Cárcar, "Evaluation and selection of AC transmission lay-outs for large offshore wind farms", *Power Electronics and Applications*, 2009. *EPE '09*, 8-10 Sept. 2009, pp. 1 – 8.
25. S. Lundberg, "Wind farm configuration and energy efficiency studies series DC versus AC layouts," Thesis, Chalmers University of Technology 2006.

26. A. Lazaros P. Lazaridis, "Economic comparison of HVAC and HVDC solutions for large offshore wind farms under special consideration of reliability," Thesis, KTH.
27. S. Dobakhshari, M. Fotuhi-Firuzabad, "A Reliability Model of Large Wind Farms for Power System Adequacy Studies," *IEEE Transactions on Energy Conversion*, vol. 24, no. 3, pp. 792-801, 2009.
28. IEEE Gold Book, *IEEE Recommended Practice for the Design of Reliable Industrial and Commercial Power Systems*, 1997
29. S. Lundberg, "Evaluation of wind farm layouts," in *Nordic Workshop on Power and Ind. Electron.*, Trondheim, Norway, Jun. 2004.
30. B. K. Bose, *Modern Power Electronics and AC Drives*. New Jersey: Prentice Hall, 2002.
31. J. Arrillaga, Y. H. Liu, and N. R. Watson, *Flexible Power Transmission: The HVDC Options*. Hoboken, NJ: Wiley, 2007.
32. B. Wu, *High-Power Converters and AC Drives*. Hoboken, NJ: Wiley, 2006.
33. P. C. Krause, O. Wasynczuk, and S. D. Sudhoff, *Analysis of Electric Machinery and Drive Systems*, 2nd ed. IEEE Press, 2002.
34. B. R. Pelly, *Thyristor Phase-Controlled Converters and Cycloconverters*. New York: Wiley, 1971.
35. A. R. Bergen and V. Vittal, *Power System Analysis*, 2nd edition. New Jersey: Prentice Hall, 2000.
36. J. Arrillaga and N. R. Watson, *Power System Harmonics*, 2nd edition. Hoboken, NJ: Wiley, 2003.
37. XLPE Land Cable Systems User's Guide. [Online]. Available: <http://www.abb.com>
38. XLPE Submarine Cable Systems. [Online]. Available: <http://www.abb.com>.
39. "2010 offshore development information statement," National Grid, Tech. Rep., Sep. 2008. [Online]. Available: <http://www.nationalgrid.com/uk/Electricity/ODIS/Archive/>
40. L. Freris and D. Infield, *Renewable Energy in Power Systems*. Wiley, 2008.
41. P. Bresesti, W. L. Kling, R. L. Hendriks, and R. Vailati, "HVDC connection of offshore wind farms to the transmission system," *IEEE Trans. Energy Convers.*, vol. 22, no. 1, pp. 37-43, Mar. 2007.
42. PLECS User Manual. [Online]. Available: <http://www.plexim.com/downloads/>
43. \_\_ "Available Transfer Capability Definitions and Determination," North Amer. Elect. Rel. Council, Princeton, NJ, June 1996
44. R. Pelly, "Cycloconverter Circuits," in *Thyristor Phase-Controlled Converters and Cycloconverters*, New York: Wiley, 1971

45. P. Kundur, J. Paserba, V. Ajarapu, G. Andersson, etc., "Definition and Classification of Power System Stability" *IEEE Transactions on Power Systems*, Vol. 19, no. 2, May, 2004, pp 1387 - 1401.
46. A. P. Meliopoulos, G. J. Cokkinides, and G. K. Stefopoulos, "Voltage stability and voltage recovery: Effects of electric load dynamics," *presented at the 2006 IEEE International Symposium on Circuits and Systems*, Island of Kos, Greece, May 21-24, 2006.
47. Kundur P, Paserba J, Ajarapu V, et al. Definition and classification of power system stability. *IEEE Trans on Power Systems*, 2004, 19(3): 1387-1401.
48. S. M. Mueen, *et al.*, "Low Voltage Ride-Through Capability Enhancement of Wind Turbine Generator System during Network Disturbance," *Renewable Power Generation*, Vol. 3, No. 1, 2009, pp. 65-74.
49. J. Pontt, J. Rodriguez, E. Caceres, E. Illanes, and C. Silva, "cycloconverter Drive System for Fault Diagnosis Study: Real Time Model, Simulation and Construction," *in Proceedings of Power Electronics Specialists*
50. N. Mohan, M. Undeland, and W. Robbins, "Snubber Circuits" *in Power Electronics*, 3th ed. New York: Wiley, 1995, pp. 668–670.
51. M. Malinowski and M. P. Kazmierkowski, "Direct power control of three-phase PWM rectifier using space vector modulation—Simulation study," *in Proc. IEEE Int. Symp. Ind. Electron. ISIE 2002*, vol. 4, 2002, pp. 1114–1118.
52. Y. Tang and L. Xu, "A flexible active and reactive power control strategy for a variable speed constant frequency generating system," *Proc. Conf. Rec. IEEE/IAS Annu. Meeting*, pp. 568–573, 1993.
53. L. Xiao, S. Huang, T. Liu, Q. Xu, and K. Huang, "A novel SVM-DPC control method for Grid Connected AC-DC Converters under Asymmetrical Fault," *Power Engineering, Energy and Electrical Drives (POWERENG), 2011 International Conference on*, pp.1 – 6, May 2011.
54. L. Xu and P. Cartwright, "Direct active and reactive power control of DFIG for wind energy generation," *IEEE Trans. Energy Convers.*, vol. 21, no. 3, pp. 750–758, Sep. 2006.
55. S. Bozhko, R. V. Blasco-Gimenez, R. Li, J. Clare, and G. Asher, "Control of offshore DFIG-based wind farm grid with line-commutated HVDC connection," *IEEE Trans. Energy Convers.*, vol. 22, no. 1, pp. 71–78, Mar. 2007.
56. D. Xiang, L. Ran, J. R. Bumby, P. J. Tavner, and S. Yang, "Coordinated control of an HVDC link and doubly fed induction generators in a large offshore wind farm," *IEEE Trans. Power Del.*, vol. 21, no. 1, pp. 463–471, Jan. 2006.
57. Wu, Bin, *High-Power Converters and AC Drives*, IEEE Press, USA, 2006

58. F. Blaabjerg and Z. Chen, *Power Electronics for Modern Wind Turbines*, 1st edition. USA: Morgan & Claypool, 2006.
59. A. Meliopoulos, G. Cokkinides, and G. Stefopoulos, "Quadratic integration method," in *Proceedings of the 2005 International Power System Transients Conference (IPST 2005)*. Citeseer, pp. 19–23.
60. M. Roitman and P. Diniz, "Simulation of Nonlinear and Switching Elements for Transient Analysis Based on Wave Digital Filters," *IEEE Power Engineering Review*, vol. 17, no. 13, pp. 72–72, 1996.

## Appendix A: Nomenclature

---

<b>A</b>	ACF	Algebraic companion form
	ACB	Alternating Current Bus
<b>B</b>	BESS	Battery energy storage system
<b>C</b>	CF	Capacity Factor
	Conv	Converter
<b>D</b>	DFIG	Doubly-fed induction generator
	DSP	Digital signal processor
	DPC	Direct power control
	DPC-SVM	Direct power control-space vector modulation
	DCB	Direct Current Bus
<b>E</b>	EMTP	Electro-Magnetic Transients Program
	EAWWE	Expected Available Wind Energy
	EGWE	Expected Generated Wind Energy
<b>F</b>	FDC	In-Farm DC Transmission
<b>G</b>	GSC	grid-side converter
	GR	Generation Ratio
<b>H</b>	HVDC	High-voltage direct-current
	HVRT	high-voltage ride through
<b>K</b>	kVdc	DC-voltage level
<b>L</b>	LFAC	Low-frequency alternating-current
	LVRT	Low voltage ride through
	IT	Large Transformer
	ISw	Large Switch
	l AC/DC	Large AC/DC Converter
<b>M</b>	MPTC	Maximum power transfer capability
	MSC	Machine-side converter
<b>N</b>	NERC	North American Electric Reliability Corporation
<b>P</b>	PCC	Point of common connection
	PWM	Pulse-width modulation
	PMSG	Permanent-magnet synchronous generator



	PI controller	Proportional-integral controller
<b>R</b>	RSC	Rotor side converter
<b>S</b>	SG	Synchronous generator
	SSC	Stator-side converter
	SVM	Space vector modulation
	Sw	Switch
	sSw	Small Switch
	sT	Small Transformer
	s AC/DC	Small AC/DC Converter
<b>T</b>	THD	Total harmonic distortion
<b>V</b>	VSC	Voltage source converter
	VRT	Voltage ride through
<b>W</b>	WTG	Wind-turbine generator
	WT	Wind Turbine
<b>Num.</b>	20T	20Hz Transformer
	20AC	20Hz AC Transmission Line

## Appendix B: Example Wind Farm Model

This Appendix presents the organization and a substation of the future that serves a wind farm. We discuss the organization and the functions of this case. Generally, wind farm systems consist of wind-turbine generators (WTGs), a local wind-turbine grid, a point of common connection (PCC), and transmission systems as shown in Figure B.1.

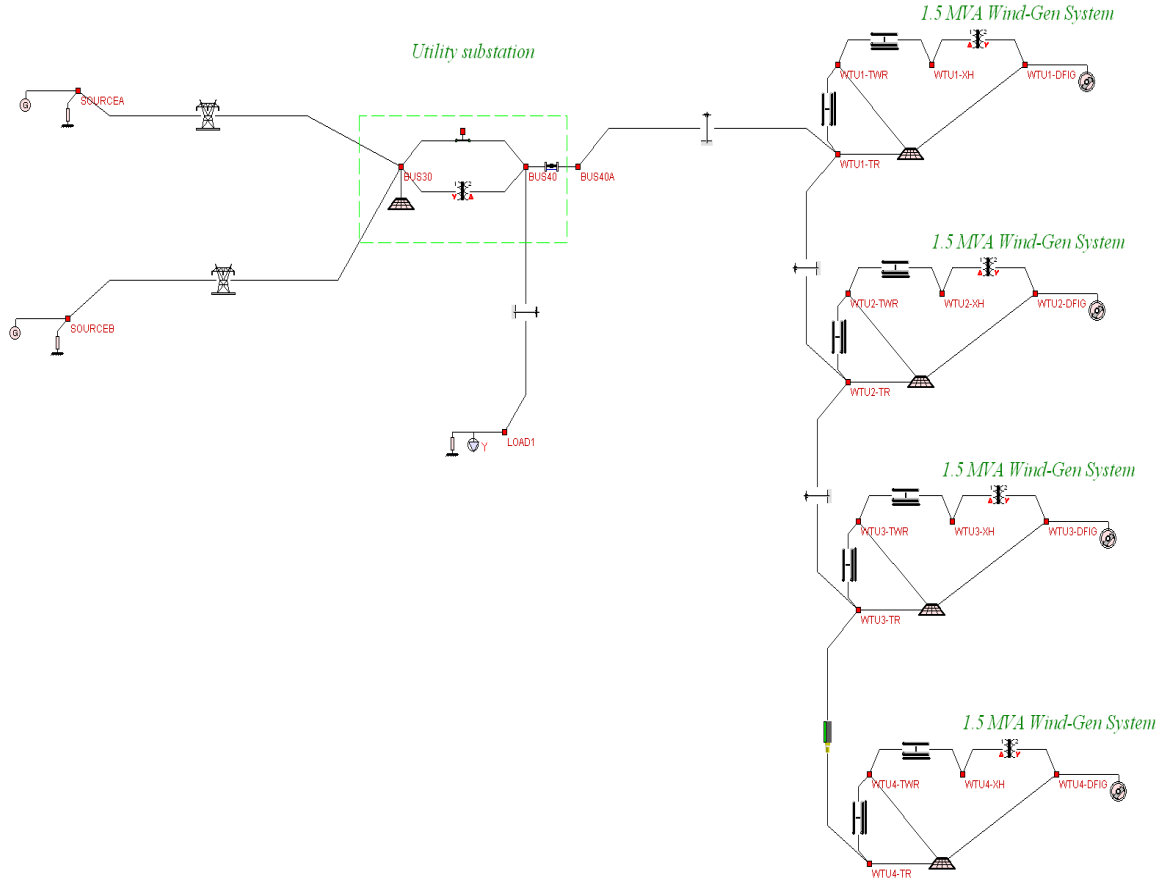


Figure B.1: Example Wind Farm Configuration

Wind turbines capture and convert the fluctuating and randomly varying wind energy into mechanical energy. To capture certain energy without mechanical damage from high wind speed, it is important to control and limit the rotor blades. Since wind turbines have their own operating ranges, rotor blades should be controlled in certain safe operating ranges using pitch control and stall control. The stall control regulates the pitch angle of blades and the pitch control turned rotor blades out from high speed wind [58].

In recent wind-turbine design, variable-speed wind-turbine systems are attractive for increasing energy capture and reducing mechanical fatigue damage. Variable-frequency generator and converters are essential so as to interconnect variable-frequency systems and constant-frequency systems. Among various wind-turbine systems, Type-3 wind-

generation unit using doubly-fed induction machines (DFIM) and Type-4 wind-generation unit using permanent magnetic synchronous generators (PMSG) are popularly used and researched for more efficient wind-energy extraction from wind-turbines. The basic configurations are shown in Figure B.2.

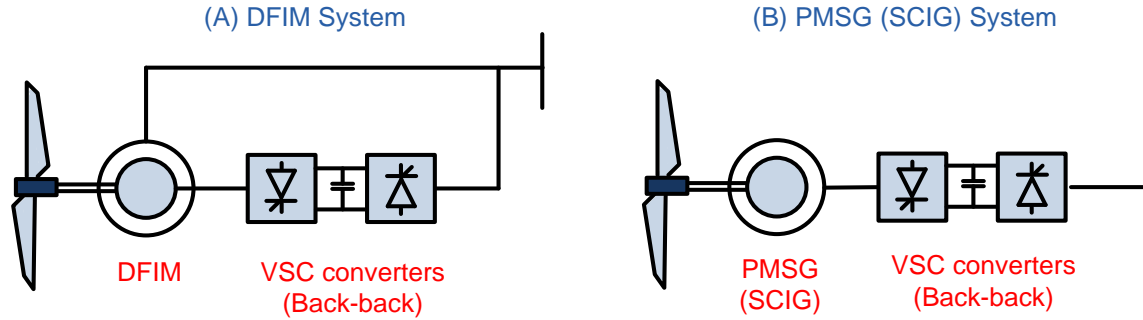


Figure B.2: (A) Type-3 Wind-Generation Unit and (B) Type-4 Wind-Generation Unit

The Type-3 wind generation unit is based on a DFIG and a back-to-back converter system. The stator of the DFIG is directly connected to the grid, and the back-to-back converter system is placed between the rotor of the DFIG and the grid. The back-to-back converter system consists of a rotor-side converter (RSC) and a grid-side converter (GSC). The RSC transmits real power and imaginary power into the rotor of the DFIG, and the GSC is needed to support the DC-voltage level and to offer the controllability of imaginary power at the grid.

The Type-4 wind generation unit is based on a full size back-to-back converter system and a PMSG or a SCIG. In the system, the back-to-back converter system is placed between the stator of the generator and the grid. The back-to-back converter system consists of a stator side converter (SSC) and a grid side converter (GSC), and deals with the full ranges of the generated power from wind turbines. The SSC controls the amount of the real power and imaginary power from the generator; and the GSC offers the DC-voltage support and the controllability of imaginary power at the grid.

In the local-grid system, the electrical voltage from wind-turbine systems is first boosted into high-voltage level of tens of kV to avoid low-voltage transmission via cables. Step-up transformer can be used for voltage boosting and allow electrical isolation between the wind-turbine system and the local-grid. High potential in the local-grid can shock and destroy wind-turbine systems. For example, assuming that the wind-turbines are connected in DC-series interconnection, the total DC-voltage are huge, and the electrical potential can offer harmful damages in wind-turbine systems. In this case the transformer can allow electrical isolation between wind-generators and local-grid potential and ground connection.

Wind-turbine units are connected to transmission system and electrical energy from wind-turbine units are corrected at a point of common connection (coupling). In case of nominal-frequency transmission system, only a step-up transmission can be used to boost

electrical voltage into transmission voltage-level. Otherwise, in case of HVDC transmission system, a rectifier station is also required to convert AC- to DC-power. Also, protection systems such as relays and circuit breakers are necessary to protect and disconnect the wind farm at the PCC.

For electrical energy transmission, nominal-frequency transmission systems, direct-voltage direct-current (HVDC) systems, and low-frequency alternating-current (LFAC) transmission systems can be used for efficient electrical-power transmission and the interconnection between wind farm and grid systems. The selection among them depends on the investment cost, the transmission distance, the power transmission capacity, etc.

## Appendix C: Advanced Time-Domain Method (Quadratic)

Mathematical models of physical components in power systems are generally modeled by state equations containing differential equations and algebraic equations [59]. Since the state equations cannot be solved exactly in explicit calculations, approximate methods are needed to model power systems, and the quadratic integration method is proposed in this paper for power systems with nonlinearities and switching subsystems. In this section, the basic concept and the superior properties of the quadratic integration are presented.

### Basic Concept of the Quadratic Integration method

The quadratic-integration method is based on two concepts: (a) the model of the systems is written as a combination of linear and quadratic equations within time step and (b) the quadratic integration is applied to these equations assuming the quadratic variation of the equations within the integration time step. Under these assumptions, the general quadratic form can be shown in Figure C.1 and the quadratic equation is written as  $x(t)=a+bt+ct^2$ .

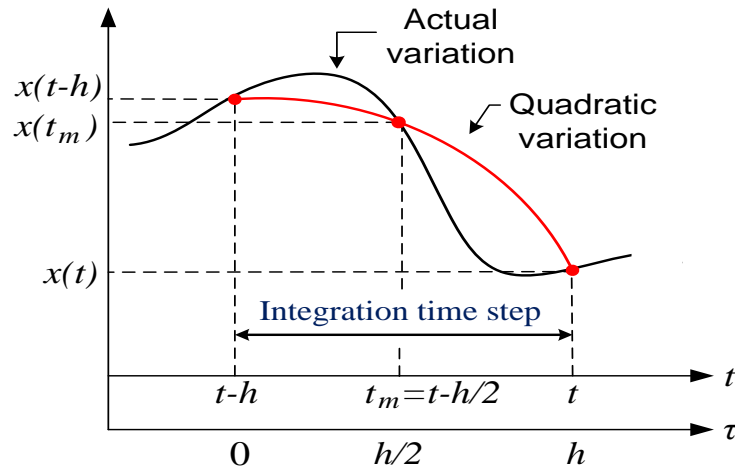


Figure C.1: Graphical Illustration of Quadratic Integration

The three parameters in the quadratic equation can be presented as a function of time at three collocation points: the two end of the interval are  $x(t-h)$  and  $x(t)$ , and the midpoint is  $x(t-h/2)$ . When the new variable  $\tau$  is used instead of  $t$  then it holds:  $x(t-h)=x(\tau=0)$ ,  $x(t)=x(\tau=h)$ , and  $x(t-h/2)=x(\tau=h/2)$ . With the assumption above, the three parameters  $a$ ,  $b$ , and  $c$  of the quadratic equation can be calculated and expressed as follows:

$$a = x(t-h), \quad (C.1)$$

$$b = \frac{1}{h} \left( -3x(t-h) + 4x_m - x(t) \right), \text{ and} \quad (C.2)$$

$$c = \frac{2}{h^2} \left( x(t-h) - 2x_m + x(t) \right). \quad (\text{C.3})$$

Using the three parameters, the algebraic-companion equations are calculated by integration of the state equations of the power device. Suppose that a first-order, dynamic system is given as  $\frac{dx}{dt} = Ax$ , the integration results are as follows:

$$x(t) - x(t-h) = A \cdot \int_0^h x(\tau) d\tau, \text{ and} \quad (\text{C.4})$$

$$x_m - x(t-h) = A \cdot \int_0^{h/2} x(\tau) d\tau \quad (\text{C.5})$$

Therefore, the algebraic-companion equations can be written as follows:

$$x(t) = x(t-h) + A \cdot \left( \frac{h}{6} x(t-h) + \frac{2h}{3} x_m + \frac{h}{6} x(t) \right) \text{ and} \quad (\text{C.6})$$

$$x(t) = x(t-h) + A \cdot \left( \frac{5h}{24} x(t-h) + \frac{h}{3} x_m - \frac{h}{24} x(t) \right). \quad (\text{C.7})$$

Note that  $h$  is the integration time step, and the state variable at mid-point ( $t_m$ ) is discarded since  $x_m$  is only introduced to compute the present value  $x(t)$ .

### Superior Properties of the Quadratic Integration

The superior properties of the quadratic integration are presented by comparison with the properties of the trapezoidal integration. First, accuracy property is an important characteristic of numerical-integration methods, since the reliability of power-transient analysis depends on it. The trapezoidal integration method is known as a second-order accurate method with two collocation points and the quadratic integration is a fourth-order accurate method with three-collocation points [59]. The dominant truncation error of both the trapezoidal integration and the quadratic integration can be denoted as  $E_{trapezoidal} = O(h^2)$  and  $E_{quadratic} = O(h^4)$  over the time interval  $[t-h, t]$ . That is, the dominant truncation error of the trapezoidal integration is proportional to  $h^2$  while that of the quadratic integration is proportional to  $h^4$ . For the accuracy comparison, a simple switching system is introduced in Figure C.2. The switches shown are ideal electronic, and the sequence of switching given with: Switches  $S1$  are closed at  $t=0.0T+KT$ , and opened at  $t=0.5T+KT$ , and switches  $S2$  are reversely operated, where the switching period  $T$  is 0.02 seconds, and  $k=\{0,1,2,\dots\}$ .

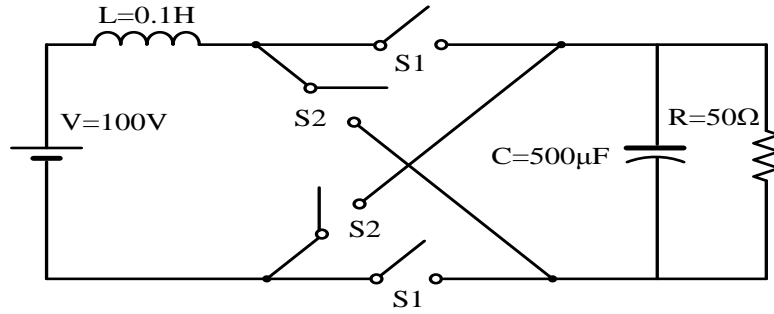


Figure C.2: A Simple Switching System

Figure C.3 shows the results (inductor current and the capacitor voltage) from the direct analytical solution by the Laplace transform. In order to show the error clearly, Figure A. 6 shows the absolute errors of both numerical methods during the last 0.1 second and for two different integration time steps. The absolute error is defined as  $Error = abs(v_{LT}(t) - v_N(t))$ , where  $v_{LT}$  is the capacitor voltage from the Laplace transform and  $v_N$  is that from the numerical methods.

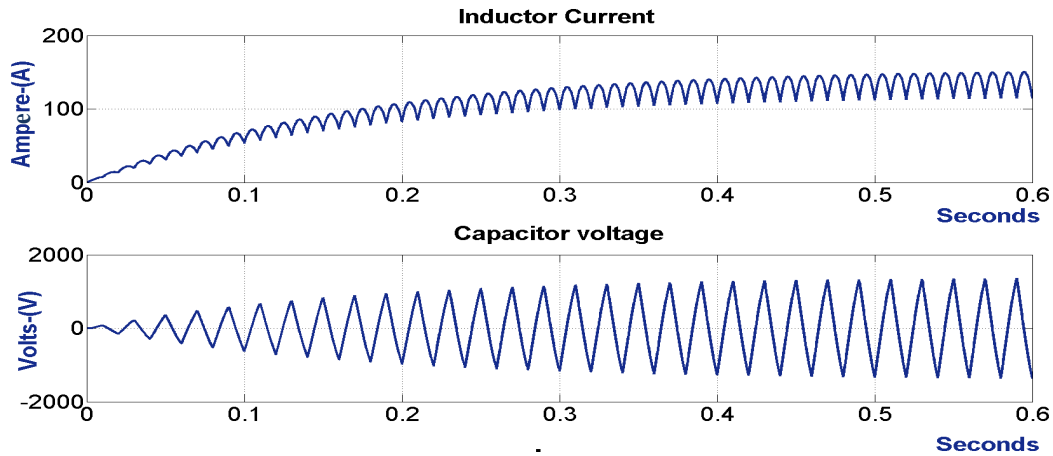


Figure C.3: Inductor Current and Capacitor Voltage from Laplace Transform

The absolute errors of the quadratic integration are about five orders of magnitude smaller than the errors of the trapezoidal integration. The example clearly shows the substantially higher accuracy of the quadratic integration method as compared to that of the trapezoidal integration. The computational cost of the quadratic integration is almost twice as much as that of the trapezoidal integration with the same time step. However, the quadratic integration with time step of 50 micro-seconds as compared to the trapezoidal integration with time step of 10 microseconds offers more accurate simulation results (more than three orders of magnitude) at a fraction of the execution time (about 50% of the execution time of trapezoidal integration).

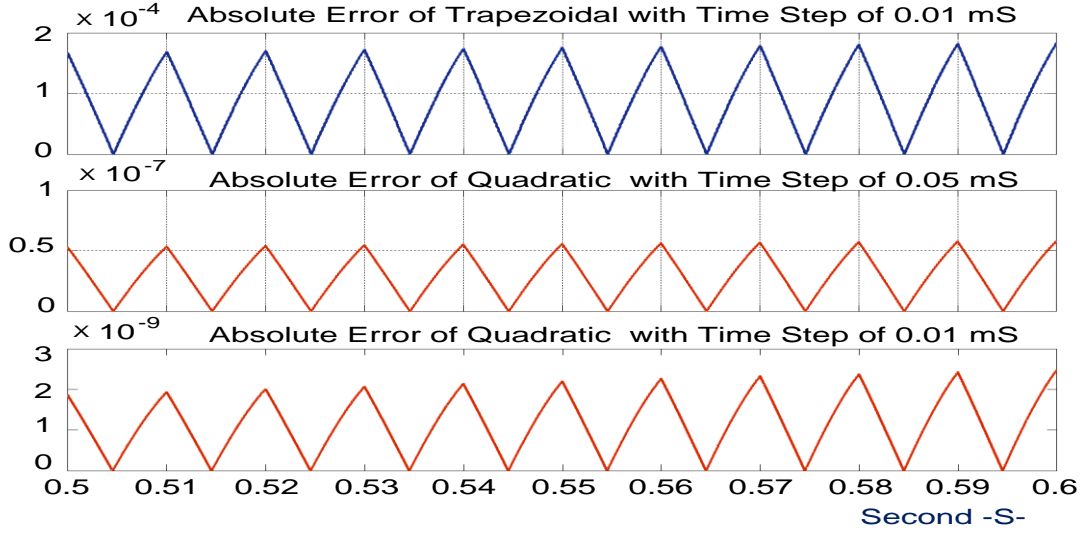


Figure C. 4: Absolute Error of the Capacitor Voltage

Second, power-transient analysis by application of trapezoidal integration has suffered from numerical oscillations especially in systems with nonlinearities and switching subsystems. The root cause of the fictitious oscillations is well known. The fictitious oscillations has been studied and reported in previous publications [59], [60]. The possibility of fictitious-oscillatory solution can be studied from the general form of the numerical solution of a simple dynamical system. Consider for an example a first-order dynamical system:  $\frac{dx}{dt} = ax$ , where  $a < 0$ .

The physical system is stable, since  $a < 0$ . Therefore the direct analytical solution is also stable. The numerical solution using trapezoidal integration is:

$$x(t) = \left( \frac{2+z}{2-z} \right) x(t-h), \text{ where } z = ah, \text{ and } h \text{ is positive.}$$

If the integration time step is selected such that  $z < -2$ , the numerical solution for  $x(t)$  will oscillate around the true values. Because the method is absolutely stable, the true values can be approximated by filtering the oscillations. The numerical solution using the quadratic integration, after eliminating the mid-point,  $x_m$ , is:

$$x(t) = \left( \frac{12 + 6z + z^2}{12 - 6z + z^2} \right) x(t-h) \quad (\text{C.8})$$

Note that in Equation (8) the coefficient cannot become negative for any selection of the time step ( $a$  is negative and  $h$  is positive). Therefore, the quadratic integration is free of fictitious oscillations as compared to the trapezoidal integration. To demonstrate numerical oscillations graphically, the six- pulse converter model is simulated with three



methods and with an appropriately selected integration time-step (same for all methods) as shown in Figure C.5. Trace (A) is the Line-to-Line voltage (A-B) solution using the trapezoidal integration and trace B is the filtered version of this solution. The results clearly demonstrate the existence of fictitious oscillations around the true solution of the system. Trace (C) shows the solution when numerical stabilizers are used in the trapezoidal integration. Trace (D) shows the solution by application of the quadratic integration which is free of fictitious oscillations.

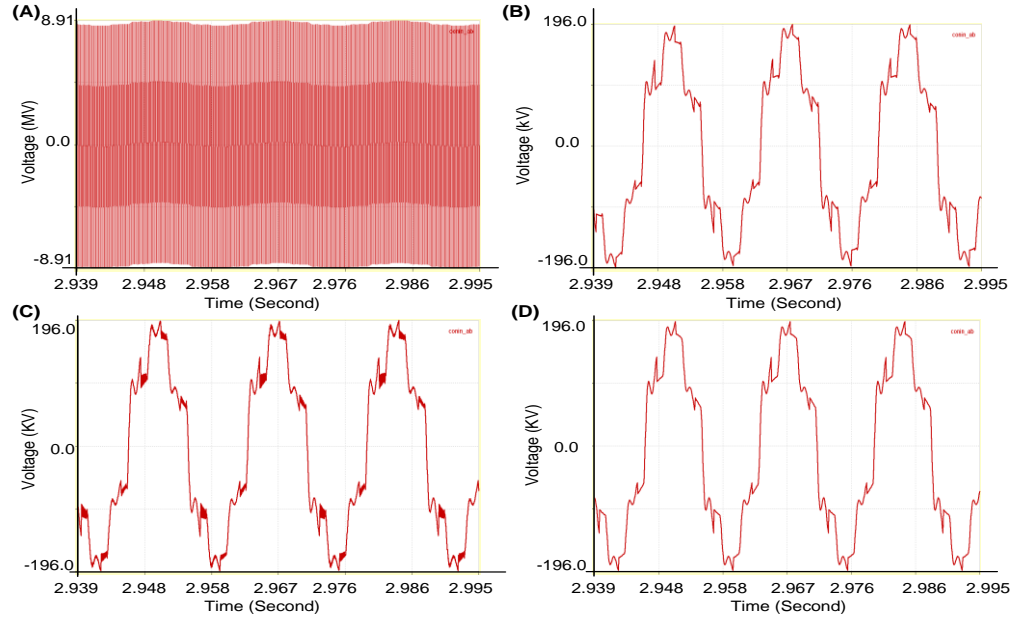


Figure C.5: Line-to-Line Voltage of a Six-Pulse Converter: (A) Trapezoidal, (B) Filtered Waveform, (C) Trapezoidal with Stabilizers, and (D) Quadratic Integration

Third, the quadratic integration method is also absolutely stable method. Assuming that a system to model is stable, the coefficient in the numerical solution from the quadratic integration is smaller than  $1$  over any combinations of time steps and system natural-frequencies as shown in Equation (C.8).

## Appendix D: Reliability Model Parameters

This appendix provides the symbols and typical values of component reliability parameters. The list shows all the components that appear in the 8 wind farm configurations discussed above. These parameters are used for the example calculation of the 8 configurations provided in the previous subsections.

Table D.1: Reliability Parameters of Components




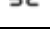





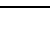


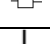


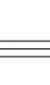


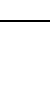
Icon	Component	Failure Rate	Typical Value of Failure Rate	Repair Rate	Typical Value of Repair Rate
	Wind Turbine	$\lambda_{WT}$	$\lambda_{WT} = 0.402$	$\mu_{WT}$	$\mu_{WT} = 69.546$
	Small Switch	$\lambda_{SSW}$	$\lambda_{SSW} = 0.0061$	$\mu_{SSW}$	$\mu_{SSW} = 14.84$
	Small Transformer	$\lambda_{sT}$	$\lambda_{sT} = 0.003$	$\mu_{sT}$	$\mu_{sT} = 0.533$
	Small AC/DC Converter	$\lambda_{sAC/DC}$	$\lambda_{sAC/DC} = 0.0298$	$\mu_{sAC/DC}$	$\mu_{sAC/DC} = 3.233$
	Large AC/DC Converter	$\lambda_{lAC/DC}$	$\lambda_{lAC/DC} = 0.0298$	$\mu_{lAC/DC}$	$\mu_{lAC/DC} = 3.233$
	In Farm AC Transmission Line	$\lambda_{FAC}$	$\lambda_{FAC} = 0.0189$	$\mu_{FAC}$	$\mu_{FAC} = 3.88$
	In Farm DC Transmission Line	$\lambda_{FDC}$	$\lambda_{FDC} = 0.0141$	$\mu_{FDC}$	$\mu_{FDC} = 3.04$
	Large Switch	$\lambda_{lSW}$	$\lambda_{lSW} = 0.0096$	$\mu_{lSW}$	$\mu_{lSW} = 8.75$
	AC Bus	$\lambda_{ACB}$	$\lambda_{ACB} = 0.000125$	$\mu_{ACB}$	$\mu_{ACB} = 0.0084$
	DC Bus	$\lambda_{DCB}$	$\lambda_{DCB} = 0.000125$	$\mu_{DCB}$	$\mu_{DCB} = 0.0084$
	DC/AC Converter	$\lambda_{DC/AC}$	$\lambda_{DC/AC} = 0.0298$	$\mu_{DC/AC}$	$\mu_{DC/AC} = 3.233$
	20 Hz Transformer	$\lambda_{20T}$	$\lambda_{20T} = 0.0032$	$\mu_{20T}$	$\mu_{20T} = 0.454$
	DC Transmission Line	$\lambda_{DC}$	$\lambda_{DC} = 0.0123$	$\mu_{DC}$	$\mu_{DC} = 3.04$

Table D.1: Reliability Parameters of Components (continued)

	20Hz AC Transmission Line	$\lambda_{20AC}$	$\lambda_{20AC} = 0.0075$	$\mu_{20AC}$	$\mu_{20AC} = 3.75$
	Cyclo Converter	$\lambda_{Conv}$	$\lambda_{Conv} = 0.0298$	$\mu_{Conv}$	$\mu_{Conv} = 3.233$
	60Hz AC Transmission Line	$\lambda_{60AC}$	$\lambda_{60AC} = 0.0141$	$\mu_{60AC}$	$\mu_{60AC} = 3.04$
	Large/ Substation Transformer	$\lambda_{IT}$	$\lambda_{IT} = 0.0032$	$\mu_{IT}$	$\mu_{IT} = 0.454$
	20Hz Inter- Transmission Line	$\lambda_{Inter20}$	$\lambda_{Inter20} = 0.0075$	$\mu_{Inter20}$	$\mu_{Inter20} = 3.75$
	60Hz Inter- Transmission Line	$\lambda_{Inter60}$	$\lambda_{Inter60} = 0.0141$	$\mu_{Inter60}$	$\mu_{Inter60} = 3.04$

## Appendix E: Cost Parameters

---

This appendix provides the typical values of individual acquisition cost for the components in the configurations. The list shows all the components that appear in the 8 wind farm configurations discussed above. These parameters are used for the example calculation of the 8 configurations provided in the previous subsections. It should be noted that the acquisition cost of one type of component, such as wind turbine, is different in different kV levels. For example, the wind turbine operating at 25 kV is more expensive than the turbine operating at 13.8 kV. Table E.1 only provides a typical acquisition cost of the components operating at 13.8 kV.

E.1: Typical Acquisition Cost of Components in the 8 Configurations

Component	Typical Acquisition Cost (\$)
Wind Turbine	1000,000
Small Switch	300
Small Transformer	5000
Small AC/DC Converter	2000
Large AC/DC Converter	30,000
In Farm AC Transmission Line	500
In Farm DC Transmission Line	500
Large Switch	5000
AC Bus	1000
DC Bus	1000
DC/AC Converter	20,000
20 Hz Transformer	20,000
DC Transmission Line	2000
20Hz AC Transmission Line	2000
Cyclo Conveter	5000
60Hz AC Transmission Line	2000
Large/ Substation Transformer	50,000
20/60 internal transmission line	1000

Table E.2 provides the data of cost of transmission lines, which is the mean per-mile cost of the lines.

## E.2: Cost of Transmission Lines

Voltage (kV)	Range of per-mile Costs (k\$)	Mean per-mile Cost from Composite Database (k\$)
13.8	41 - 50	44
34.5	43 – 55	48
46	46-56	49
69	60 – 238	107
115	91 – 228	124
138	96 – 308	165
161	105 – 333	182
230	129 – 371	235
345	218 – 503	341
500	364 – 972	519
765	Extrapolated	782
Based on flat terrain. Does not include land, environmental, planning, or construction supervision costs.		